

STOL TACTICAL AIRCRAFT INVESTIGATION

Volume IV

**Analysis of Wind Tunnel Data :
Vectored Thrust/Mechanical Flaps and
Internally Blown Jet Flaps**

*John R. Monk
Jerry L. Lee
J. Patrick Palmer*



Approved for public release; distribution unlimited.

FOREWORD

This report was prepared for the United States Air Force by The Boeing Company, Seattle, Washington in partial fulfillment of Contract F33615-71-C-1757, Project No. 643A. It is one of eight related documents covering the results of investigations of vectored-thrust and jet-flap powered lift technology, under the STOL Tactical Aircraft Investigation (STAI) Program sponsored by the Air Force Flight Dynamics Laboratory, Air Force Systems Command, Wright-Patterson Air Force Base, Ohio. The relation of this report to the others of this series is indicated below:

AFFDL TR-73-19 STOL TACTICAL AIRCRAFT INVESTIGATION

Vol I Configuration Definition:
Medium STOL Transport with
Vectored Thrust/Mechanical Flaps

Vol II Aerodynamic Technology:
Part 1 Design Compendium,
Vectored Thrust/Mechanical Flaps

Vol II A Lifting Line Analysis Method
Part 2 for Jet-Flapped Wings

Vol III Takeoff and Landing Performance
Ground Rules for Powered Lift
STOL Transport Aircraft

Vol IV Analysis of Wind Tunnel Data;
Vectored Thrust/Mechanical
Flaps and Internally Blown
Jet Flaps

THIS
REPORT

Vol V Flight Control Technology: System
Part 1 Analysis and Trade Studies for a
Medium STOL Transport with Vectored
Thrust/Mechanical Flaps

Vol V Flight Control Technology: Piloted
Part 2 Simulation of a Medium STOL Transport
with Vectored Thrust/Mechanical Flaps

Vol VI Air Cushion Landing System Study

The work reported here was performed in the period June 1971 through December 1972 by the Aero/Propulsion Staff of the Research and Engineering Division and by the Tactical Airlift Program, Aeronautical and Information Systems Division, both of the Aerospace Group, The Boeing Company. Mr. Franklyn J. Davenport served as Program Manager.

Contrails

The success of the work is also due to the contributions of the following persons in the areas designated.

Dennis L. Berry Investigated effects of tunnel wall corrections on ground effect test results. Compared ground effect test results with theory. Authored control power and engine-out thrust interference sections of this report.

Lorin D. Hawkins Performed analysis of lateral stability derivatives and the thrust interference effect on lift.

Fred W. May Conducted jet flap test. Performed analysis of jet flap data. Authored jet flap section of this report.

The help of the following persons is gratefully acknowledged: William G. F. Hardy (Vertol), Gary R. Letsinger, Harold S. Lewis, Edward J. Monell, Bernard F. Ray, William J. Runciman and Donald E. West.

The Air Force Project Engineer for this investigation was Mr. Garland S. Oates, Air Force Flight Dynamics Laboratory, PTA, Wright-Patterson Air Force Base, Ohio.

This report was released within The Boeing Company as document D180-14411-1 and submitted to the U.S. Air Force in December 1972.

This technical report has been reviewed and is approved.



E. J. Cross Jr., Lt. Col., USAF
Chief, Prototype Division
Air Force Flight Dynamics Laboratory

Contrails

ABSTRACT

This document presents the analysis of 728 hours of testing, conducted in the Boeing V/STOL 20 x 20 ft. Wind Tunnel, on a model of a medium STOL transport with vectored thrust and jet flap powered-lift systems. The work is part of the STOL Tactical Aircraft Investigation, U. S. Air Force Flight Dynamics Laboratory Contract Number F33615-71-C-1757, (A Study of the Aerodynamic and Flight Controls Technology of Vectored Thrust for STOL Transport Aircraft).

The interactions between the two powered lift systems and the basic airplane aerodynamics are presented for a systematic series of configuration changes which include sweep and nacelle location.

Contrails

Contracts

TABLE OF CONTENTS

		<u>Page</u>
Section I	Introduction	1
1.1	Background	1
1.2	State of the Art Prior to the STAI	1
1.3	Test Program	2
1.4	Document Organization	2
Section II	Test Program	3
2.1	Program Outline	3
2.2	Model Description	3
2.3	Facility	25
Section III	Unpowered Aerodynamic Characteristics	31
3.1	Lift and Drag Effects	31
3.2	Longitudinal Static Stability	43
3.3	Lateral-Directional Stability	48
Section IV	Vectored Thrust Characteristics	67
4.1	Thrust Interference Effects	67
4.2	Engine-Out Thrust Interference	106
4.3	Ground Effect on Gross Forces and Moments	135
4.4	Maximum Lift	155
4.5	Longitudinal Stability	170
4.6	Lateral Stability	191
4.7	Control Power	218
Section V	Internally Blown Jet Flap	229
5.1	Aerodynamic Data for Internally Blown Jet Flap and Vectored Thrust	229
5.2	Residual Nacelle Thrust Interference Effects	236
5.3	Flow Survey	245
5.4	Augmentor Wing Jet Flap	245
Appendix		257
References		285

Contracts

LIST OF ILLUSTRATIONS

Figure		Page
1	Vectored Thrust Model	4
2	Air Supply	6
3	Model Assembly Drawing	11
4	Trailing Edge Flaps	18
5	Installation of Balance	26
6	Boeing V/STOL Wind Tunnel	27
7	Unpowered Characteristics of Reference Configurations	33
8	Effect of Flap Deflection on Lift	34
9	Effect of Flap Deflection on Lift-Drag Ratio	36
10	Effect of Flap Span on Lift	37
11	Effect of Leading Edge Flap Angle on Maximum Lift	38
12	Effect of Sweep and Leading Edge Blowing on Maximum Lift Coefficient	39
13	Effect of Spanwise Break in Leading Edge Blowing	40
14	Effect of Sweep on Maximum Lift Coefficient	41
15	Effect of Aspect Ratio on Maximum Lift	42
16	Effect of Sweep on Lift	44
17	Effect of Nacelles on Lift	45
18	Lift Curve Slope and Aerodynamic Center - Effect of Aspect Ratio - Flaps Up	46
19	Lift Curve Slope and Aerodynamic Center - Effect of Sweep - Flaps Up	47
20.	Lift Curve Slope and Aerodynamic Center - Effect of Trailing Edge Flap Angle	49
21	Lift Curve Slope and Aerodynamic Center - Effect of Flap Span	50
22	Lift Curve Slope and Aerodynamic Center - Effect of Wing Sweep	51
23	Effect of Aspect Ratio on β Stability Derivatives - Flaps Up	56
24	Effect of Aspect Ratio on β Stability Derivatives - Flaps Down	57
25	Effect of Sweep on β Stability Derivatives, Nacelles On and Off, T.E. Flaps Up	58
26.	Effect of Sweep on β Stability Derivatives, Nacelles On and Off, Flaps Down	59

Contrails

LIST OF ILLUSTRATIONS (CONT)

Figure		Page
27	Effect of T.E. Flap Angle on β Stability Derivatives	60
28	Effect of T.E. Flap Span on β Stability Derivatives	61
29	Effect of L.E. Flap Angle on β Stability Derivatives	62
30	Effect of L.E. BLC on β Stability Derivatives	63
31	Effect of Tail - β Stability Derivatives	64
32	Effect of Angle of Attack on β Stability Derivatives	65
33	Determination of Thrust Interference on Lift	74
34	Effect of Thrust Coefficient on Thrust Interference	75
35	Effect of Thrust Vector Angle on Thrust Interference	76
36	Effect of Nacelle Chordwise Location on Thrust Interference	78
37	Effect of Nacelle Chordwise Location on Drag Interference at Given ΔC_{LINT}	79
38	Effect of Nacelle Chordwise Location on Pitching Moment Interference at Given ΔC_{LINT}	80
39	Effect of Nacelle Height on Thrust Interference	82
40	Thrust Interference, Single-Pods versus Dual-Pods	83
41	Effect of One Engine Failure on Thrust Interference	85
42	Effect of T.E. Flap Angle on Thrust Interference	86
43	Effect of Sweep on Thrust Interference	89
44	Effect of Test Conditions on Thrust Interference	90
45	Effect of Thrust Coefficient on Thrust Interference in Ground Effect versus Free Air	95
46	Effect of Thrust Coefficient on Thrust Interference in Ground Effect	96
47	Effect of Thrust Vector Angle on Thrust Interference in Ground Effect versus Free Air	98
48	Effect of Nacelle Chordwise Location on Thrust Interference in Ground Effect	99
49	Single Pods versus Dual Pods, Thrust Interference in Ground Effect	100
50	Effect of One Engine Failure on Thrust Interference in Ground Effect	102
51	Effect of T.E. Flap Angle on Thrust Interference in Ground Effect versus Free Air	103

Contrails

LIST OF ILLUSTRATIONS (CONT)

Figure		Page
52	Effect of Sweep on Thrust Interference in Ground Effect versus Free Air	105
53	Rolling Moment Due to Lift Interference	112
54	Comparison of Rolling Moment and Lift Thrust Interference	114
55	Comparison of Yawing Moment and Drag Thrust Interference	115
56	Longitudinal Thrust Interference, Effect of α and σ , Inboard Engine Out	117
57	Lateral-Directional Thrust Interference, Effect of α and σ , Inboard Engine Out	118
58	Longitudinal Thrust Interference, Effect of α and σ , Outboard Engine Out	119
59	Lateral-Directional Thrust Interference, Effect of α and σ , Outboard Engine Out	120
60	Longitudinal Thrust Interference, Effect of Nacelle Spanwise Location	122
61	Lateral-Directional Thrust Interference, Effect of Nacelle Spanwise Location	123
62	Longitudinal Thrust Interference, Effect of Trailing Edge Flap Angle	124
63	Lateral-Directional Thrust Interference, Effect of Trailing Edge Flap Angle	125
64	Longitudinal Thrust Interference, Effect of Wing Sweep, Inboard Engine Out	127
65	Lateral-Directional Thrust Interference, Effect of Wing Sweep, Inboard Engine Out	128
66	Longitudinal Thrust Interference, Effect of Wing Sweep, Outboard Engine Out	129
67	Lateral-Directional Thrust Interference, Effect of Wing Sweep, Outboard Engine Out	130
68	Longitudinal Thrust Interference, Effect of Ground Height, Inboard Engine Out	131
69	Lateral-Directional Thrust Interference, Effect of Ground Height, Inboard Engine Out	132
70	Longitudinal Thrust Interference, Effect of Ground Height, Outboard Engine Out	133

Contrails

LIST OF ILLUSTRATIONS (CONT)

Figure		Page
71	Lateral-Directional Thrust Interference, Effect of Ground Height, Outboard Engine Out	134
72	Comparison of Free Air and Ground Effect Characteristics, Power-Off	140
73	Comparison of Free Air and Ground Effect Characteristics, Power-On	142
74	Effect of Ground Height on Longitudinal Characteristics	143
75	Effect of Thrust Coefficient and Angle of Attack on Ground Effect	144
76	Effect of Thrust Vector Angle on Ground Effect	145
77	Effect of Nacelle Chordwise Location on Ground Effect	147
78	Effect of Nacelle Height and Spanwise Location on Ground Effect	148
79	Effect of Nacelle Type on Ground Effect	150
80	Effect of an Engine Failure on Ground Effect	151
81	Effect of Flap Angle on Ground Effect	152
82	Effect of Sweep Angle on Ground Effect	154
83	Effect of Thrust Coefficient on $C_{L_{MAX}}$	157
84	Effect of Thrust Vector and Nacelle Chordwise Location on $C_{L_{MAX}}$	158
85	Effect of Nacelle Spanwise Location and Nacelle Type on $C_{L_{MAX}}$	159
86	Effect of Nacelle Height on $C_{L_{MAX}}$	160
87	Effect of an Engine Failure on $C_{L_{MAX}}$	162
88	Effect of Flap Angle on $C_{L_{MAX}}$	163
89	Effect of L.E. Flap on $C_{L_{MAX}}$	164
90	Comparison of $C_{L_{MAX}}$ for 15° and 30° Wing Sweep	165

Contrails

LIST OF ILLUSTRATIONS (CONT)

Figure		Page
91	Comparison of Lift for 15° and 30° Wing Sweep, Flaps Up	167
92	Effect of Ground Proximity on $C_{L_{MAX}}$	168
93	Effect of Reynold's Number on $C_{L_{MAX}}$	169
94	Effect of Thrust on Longitudinal Stability	173
95	Direct Pitching Moment Due to Vectored Thrust	174
96	Effect of Thrust on Longitudinal Stability $\Lambda = 15^{\circ}$	175
97	Effect of Thrust on Longitudinal Stability $\Lambda = 30^{\circ}$	176
98	Effect of Thrust Deflection Angle on Longitudinal Stability	177
99	Effect of Nozzle Chordwise Position on Longitudinal Stability $\Lambda = 15^{\circ}$	178
100	Effect of Nozzle Chordwise Position on Longitudinal Stability $\Lambda = 30^{\circ}$	179
101	Effect of Nacelle Spanwise Location on Longitudinal Stability	181
102	Effect of One Engine Inoperative on Longitudinal Stability	182
103	Effect of Sweep on Longitudinal Stability	183
104	Effect of Flap Deflection on Longitudinal Stability	184
105	Effect of Angle of Attack on Pitching Moment Interference	186
106	Effect of Ground Height on Longitudinal Stability	187
107	Effect of Vectored Thrust on Downwash at the Horizontal Tail	188
108	Effect of One Engine Inoperative on Downwash	189
109	Effect of Ground Height on Downwash	190
110	Effect of Thrust on Sideforce Derivative	195
111	Effect of Thrust on Yawing Moment Derivative	196
112	Effect of Thrust on Rolling Moment Derivative	197
113	Effect of Thrust on Tail Input to Sideslip Derivatives	198

LIST OF ILLUSTRATIONS (CONT)

Figure		Page
114	Effect of Thrust Deflection Angle on Side Force Derivative	199
115	Effect of Thrust Deflection Angle on Yawing Moment Derivative	200
116	Effect of Thrust Deflection Angle on Rolling Moment Derivative	201
117	Effect of Nacelle Chordwise Location on Side Force Derivative	202
118	Effect of Nacelle Chordwise Location on Yawing Moment Derivative	203
119	Effect of Nacelle Chordwise Location on Rolling Moment Derivative	204
120	Effect of Thrust Deflection Angle on Side Force Derivative, Engine Out	206
121	Effect of Thrust Deflection Angle on Yawing Moment Derivative, Engine Out	207
122	Effect of Thrust Deflection Angle on Rolling Moment Derivative, Engine Out	208
123	Effect of Wing Sweep on Sideslip Derivatives	209
124	Effect of T.E. Flap Angle on Sideslip Derivatives	210
125	Effect of Angle of Attack on Side Force Derivative	211
126	Effect of Angle of Attack on Tail Input to Side Force Derivative	212
127	Effect of Angle of Attack on Yawing Moment Derivative	213
128	Effect of Angle of Attack on Tail Input to Yawing Moment Derivative	214
129	Effect of Angle of Attack on Rolling Moment Derivative	215
130	Effect of Angle of Attack on Tail Input to Rolling Moment Derivative	216
131	Sidewash at the Vertical Tail	217
132	Effect of Aileron Deflection and Blowing on Effectiveness	219
133	Aileron Effectiveness - Effect of Wing Leading Edge Blowing	220
134	Effect of Aileron Blowing and Engine Thrust on Aileron Effectiveness	221

Contracts

LIST OF ILLUSTRATIONS (CONT)

Figure		Page
135	Spoiler Effectiveness	222
136	Lateral Control - Combined Aileron and Spoiler	224
137	Rudder Effectiveness - Power Off	225
138	Effect of Sideslip on Rudder Power	226
139	Stabilizer Effectiveness	227
140	Comparison of Aerodynamic Characteristics of Jet Flap to Vectored Thrust	230
141	Comparison of Aerodynamic Characteristics of Jet Flap to Vectored Thrust	231
142	Maximum Lift Comparison	233
143	Leading Edge Boundary Layer Control Effectiveness	234
144	Lateral Stability	235
145	Spoiler Effects - Jet Flap and Vectored Thrust	237
146	Jet Flap Aileron	238
147	Jet Flap Aileron - No Blowing on Upgoing Aileron	239
148	Effect of Thrust Division Between Nacelle and Jet Flap	241
149	Effect of Jet Flap Thrust Coefficient on Residual Nacelle Thrust Interference - $\delta_f = 80^\circ$	242
150	Effect of Jet Flap Angle and Thrust Coefficient on Residual Nacelle Thrust Coefficient ($C_{J_{Nac}} = 2.0$)	243
151	Effect of Residual Nacelle Thrust Level on Interference $\delta_f = 80^\circ$, $\alpha_w = 8^\circ$	244
152	Ground Effect on Jet Flap Characteristics	246
153	Effect of Ground Proximity on Residual Nacelle Thrust Interference Effects - $C_{J_{Nac}} = 2.0$	247
154	Effects of Power on Downwash - Free Air	248
155	Effect of Sideslip Angle on Sidewash	249
156	Comparison of Performance of Jet Flap and Augmentors at $q = 20$ psf	250
157	Definition of Geometry Parameters	252
158	Effect of Augmentor Flap Geometry on Static Thrust Augmentation Ratio	

LIST OF ILLUSTRATIONS (CONT)

Figure		Page
159	Representative 2-D Aerodynamic Data for the Augmentor Wing at $C_j = 1.16$	254
160	Variation of Lift and Streamwise Force with C_j for the Augmentor Wing	255
161	Predicted versus Flight Test Aerodynamic Characteristics for the NASA Program Augmentor Wing Buffalo	256

Contrails

LIST OF TABLES

Table		Page
I	Wind Tunnel Test Program Outline	9
II	Wing Geometric Parameters	16
III	Trailing Edge Flap Deflection Angles	16
IV	Location of Vectored Nozzle Exit	23
V	Lift and Drag Characteristics - Unpowered	32
VI	Lateral-Directional Characteristics - Unpowered	52
VII	Effect of Vectored Thrust on Thrust Interference in Free Air	71
VIII	Effect of Vectored Thrust on Thrust Interference in Ground Effect	93
IX	Effect of Airplane Variables on Engine-Out Thrust Interference	107
X	Ground Effect on Gross Forces	137
XI	Effect of Vectored Thrust on Maximum Lift	155
XII	Effect of Vectored Thrust on Longitudinal Stability	171
XIII	Sideslip Derivative Behavior	192

LIST OF ABBREVIATIONS AND SYMBOLS

The data presented herein are referred to the stability-axis system about a moment center located longitudinally at .25 MAC and at a point 32.4% of the body height below the top of the body (WL 12.132). See Table II, Page 16.

1. Symbols

AR	Aspect ratio, b^2/S
a.c.	Aerodynamic Center
b	Wing Span, in.
c	Local Wing Chord, in.
c'	Extended Wing Chord (with flaps extended and rotated up)
\bar{c}	Wing Mean Aerodynamic Chord
C_D	Drag Coefficient, Drag/qS
C_J	Thrust Coefficient, Thrust/qS
C_j	Two-Dimensional Thrust Coefficient
C_L	Lift Coefficient, Lift/qS
$C_{L\alpha}$	Lift Derivative with Respect to α
$C_{L_{MAX}}$	Maximum Lift Coefficient
C_l	Two-Dimensional Lift Coefficient
C_{ξ}	Rolling Moment Coefficient, Rolling Moment/qSb
$C_{\xi\beta}$	Rolling Moment Derivative with Respect to β
C_m	Pitching Moment Coefficient, Pitching Moment/qSc
C_n	Yawing Moment Coefficient, Yawing Moment/qSb
$C_{n\beta}$	Yawing Moment Derivative with Respect to β
C_x	Augmentor Wing Longitudinal Force Coefficient, Positive Aft
C_Y	Side Force Coefficient, Side Force/qS
$C_{Y\beta}$	Side Force Derivative with Respect to β

Contracts

LIST OF ABBREVIATIONS AND SYMBOLS (Continued)

D	Drag, lbs.
H	Distance between $.25\bar{c}$ and Ground Level, in.
h	Distance between WDP and Centerline of Nacelle, in.
K_{ℓ}	Rolling Moment Coefficient Zero Offset Caused by Mutual Interference between Two Engines Operating Side by Side (Fig. 53)
K_n	Yawing Moment Coefficient Zero Offset Caused by Mutual Interference between Two Engines Operating Side by Side (Page 113)
L	Lift, lbs.
l_H	Distance from Wing $\bar{c}/4$ to Horizontal Tail $\bar{c}/4$, in.
l_V	Distance from Wing $\bar{c}/4$ to Vertical Tail $\bar{c}/4$, in.
M	Mach Number
q	Dynamic Pressure, psf
R_e	Reynolds Number
S	Wing Reference Area, sq. ft.
S_H	Horizontal Tail Area, sq. ft.
S_V	Vertical Tail Area, sq. ft.
t	Local Wing Thickness, in.
\bar{V}_H	Horizontal Tail Volume Coefficient, $\frac{l_H S_H}{S \bar{x}}$
\bar{V}_V	Vertical Tail Volume Coefficient, $\frac{l_V S_V}{S b}$
x	Distance Nozzle Exit is Moved Aft from Leading Edge of Wing (positive as nacelle moves aft), in.
x_i, y_i, z_i	Three-Dimensional Location of Nozzle Exit Centerline with Respect to Moment Reference Center (x_i positive forward, y_i positive out right wing, z_i positive down), in.
Y	Effective Moment Arm (positive out right wing), in.
Y_M	Mean Effective Moment Arm, in.
Z_H	Distance from Wing Chord Plane to Horizontal Tail Chord Plane, in.

LIST OF ABBREVIATIONS AND SYMBOLS (Continued)

2. Greek Symbols

α	Angle of Attack, degrees
β	Sideslip Angle, degrees
Δ	Increment
δ	Deflection Angle, degrees
δ_f	T.E. Flap Deflection Angle, degrees
$\delta_{\text{R}}^{\text{EFFECTIVE}}$	Effective Rudder Deflection Angle, degrees
ϵ	Downwash Angle, degrees
η	Fraction of Semi-Span
η_{ENG}	Semi-Span Engine Location
η_f	Spanwise Location of Outboard End of T.E. Flap
Λ	Sweep Angle of the Wing $.25\bar{c}$
C_{μ}	Boundary Layer Control Momentum Coefficient
σ	Thrust Vector Angle, Sidewash Angle, degrees

3. Abbreviations

BLC	Boundary Layer Control
BVWT	Boeing V/STOL Wind Tunnel
DEGS	Degrees
IBJF	Internal Blown Jet Flap
MAC(m.a.c.)	Mean Aerodynamic Chord
MBGP	Moving Belt Ground Plane
MS	Model Station
OEI	One Engine Inoperative
psf	Pounds per Square Foot
WBL	Wing Buttock Line
WDP	Wing Definition Plane

Contrails

LIST OF ABBREVIATIONS AND SYMBOLS (Continued)

WL	Water Line
4. Subscripts	
α	With Respect to Angle of Attack
AIL	Aileron
A_L	Left Aileron
A_R	Right Aileron
β	With Respect to Sideslip Angle
ENG	Engine
f	Flap
∞	Remote Conditions
F.A.	Free Air
GROSS	Denotes Total Measured Force or Moment Including Aerodynamic, Thrust and Interference Components
G.E.	Ground Effect
H	Horizontal Tail
INT	Denotes Interference Term, which is Total Measured Force or Moment Less Aerodynamic and Thrust Components
J	Thrust
JET	Nozzle Efflux Condition
L.E.	Leading Edge
NAC	Nacelle
NET	Denotes Total Measured Force or Moment Less the Thrust Component
r	Rudder
S	Right Wing Spoiler
t	Tail
T.E.	Trailing Edge
V	Vertical Tail

xx

LIST OF ABBREVIATIONS AND SYMBOLS (Continued)

TEST	WING FENCE	WING	WING LE BLOWING	LE FLAPS	TE FLAPS	VERTICAL TAIL	HORIZONTAL STABILIZER	NACELLE	PYLON	SPOILER (RIGHT HAND ONLY)	BODY
B-4 BVWT 097	Z ₃	W _{x,y} ^Z	W _{x,1,y} ^Z	L _{1,1-6} ^{xx} L _{1,1,6} ⁷⁰ L _{1,2} ^{xx}	F _{1,1-5} ^{xx}	V ₁ ^{xx}	H ₁ ^{xx}	N ₁ ^{1,2,3,4}	P _{2,1} P _{5,1} P ₈ P _{1,2,3,4} P _x	-	B ₁
B-5 BVWT 099	-	W _{x,y} ^Z	W _{x,1,y} ^Z	L _{1,1-6} ^{xx} L _{1,2} ^{xx}	F _{1,1-5} ^{xx}	V ₁ ^{xx}	H ₁ ^{xx}	N ₂ ^{xx} N ₃ ^{xx} N _{2,1}	P _{2,3} P _{5,3} P _{1,2,3,4} P _x	-	B ₁
B-6 BVWT 101 BVWT 103	-	W _{x,y} ^Z	W _{x,1,y} ^Z	L _{1,1-6} ^{xx}	F _{1,1-5} ^{xx} F ₃	V ₁ ^{xx}	H ₁ ^{xx}	-	P _{1,2,3,4} P _x	S _{2,1-6} ⁴⁹	B ₁

DEFINITIONS:

W _{x,y} ^Z	x ~ General Configuration and Aspect Ratio	N ₁ ^{1,2,3,4}	~ Nacelle Location Spanwise
L _{1,1-6} ^{xx}	y ~ Sweep ~ Degrees	N ₂ ^{xx}	~ Thrust Angle ~ Degree
F _{1,1-5} ^{xx}	Z ~ Dihedral ~ Degrees	2	~ Vector Thrust Blowing Single Nacelles
F ₃	xx ~ Flap Deflection Angle ~ Degrees { $\Lambda = 15^\circ$	3	~ Vector Thrust Blowing Dual Nacelles
V ₁ ^{xx}	1-6 ~ LE Flap Section	2,1	~ Vector Thrust Blowing Nacelles with Plug to Simulate N ₁
H ₁ ^{xx}	xx ~ Main Flap Deflection Angle ~ Degrees	x	~ Pylon Configuration to Position Nacelles at Various Location
	1-5 ~ Flap Spanwise Section	1,2,3,4	~ Pylon Position
	Jet Flap	x,1	~ Clax Contour
	xx ~ Vertical Tail Incidence Angle ~ Degrees (Moveable Rudder and Tab)	x,3	~ Blowing Nacelle Pylon
	xx ~ Stabilizer Angle ~ Degrees (-20°, -15°, -10°, 0°, +15°)	P ₈	~ Blowing Nacelle in Position 8
	(Moveable Elevator -60°, -30°, 0°, +30°)	49	~ Deflection Angle ~ Degrees Streamwise
		1-6	~ Spoiler Sections

Model Configuration Symbol Summary

Contrails

SECTION I

INTRODUCTION

1.1 Background

The U.S. Air Force's need for modernization of its Tactical Airlift capability led to establishment of the Tactical Airlift Technology Advanced Development Program (TAT-ADP), contributing to the technology base for development of an Advanced Medium STOL Transport (AMST).

The AMST must be capable of handling substantial payloads and using airfields considerably shorter than those required by large tactical transports now in the Air Force inventory. If this short field requirement is to be met without unduly compromising aircraft speed, economy, and ride quality, an advanced-technology powered-lift concept will be required.

The STOL Tactical Aircraft Investigation (STAI) is a major part of the TAT-ADP, and comprises studies of the aerodynamics and flight control technology of powered-lift systems under consideration for use on the AMST. Under the STAI, The Boeing Company was awarded Contract No. F33615-71-C-1757 by the USAF Flight Dynamics Laboratory to conduct investigations of the technology of the vectored-thrust and internally blown jet flap powered-lift concepts. These investigations included:

- o Aerodynamic analysis and wind tunnel testing.
- o Configuration studies.
- o Control system design, analysis, and simulation.

1.2 State of the Art Prior to the STAI

Early in the STAI, the available literature and test data on vectored thrust was surveyed. It was found that the data base for vectored thrust interference effects on transport-type configurations was almost nonexistent. Consequently, the "State-of-the-Art Design Compendium" compiled from the information then available consisted only of procedures for estimating power-off characteristics and the recommendation to correct for power simply by direct vector addition of the propulsive forces. That is, interference effects were assumed to be zero.

1.3 Test Program

To provide the required data base, an extensive program of testing was conducted in the Boeing V/STOL Wind Tunnel. The unpowered, vectored thrust, and control characteristics of a vectored-thrust STOL transport configuration were defined in three separate test periods.

To provide better perspective for comparison of vectored thrust with other powered lift concepts being considered for the AMST, a limited additional program of wind tunnel tests was run with the same basic model equipped with internally blown jet flaps.

1.4 Document Organization

Section II defines the test program and provides a model description and a facility description. Section III presents the unpowered aerodynamic characteristics, establishing a reference level for subsequent powered testing. Section IV presents the vectored thrust characteristics. Section V presents the jet flap characteristics, together with data obtained from outside sources on augmentor wing jet flap performance.

SECTION II

TEST PROGRAM

2.1 Program Outline

The STAI wind tunnel test program consisted of four separate test periods. Each of these test periods was conducted to accomplish specific goals in the overall program. The first, BVWT 097, was conducted to define the basic unpowered airplane characteristics. The second, BVWT 099, defined the aerodynamic characteristics with vectored thrust. The third, BVWT 101, was devoted to determination of vectored thrust effects on control power. The fourth and final test period, BVWT 103, was a test of the internally blown jet flap concept.

The tests followed the outline defined in the STAI Wind Tunnel Test Program Description (Reference 16). The program was approved by the Air Force prior to execution, and was designed to exploit efficiently the configuration and vectored thrust capabilities of the model, as well as special features of the Boeing Vertol Wind Tunnel facility.

The test conditions, including wind tunnel, vectored thrust and airplane parameters are summarized in Table I.

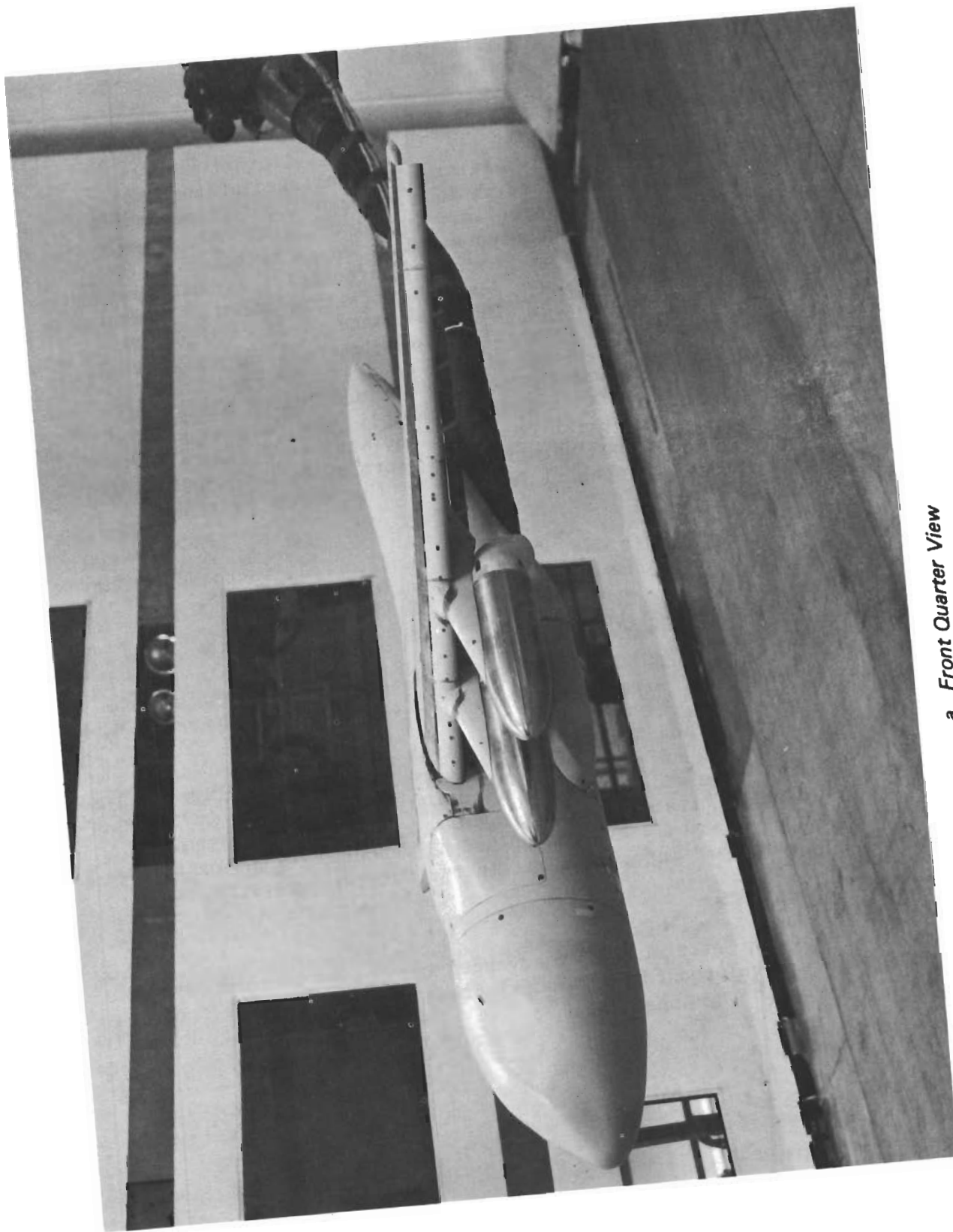
2.2 Model Description

The wind tunnel model used for the Boeing STAI test program was built to represent a typical medium STOL transport at .06 scale.

Quarter front and rear views of the model installed in the Boeing V/STOL wind tunnel are shown in Figures 1-a and 1-b. Figures 2-a through 2-c show the air supply distribution control system inside the model. The detailed features of the model are shown in the assembly drawing, Figures 3-a and 3-b. The principal features of the configuration will be described in more detail in the following paragraphs.

2.2.1 Wing Design

The wing section was an advanced technology section based on tests of wings developed for commercial transport applications. (Ordinates are given in the Appendix.)



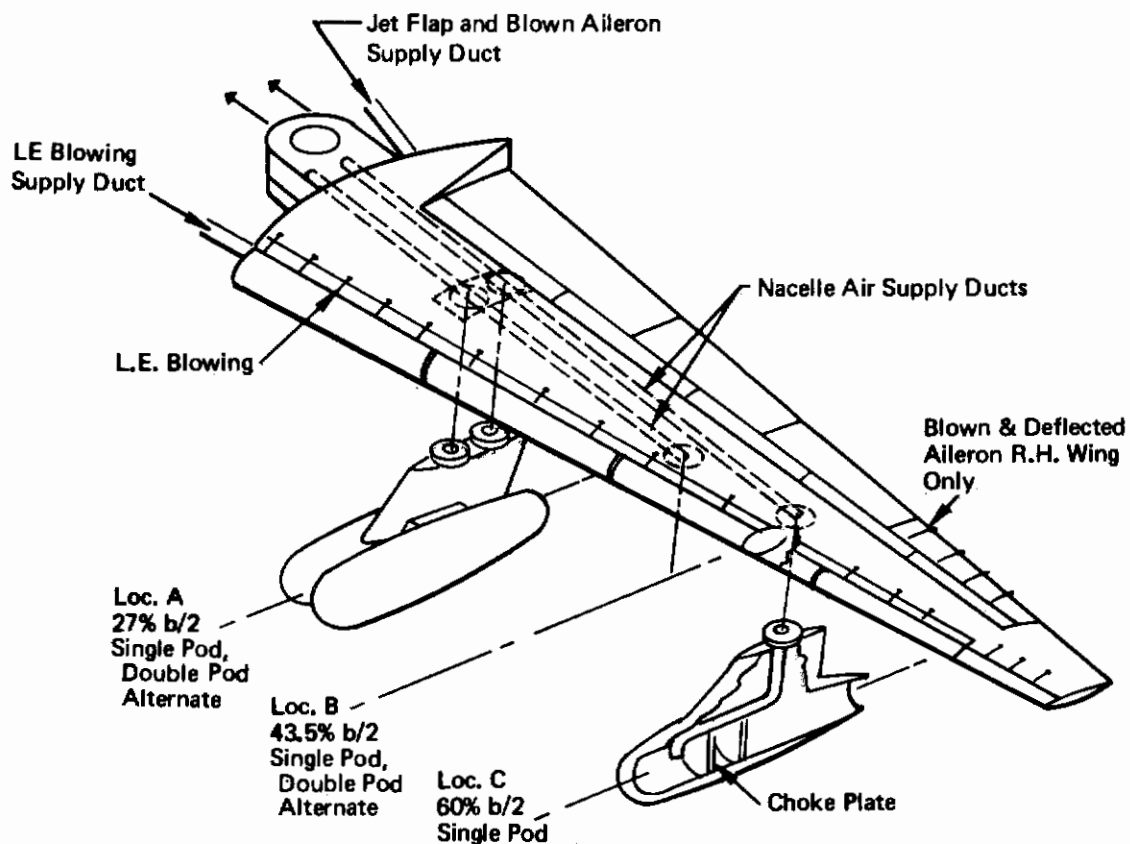
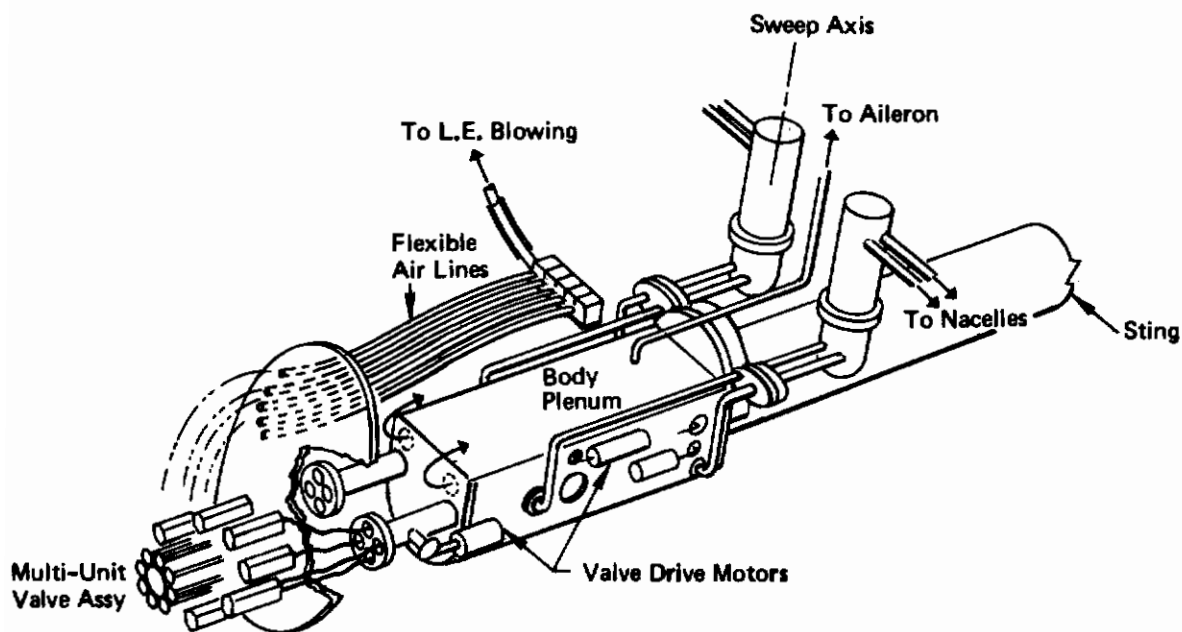
a. Front Quarter View

Figure 1: Vectored Thrust Model



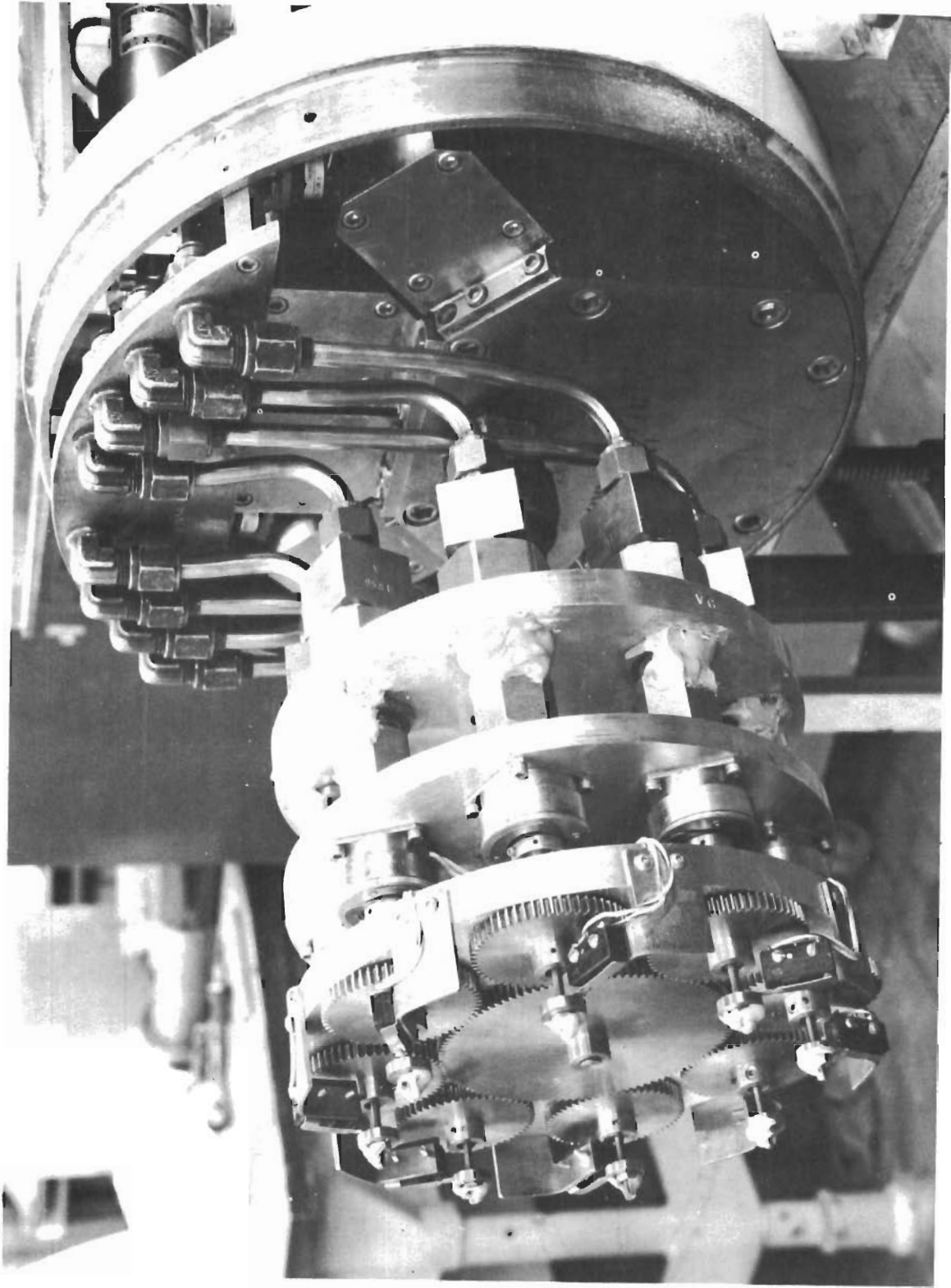
b. Rear Quarter View

Figure 1: Vectored Thrust Model (Concluded)



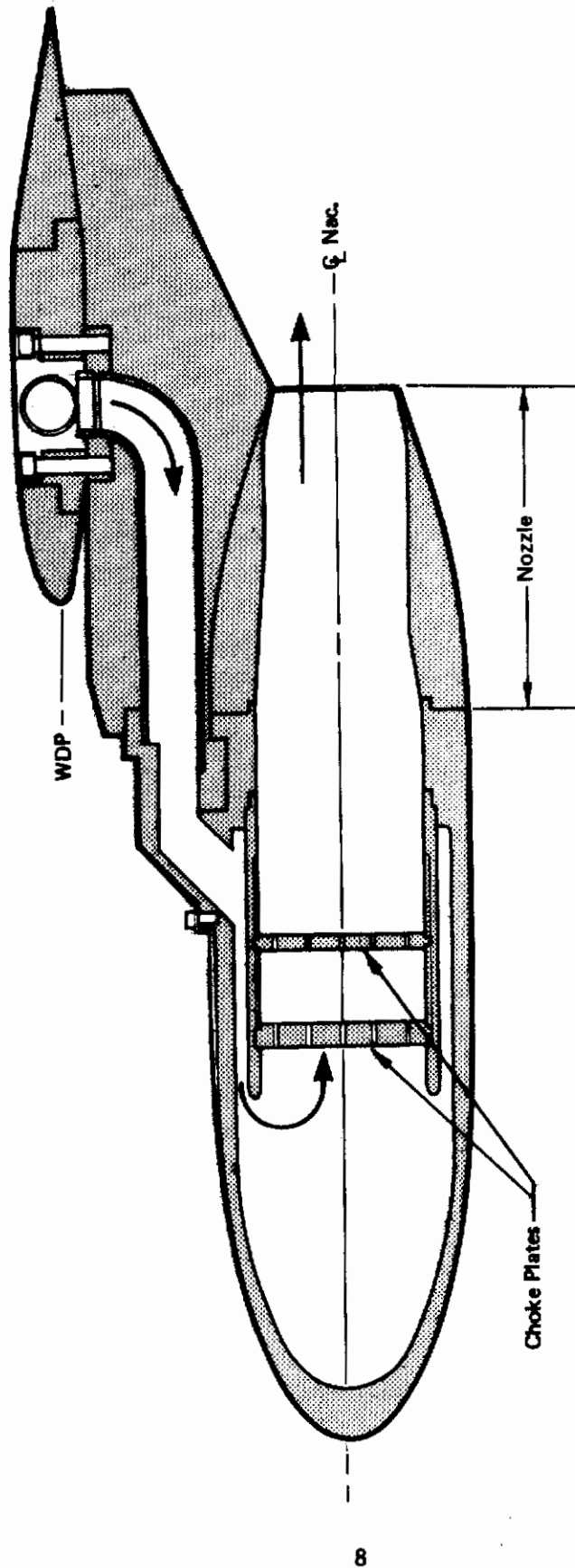
a. Schematic Diagram of Model

Figure 2: Air Supply



b. Internal Valve Control System

Figure 2: Air Supply (Continued)

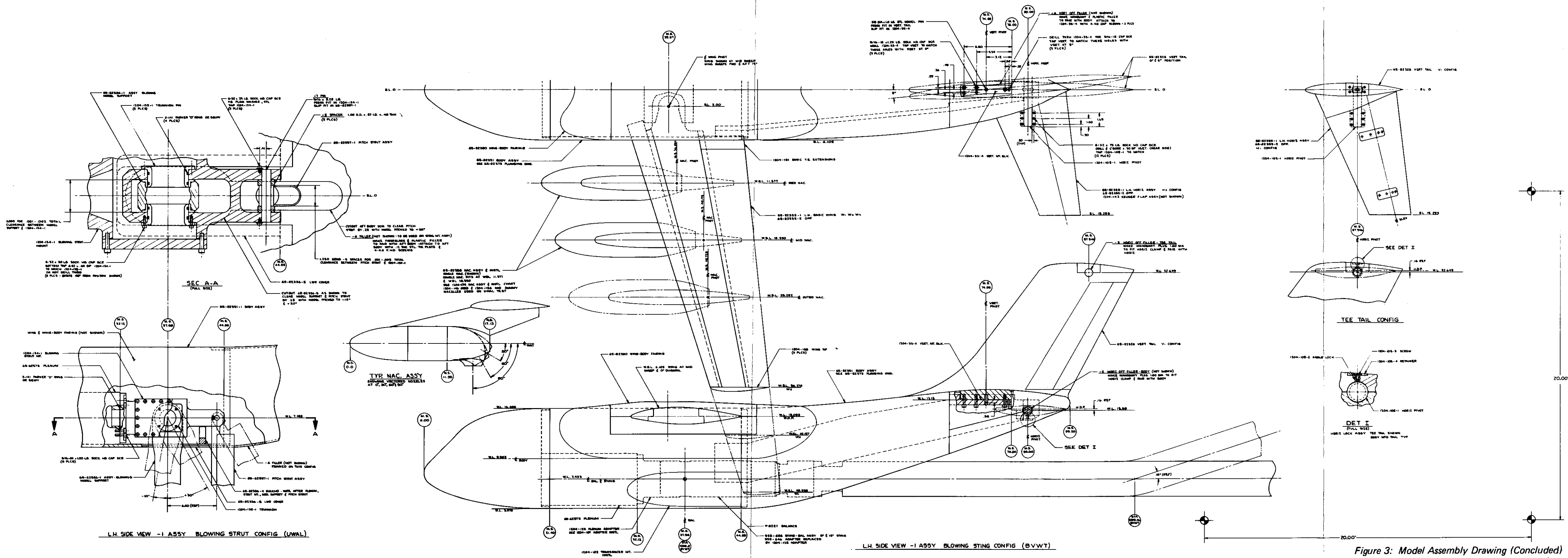


c. Internal Ducting of Blown Nacelle

Figure 2: Air Supply (Concluded)

Table I: Wind Tunnel Test Program Outline

BVWT TEST	PURPOSE	WIND TUNNEL CONDITIONS	VECTORED THRUST PARAMETERS						AIRPLANE PARAMETERS						Control Parameters	TEST ACCOMPLISHED
			C _J	α	NACELLE POSITION		Eng. Out	Eng. Type	Sweep	A R	T.E. Flaps	L.E. Flaps	Tail			
097 dates 3-13 3-31 123 hours	Determine unpowered characteristics.	Solid floor, q=22 psf, internal strain gauge balance. Re/Ft = .82 x 10 ⁶	0	0°	Off or 35% chord span	Off or 27/43.5% span	Off or h/c = .371 or .406	Does not apply.	Solid plug (no flow), 4 single pods.	0° 15° 30°	5.37 to 10.46	3-Slot flaps Variable span. δ _f =0° to 55%	δ=60° 70° 80° C _μ =0 to .06 Vary gap	On	Not Tested	The airplane parameters shown to the left varied and 6-component force data were obtained. These data formed the unpowered reference level to which the various interference and control effects of subsequent tests could be applied. The leading-edge flap configuration was optimized and the trailing-edge flap configurations for further testing were defined.
099 dates 5-23 6-30 395.4 hours	Determine vectored thrust interference effects.	Moving belt ground plane installed, q=22 & 10 psf, internal strain gauge balance. Re/Ft = .82 x 10 ⁶ and .55 x 10 ⁶	0.0 to 6.0	0° to 90°	0% or 35% or 70%	Single pods 27/43.5% or 43.5/60% dual pods 27 or 43.5%	h/c = .371 to .453	Yes, at various positions	Blown, 4 single pods or 2 dual pods.	15° 30°	8.0 6.62	3-Slot Flaps δ _f =0° to 48°	δ=70° C _μ =.06 No gap	On and Off	Not Tested	The vectored thrust and airplane parameters shown to the left were varied and 6-component force data were obtained in such a manner that the various aerodynamic and thrust interference effects could be isolated and identified. The tests were conducted in both free air and in close proximity to the moving belt ground plane.
101 dates 7-18 7-27 108 hours	Determine effect of vectored thrust on aileron and rudder control requirements; define downwash and sidewash.	Moving belt ground plane installed, q=22 psf, internal strain gauge balance, wake rake. Re/Ft = .82 x 10 ⁶	0.0 to 3.0	0° to 90°	0% or 35% or 70%	Single pods 27/43.5% or h/c = .371 or .406	Yes, at various positions.	Blown, 4 single pods.	15° 30°	8.0 6.62	3-Slot Flaps δ _f =0° to 35°	δ=70° C _μ =.06 No gap	On and Off	δAILERON 0,25,40,60,80° -40,-25° C _μ ALL 0, .02, .04, .06 δSPOILER 60° δRUDDER 0,10,20,30° δSTAB 0,10,20,30°	The tests conducted with various combinations of control deflections, vectored thrust parameters and airplane parameters. Six-component pitch and yaw data were obtained. The wake rake pressure data were obtained for various vectored thrust and airplane parameters. Not every point on the matrix of possible vectored thrust, airplane or control parameter combinations was obtained, but a sufficient cross-section of combinations were tested to allow the program objectives to be realized. Data in close proximity to the ground plane were obtained.	
103 dates 8-28 9-7 102 hours	Determine the characteristics of a jet flap AMST configuration.	Moving belt ground plane installed q = 10 psf, internal strain gauge balance, wake rake. Re/Ft = .82 x 10 ⁶	For jet flap 0-2.2 For nacelle 0-2.0	0°	35%	Single pods 27/43.5% or h/c = .371	None	Blown, 4 single pods.	15°	8.0	Jet Flap δ _f = 0° to 80°	δ=70° C _μ 0 to .10	Off	Not Tested	Various combination of jet flap and engine thrust, and jet flap deflections were tested. The 6-component pitch and yaw data were obtained using an internal strain gauge balance. A flow survey was also conducted during this test phase with a wake rake. Data in ground effect were obtained.	



The wing was pivoted to allow variable sweep. The wing was tested at 0° dihedral and with the wing design plane parallel to the body centerline.

The wing had two tip extensions to change aspect ratio. Most of the testing was done at the middle aspect ratio at sweeps of 15 and 30 degrees.

The wing geometric parameters are given in Table II.

2.2.2 Trailing Edge Mechanical Flaps

The triple slotted trailing edge flaps are of the type used on the Boeing 727 airliner. The shape of the main flap and the gap settings have been changed from the 727 geometry to improve the flap lift increment on the basis of two-dimensional tests conducted in the Boeing 4' x 8' low speed tunnel. Figure 4-a shows sections of the flaps taken streamwise at a wing sweep of 15° . The extended wing chord with the flaps rotated up, ratioed to the basic chord, is 1.302. The flap ordinates are given in Appendix.

The main flap deflection angle is defined two ways:

- (1) The angle between the flap local chord and the wing design plane;
- (2) The angle between the flap local chord in the extended and retracted position.

Because of the way the flap is stowed in the retracted position, the latter is greater than the former. The flap rotation definition of flap angle is used in the design compendium (Reference 6).

Table III gives the relationship between the two ways of measuring the angle.

The right hand column of Table III gives the angle a simple flap would have to give the same lift, assuming a linear relationship between flap deflection angle, flap chord ratio, and lift increment due to flap.

For the purposes of the model nomenclature, the main flap angle is used as a superscript on the flap symbol to denote a particular flap angle combination. The flap type and flap spanwise section are indicated by subscripts. For example:

Table II

WING GEOMETRIC PARAMETERS

Sweep c/4	Aspect Ratio	Area (ft) ²	Span (in)	Taper Ratio	MAC (in)	.25 MAC (MS, in.)	Y _{mac} ^w (in) ^w
0	6.818	5.696	74.782	0.481	11.417	33.897	16.513
	8.380	6.237	86.752	0.398	10.993		18.576
	10.461	6.741	100.768	0.301	10.561		20.680
15	6.5	5.624	72.556	0.483	11.613	37.437	16.034
	8.0	6.164	84.274	0.400	11.179	37.980	18.059
	10.0	6.669	97.996	0.302	10.737	38.533	20.124
30	5.374	5.584	65.738	0.485	12.723	40.481	14.534
	6.620	6.126	76.420	0.401	12.245	41.549	16.384
	8.283	6.630	88.928	0.303	11.759	42.638	18.270

Moment Reference Center at WL 12.132 and .25 MAC

TABLE III

TRAILING EDGE FLAP DEFLECTION ANGLES

Configuration Symbol	Angle of Flap Local Chord to Wing Defini- tion Plane (Degrees)			Total Flap Rotation (Degrees)		Equivalent Simple Flap Rotation (Degrees)
	Fore Flap	Main Flap	Aft Flap	Main Flap	Aft Flap	
F ₁ ²⁰	5	20	30	28.5	32.5	30
F ₁ ³⁰	10	30	40	38.5	42.5	40
F ₁ ³⁵	12	35	60	43.5	62.5	50.5
F ₁ ⁴⁸	20	48	60	56.5	62.5	58.7
F ₁ ⁵⁵	22	55	70	63.5	72.5	66.8
Flaps Up		-8.5	-2.3			

Contrails

F 35 ← flap angle, degrees
 type → 1, 12 ← flap spanwise segments

1 is mechanical flap

3 is jet flap

For the wing with 15° sweep and aspect ratio 8, the flap spanwise breaks occur at the following locations:

Flap Section	1	2	3	4	5
Fraction of Span	Body side to .565	.565 to .75	.75 to .861	.861 to 1.0	Not used at AR = 8.0

location of
aileron

Used for
AR = 10.45 wing

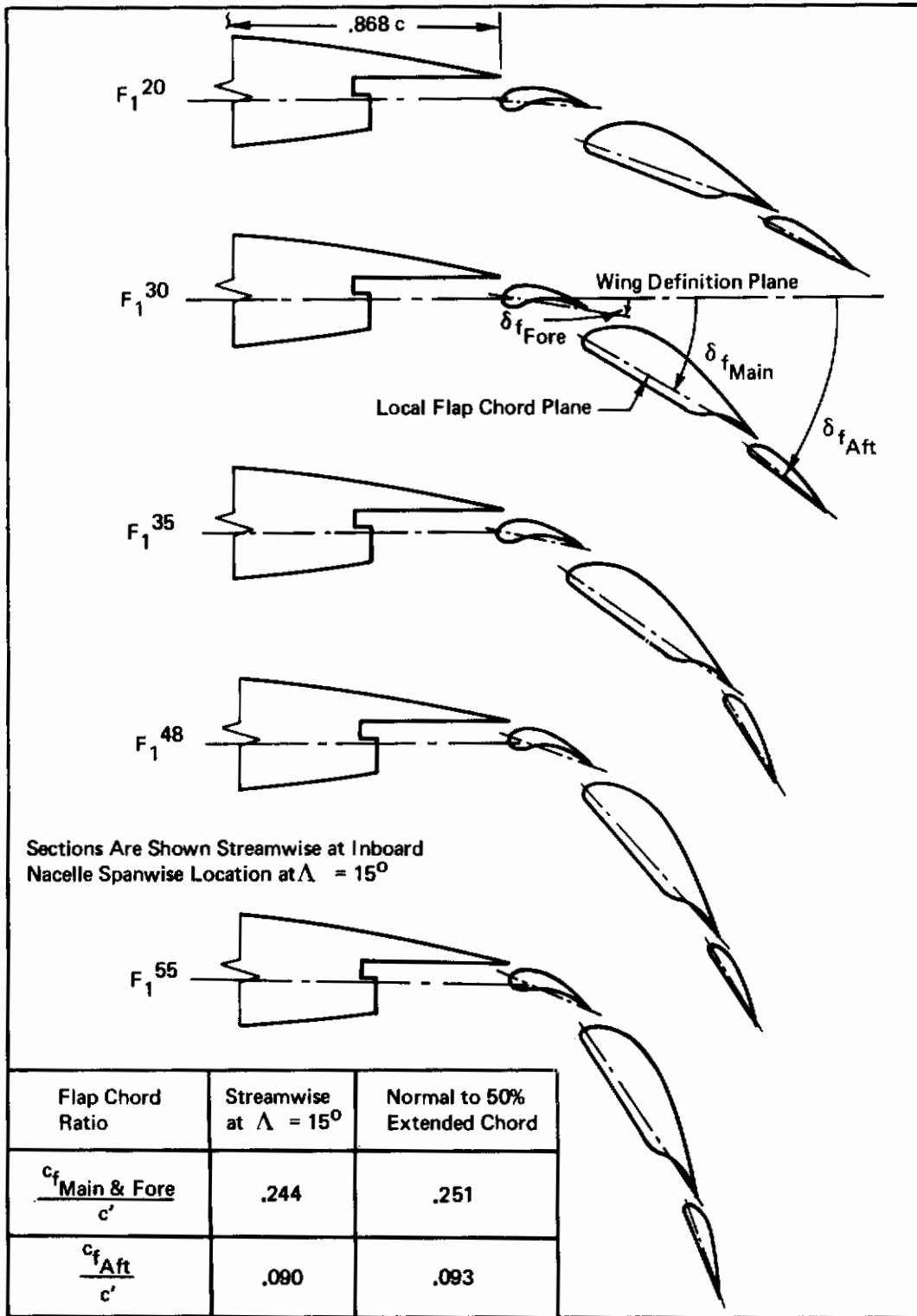
2.2.3 Jet Flap

Figure 4-b shows a section of the jet flap and air supply plenum. The end of the fixed upper surface (cove) is in the same location as for the triple slotted flap. The geometry corresponds to a 15% Fowler motion and gives a flap to extended total chord ratio of 1.25.

The blowing slot is tapered from 0.1 inch at the root to .04 inch at the tip to give a constant slot size to extended chord ratio of 0.62%. This slot size allows a jet momentum coefficient of 2.2 at a tunnel q of 10. The flap angle could be varied remotely. The flap has two sections, one out to the aileron and a second which replaces the aileron.

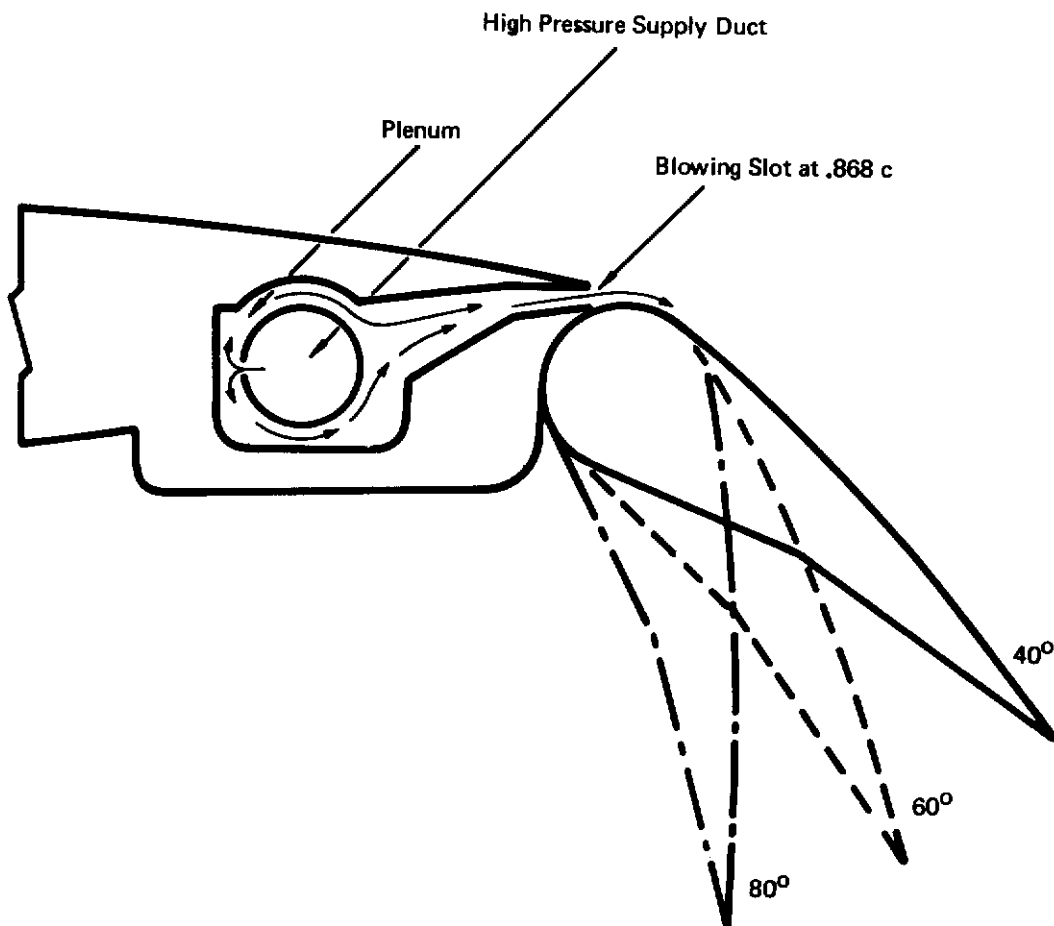
2.2.4 Leading Edge Flap

The leading edge flap is cambered and has a constant chord equal to 15% of the MAC of the basic wing. The blowing slot is at the trailing edge of the flap and has a constant gap of .003 inch. There is no blowing slot on the outermost wing tip extension. The flap is divided into six segments and can be set to 60° , 70° , and 80° angles with brackets.



a. Triple Slotted

Figure 4: Trailing Edge Flaps



Section Taken Normal to Flap Hinge Line at WBL = 15.58

$$\frac{c_f}{c'} = .247$$

b. Jet Flap

Figure 4: Trailing Edge Flaps (Concluded)

2.2.5 Spoilers

The spoilers were simple unvented plates set at 60° to the hinge line at 70% wing chord (49° streamwise at 30° sweep). There were six segments available for each side of the wing. The spoilers have a constant chord equal to 14% of the m.a.c.

2.2.6 Aileron

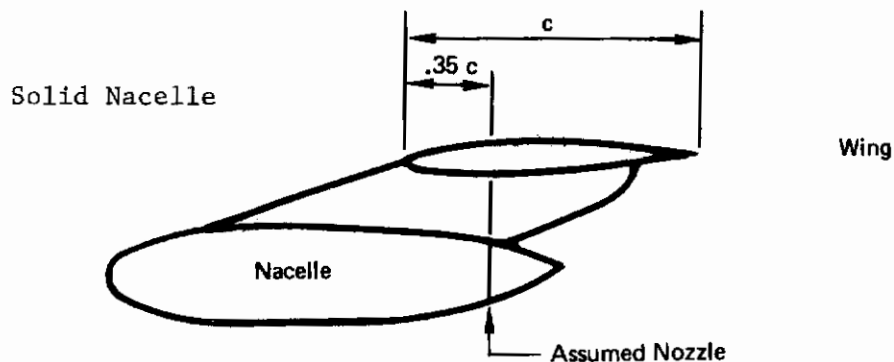
The aileron was a 25% local chord control surface mounted on the outboard 25% of the semi-span. The right hand aileron has a .005 inch blowing slot which improves aileron performance at the higher deflections. The blowing nozzle restricts the available right hand aileron deflection to the range $20^\circ - 80^\circ$ down. The left hand aileron is unblown and has a range of deflection from -40° (up) to $+60^\circ$.

2.2.7 Nacelle Geometry

o Nacelle Description

The nacelles were sized to represent engines in the 20,000 lbs. thrust class at .06 scale. Two types of nacelles were available.

1. Faired Body Type. The nacelle is represented by a solid body. No inlet or exit flow is simulated. Used in unpowered test only.



2. Blown Nacelle Type. The forward part of the nacelle is externally the same as the solid type nacelle above. The nozzle is blown with an external source of compressed air via a supply pipe built into the model. The nozzle can be set at a choice of 4 vectored thrust angles: 0° , 30° , 60° , 90° .

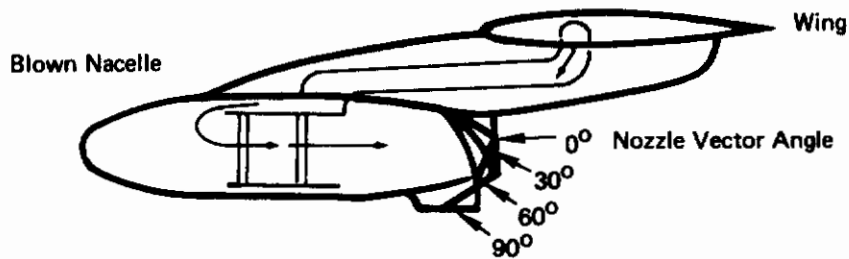
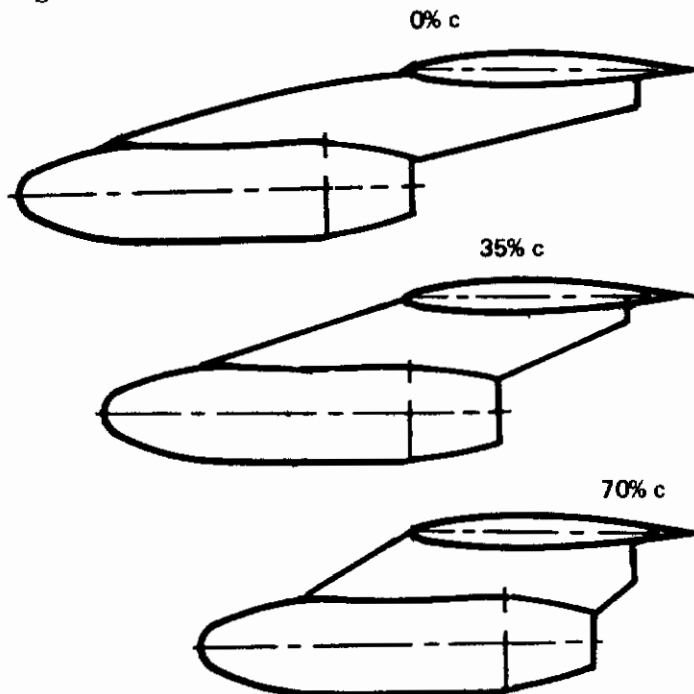


Figure 2-c shows the internal arrangement of the nacelle. Note the two choke plates.

o Nacelle Location

The nacelle can be mounted on the wing in a selection of chordwise, spanwise, and vertical locations by means of interchangeable pylons, as outlined below.

Chordwise Location. Three fore and aft nacelle locations were available which placed the plane of the undeflected nozzle at zero, 35, and 70% of the local wing chord as illustrated in the following sketch:



Contrails

These positions are referred to as the nominal nozzle locations which are used to define the model parts. When the nozzle is deflected, the center of the nozzle moves down and forward. The resulting nozzle locations are given in Table IV.

Spanwise Location. Three spanwise stations were available on the wing as nacelle mounting points, at 0.27, 0.435, and 0.60 semi-span. The combinations which were tested are shown in the diagram below. The double pods were restricted to the 15° wing sweep case.

Nacelle Spanwise Locations:

Single Pods



Double Pods



Height. The nacelle could be lowered one inch from its nominal vertical position by a spacer in the pylon. The available h/\bar{c} for the nacelle (where h is the distance from the WDP to the nacelle centerline) were:

Λ	0°	15°	30°
h/\bar{c}	.41	.406	.371
	.5	.496	.452

NOMINAL

LOWERED 1 IN.

Table IV: Location of Vectored Nozzle Exit

SWEEP	NOZZLE VECTOR ANGLE-DEG.	NOMINAL CHORDWISE LOCATION % LOCAL CHORD	ACTUAL CHORDWISE LOCATION % LOCAL CHORD - CENTER OF NOZZLE			ACTUAL CHORDWISE LOCATION % MAC - CENTER OF NOZZLE			DEPTH OF NOZZLE PLANE BELOW WDP % MAC
			INBD	MID	OUTBD	INBD	MID	OUTBD	
0° AR = 8.38		0	(WBL) 11.31	(WBL) 18.89	(WBL) 25.75				
		35	-1.45	-2.16	-	-5.23	-2.33	-	
		70	33.93	33.51	33.85	34.97	33.15	32.21	41.30
		0	69.25	69.10	-	75.09	68.54	-	
		30	-3.51	-4.52	-	-7.58	-4.68	-	
		35	31.87	31.15	31.14	32.62	30.80	29.86	52.20
		70	67.19	66.74	-	72.74	66.19	-	
		0	-9.27	-11.10	-	-14.12	-11.22	-	
		35	26.11	24.57	23.58	26.08	24.26	23.32	61.01
		70	61.43	60.16	-	66.20	59.65	-	
		0	-17.45	-20.44	-	-23.40	-20.50	-	
		35	17.93	15.23	12.85	16.80	14.98	14.04	66.15
	70	53.25	50.82	-	56.92	50.37	-		
15° AR = 8.00		0	(WBL) 11.337	(WBL) 18.38	(WBL) 25.882				
		35	-0.02	-0.04	-	-19.24	0.72	-	
		70	35.03	35.02	35.03	20.29	35.61	50.95	40.61
		0	70.00	70.00	-	59.74	70.41	-	
		30	-2.06	-2.36	-	-21.55	-1.59	-	
		35	32.99	32.70	32.35	17.98	33.30	48.64	51.33
		70	67.96	67.68	-	57.43	68.10	-	
		0	-7.77	-8.82	-	-27.98	-8.02	-	
		35	27.28	26.24	24.89	11.55	26.87	42.21	60.00
		70	62.25	61.22	-	51.00	61.67	-	
		0	-15.86	-18.01	-	-37.11	-17.15	-	
		35	19.19	17.05	14.29	2.42	17.74	33.08	65.05
	70	54.16	52.03	-	41.87	52.54	-		
30° AR = 6.62		0	(WBL) 10.80	(WBL) 16.66	(WBL) 23.30				
		35	3.70	5.30	-	-24.99	7.01	-	
		70	35.97	37.31	36.28	11.10	38.86	67.40	37.08
		0	68.19	69.24	-	47.18	70.62	-	
		30	1.82	3.18	-	-27.10	4.90	-	
		35	34.09	35.19	33.82	8.99	36.75	65.29	46.86
		70	66.31	67.12	-	45.07	68.51	-	
		0	-3.43	-2.72	-	-32.97	-0.97	-	
		35	28.84	29.29	26.96	3.12	30.88	59.42	54.77
		70	61.06	61.22	-	39.20	62.64	-	
		0	-10.88	-11.10	-	-41.31	-9.31	-	
		35	21.39	20.91	17.22	-5.22	22.54	51.08	59.39
	70	53.61	50.72	-	30.86	54.30	-		

Contracts

2.2.8 Body Proportions

The full scale body corresponded to 204 inch diameter and 110 ft. length (assuming the full size to model scale of .06). This would provide a 138"W x 148"H x 540"L cargo box. The aft body is designed for a rear loading door with a ramp and a truck-bed height cargo floor with doors closed. The aft body has a keel line upswept 19.3°.

2.2.9 Empennage

The geometric characteristics of the horizontal and vertical tail were as follows:

	Horizontal Tail	Vertical Tail
Area	1.624 ft ²	1.359 ft ²
Sweep at Quarter Chord	20°	35°
Aspect Ratio	4	1.08
Thickness/Chord Ratio	.13	.11
Camber	-2%	0

Wing Sweep	Wing Aspect Ratio	Tail Arm	\bar{V}_H	Tail Arm	\bar{V}_V
0°	6.818	53.254	1.327	44.772	0.143
	8.380		1.258		0.112
	10.461		1.212		0.090
15°	6.5	49.714	1.233	41.232	0.137
	8.0	49.171	1.156	40.689	0.106
	10.0	48.618	1.100	40.136	0.083
30°	5.374	46.670	1.064	38.188	0.141
	6.620	45.602	0.985	37.120	0.108
	8.283	44.513	0.925	36.031	0.083

The double segmented rudder had a constant percentage chord of 38% chord measured streamwise with a span of 90% of the vertical fin height. The trailing-edge segment was 40% of the chord of the rudder.

2.2.10 Internal Strain Gauge Balance

The model used the Boeing 6227 six-component strain gauge balance containing an internal flow passage which allowed the air supply to cross the balance. In the first three test periods there was a large pressure tare effect on the axial force corresponding to the supply pressure acting on the internal cross-sectional area of the balance bellows. The pressure tares were the principal source of error of the balance, which resulted in a maximum uncertainty in axial force of 2% of thrust or .05 in drag coefficient. However, the repeatability of the data seems to be very much better than this. The error in normal force was less than 0.5%. The balance was modified for the fourth jet flap test with an opposed bellows system which gave internal cancellation of the pressure forces to greatly reduce the tare. The balance installation prior to the modification is shown in Figure 5.

The model was installed so that the balance moment reference center was located horizontally at tunnel station 1000; laterally 20.5 inches to the left looking downstream and vertically at waterline 1000 (120 inches above the solid floor reference for the free air testing).

2.3 Facility

The STAI wind tunnel tests, BVWT 097, 099, 101 and 103, were conducted in the 20-foot by 20-foot test section of the Boeing V/STOL Wind Tunnel. The Moving Belt Ground Plane was installed for all of the tests except BVWT 097. The dynamic pressure was generally 22 psf except for BVWT 103, which was run at 10 psf to allow the jet flap nozzle pressure to remain below the value at which the jet separated from the flap surface. The corresponding Reynolds numbers per foot were .82 and $.55 \times 10^6$, respectively. The test section was in the conventional (solid wall) configuration. The wind tunnel facilities are shown on Figure 6-b.

2.3.1 The model was mounted on the Boeing 6227 internal six-component strain gauge balance installed on an 18-degree preband sting, which was in turn attached to the standard BVWT sting assembly consisting of the short 'cannon', the offset adapter, and the yaw adapter. The model installation in the wind tunnel test section is presented on Figure 6-a.

2.3.2 The installation of the Moving Belt Ground Plane is shown on Figure 6-a. The moving ground belt is 18 feet wide and stretched between rollers 27 feet apart. For testing in ground effect, the model was lowered into close proximity with the Moving Belt Ground Plane, with physical interference between the model support sting and the moving belt the limiting factor. The Moving Belt Ground Plane was operated at the same speed as the air flow through the test section. A boundary layer bleed scoop removed the tunnel floor boundary layer ahead of the belt to assure full total head conditions near the surface of the ground plane.

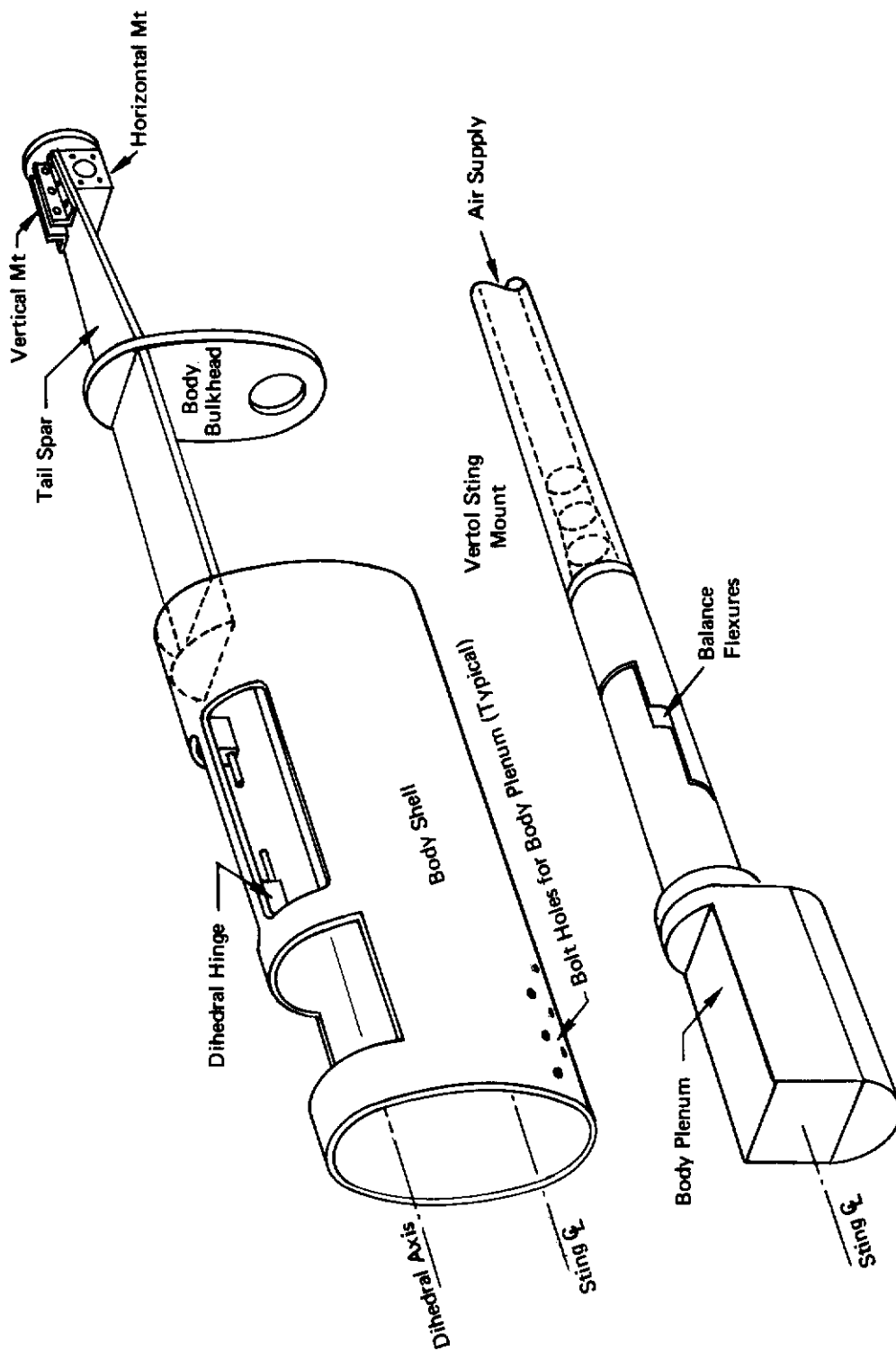
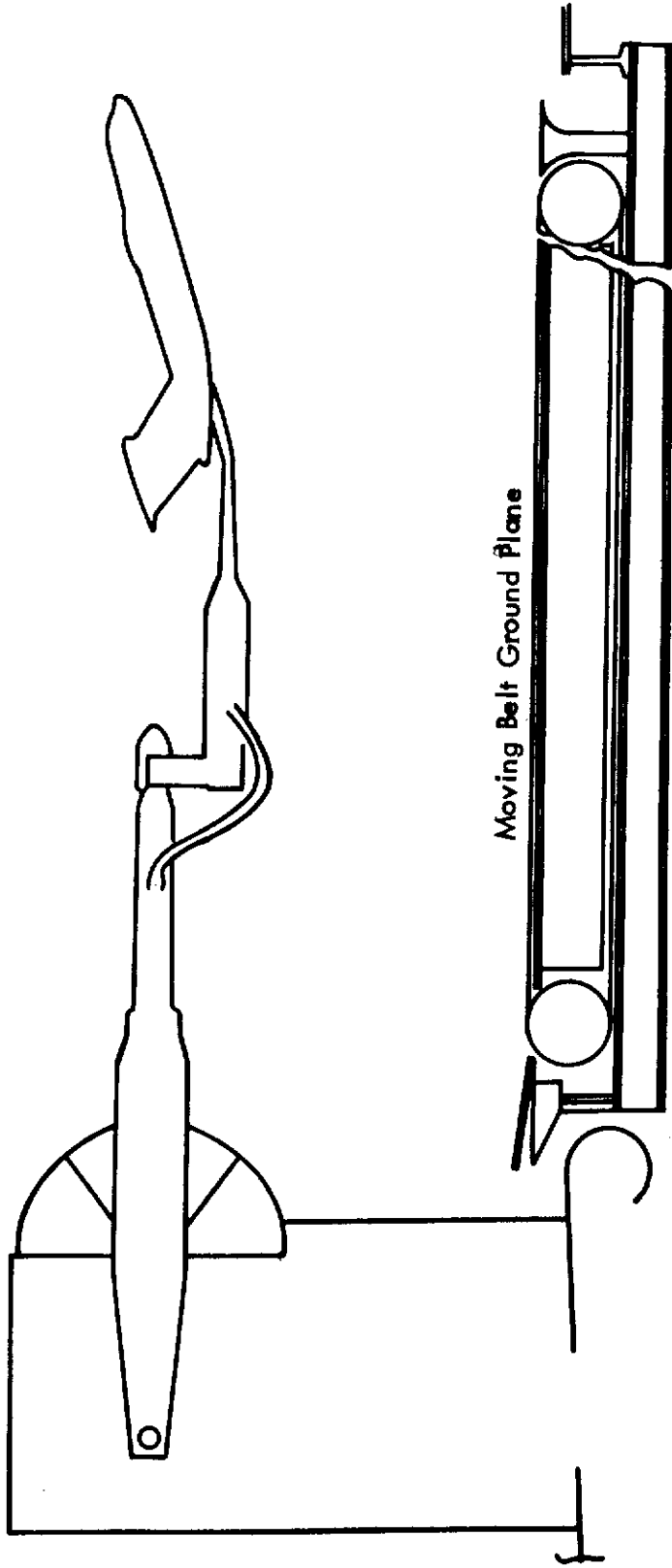
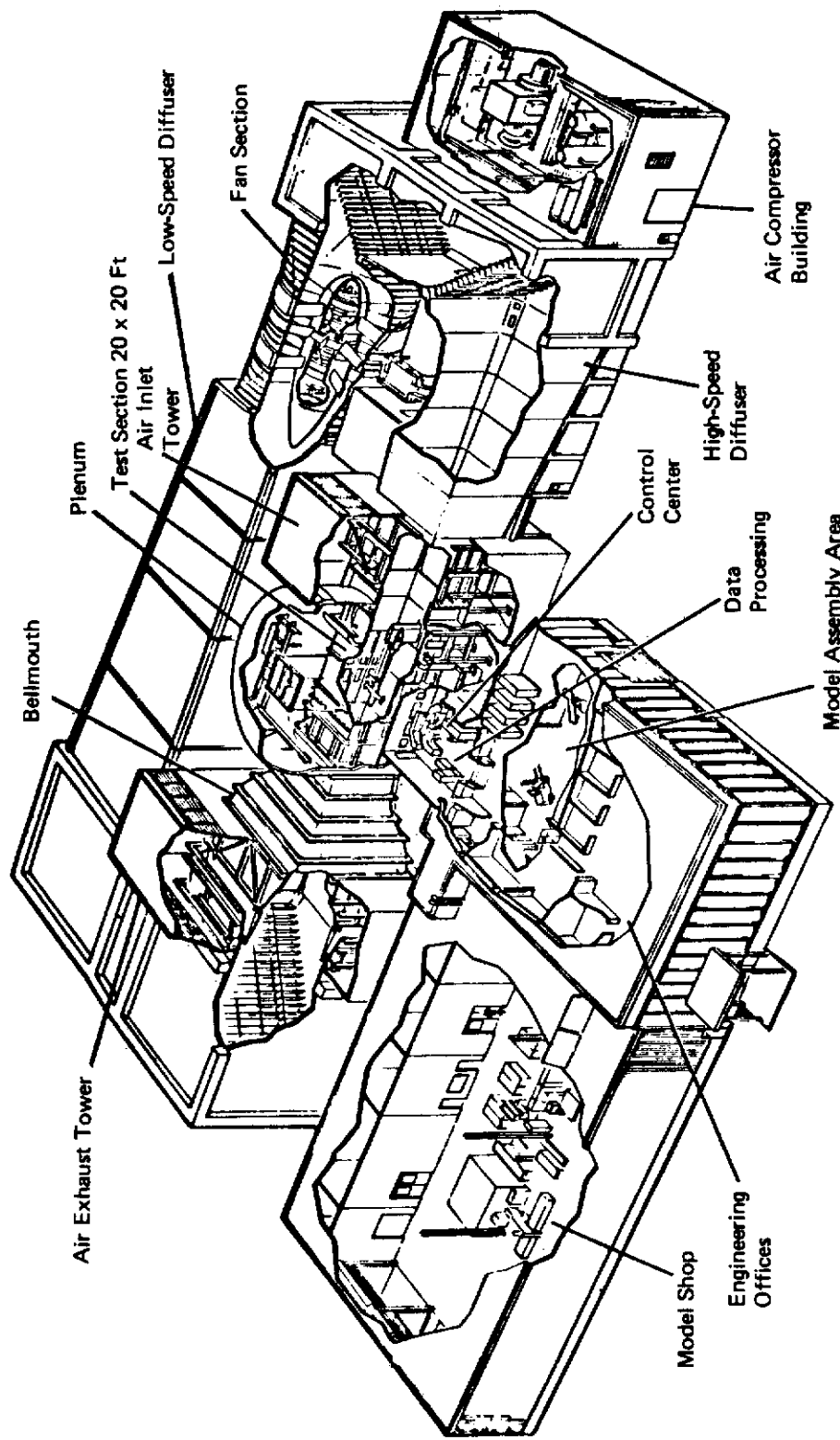


Figure 5: Installation of Balance



a. Model Installation

Figure 6: Boeing V/STOL Wind Tunnel



b. General View

Figure 6: Boeing VSTOL Wind Tunnel (Concluded)

2.3.3 Air Supply

The 1000 psi/20 pounds per second compressed air supply was limited to a flow of 16 pounds per second at 900 psi by the size of the duct through the balance.

2.3.4 Data System

The force and pressure data from the model were converted into digital signals and fed into an IBM 1800 computer. Printed output of the data in coefficient form (on microfiche) and the gross coefficient plots were issued as wind tunnel data reports (References 8 through 11). The data was further processed to derive net coefficients and terms relating to the analysis using a CDC 6600 computer. This latter data was released in References 1 through 5.

2.3.5 Flow Visualization

Flow visualization using smoke generated from ammonia and sulfur dioxide was conducted on the model to show the air flow patterns in the presence of the ground plane and to show the effects of thrust. 16 mm motion pictures were taken.

Contrails

SECTION III

UNPOWERED AERODYNAMIC CHARACTERISTICS

3. SUMMARY

Table V summarizes the more significant lift and drag characteristics of the wind tunnel model with power off.

3.1 Lift and Drag Effects

The characteristics of the model without powered lift (other than leading-edge BLC) were obtained for the complete range of configuration variables described in Section II.

The three configurations which represented the central area of the unpowered test matrix were:

REFERENCE CONFIGURATIONS FOR UNPOWERED TEST

Sweep	0°	15°	30°
Aspect Ratio	8.38	8	6.62
Trailing Edge Flap Angle	35°		
Trailing Edge Flap Span Ratio	.75		
Leading Edge Flap Angle	70°		
Leading Edge C_{μ}	.06		
Tail	Off		
Nacelles	On		

Figure 7 gives the lift, drag and pitching moment for these configurations to establish the level about which the effects of the various configurations can be applied. The leading-edge blowing C_{μ} of .06 was chosen to be representative of a practical case. The corresponding value for a "well tempered" full-scale airplane would be about .04.

The stall began at the wing root which did not have an optimum aerodynamic fairing because of the variable sweep feature of the model. At 30° sweep, the root stall produced a pronounced break in the lift curve before $C_{L_{max}}$ was reached.

3.1.1 Effect of Trailing Edge Flap Deflection

Figure 8 shows that the flaps were effective in increasing the lift up to 35° main flap deflection. Note that the increasing slope of $C_{L_{FLAP, \alpha=0}}$ with main flap angle between 30° and 35° becomes linear if the equivalent angle flap angle defined in Table III is used as the abscissa. The 48° deflection gave reduced lift except at 30° of sweep where the $C_{L_{max}}$ was obtained with 48° flaps. As flap angle was increased, the angle of attack for $C_{L_{max}}$ was reduced, as would be expected for a fixed leading edge device.

Table V: Lift and Drag Characteristics — Unpowered

Effect of	Fig.	C_{Lmax} , $C_{L\alpha}$	C_D , L/D	Aerodynamic Center
Wing Flap Angle	8,9	At sweep = 0° and 15°, flaps were effective in increasing C_{Lmax} up to flap angle of 35°. At 30° of wing sweep, C_{Lmax} continued to increase up to flap angles of 55°.	Increasing flap deflection decreases L/D.	With initial flap deflection the aerodynamic center shifts aft. Then, as the flaps are deflected past 25°, the aerodynamic center moves back toward its original location.
Wing Flap Span	10	Increasing flap span increases C_{Lmax} and $\Delta C_{L(\alpha=0)}$. Flap span influences $C_{L\alpha}$, with minimum $C_{L\alpha}$ occurring at flap span of .75b.		The aerodynamic center moves aft as the flap span increases.
Wing Sweep	14,16	Lift curve slope decreases as wing sweep increases. C_{Lmax} also decreases.		Aerodynamic center shifts aft about 3% MAC due to 30° of wing sweep, tail off. Aerodynamic center shifts forward about 5% MAC for 30° of wing sweep, tail on.
Wing Aspect Ratio	15	C_{Lmax} increases with aspect ratio up to aspect ratio of 7 for the 30° sweep and 8 for 15° sweep. Lift curve slope is relatively unaffected.		Tail off, the effect is negligible. Tail on, the aerodynamic center shifts aft as aspect ratio increases.
Nacelles	17	Nacelles cause a lift loss but have no significant influence on lift curve slope.		The presence of the nacelles cause the a.c. to shift forward about 7% MAC.

Aspect Ratio 8.38
 Sweep 0°
 TE Flap Angle 35°
 Flap Span Fraction .75
 LE Flap Angle 70°
 $C_{\mu_{LE}} = .06$
 Tail Off *
 Nacelles On

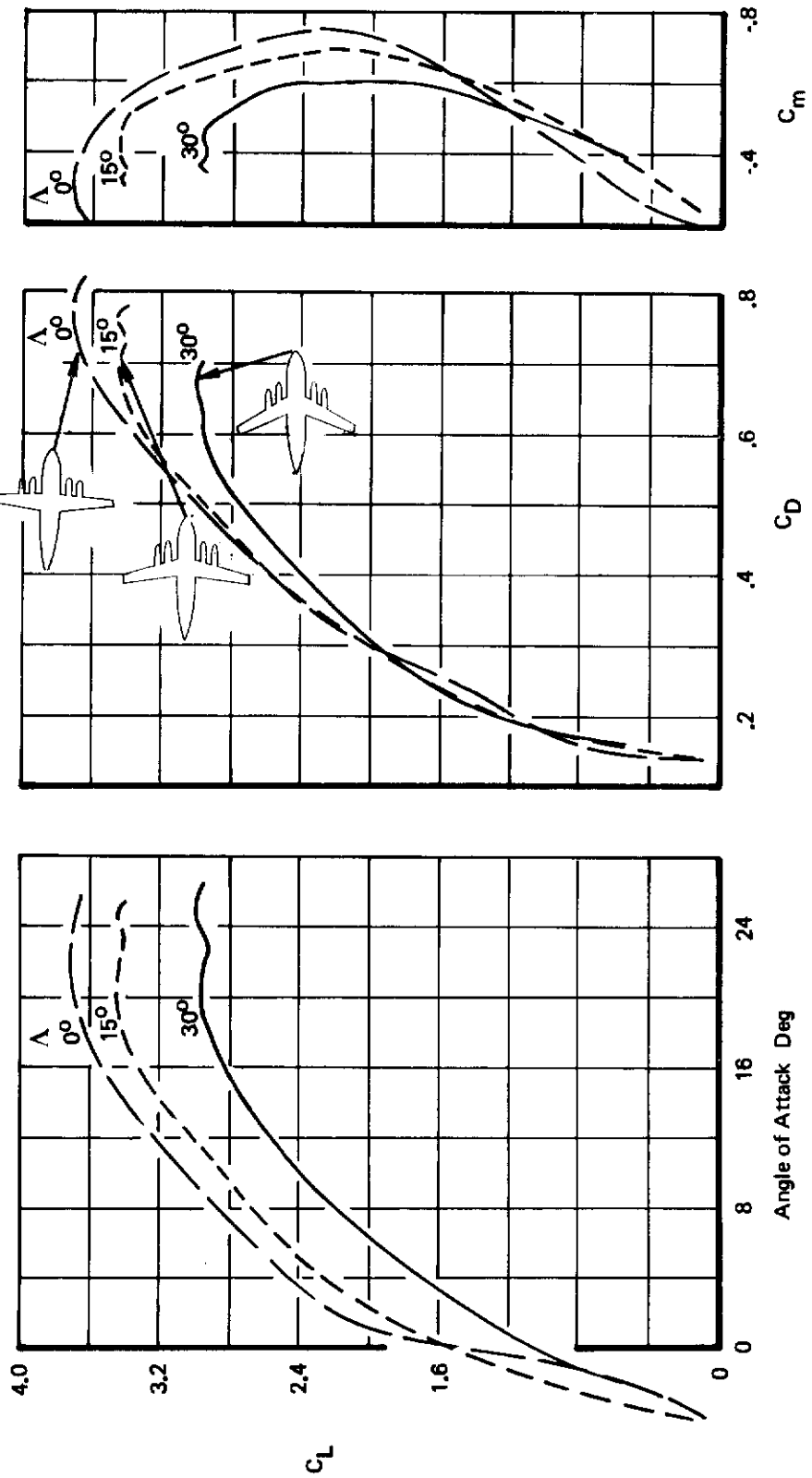


Figure 7: Unpowered Characteristics of Reference Configurations

Contrails

$C_{\mu LE} = .06$

LE Flap Angle 70°

Tail Off

Aspect Ratio 8.38 8.00 6.62

Nacelles On

Sweep 0° 15° 30°

Part Span Flap .74

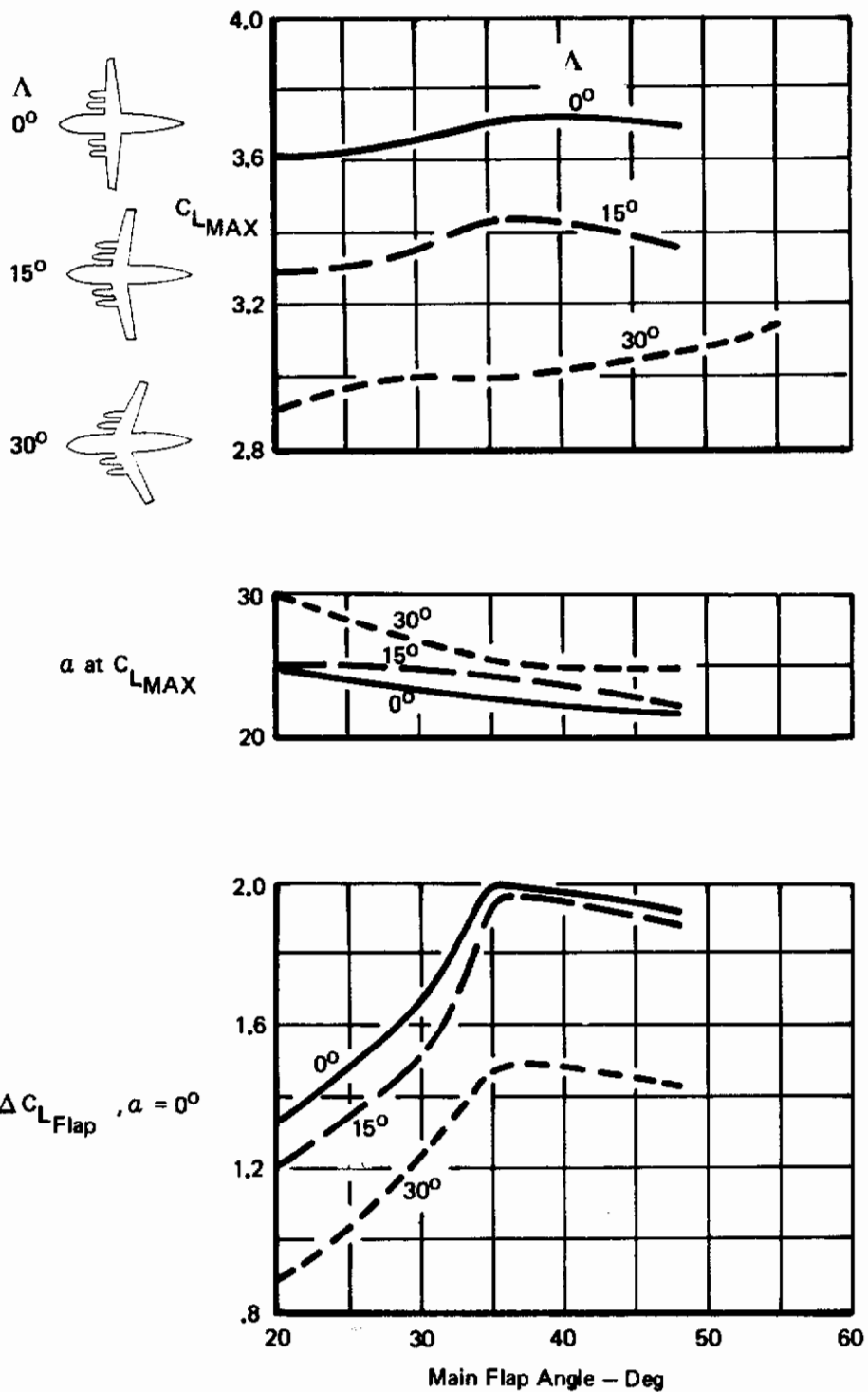


Figure 8: Effect of Flap Deflection on Lift

Figure 9 shows that the model L/D reduces as flap angle is increased. The best L/D for the model, tail off at 15° sweep was 6.3.

3.1.2 Effect of Trailing Edge Flap Span

Figure 10 shows the effect on lift of variation of flap span from 58% to full span. The low value of $C_{L_{max}}$ for the 75% span flap is probably not typical and is most likely due to the spreading of the separation behind the small (.375") breaks in the leading edge blowing slot. Elimination of the discontinuities for the last two test periods did increase $C_{L_{max}}$ for this case by 0.2.

3.1.3 Effect of Leading-Edge Flap

The blown leading edge flap gave an increase of $C_{L_{max}}$ of approximately 1.0 relative to the wing with no leading-edge device at 30° sweep, somewhat less at 15°. Figure 11 shows the effect on $C_{L_{max}}$ of leading edge flap angle for varying amounts of leading edge blowing. At 30° sweep, the 70° flap angle was best, essentially at all values of C_{μ} . At 15° sweep at .06 C_{μ} the 60° flap was best, however, 70° flap was used for most of the testing.

Mounting the leading edge flap with a 1% gap improved the $C_{L_{max}}$ when it was used in conjunction with leading-edge blowing ($C_{\mu} = .06$) but gave no improvement by itself.

Figure 12 shows the effect of increase of leading-edge blowing quantity at the three sweeps tested. The blowing effectiveness (ratio of lift increase to blowing momentum) was in the vicinity of 6.0. This is considerably less than the data shown in Figure 13 of Volume II. This result is attributed to the interruptions in the blowing slot (4 interruptions per side of width .375"). For the control power and jet flap tests, the interruptions were greatly reduced in size giving the improvement shown in Figure 13.

3.1.4 Effect of Sweep and Aspect Ratio

Figure 14 shows the effect of sweep on the $C_{L_{max}}$ with leading and trailing edge flaps extended. The wing in this case was fixed geometry so that aspect ratio changes with sweep. However, Figure 15 shows that the aspect ratio does not effect $C_{L_{max}}$ significantly in the range of aspect ratio shown in Figure 14. Figure 14 also shows the effect of sweep on the trailing edge flaps up with the leading edge flap down case and for the clean wing.

Figure 15 shows that lift increases with aspect ratio up to a value of aspect ratio of 7 for the 30° sweep or 8 for the 15° sweep wing beyond which there is no further improvement due apparently to the reduction in angle of attack at stall. This effect is more pronounced at a higher sweep which would suggest that with the higher aspect ratio the outward drift of boundary layer causes an earlier stall at the tip.

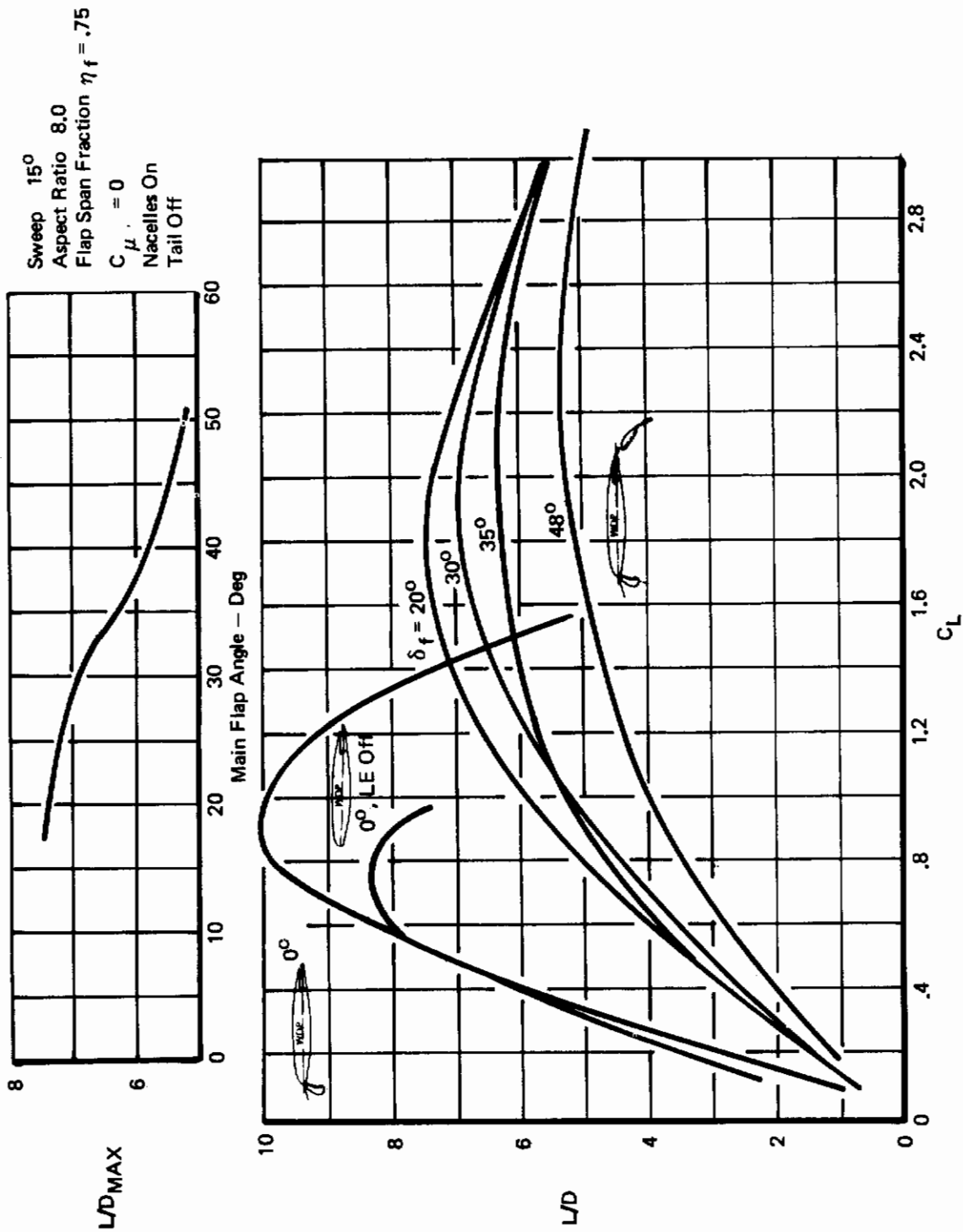


Figure 9: Effect of Flap Deflection on Lift-Drag Ratio

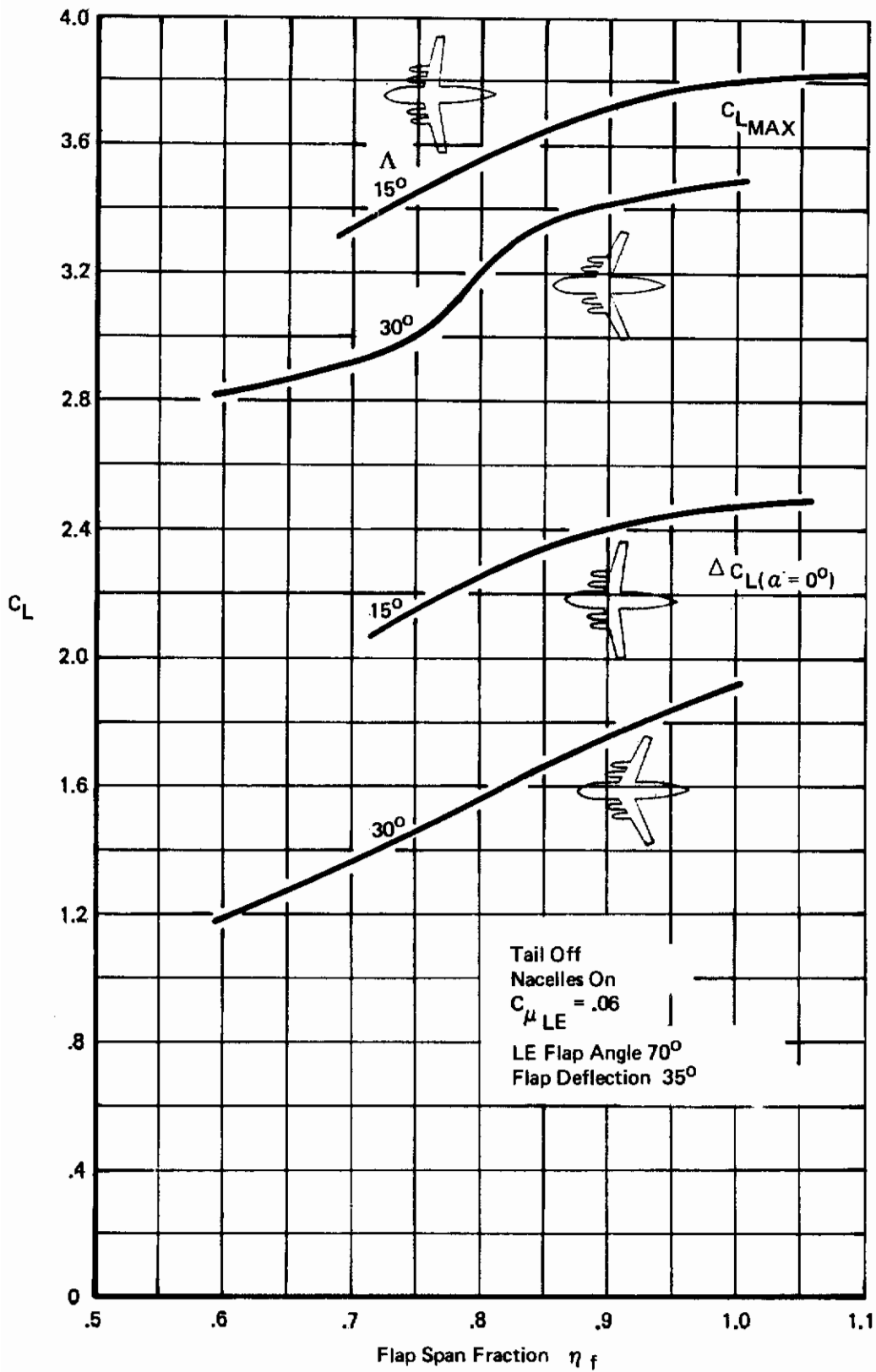


Figure 10: Effect of Flap Span on Lift

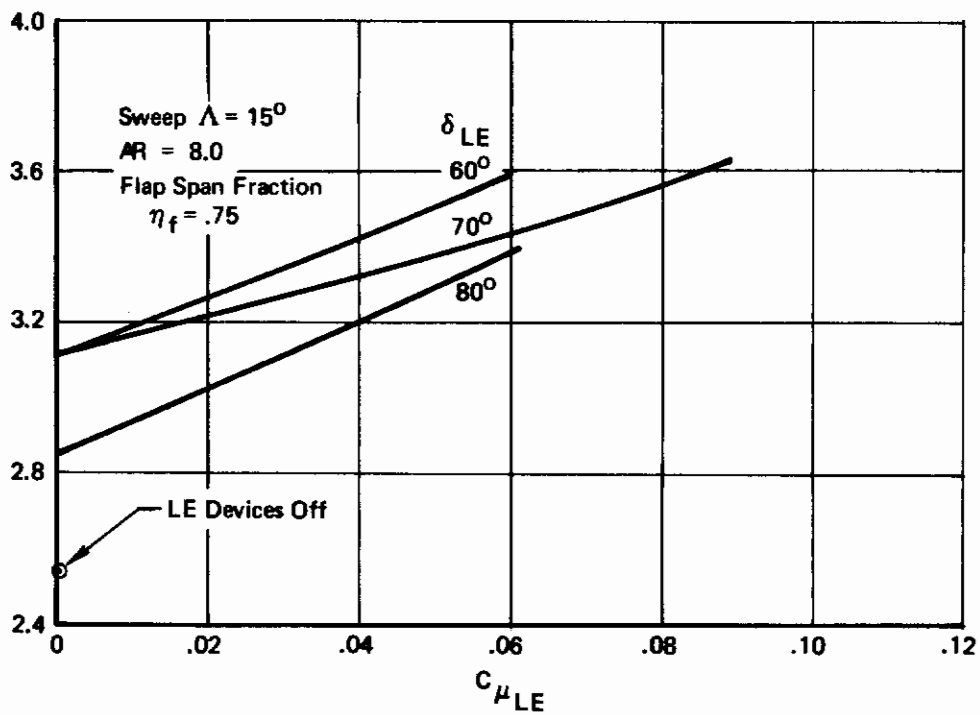
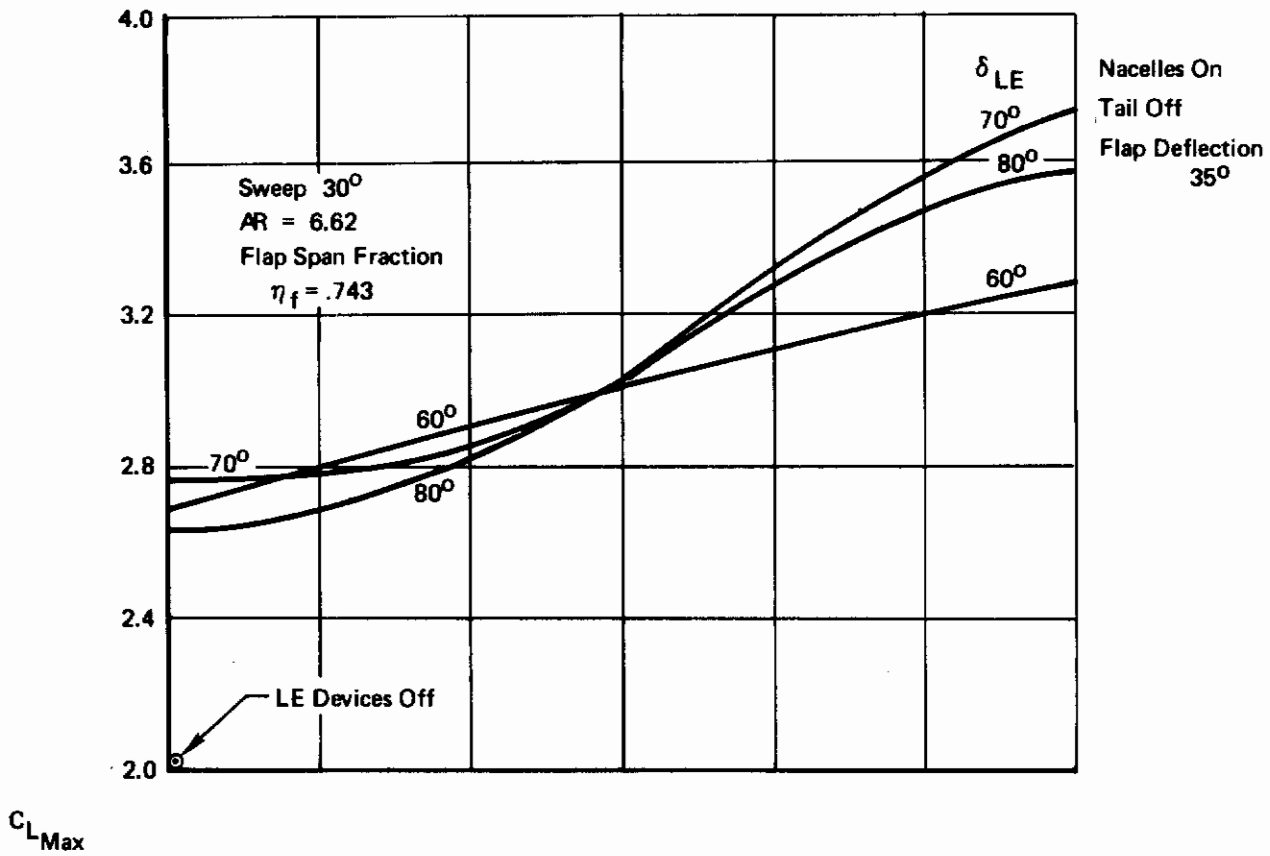


Figure 11: Effect of Leading Edge Flap Angle on Maximum Lift

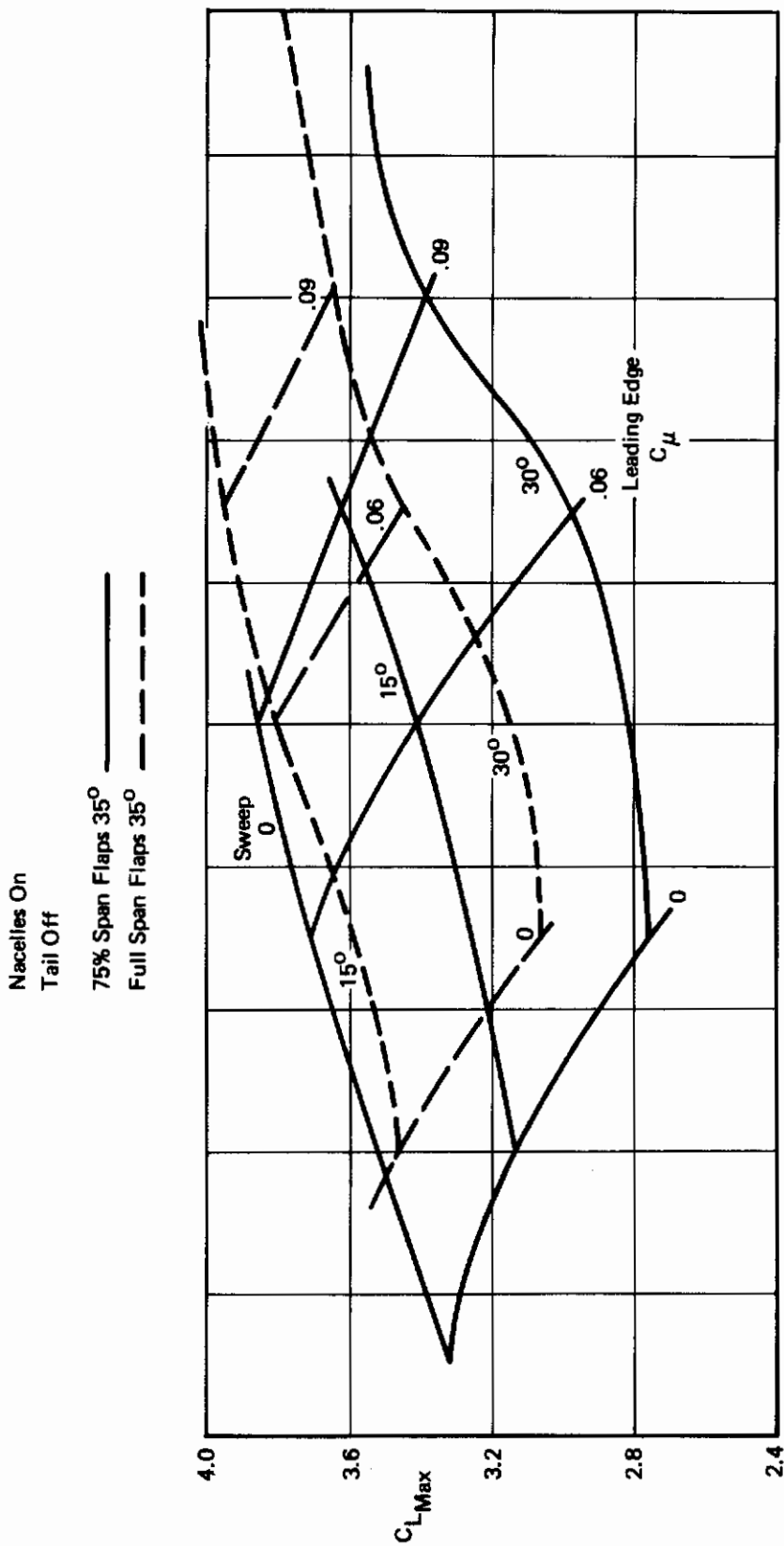
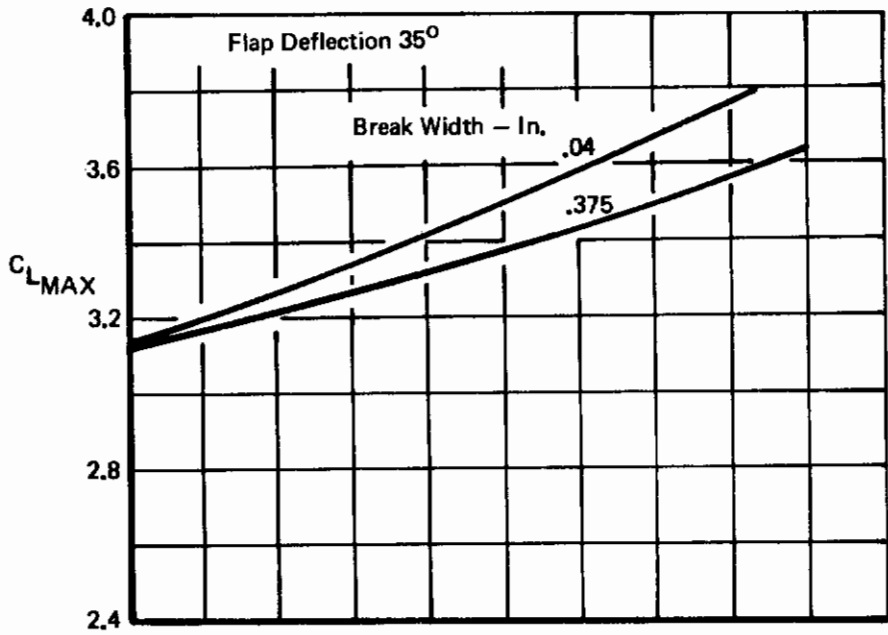


Figure 12: Effect of Sweep and Leading Edge Blowing on Maximum Lift Coefficient



Sweep 15°
 Aspect Ratio 8.0
 Flap Span Fraction $\eta_f = .75$
 LE Flap Angle 70°
 Nacelles On
 Tail Off

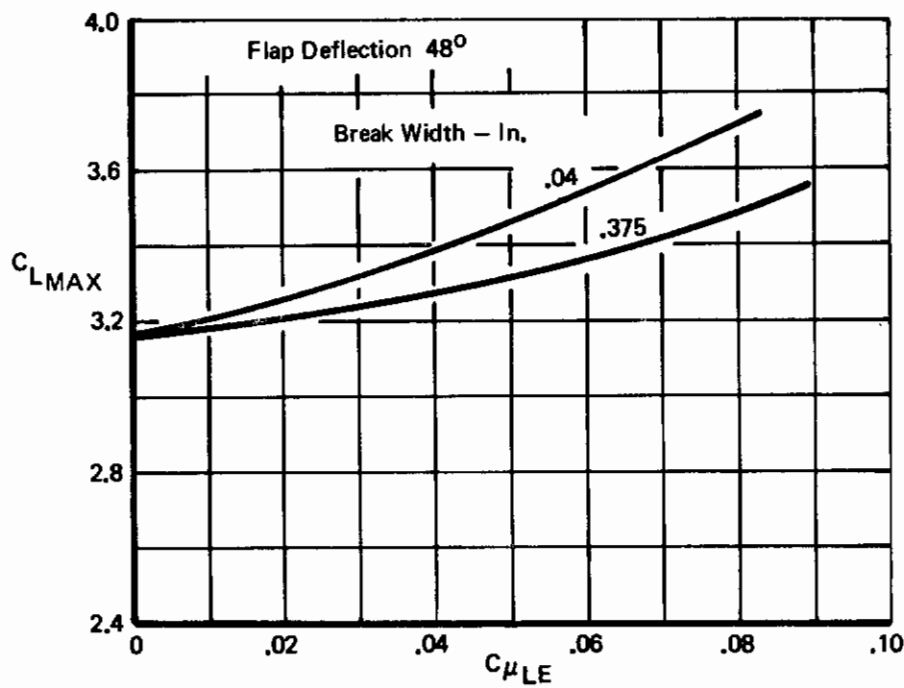
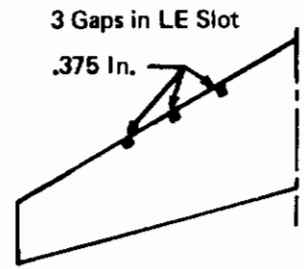


Figure 13: Effect of Spanwise Break in Leading Edge Blowing

Contrails

Nacelles On
 Tail Off
 Aspect Ratio 8.38 8.00 6.62
 Sweep 0° 15° 30°

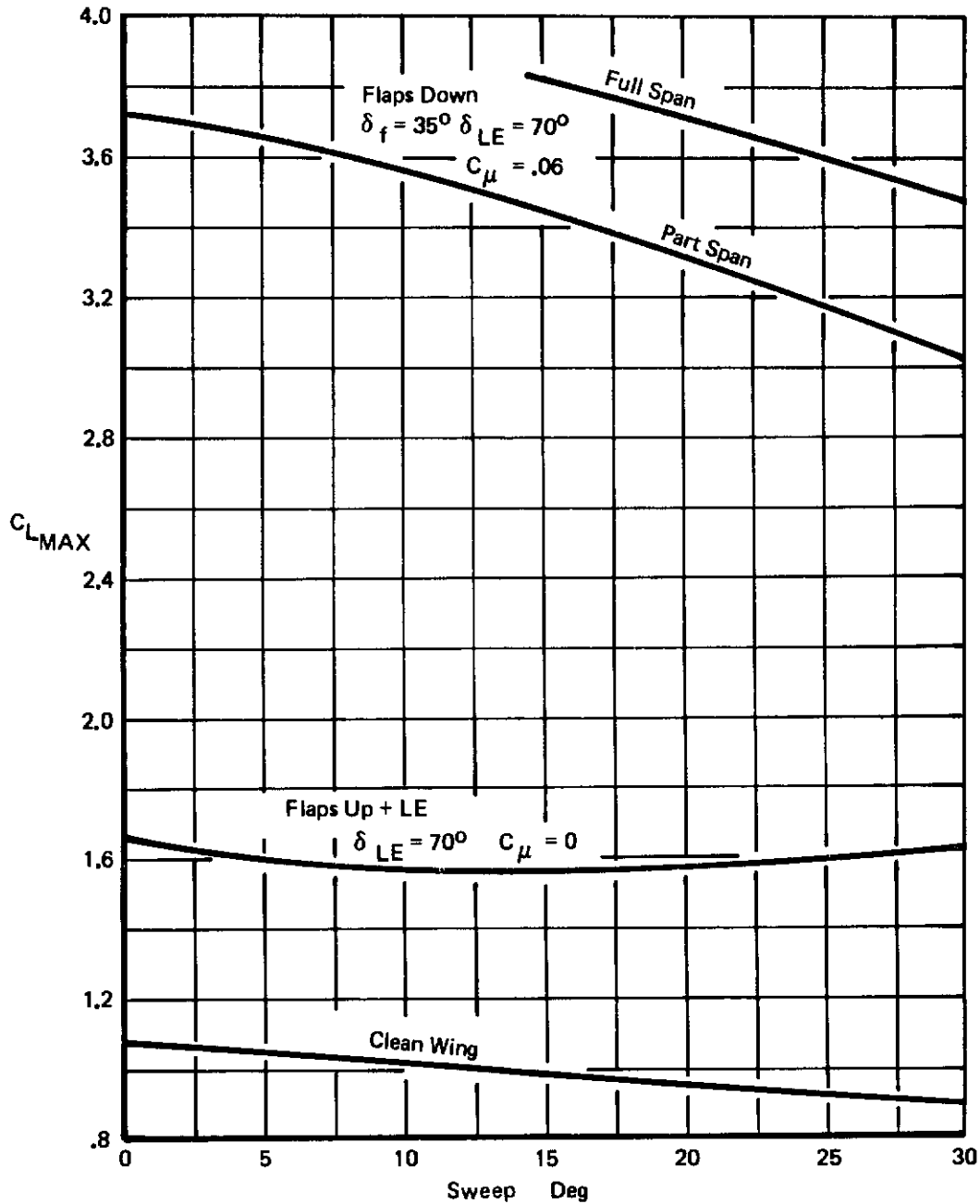


Figure 14: Effect of Sweep on Maximum Lift Coefficient

Contrails

Nacelles On
Tail Off
Flap Deflection 35°
Full Span Flaps
LE Flap Angle 70°
 $C_{\mu LE} = 0$

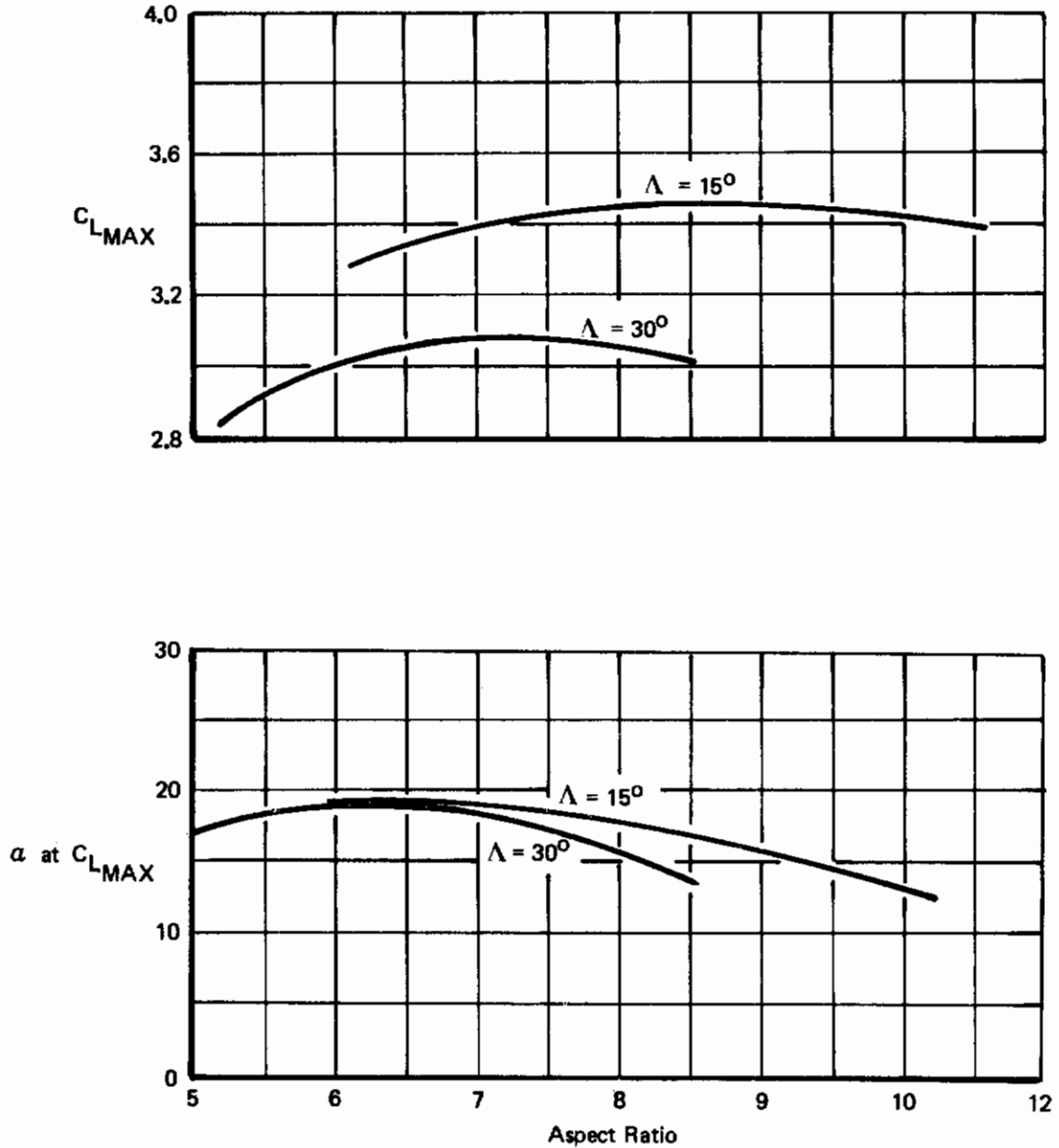


Figure 15: Effect of Aspect Ratio on Maximum Lift

Figure 16 shows the effect of sweep on lift curve. The lift is everywhere reduced as sweep increases with the exception of the post stall region flaps-up when the 30° sweep does not reach stall within the angle of attack tested.

At $\alpha = 8^\circ$, flaps-down, the 30° sweep has a higher slope than the 15° sweep. This is not considered typical and is the result of using the model in a general purpose way without (for example) retaylor-ing the leading-edge flap or the wing root intersection at each sweep.

3.1.5 Effect of Nacelles

Figure 17 shows a comparison of the lift of the basic con-figuration with and without the solid nacelles in the more inboard loca-tions. The nacelles cause a loss of lift at both low and high angles of attack. There is a 0.4 loss of maximum lift coefficient at both of the sweeps shown. Data shown in Section IV would indicate that this loss would be reduced if the nacelles were moved outboard.

3.2 Longitudinal Static Stability

3.2.1 Longitudinal stability data were taken at wing sweep angles of 0°, 15° and 30°. Several flap configurations were tested. Aspect ratio was also varied. Tail on and tail off, as well as nacelles on and off, were also tested. Lift curve slopes and aerodynamic centers were measured at an angle of attack of 8 degrees.

3.2.2 The flaps-up lift curve slope and aerodynamic center are shown in Figures 18 and 19. Figure 18 shows the effect of aspect ratio at wing sweeps of 15° and 30° tail off, and 30° tail on. The effect of the horizontal tail can also be seen on these figures. Aspect ratio has very little effect tail off. Lift curve slope varies about .01 per degree, and the aerodynamic center moves only about two percent. How-ever, with the tail on, aspect ratio has a strong influence on the aero-dynamic center. The lift curve slope is still relatively unaffected. As the aspect ratio is increased from about 7 to 8.3, the aerodynamic center shifts aft about 15% MAC, even though the horizontal tail volume coefficient decreases as the aspect ratio is increased.

3.2.3 Wing sweep and nacelle effects on the flaps-up configuration are shown in Figure 19. Wing sweep was varied nacelles on and off for the tail-off configuration. The nacelles cause a 7% MAC shift in the aerodynamic center, but do not affect the lift curve slope. For both tail on and tail off, the lift curve slope decreases slightly as the wing sweep is increased. The tail-off aerodynamic center shifts aft about 3% MAC for 30° of wing sweep. However, with the tail on, the aerodynamic center moves forward about 5% MAC for 30° of wing sweep.

Contrails

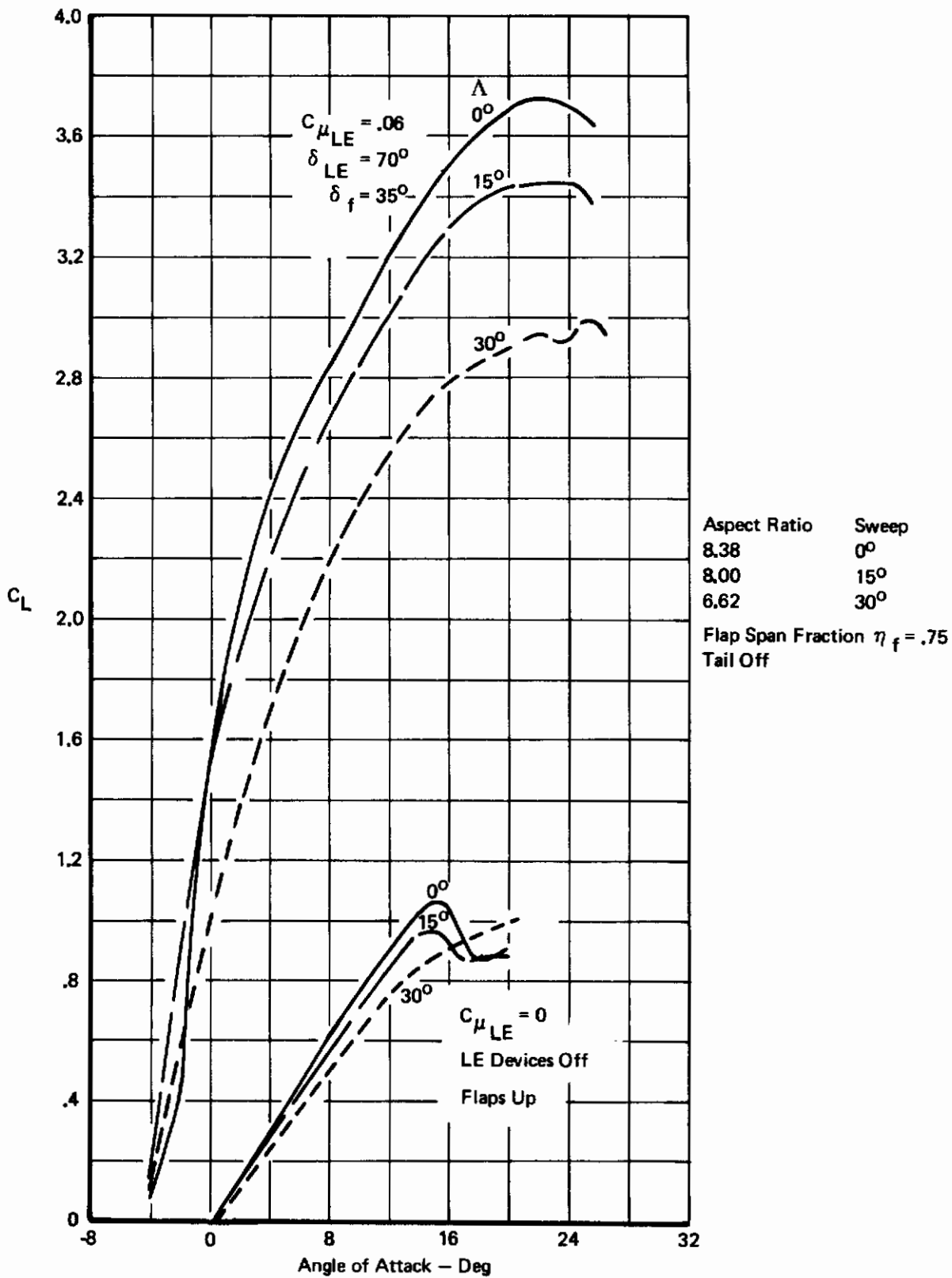


Figure 16: Effect of Sweep on Lift

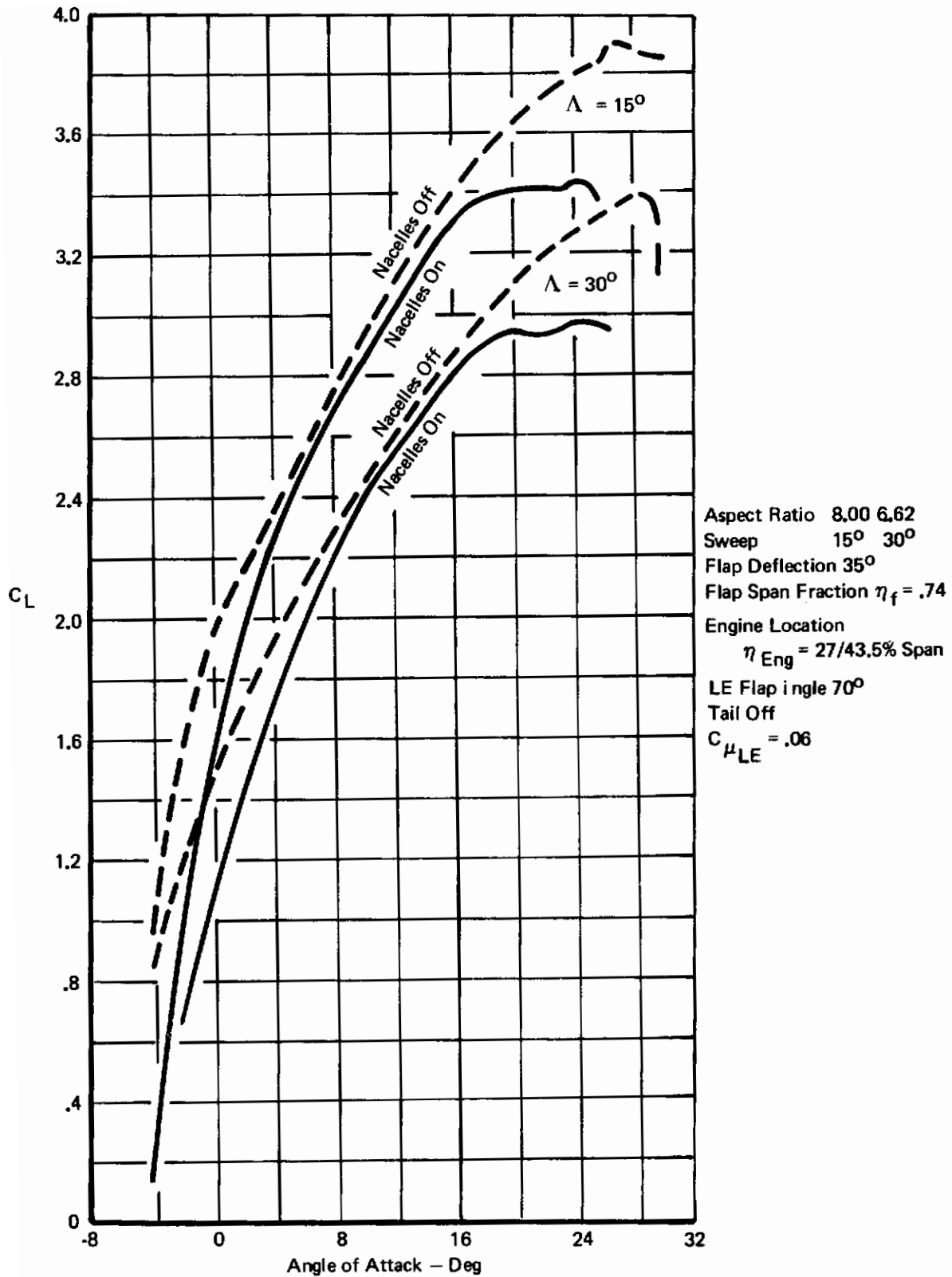


Figure 17: Effect of Nacelles on Lift

Flaps Up, $\alpha = 8^\circ$

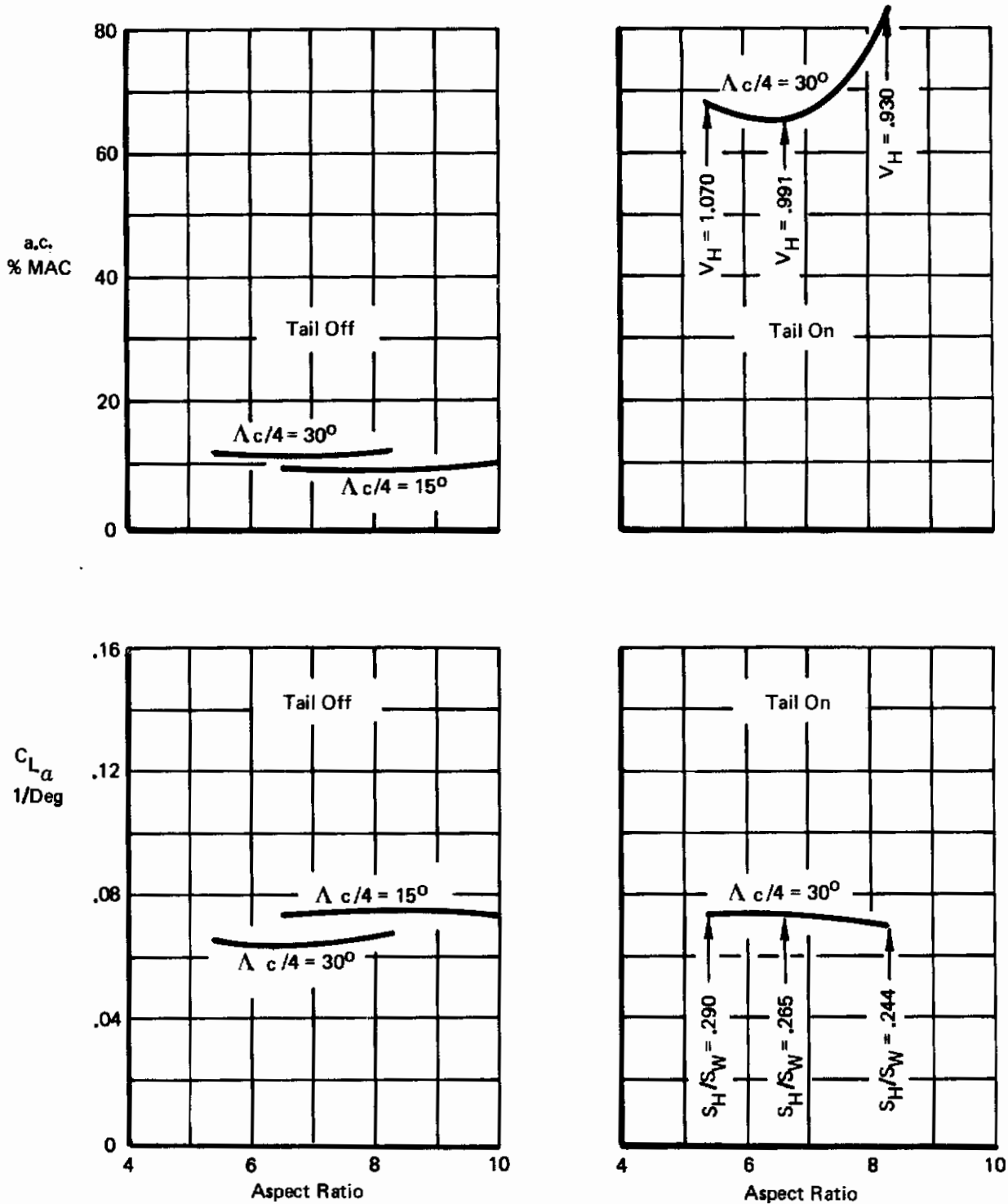


Figure 18: Lift Curve Slope and Aerodynamic Center – Effect of Aspect Ratio – Flaps Up

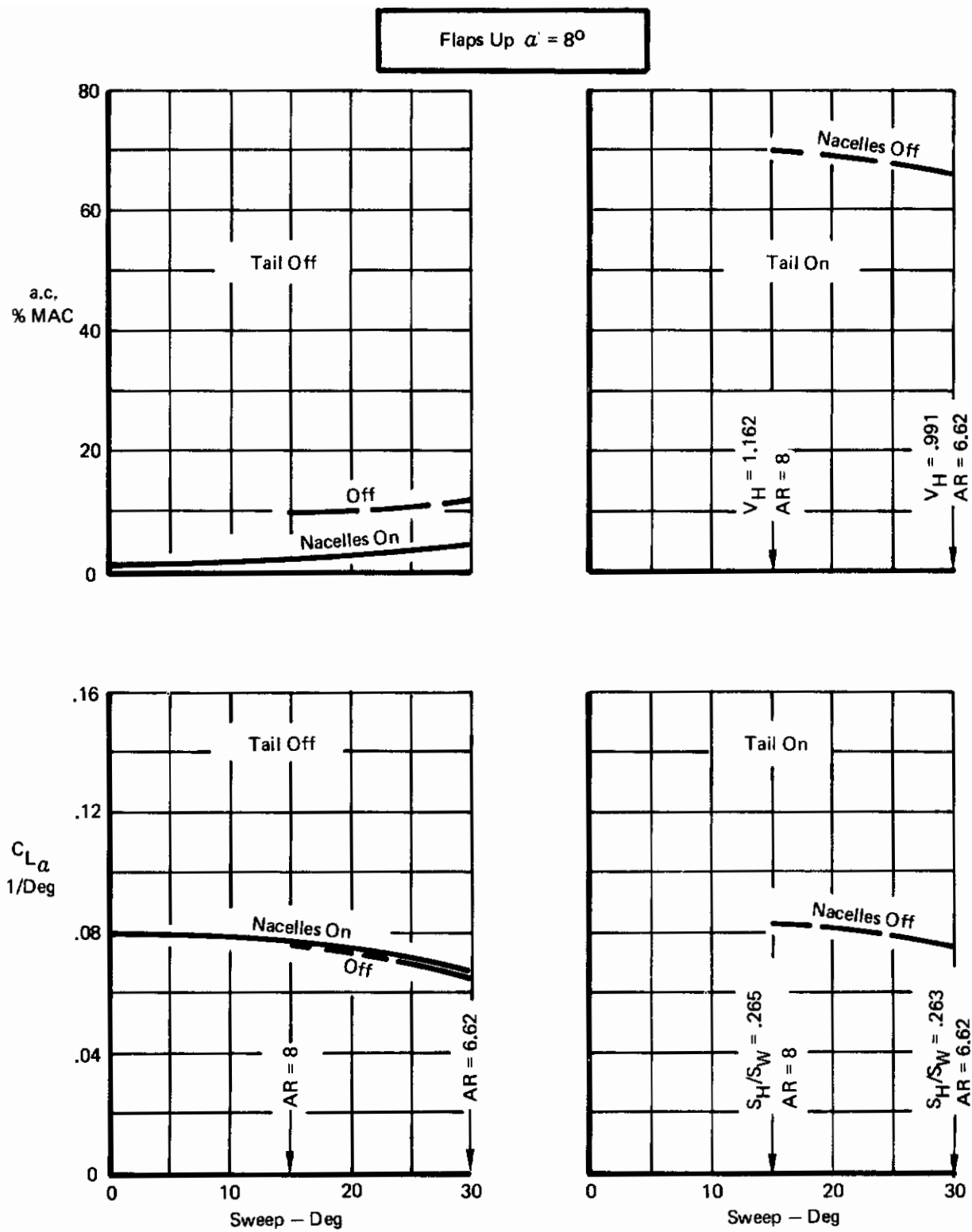


Figure 19: Lift Curve Slope and Aerodynamic Center – Effect of Sweep – Flaps Up

Contrails

3.2.4 The effect of flap angle is shown in Figure 20. Tail-on and tail-off configurations were tested. Wing sweeps of 0° , 15° and 30° were tested with the tail off. Tail on was tested only at 30° of wing sweep. The effect of flap angle showed the same trend at all three sweep angles. Lift curve slope rose sharply, about .02 per degree, for the first 20° of flap deflection. The rate of change of lift curve slope with respect to flap angle goes to zero at about 25° of flap. Then the lift curve slope drops sharply, about .012, as the flaps are deflected to 40° . This effect is greater at zero wing sweep and less pronounced as sweep is increased. The tail-off aerodynamic center moves aft almost 10% MAC as the flaps are deflected from zero to about 25° . As the flaps are further deflected, the aerodynamic center shifts back toward the initial location. Tail-on data are less complete. However, the same trend appears to be present. The changes in aerodynamic center and lift curve slope occur when the Fowler action is taking place, low flap angles, and then at the higher flap angles where the flow is starting to separate.

3.2.5 Flap span effect is shown in Figure 21. Flap span was varied for the 30° sweep, flaps deflected 35° configuration. Tail on and tail off were both tested. Flap span has a strong influence on lift curve slope both tail on and tail off. As the flap span is increased from 50% to 75% of the wing span, the lift curve slope drops by about .02 per degree (both tail on tail off), then the lift curve slope increases as the flaps are extended to the wing tips. With the tail on, the same trend exists for the lift curve slope although a little less pronounced. With the tail on, the a.c. shift is only 5% MAC as the flap span is increased from 60% to 100% span.

3.2.6 Figure 22 shows the effect of wing sweep with the flaps deflected 35° . Tail on and off, as well as nacelles on and off, were tested. The trends are about the same with the nacelles on or off. The aerodynamic center shift is about 15% MAC aft due to 30° of sweep tail off and about 6% with the tail on. This is quite a bit more than the case with flaps up shown in Figure 19. With the tail on, sweep had no influence on lift curve slope. Tail off, the lift curve slope increased .01 per degree as the wing sweep was increased from zero to 15° . Then as the sweep was further increased to 30° , the lift curve slope decreased to its initial zero sweep value. There were slight aspect ratio changes as the wing was swept. This may be masking some of the sweep effects.

3.3 Lateral-Directional Stability

Table VI is a summary of the results of all the lateral-directional runs made during this phase of the test program. Figures 23 through 32 present lateral-directional sideslip derivatives obtained during Phase I testing of the unpowered configuration. The majority of these data plots reflect derivatives for a sideslip range of $\pm 10^\circ$ at an angle of attack of 8° . No aileron, rudder or elevator power data were obtained during this phase. All coefficients are based on the geometry of each particular configuration as tabulated in Table II.

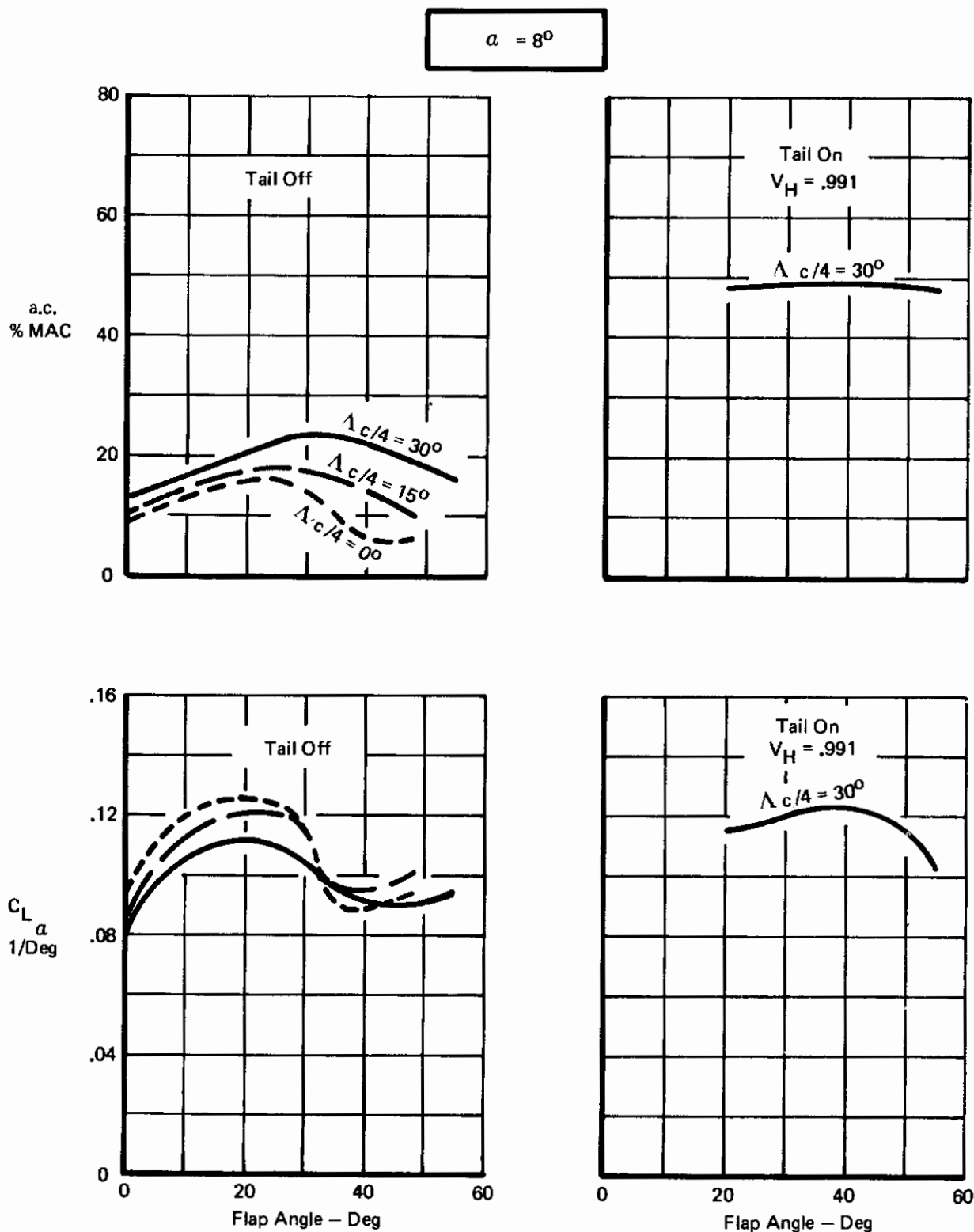


Figure 20: Lift Curve Slope and Aerodynamic Center — Effect of Trailing Edge Flap Angle

Contrails

$\Lambda = 30^\circ$ 35° Flaps $\alpha = 8^\circ$

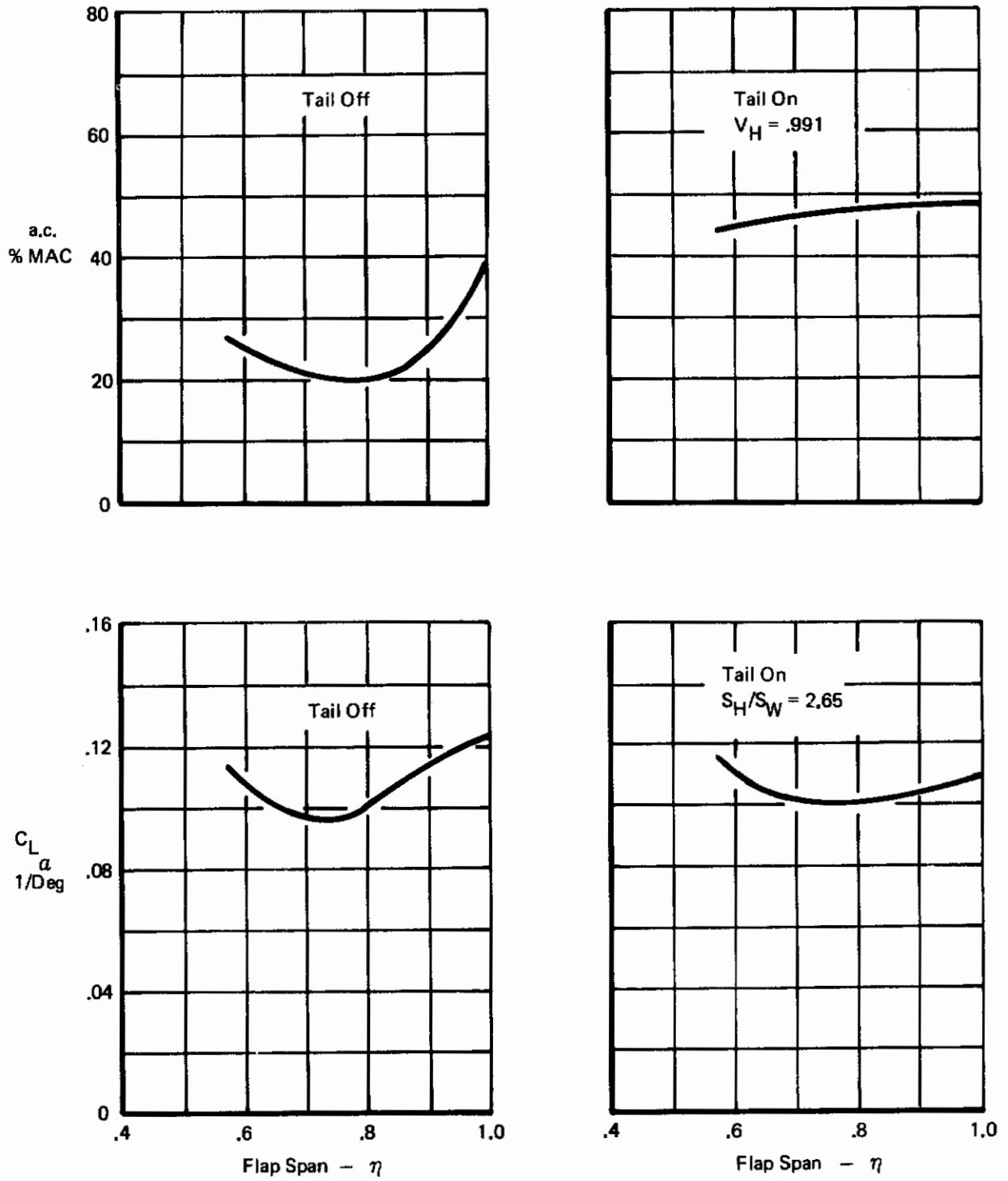


Figure 21 : Lift Curve Slope and Aerodynamic Center – Effect of Flap Span

35° Flaps
 $\alpha = 8^\circ$

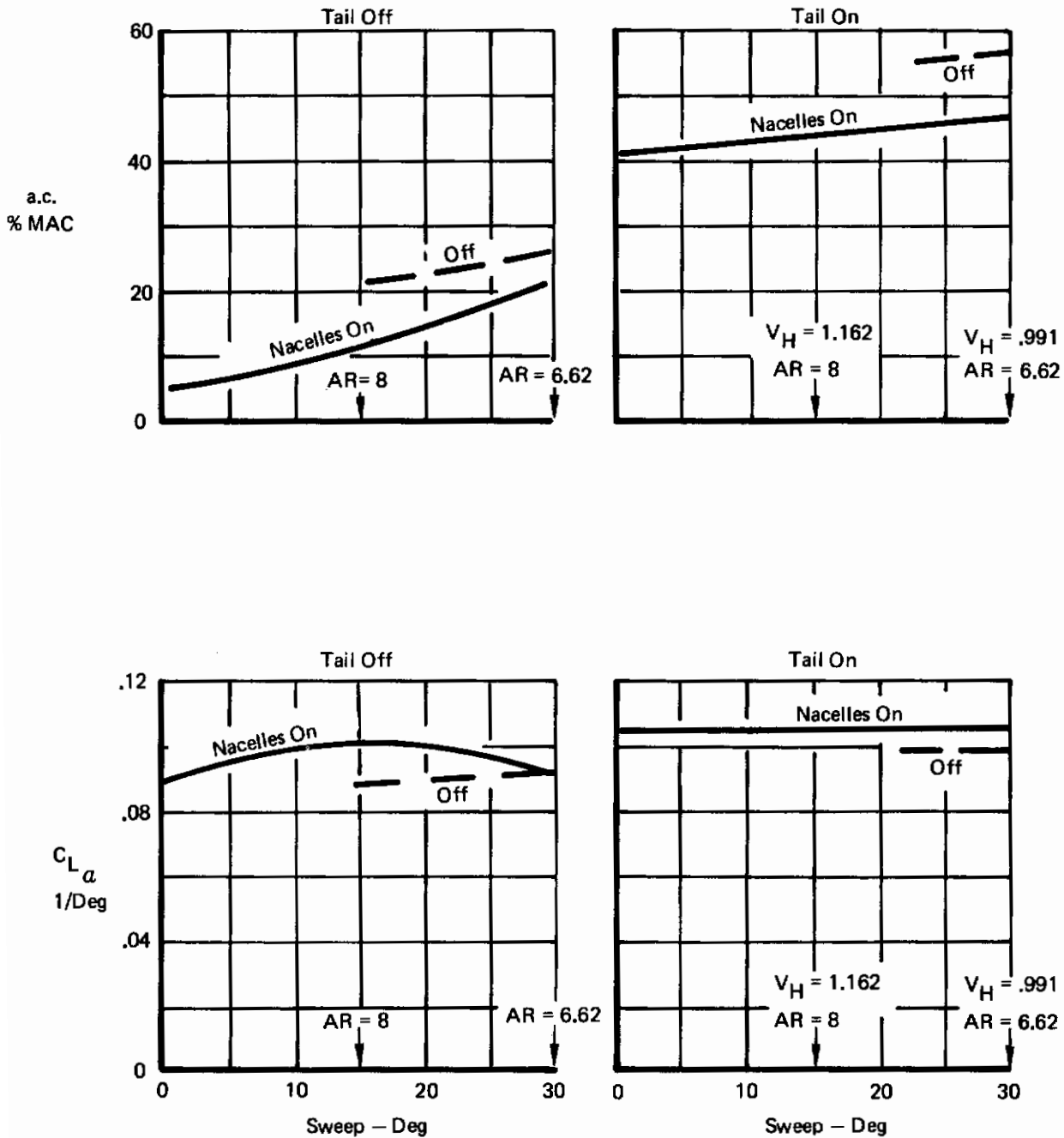


Figure 22 : Lift Curve Slope and Aerodynamic Center – Effect of Wing Sweep

Table VI: Lateral-Directional Characteristics - Unpowered

Effect of	on	$C_{Y\beta}$	$C_{n\beta}$	$C_{l\beta}$
Wing Aspect Ratio	Tail off	Negligible	Increasing aspect ratio has a stabilizing influence.	Increasing aspect ratio makes $C_{l\beta}$ less negative flaps up except for $\Lambda = 30^\circ$ flaps down where $C_{l\beta}$ gets more negative.
	Tail on	Increasing aspect ratio makes $C_{Y\beta}$ slightly less negative.	Increasing aspect ratio has a destabilizing influence.	Increasing aspect ratio makes $C_{l\beta}$ less negative.
Wing Sweep	Tail off	Negligible	Increasing sweep is slightly destabilizing except for flaps down, nacelles off, when it is stabilizing.	Increasing sweep makes $C_{l\beta}$ more negative, especially with flaps down.
	Tail On		Increasing sweep causes slight decrease $C_{n\beta}$.	
Wing Trailing Edge Flap Angle	Tail off		Increases with flap angle.	Effect varies with sweep. At $\Lambda > 15^\circ$, increasing flap angle makes $C_{l\beta}$ more negative. At $\Lambda = 0^\circ$, $C_{l\beta}$ gets less negative as flaps are deflected to 35° .
	Tail on	Negligible	Increasing flap deflection has a stabilizing effect especially at low flap angles.	
Wing Trailing Edge Flap Span	Tail off	Negligible.	Increasing flap span has a stabilizing effect.	Increases with flap span.
	Tail on	$C_{Y\beta}$ gets less negative as flap span is increased.	Slight reduction as flap span is increased.	

Table VI: Lateral-Directional Characteristics--Unpowered (Continued)

Effect of ↓	on →	$C_{Y\beta}$	$C_{n\beta}$	$C_{l\beta}$
Wing Leading Edge Flap Angle	Tail off	Negligible	Negligible	$C_{l\beta}$ gets slightly less negative as flap angle is increased.
	Tail on			Negligible
Angle of Attack	Tail off	Negligible	With nacelles off, increasing angles of attack has a stabilizing influence on $C_{n\beta}$. With nacelles on, increasing angle of attack is destabilizing.	With nacelles off, increasing angle of attack makes $C_{l\beta}$ more negative. Nacelles on, increasing angle of attack makes $C_{l\beta}$ less negative.
	Tail on			
Nacelles	Tail off	$C_{Y\beta}$ became more negative when nacelles were added.	With flaps up, the addition of nacelles had a stabilizing influence. Flaps down the nacelles were destabilizing.	
	Tail on	$C_{Y\beta}$ became less negative when nacelles were added.		
LE BLC	Tail off	Negligible		
	Tail on			

Contrails

3.3.1 Aspect Ratio Effects

Figures 23 and 24 illustrate the effects of aspect ratio for 15° and 30° wing sweep, tail-on and tail-off, for the flaps-up and flaps-down configurations. The aspect ratio effects are fairly small with only a slight increase in tail-off $C_{n\beta}$ with increasing aspect ratio. Apparently, the tail effectiveness tends to reduce as aspect ratio increases. However, it is important to keep in mind that the derivatives are based on the geometry of the wing tested. The higher aspect ratio wings have more area and span, thus the coefficients tend to be smaller.

3.3.2 Sweep Effects

The effects of sweeping the wing from 0° to 30° are presented in Figures 25 and 26 and can also be seen in Figures 23, 24 and 27. As is illustrated, $C_{n\beta}$ generally reduces slightly while $C_{l\beta}$ increases (particularly with flaps down) as sweep increases. Note that the value of aspect ratio changes as sweep changes. Again, keep in mind that the geometry upon which the aerodynamic coefficients are based varies as the wing is swept.

3.3.3 Effects of Trailing-Edge Flap Angle

The effects of T.E. flap angle for the 75% span flaps are shown in Figure 27. Data are presented for sweeps = 0°, 15°, and 30°; and for tail-on and tail-off configurations. As flap angle increases, $C_{n\beta}$ tends to increase with smaller effects being shown at flap angles above 35°. The character of the variation of $C_{l\beta}$ with flap angle changes with sweep. This is also demonstrated in Figures 25 and 26.

3.3.4 Trailing-Edge Flap Span Effects

The effects of changing the T.E. flap span are illustrated in Figure 28. Tail-off $C_{n\beta}$ and tail on and off $C_{l\beta}$ increase as flap span increases. Tail-on $C_{n\beta}$ is relatively constant, yielding a slight decrease in tail $C_{n\beta}$ contribution as flap span increases.

3.3.5 Leading-Edge Flap Angle and BLC Effects

The effects of L.E. configuration changes on lateral-directional derivatives (Figures 29 and 30) are negligible for the β range ($\pm 10^\circ$) tested at $\alpha = 8^\circ$. With the leading-edge flap deflected and BLC operating, the linear range of the sideslip derivatives is extended to higher values of α and β .

3.3.6 Effects of Angle of Attack

Figures 31 and 32 present the effects of angle of attack. For the range of α tested (4° to 12°), $C_{n\beta}$ and $C_{l\beta}$ increase nacelles-off, and decrease nacelles-on, as α increases.

3.3.7 Effects of Nacelles

The effects of the nacelles are shown on Figures 25, 26, 31 and 32. Installation of the nacelles causes a more positive $C_{n\beta}$ and a more negative $C_{l\beta}$ with flaps-up, while with flaps-down $C_{n\beta}$ gets more negative and $C_{l\beta}$ gets more positive.

3.3.8 Tail Effects

As illustrated in Figures 23 through 32, the effects of the tail decrease with increasing wing aspect ratio (reference geometry change), increasing flap span, and decreasing flap angle.

Nacelles Off
 $\alpha = 8^\circ$
 Flaps Up

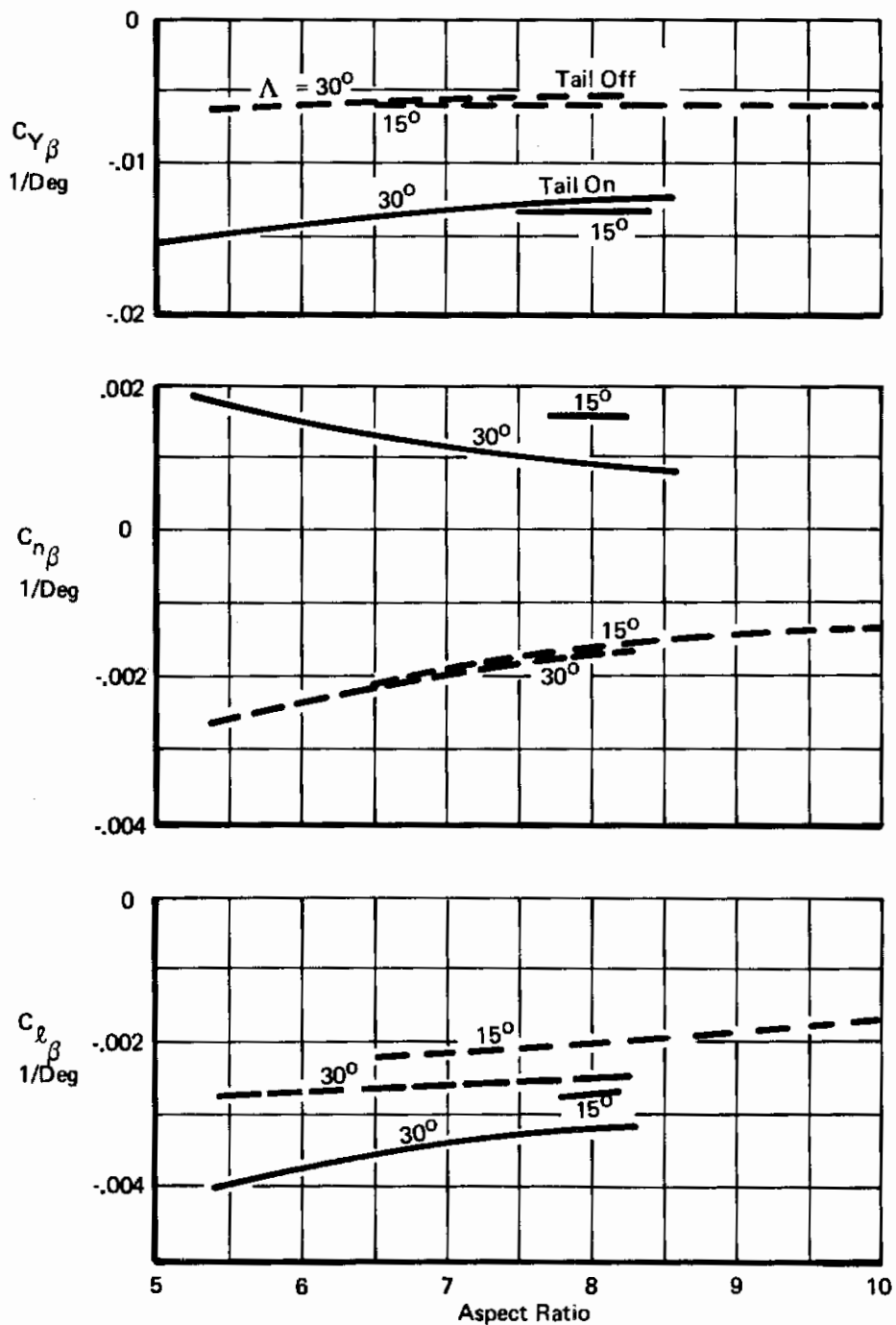


Figure 23: Effect of Aspect Ratio on β Stability Derivatives — Flaps Up

Contrails

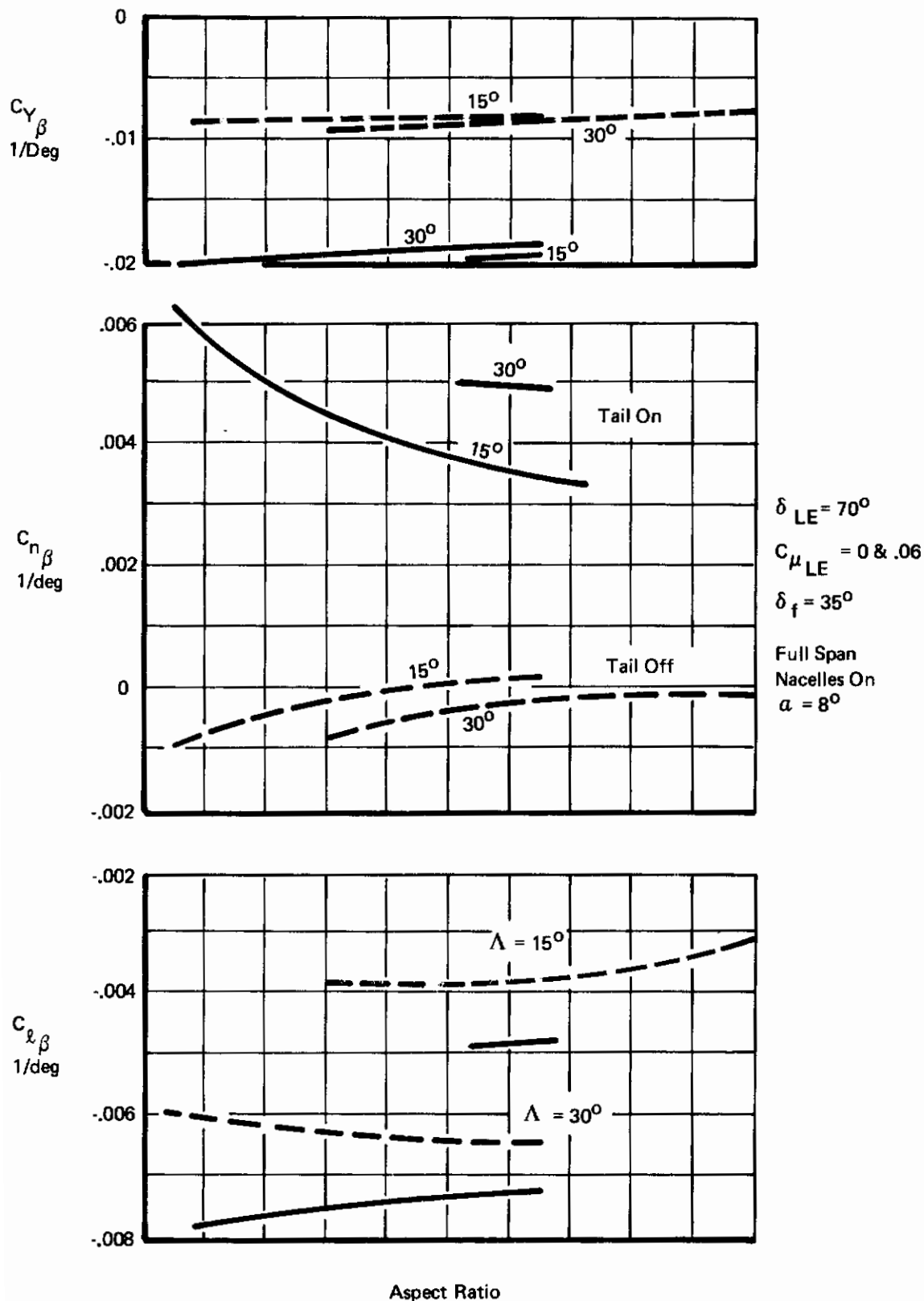


Figure 24: Effect of Aspect Ratio on β Stability Derivatives – Flaps Down

Contrails

Aspect Ratio 8.38 8.00 6.62
 Sweep 0° 15° 30°
 $\delta_{LE} = 70^\circ$ $C_{\mu_{LE}} = 0$
 $\delta_f = 0^\circ$
 Tail Off
 $\alpha = 8^\circ$

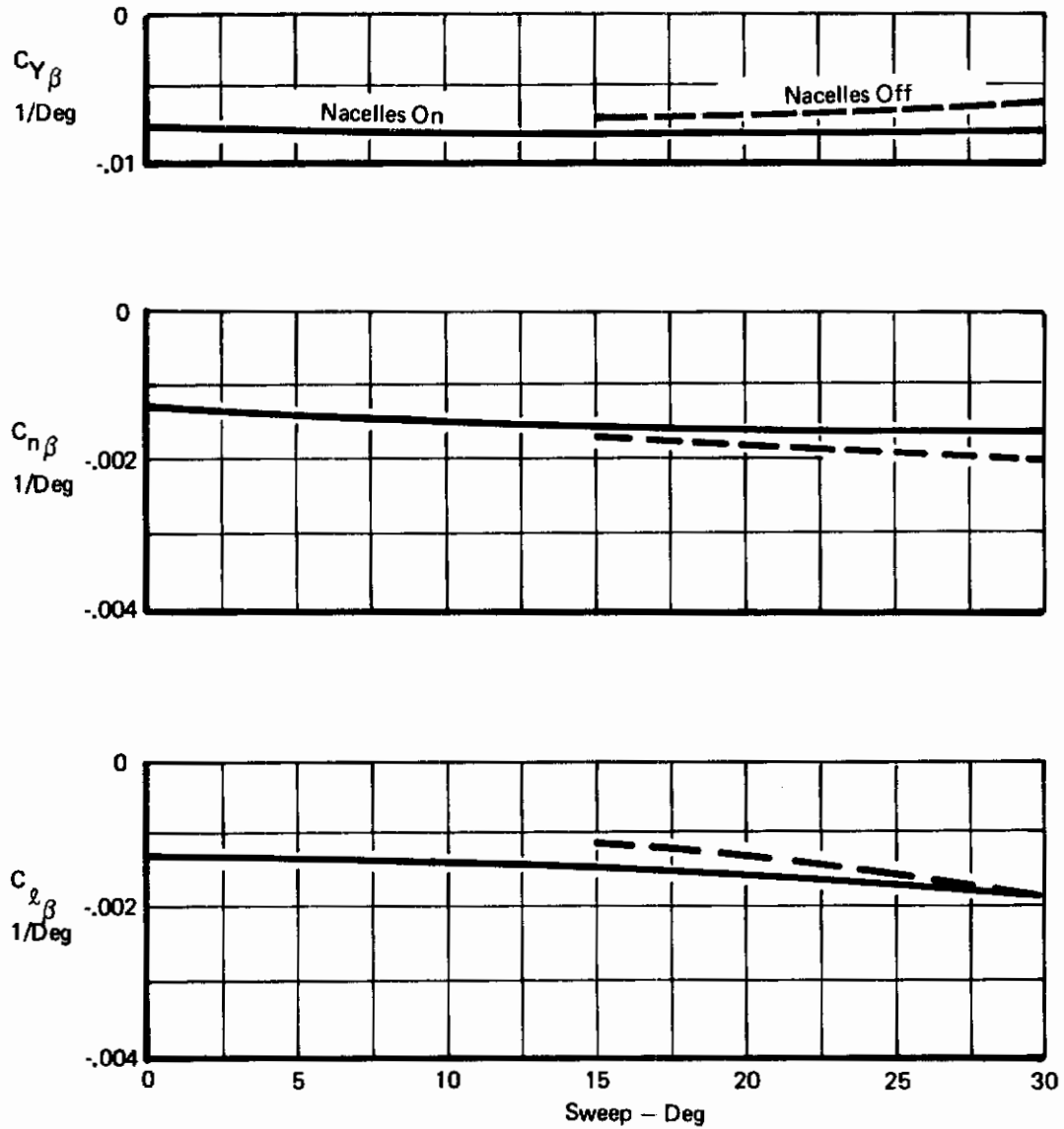


Figure 25: Effect of Sweep on β Stability Derivatives, Nacelles On and Off, T.E. Flaps Up

Contrails

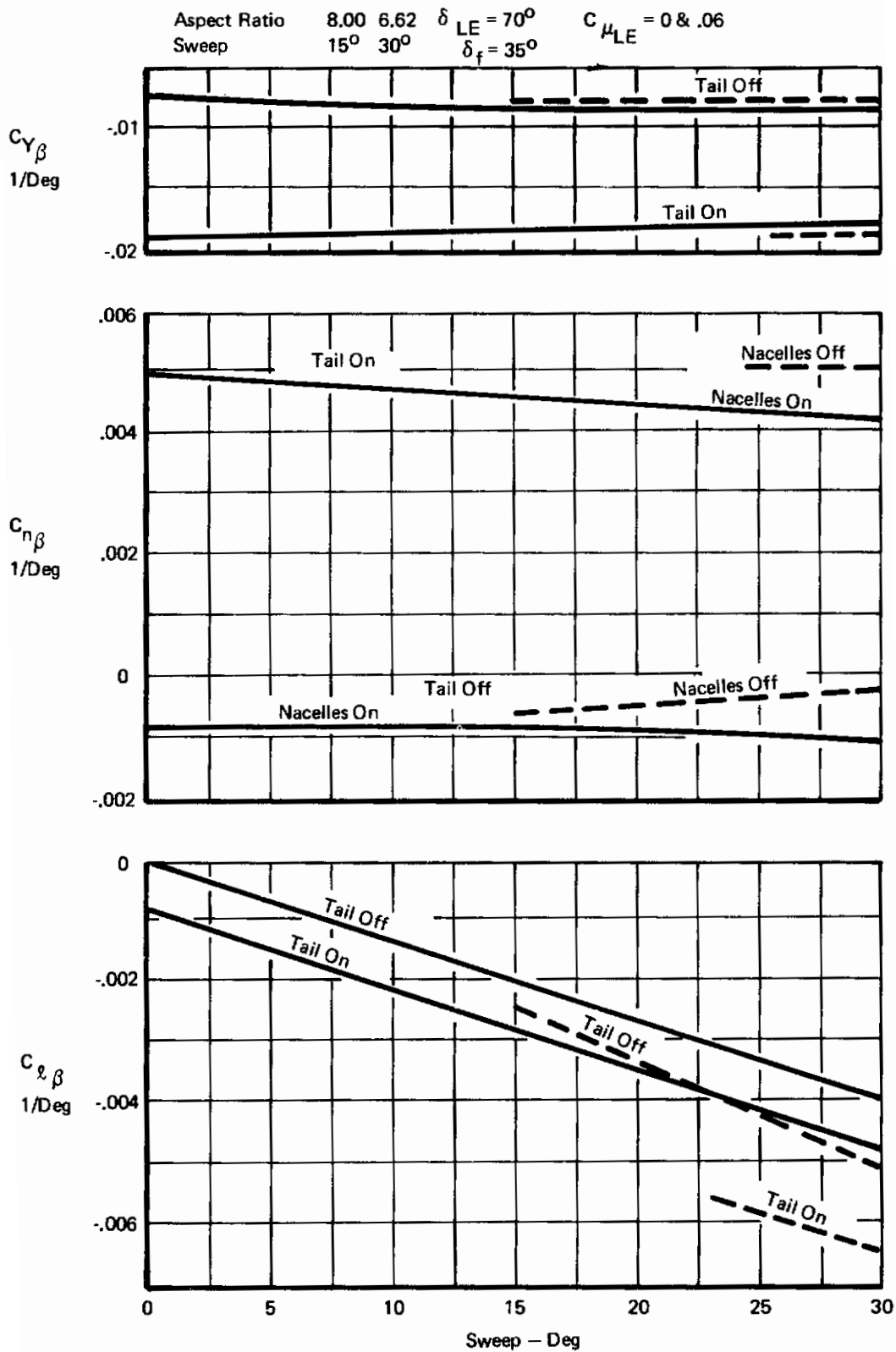


Figure 26: Effect of Sweep on β Stability Derivatives, Nacelles On and Off, Flaps Down

Contrails

Aspect Ratio 8.38 8.00 6.62 $\delta_{LE} = 70^\circ$ Nacelles On
 Sweep 0° 15° 30° $C_{\mu_{LE}} = 0 \text{ \& } .06$ $\alpha = 8^\circ$
 $\eta_f = .75$

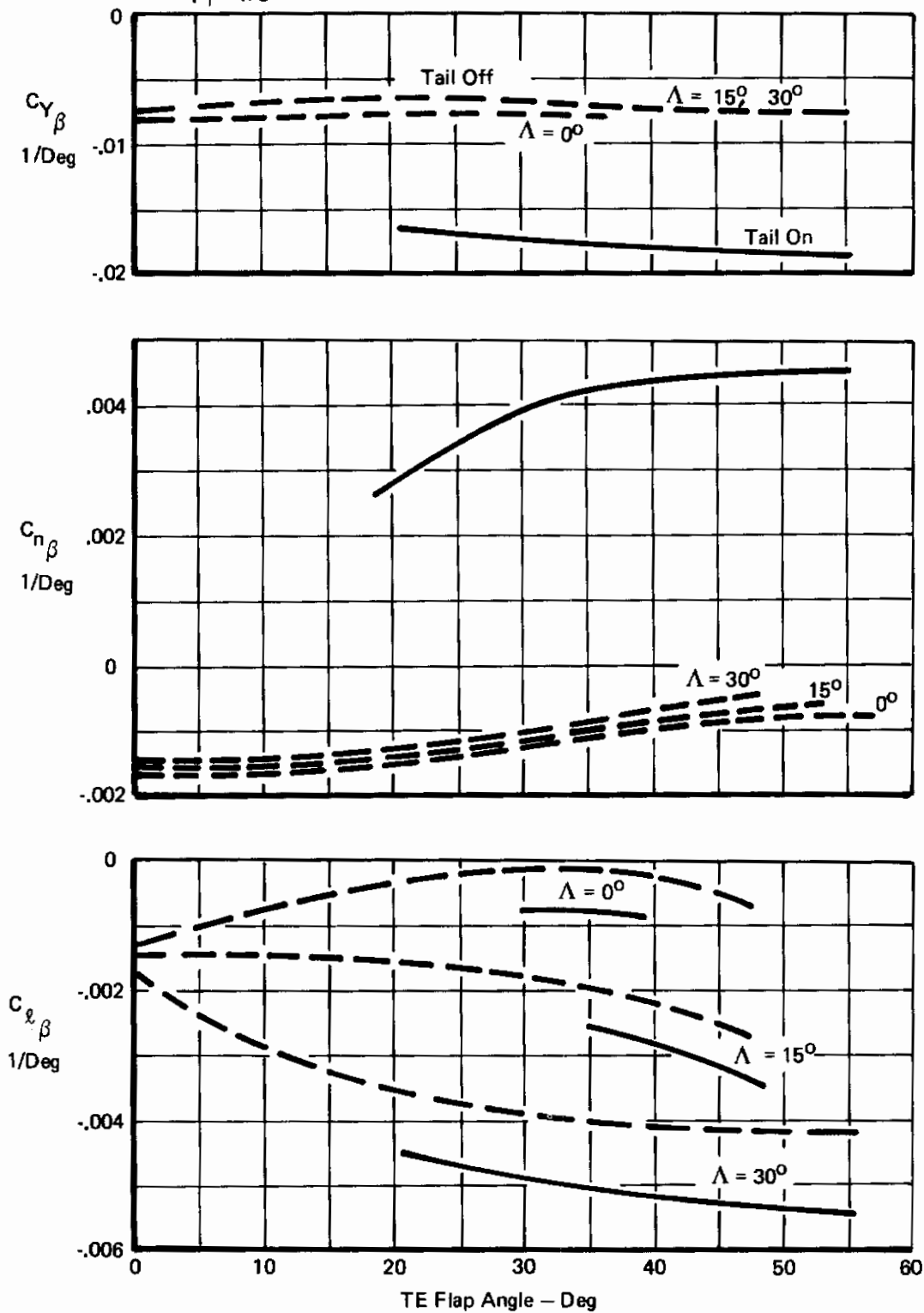


Figure 27: Effect of T.E. Flap Angle on β Stability Derivatives

Contrails

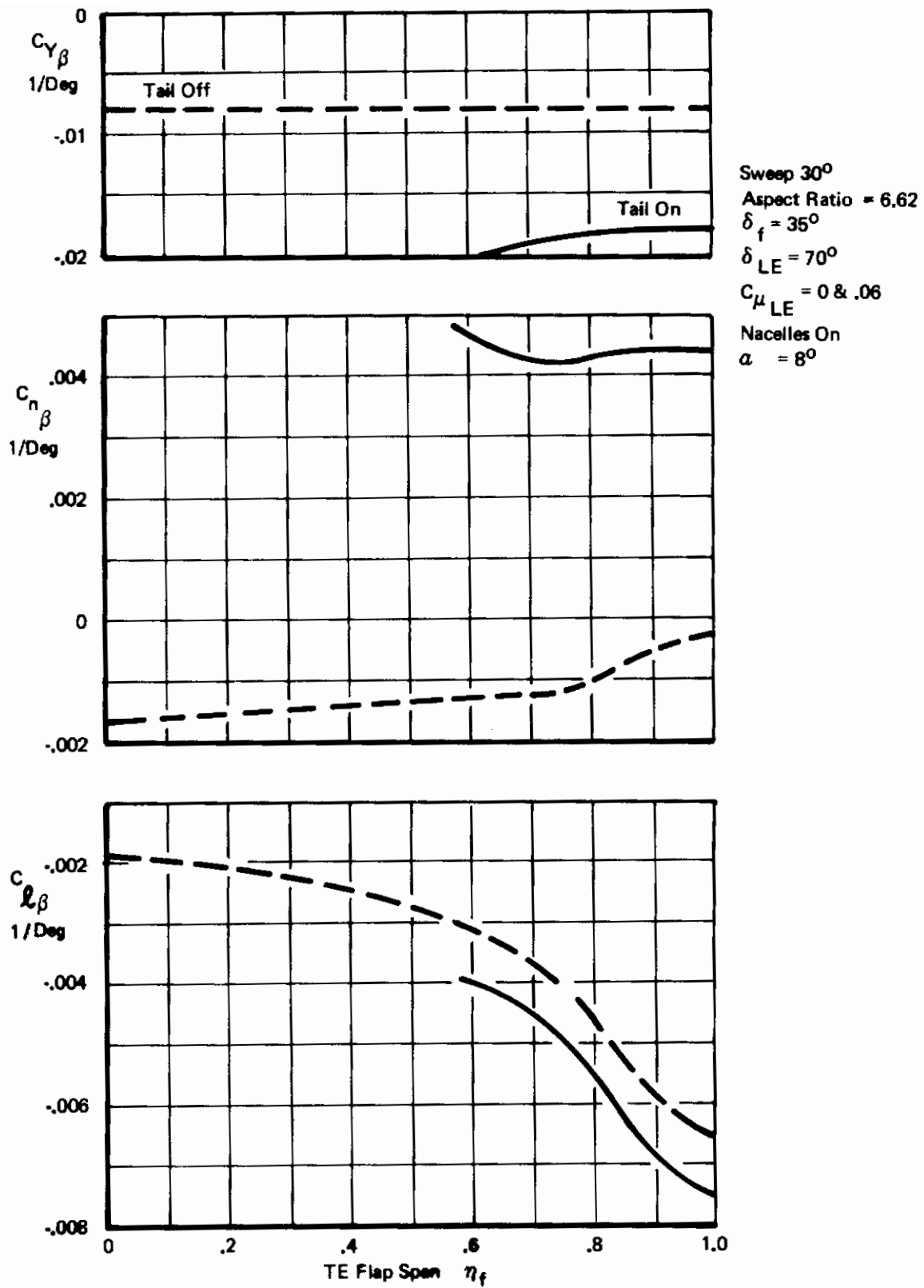


Figure 28: Effect of T.E. Flap Span on β Stability Derivatives

Contrails

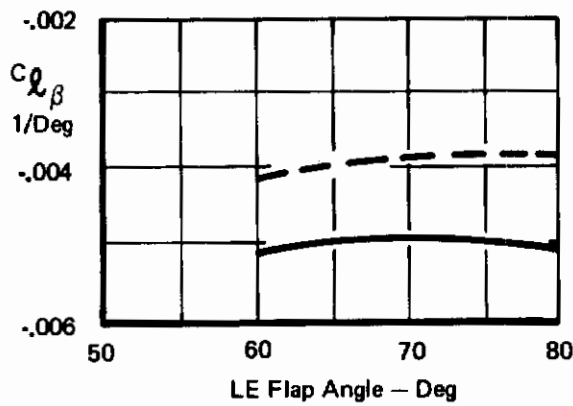
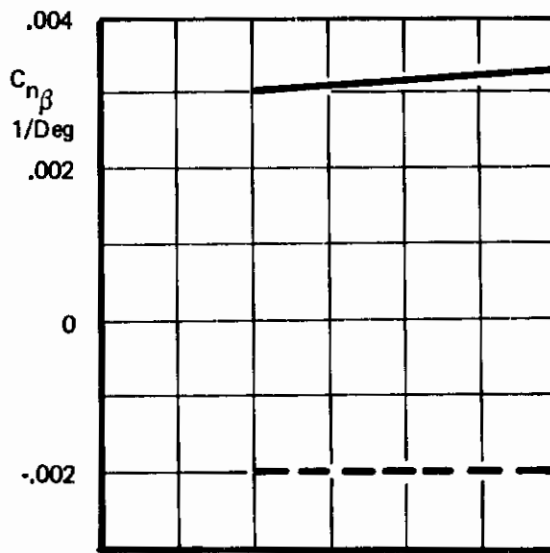
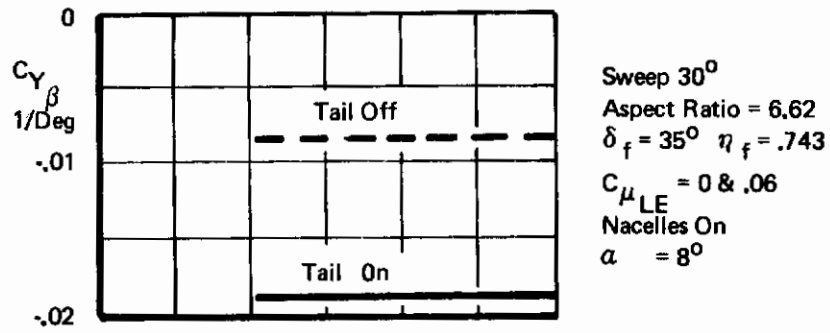


Figure 29: Effect of L.E. Flap Angle on β Stability Derivatives

Contrails

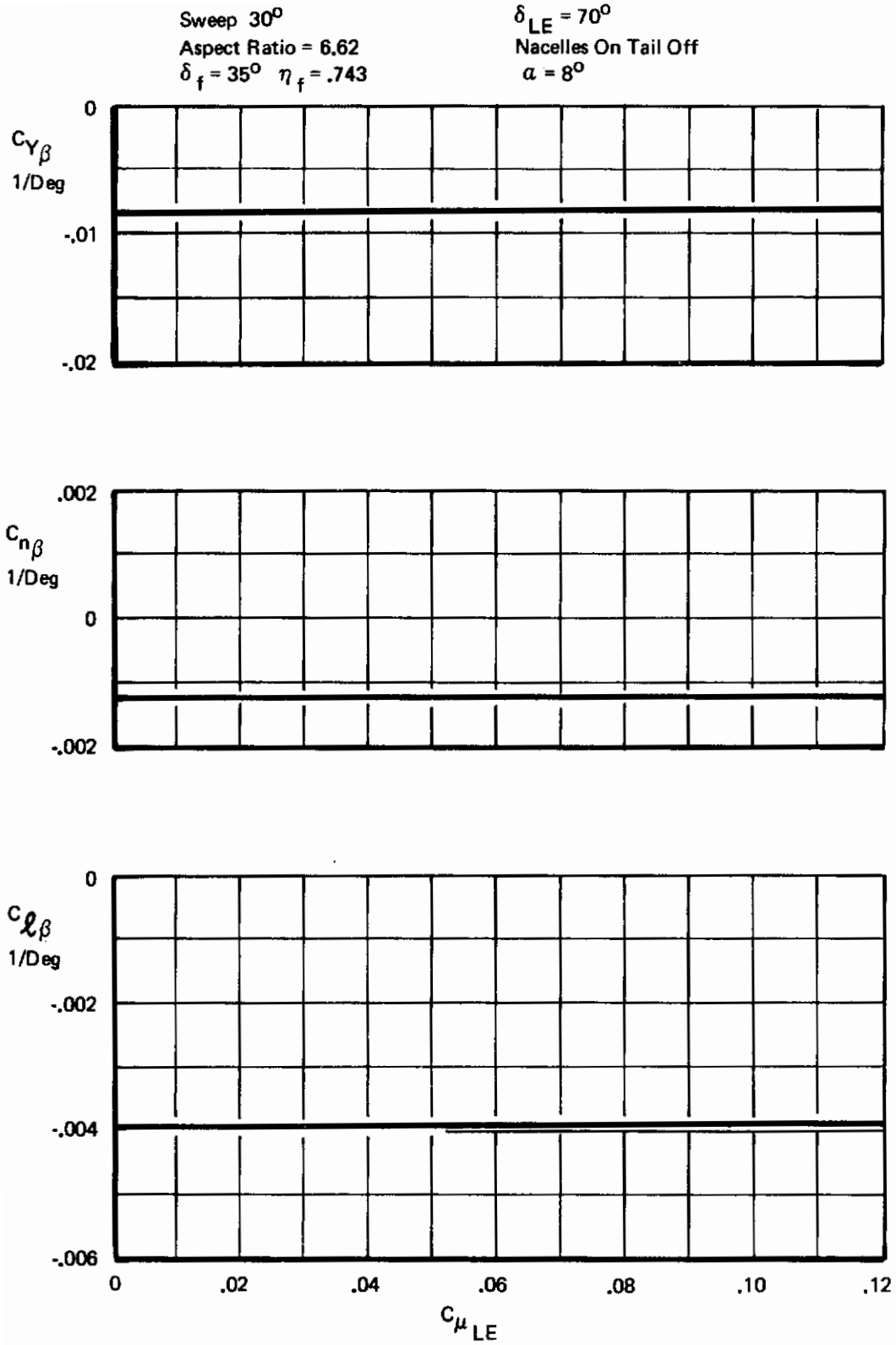


Figure 30: Effect of L.E. BLC on β Stability Derivatives

Contrails

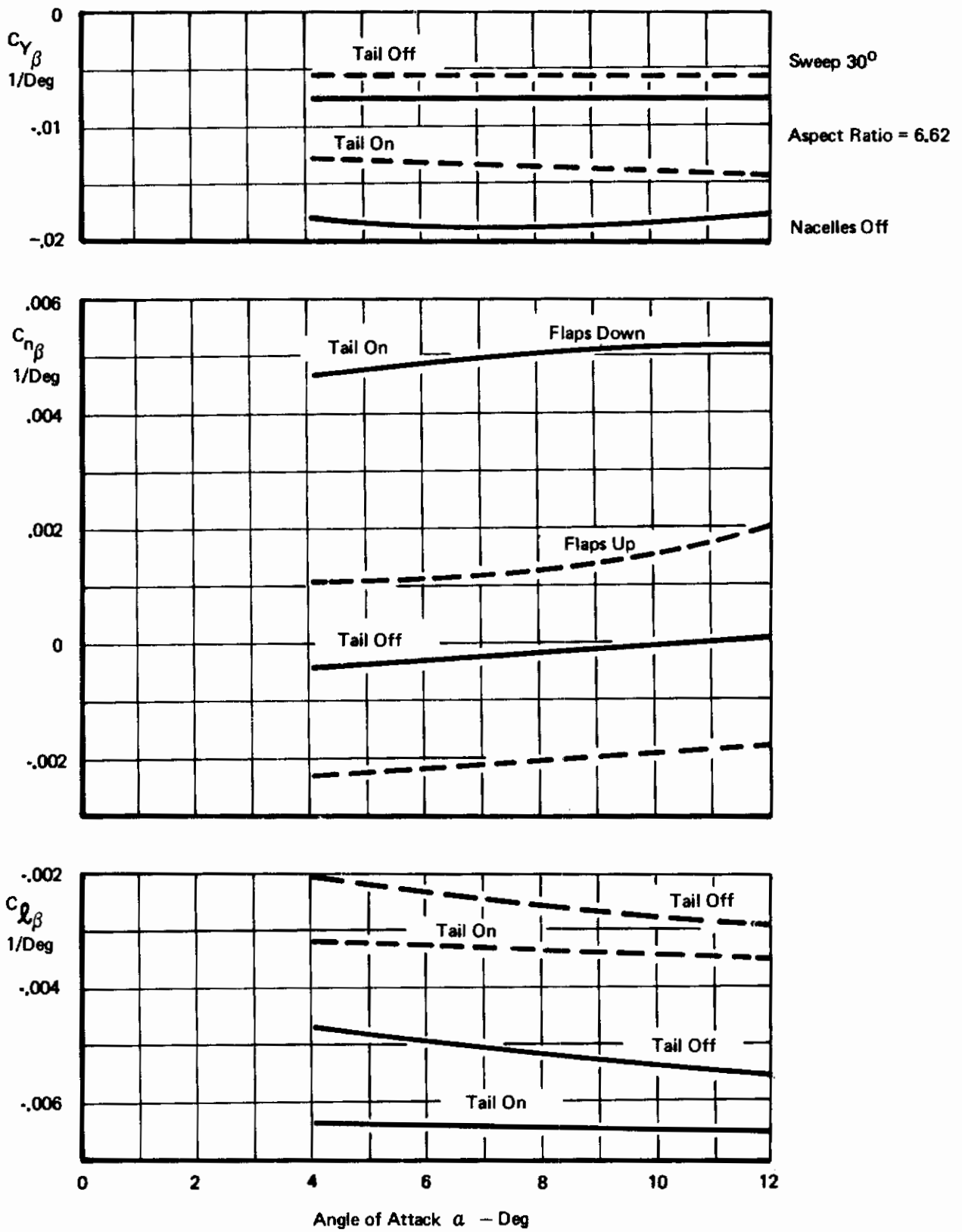


Figure 31 : Effect of Tail - β Stability Derivatives

Contrails

Aspect Ratio 8.38 6.62 Nacelles On
Sweep 0° 15° Flaps Down

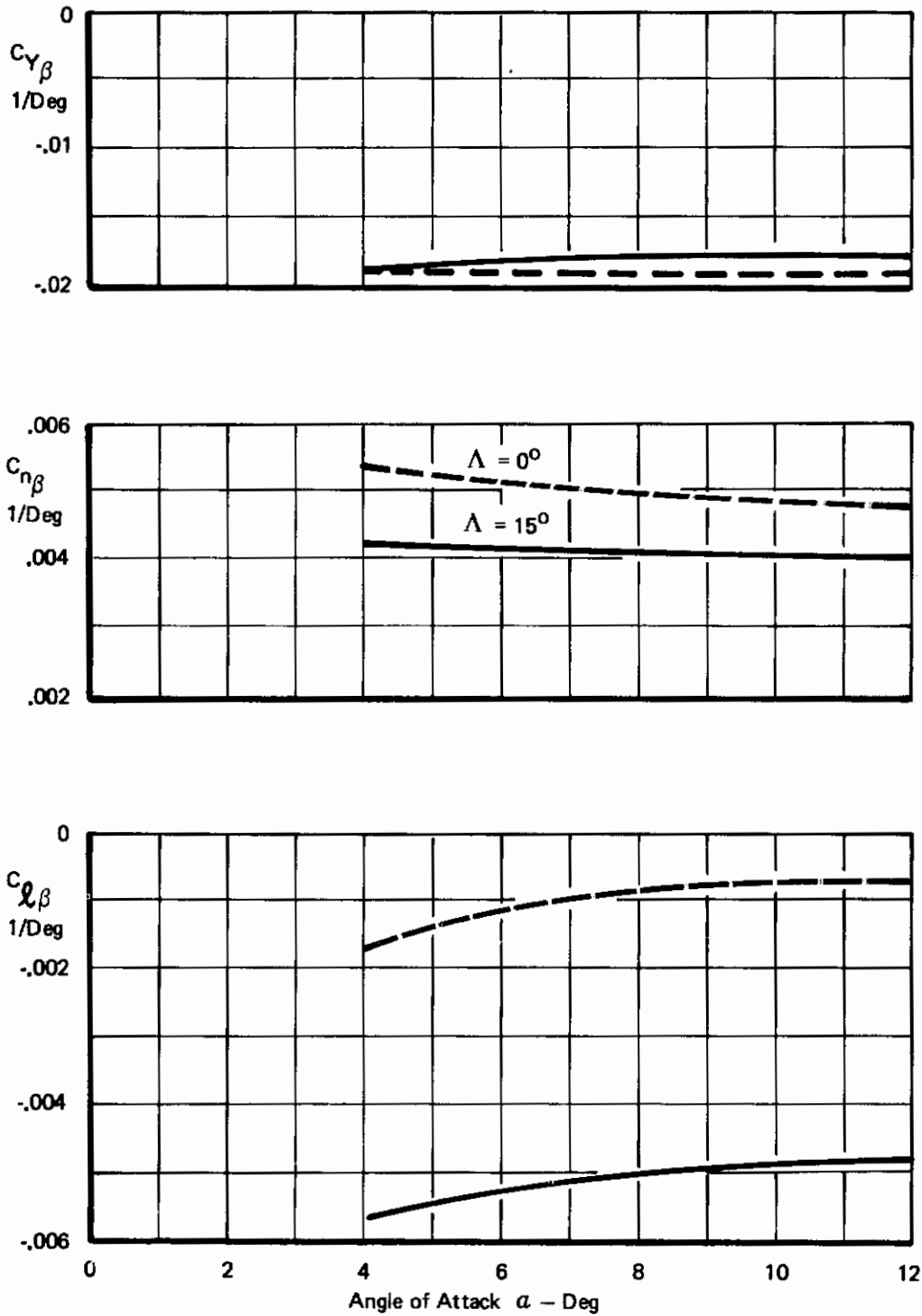


Figure 32: Effect of Angle of Attack on β Stability Derivatives

Contrails

SECTION IV

VECTORED THRUST CHARACTERISTICS

4.1 Thrust Interference Effects

The longitudinal characteristics obtained on the vectored thrust model (BVWT 099, Ref. 9) are presented in the following discussion, with particular emphasis on the aerodynamic interference effects of power from the four vectored thrust engines. The following principal parameters were studied:

- o Wing Angle of Attack $\sim \alpha$
- o Thrust Coefficient $\sim C_J$
- o Thrust Vector Angle $\sim \sigma$
- o Nacelle Location: Chord $\sim x/c$
 - Spanwise $\sim \eta_{eng}$
 - Height $\sim h/\bar{c}$

Single Pods vs Dual Pods

- o One Engine Inoperative
- o Trailing-Edge Flap Angle $\sim \delta_f$
- o Ground Height $\sim H/b$
- o Wing Sweep $\sim \Lambda$

The thrust from the blowing nacelles was included in the forces and moments recorded by the strain gauge balance on which the model was placed. Therefore, the gross force and moment coefficients produced by the model included both the aerodynamic and vectored thrust forces.

In order to determine the net aerodynamic forces acting on the model with power on, the vectored thrust components must be subtracted from the gross forces. For example, the net lift coefficient is defined as:

$$C_{L_{Net}} = C_{L_{Gross}} - C_J \sin(\alpha + \sigma)$$

In order to determine the thrust interference forces, the power-on net forces are compared to the power-off forces. For example:

$$\Delta C_{L_{INT}} = C_{L_{NET}} - C_{L_{C_J}} = 0$$

Contrails

Figure 33 gives typical lift curves and the resulting lift interference.

The drag and pitching moment are treated in a similar manner, resulting in the following equations:

$$\Delta C_{L_{Int}} = [C_{L_{Gross}} - C_J \sin(\alpha + \sigma)] - C_{L_{C_J}} = 0$$

$$\Delta C_{D_{Int}} = [C_{D_{Gross}} + C_J \cos(\alpha + \sigma)] - C_{D_{C_J}} = 0$$

$$\Delta C_{m_{Int}} = [C_{m_{Gross}} - \sum_{i=1}^4 C_{J_i} \left(\frac{x_i}{c} \sin \sigma + \frac{z_i}{c} \cos \sigma \right)] - C_{m_{C_J}} = 0$$

The bracketed terms [] are the net components and the x and z dimensions in the pitching moment equation refer to the location of the nozzle thrust vector (of each of the four nacelles) with respect to the moment reference center. These dimensions are listed, for each of the nacelle configurations tested, in Section 2.2.7, Table IV, Page 23.

The power-off reference forces used in the determination of the interference increments were measured in the same test run series (BVWT 099) as the power-on data.

Small differences were noted between the power-off data of BVWT 099 compared to the power-off characteristics shown in Section III, BVWT 097. The differences are ascribed to the cumulative effect of several adjustments to details of the model, such as flap brackets, wax fairings, etc. Use of the BVWT 099 power-off reference levels assured that the accuracy of the interference data would be unaffected by these differences.

The force and moment interference terms were calculated for the entire test by a digital computer and were subsequently plotted against angle of attack by an automatic plotting machine. Cross plots were then made from the machine plots to show the variation of the thrust interference terms versus the principal parameters studied during the vectored thrust test. The following sections present these summary crossplots.*

*Complete tabulations and plots of the gross force and moment coefficients may be found in the wind tunnel data reports (Refs. 8 through 11). The machine plots of interference effects may be found in wind tunnel data analysis supplementary reports (Refs. 2 through 5).

4.1.1 Thrust Interference in Free Air

Table VII summarizes the effects of the principal parameters studied on the lift, drag and pitching moment thrust interference terms in free air. Interference effects on maximum lift are discussed separately in Section 4.4.

Most of the data presented here is shown at an angle of attack of 8° , representing a nominal landing approach condition. Data is also shown at $\alpha = 20^\circ$ to illustrate effects occurring in a pull-up maneuver or near-stall condition.

Analysis of all the thrust interference data has shown that the drag and pitching moment interference terms tend to be directly related to the lift interference values; therefore, emphasis is placed on the lift term. It should be noted that the drag interference term as used in this report is

$$\Delta C_{D_{INT}} = C_{D_{Power-On}} - C_{D_{Power-Off}} \\ \text{(Net)}$$

and is the drag difference at a given angle of attack. It therefore contains an induced drag term caused by the change in lift due to power. Thus, the dependence of the drag interference on the lift interference is to be expected.

The thrust interference trends observed on this model were, in general, similar to those obtained in tests performed by NASA Langley (Reference 7). The NASA tests were made only at $\alpha = 0^\circ$, and indicated large unfavorable lift interferences similar to those shown here at low α 's. The NASA model had an unswept aspect ratio 6 wing with a single-slotted trailing edge flap. The vectored thrust nozzles were usually at 90° , although some data was taken for $\sigma = 60^\circ$.

Contrails

Table VII: Effect of Vektored Thrust on Thrust Interference in Free Air

Contrails

PARAMETER	FIG.	LIFT INTERFERENCE	DRAG INTERFERENCE	PITCHING MOMENT INTERFERENCE (TAIL-OFF)
Angle of Attack @ $C_J = 2$	33	Definition of lift interference.		
	34	Negative (unfavorable) interference at low α 's. Positive (favorable) interference at high α 's. (More favorable with increasing α)	Positive (unfavorable) interference at all α 's (More unfavorable with increasing α)	Positive interference at low α 's. Negative interference at high α 's. (More negative with increasing α)
Thrust Coefficient Increasing C_J :	34	Increasing thrust: the favorable interference increases at high α . At low α , the unfavorable interference becomes more unfavorable.	Unfavorable interference increases rapidly from $C_J = 0$ to 1.0. From $C_J = 1.0$ to 6.0, interference rapidly decreases for low α 's, while there is little influence at high α 's.	From $C_J = 0.0$ to $C_J = 1.0$, interference becomes negative (except for α 's to 8°). From $C_J = 1.0$ to $C_J = 6.0$, negative interference at high α 's becomes less negative and positive interference at low α 's becomes more positive.
Thrust Vector Angle Increasing σ :	35	($\alpha = 8^\circ$) Becomes more unfavorable. ($\alpha = 20^\circ$) Favorable interference increases from $\sigma = 30^\circ$ to 60° , decreases from $\sigma = 60^\circ$ to $\sigma = 90^\circ$.	For both $\alpha = 8^\circ$ and 20° unfavorable interference increases.	($\alpha = 8^\circ$) Positive interference increases. ($\alpha = 20^\circ$) Negative interference becomes slightly more negative.
Nacelle Location:		($\alpha = 8^\circ$) Most favorable interference with nacelles aft. ($\alpha = 20^\circ$) Most favorable interference with nacelles at 35% chord.	($\alpha = 8^\circ$) Unfavorable interference increases as nacelles are moved aft. ($\alpha = 20^\circ$) 35% chord gives most unfavorable interference.	($\alpha = 8^\circ$) 35% chord gives most positive interference. ($\alpha = 20^\circ$) 35% chord gives most negative interference.
<u>Chordwise</u> (Nominal Nozzle Location)	36			
(Actual Nozzle Location As Nacelle Moves Aft:	37		(Fig. 37) Unfavorable interference decreases at constant ΔC_{L_INT} .	(Fig. 38) Interference becomes more positive at constant ΔC_{L_INT} .
Height Lowering Nacelles Yields:	38			
	39	No change except at higher α where the favorable interference is slightly less.	More unfavorable interference at low α 's, yet at high α , the interference is slightly less.	Less positive interference.
<u>Spanwise</u> As Nacelles Move Inboard: ($\sigma = 60^\circ$)	40	($\alpha = 8^\circ$) Single Pods: more unfavorable Dual Pods: less unfavorable ($\alpha = 20^\circ$) Single Pods: no change Dual Pods: more favorable	($\alpha = 8^\circ$) more unfavorable largely more unfavorable ($\alpha = 20^\circ$) More unfavorable largely more unfavorable	($\alpha = 8^\circ$) increase decrease ($\alpha = 20^\circ$) more negative more negative
<u>Single Pods vs Dual Pods</u> ($\alpha=60^\circ$)	40	More favorable for single pods than dual pods.	Inboard dual pods give highest drag. Outboard dual pods give lowest drag (compared to single pods).	At $\alpha = 8^\circ$, magnitude similar. At $\alpha = 20^\circ$, more negative for single pods than dual pods.
One Engine Inoperative ($\alpha = 8^\circ, \sigma = 60^\circ$) (Also See Sec. 4.2)	41	Interference becomes less unfavorable. Outboard-out more unfavorable than inboard-out	Interference becomes less unfavorable. Inboard-out more unfavorable than outboard-out.	Positive interference decreases. Outboard-out more positive than inboard-out.
T.E. Flap Deflection Increasing δ_f :	42	Interference becomes more favorable.	Interference becomes more unfavorable.	Interference becomes more negative.
Wing Sweep Sweeping Wing from 15° to 30° :	43	($\alpha = 8^\circ$) More unfavorable. ($\alpha = 20^\circ$) Essentially no change.	($\alpha = 8^\circ$) More favorable. ($\alpha = 20^\circ$) More unfavorable.	($\alpha = 8^\circ$) Positive interference increases at $\sigma = 60^\circ$ and 90° . Decreases at $\sigma = 30^\circ$. ($\alpha = 20^\circ$) More negative.
Test Conditions Increasing q :	44	($\alpha = 8^\circ$) More unfavorable. ($\alpha = 20^\circ$) Less favorable	At $\alpha = 8^\circ$ and 20° interference reduces from $C_J = 0.0$ to 1.25, and increases from $C_J = 1.25$ to 2.0.	($\alpha = 8^\circ$) More positive. ($\alpha = 20^\circ$) Less negative.

4.1.1.1 Thrust Coefficient and Angle of Attack

Figures 33 and 34 illustrate the influence of thrust coefficient and angle of attack on the thrust interference terms.

As shown in Figure 33, a negative (unfavorable) lift interference was observed at low to moderate angles of attack while a positive (favorable) lift interference occurs at relatively high angles of attack.

Figure 34 presents the drag and pitching moment interference as well as the lift interference. Note that, for the range of α 's tested, the largest thrust interference effects generally occur between $C_J = 0$ and 1.0, with a relatively smaller change in interference at C_J 's greater than 1.0. Note also, that as α increases, the drag interference term becomes more positive (as does lift) while pitching moment interference becomes more negative.

The probable explanation for the variation of interference with angle of attack is that the jet plumes strongly entrain the surrounding air. This amounts to placing sinks directly below the wing. The sinks induce downwash at the trailing edge, which effectively reduces the trailing-edge flap angle. This leads to the observed loss in lift at low to moderate angles of attack. The sinks also induce a downward velocity at the leading edge which effectively reduces the local angle of attack felt by the leading-edge flap. Hence the undersurface separation occurring behind the leading-edge flap at low angles of attack is aggravated. The combined result at low to moderate angles of attack is a loss of lift plus an increase in parasite drag more than sufficient to offset any reduction of induced drag due to the lift loss.

As the angle of attack increases, the fact that the sink effect reduces the local angle of attack at the L. E. flap leads to a delay in the wing angle of attack at which initial separation occurs. This occurs because the sink effect reduces the pressure peak at the leading edge. The upper surface boundary layer is then relieved of the strong adverse pressure gradient behind the leading edge. This allows the flow to remain attached to a higher α (and C_L) than achieved with power-off.

4.1.1.2 Thrust Vector Angle

Figure 35 shows the effect of increasing the thrust vector angle from 30° to 90° at constant angles of attack.

- o The lift interference becomes more unfavorable at moderate angles of attack. At high angles of attack, the favorable lift interference slightly increases going from $\sigma = 30^\circ$ to 60° , but decreases again going from $\sigma = 60^\circ$ to 90° .

$\Lambda = 30^\circ$ $AR = 6.62$
 $C_J \sim$ $\sigma = 60^\circ$
 $\delta_f = 35^\circ$ $\eta_f = 74.3\%$
 $\delta_{LE} = 70^\circ$ $C_{\mu LE} = .06$
 Tail Off Free Air
 All Engines Operating
 Engine Location:
 $\eta_{Eng} = 27/43.5\%$

$h/\bar{c} = 0.371$
 $x/c = 35\%$ (Nominal)
 Note: $q = 10$ psf

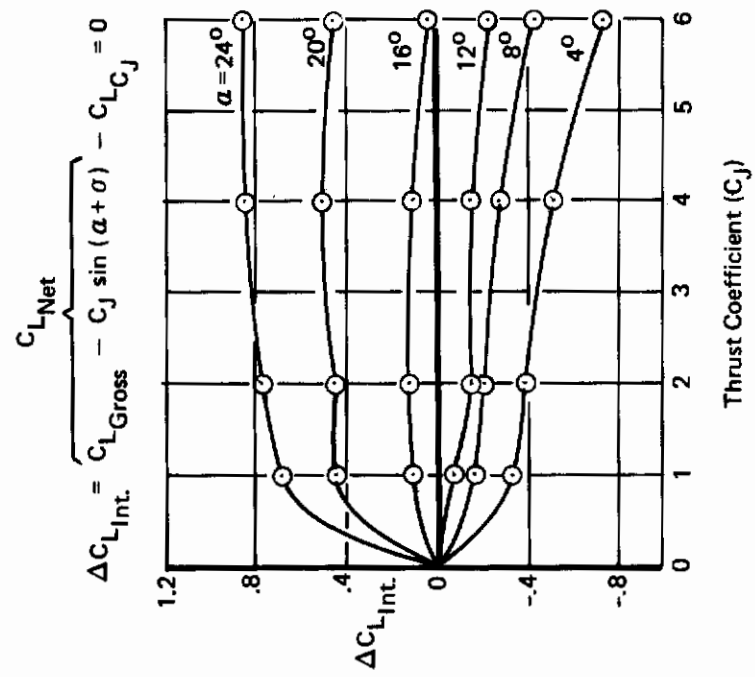
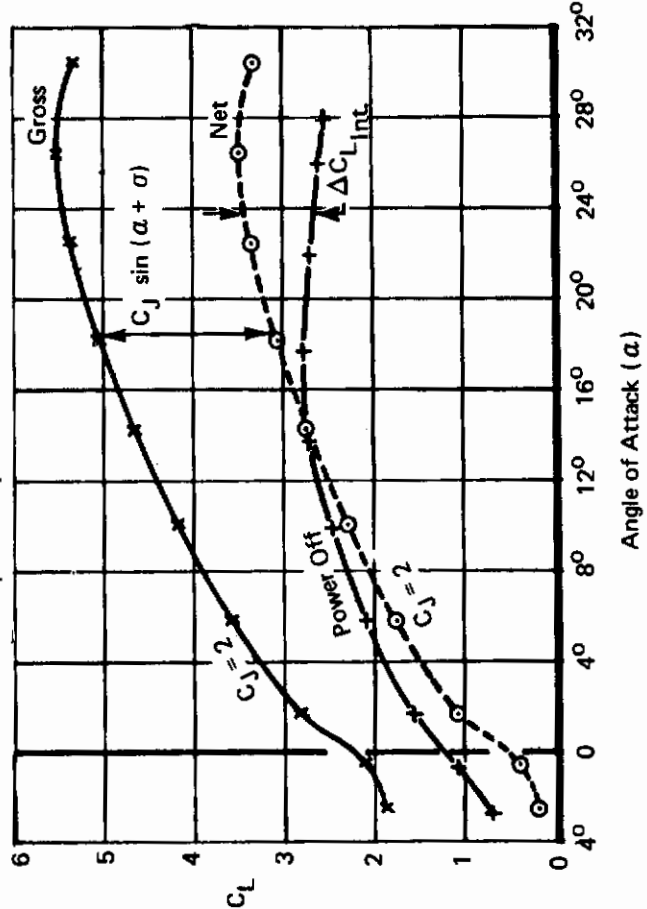
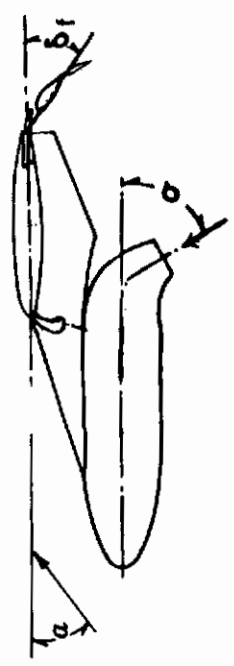


Figure 33: Determination of Thrust Interference on Lift

$\Lambda = 30^\circ$ $AR = 6.62$ $x/c = 35\%$ (Nominal) Note: $q = 10$ psf
 Tail Off Free Air $\delta_{LE} = 70^\circ$
 All Engines Operating $C_{\mu_{LE}} = .06$
 $\eta_{Flap} = 74.3\%$ $\sigma = 60^\circ$
 $\eta_{Eng} = 27/43.5\%$ $\delta_f = 35^\circ$
 $h/\bar{c} = 0.371$

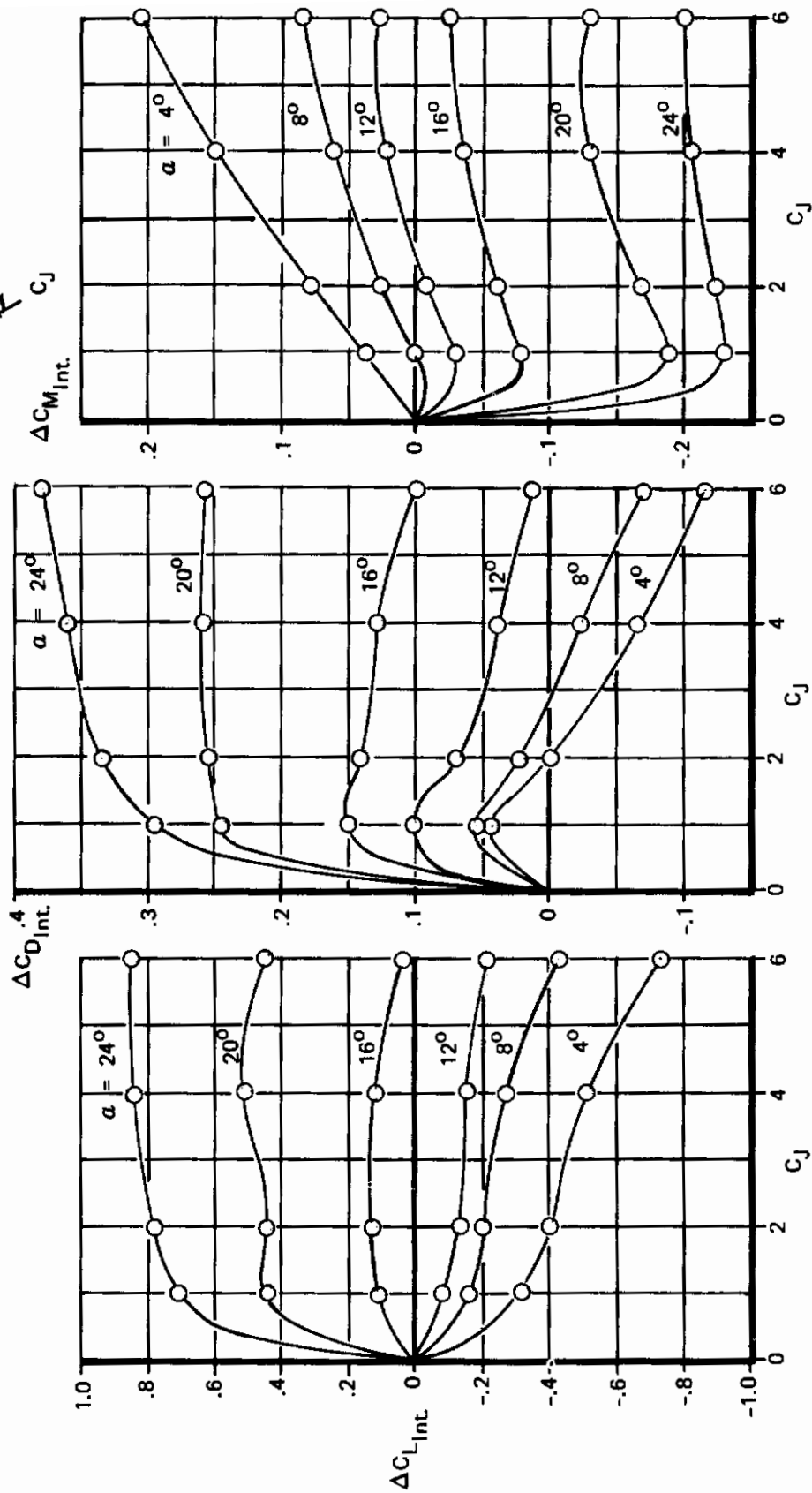
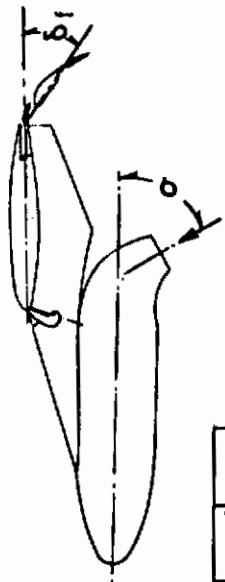


Figure 34: Effect of Thrust Coefficient on Thrust Interference

$\Lambda = 30^\circ$ $C_J = 2$
 Tail Off $AR = 6.62$
 Free Air $\eta_{Flap} = 74.3\%$
 All Engines Operating
 $\eta_{Eng} = 27/43.5\%$
 $h/\bar{c} = 0.371$
 $x/\bar{c} = 35\%$ (Nominal)
 $\delta_{LE} = 70^\circ$
 $C_{\mu_{LE}} = .06$
 $\delta_f = 35^\circ$

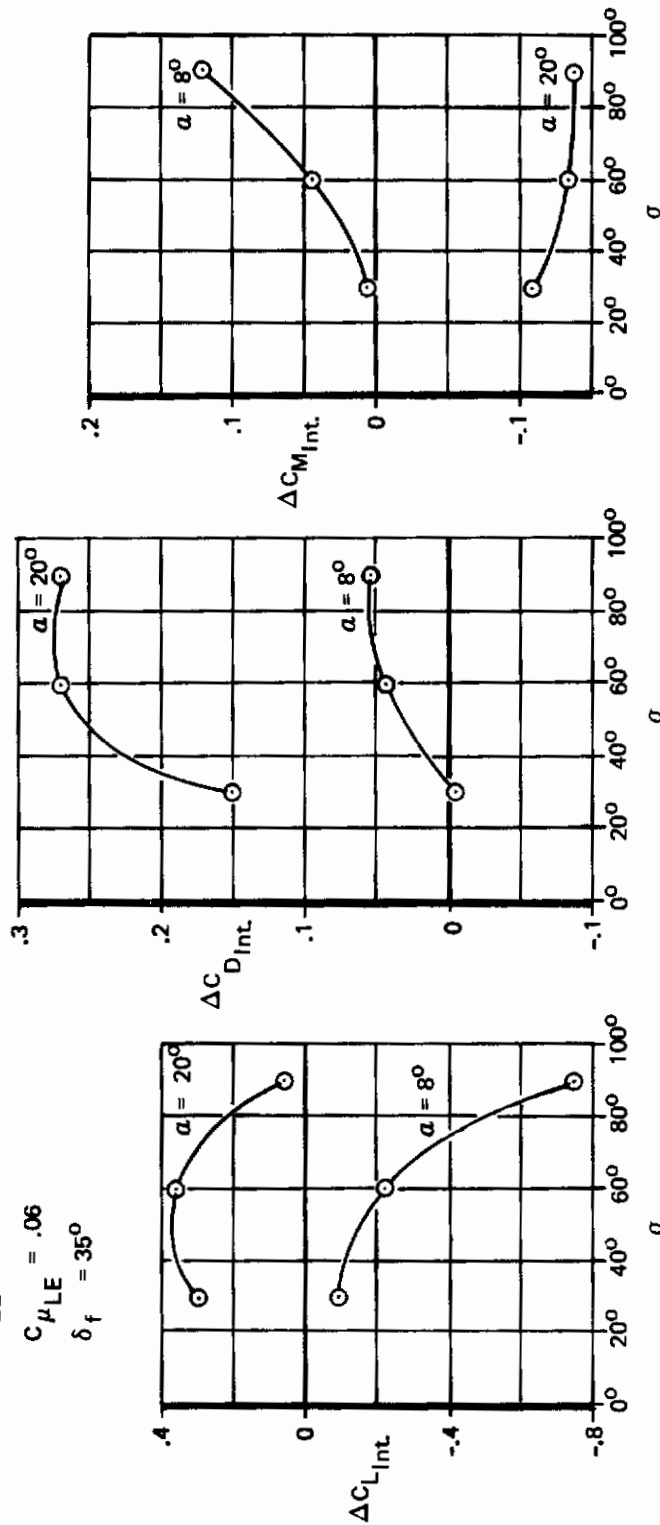
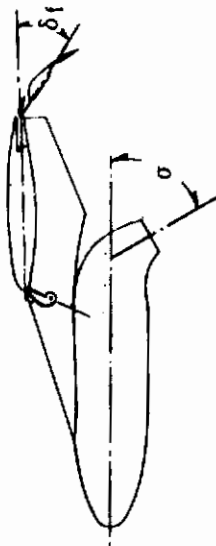


Figure 35: Effect of Thrust Vector Angle on Thrust Interference

Contrails

- o The unfavorable drag interference increases at both low and high α 's. A greater increase is observed between $\sigma = 30^\circ$ and 60° for $\alpha = 20^\circ$ than for $\alpha = 8^\circ$.
- o The positive pitching moment interference at moderate α 's increases. The negative moment interference at high α 's becomes slightly more negative.

The NASA data referred to above showed similar trends to those noted above when σ was changed from 60° to 90° .

4.1.1.3 Nacelle Location

Figures 36 through 40 summarize the thrust interference effects in free air for various nacelle locations including chordwise, height and spanwise variations as well as a comparison of the single pods versus the dual pods installation.

4.1.1.4 Chordwise Location

Figure 36 is an example of the data obtained to determine the effect of moving the nacelles fore and aft in a chordwise direction. (Note that the x/c dimension shown in Figure 36 refers to the location of the nozzle exit plane (relative to the basic wing leading edge) when the thrust vector angle is zero. Therefore, x/c is dimensionally correct only when $\sigma = 0^\circ$, since the nozzle exit plane on the wind tunnel model actually translated forward as the nozzles were rotated. Therefore the x/c shown is referred to as the "nominal" x/c. A table of the actual x/c versus the nominal x/c is given in Table IV in Section 2.1.)

The effects of moving the nacelles aft are summarized below and are shown in Figure 36 through 38. Additional data is presented in Reference 2.

Lift interference becomes more favorable for a given moderate angle of attack as the nacelles move aft, particularly, as the nacelles are moved from 35% to 70% x/c. However, the data shows that the 35% x/c position is generally better than the 70% x/c position in terms of favorable lift interference at high angles of attack.

This agrees with the NASA data, which showed lift interference becoming more favorable as the nacelles moved aft at low α 's.

The drag interference at $\alpha = 8^\circ$ tends to increase (especially at $\alpha = 90^\circ$) as the nacelles move aft; however, at high α 's the 70% x/c position shows the least interference while the 35% x/c shows the most interference. When plotted at a given level of lift interference, rather than at constant α , the drag interference tends to reduce as the nacelles move aft as shown in Figure 37. Note that the actual, rather than the nominal, x/c is shown. Also the data shown has been smoothed and averaged for several configurations.

The pitching moment interference shows that the 35% x/c position generally shows the most positive increment at $\alpha = 8^\circ$, yet it also produces

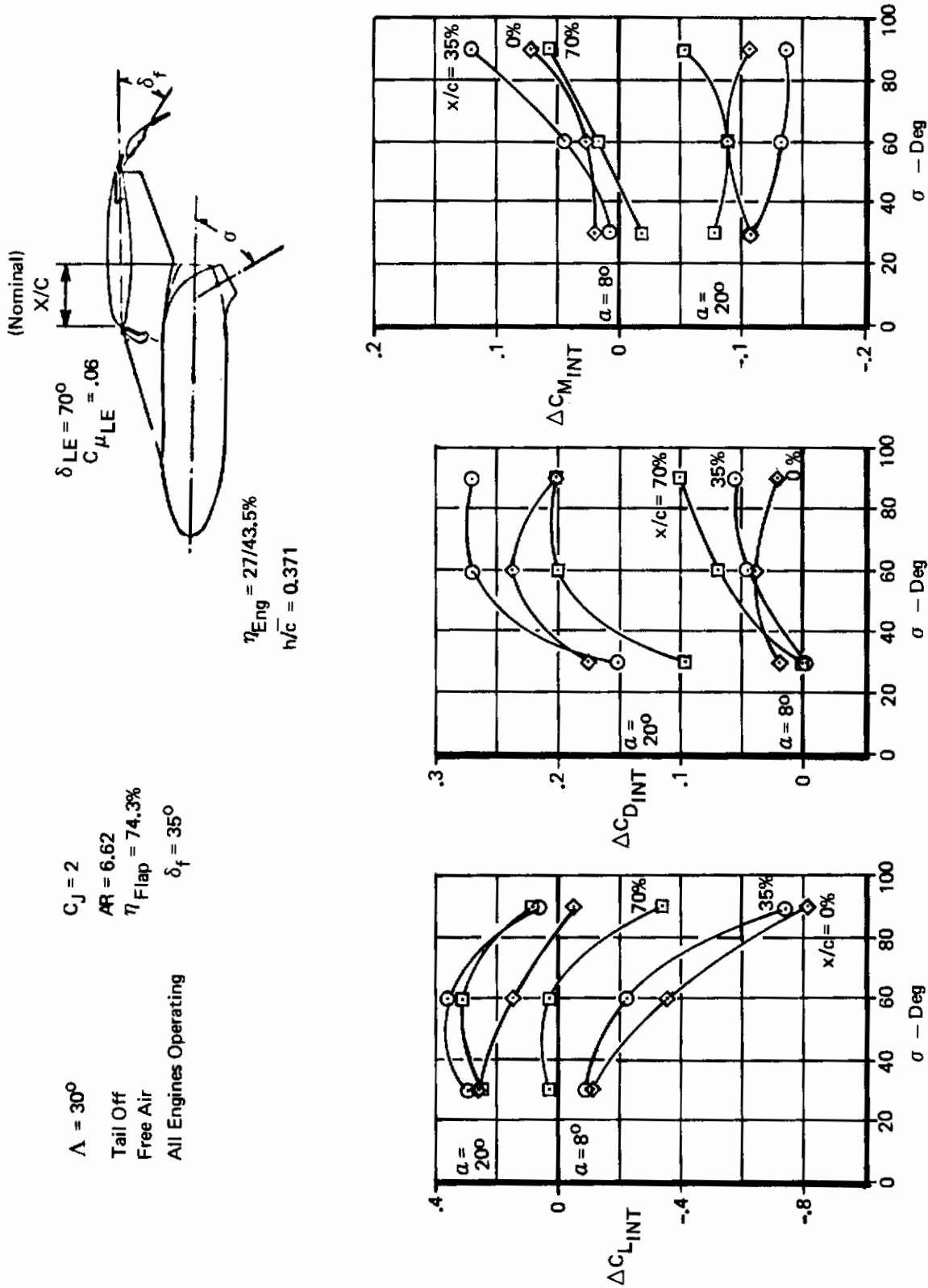


Figure 36: Effect of Nacelle Chordwise Location on Thrust Interference

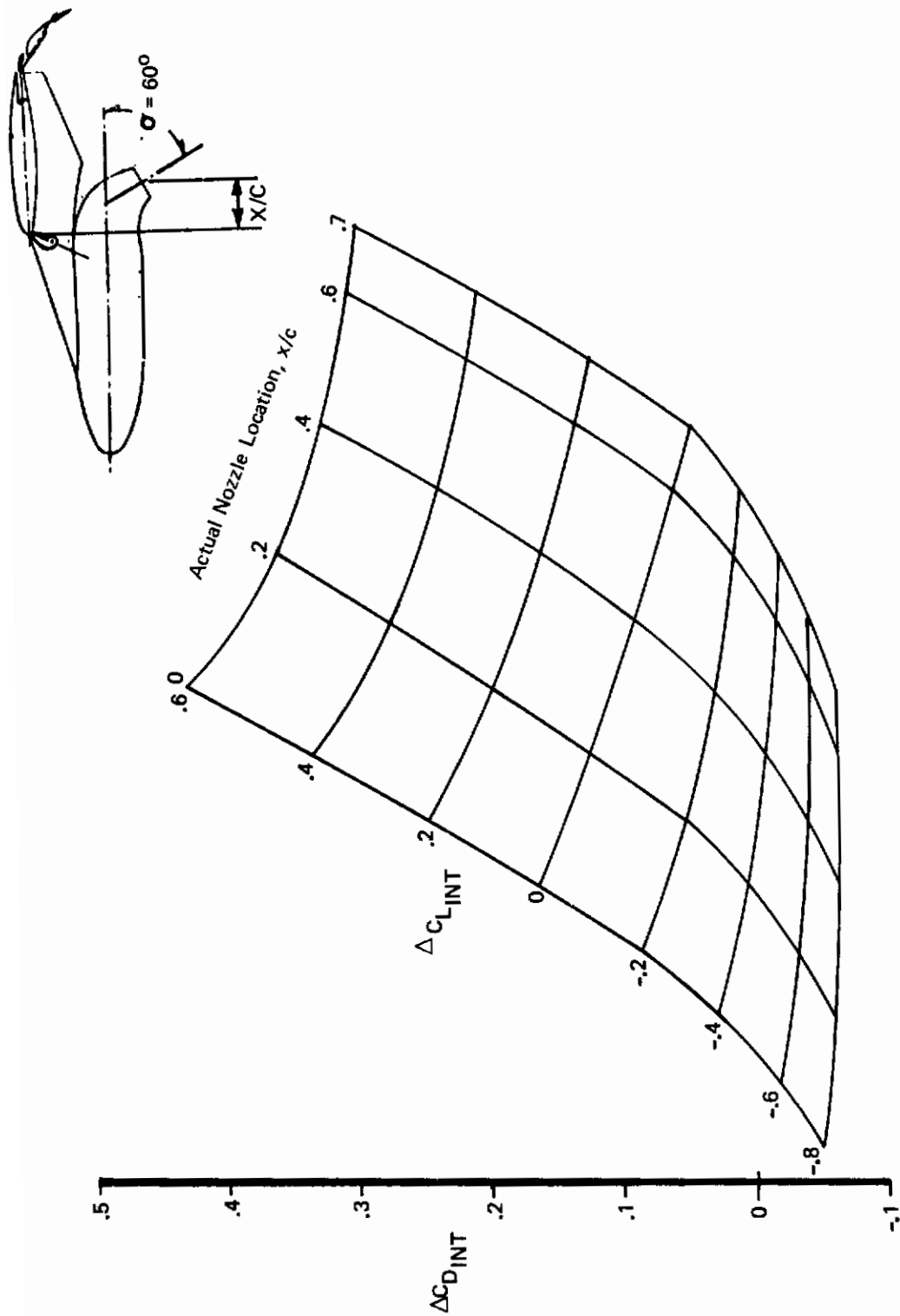


Figure 37 : Effect of Nacelle Chordwise Location on Drag Interference at Given ΔC_{L_INT}

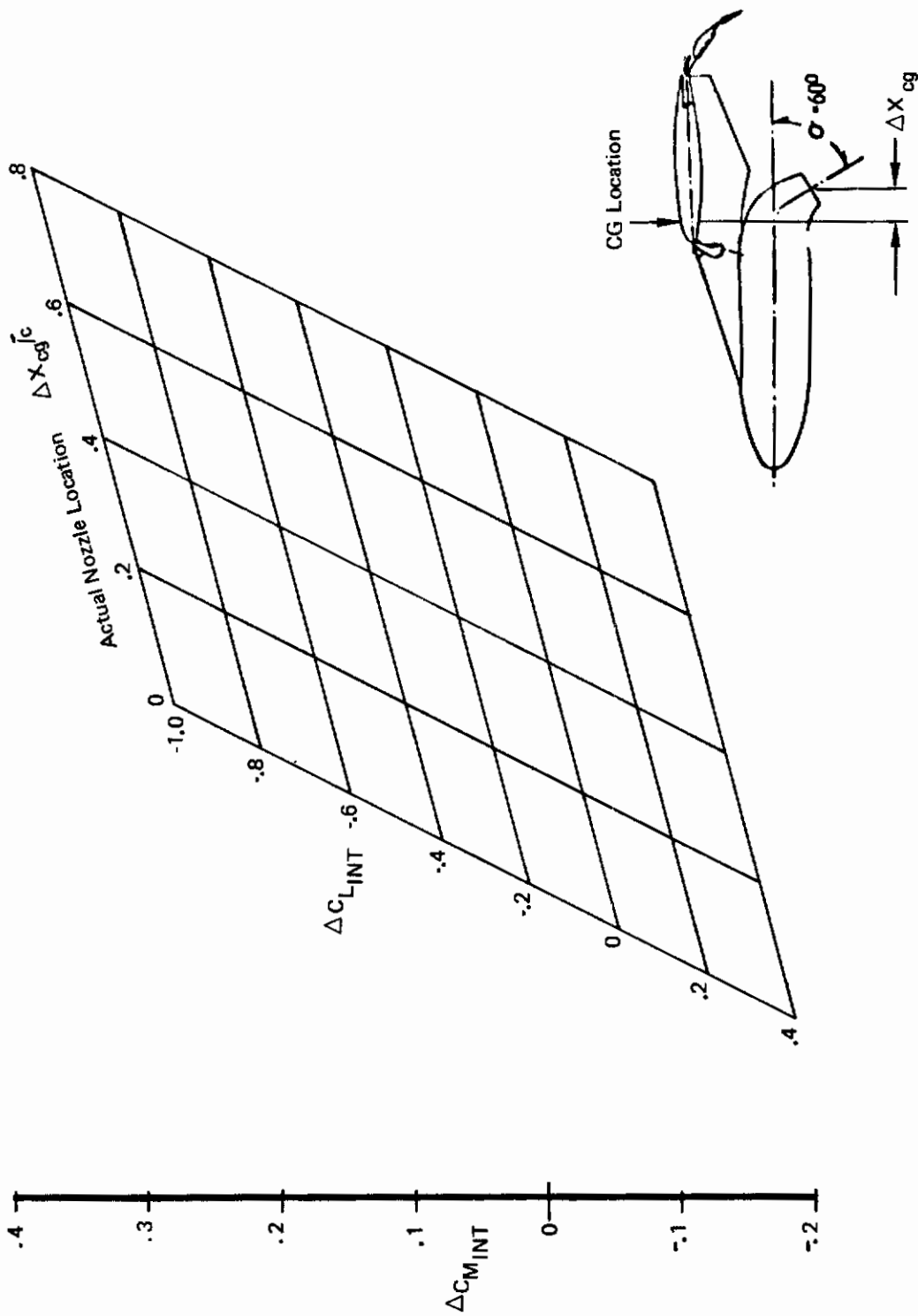


Figure 38: Effect of Nacelle Chordwise Location on Pitching Moment Interference at Given $\Delta C_{L_{INT}}$

the most negative increment at $\alpha = 20^\circ$. The 0% and 70% x/c data are nearly equal for both angles of attack. Again, when the pitching moment interference is plotted at a given level of lift interference (in a manner similar to drag interference in Figure 37), the moments tend to become more positive as the nacelles move aft, as shown in Figure 38.

4.1.1.5 Nacelle Height

Figure 39 shows the following small effects of moving the nacelle downward one inch model scale (from $h/\bar{c} = 0.406$ to 0.496):

- o The lift interference is essentially the same except above $20^\circ\alpha$, the lowered nacelle shows a little less favorable lift interference.
- o The lowered nacelle shows slightly more unfavorable drag interference at low α 's and slightly less interference above $15^\circ\alpha$.
- o The lowered nacelle shows about 0.05 less positive pitching moment interference.

4.1.1.6 Spanwise Location

The effect of moving the single pods from the 43.5%/60% b/2 position to the more inboard (27%/43.5% b/2) position is shown in Figure 40. As the single pods move inboard:

- o Lift interference becomes more unfavorable at low α 's and shows no change at high α 's.
- o Drag interference increases at both low α 's and high α 's.
- o Pitching moment interference becomes slightly more positive at low α 's yet more negative at high α 's.

Different trends were observed for the dual pods also illustrated in Figure 40. As the dual pod nacelles move inboard from the 43.5% b/2 position to the 27% position:

- o Lift interference shows slightly more favorable interference at all α 's.
- o Drag interference is much more unfavorable at all α 's.
- o Pitching moment interference is more negative at all α 's.

It is thought that the inboard dual pod nacelles were located too close to the body side. This led to an induced separation under the inboard wing due to the nacelle-body interference. The precipitation of an inboard underwing separation could lead to the trends noted above as the dual pod nacelles are moved inboard.

$\Lambda = 15^\circ$
 Tail Off
 Free Air
 All Engines Operating

$C_J = 2$ $\sigma = 60^\circ$
 $AR = 8$
 $\eta_{Flap} = 75\%$
 $\delta_f = 35^\circ$

$\eta_{ENG} = 27/43.5\%$
 $X/C = 35\%$ (Nominal)

$\delta_{LE} = 70^\circ$
 $C_{\mu,LE} = .06$

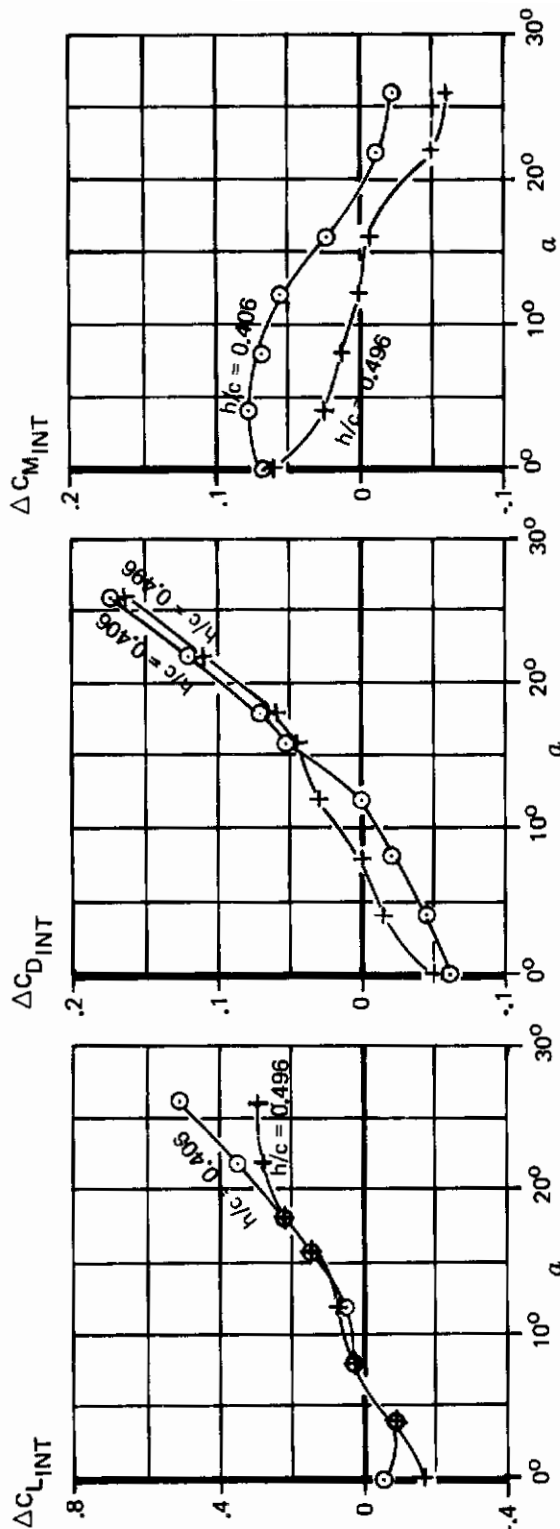
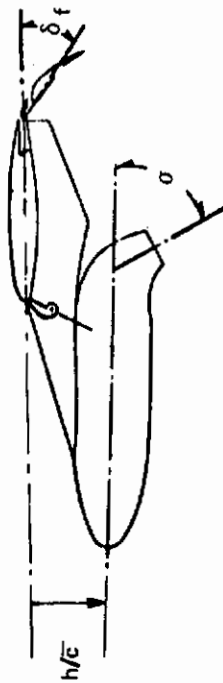


Figure 39: Effect of Nacelle Height on Thrust Interference

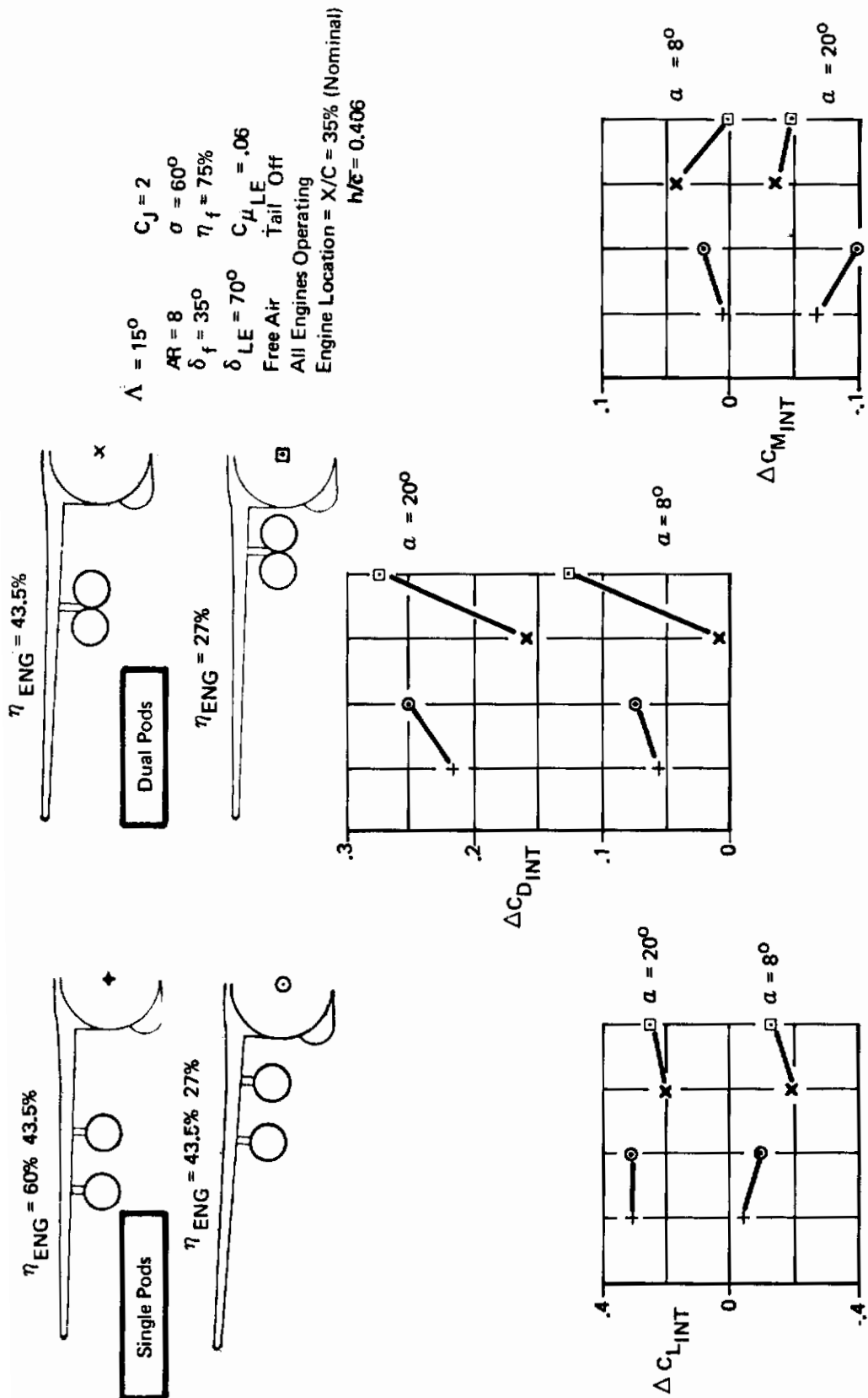


Figure 40: Thrust Interference, Single Pods versus Dual Pods

4.1.1.7 Single Pods Versus Dual Pods

The configuration with the single pods is compared to an inboard and an outboard dual pod configuration in Figure 40 in terms of the thrust interference effects for a 15° wing sweep configuration.

- o Lift Interference: The configuration with the single pods shows a more favorable lift thrust interference than either of the dual pod configurations. The inboard dual pods are more favorable in terms of lift interference than the outboard dual pod configuration as noted earlier.
- o Drag Interference: The outboard dual pods show less drag interference than either the inboard dual pods (which gave highest drag) or the configurations with the single pods.
- o Pitching Moment Interference: At low α 's, the pitching moment interference is of the same order of magnitude for all nacelle configurations shown. At high α 's the single pods show a more negative pitching moment interference than the dual pods.

4.1.1.8 One Engine Inoperative

Figure 41 shows the effects of an engine failure on the longitudinal thrust interference in free air. The unfavorable lift interference at $\alpha = 8^\circ$ is reduced by 45% for an inboard engine failure and by 29% for an outboard engine failure. Reducing the power setting to $C_J = 1.5$ with all engines operating reduces the lift interference by only 16%. It might be anticipated that the loss of one engine out of four engines would reduce the interference by 25%. However, the reductions shown are due not only to the loss of the interference induced by a single isolated engine but also to the loss of the mutual interference experienced by two engines operating side by side. This is discussed more fully in Section 4.2. The fact that the reduction in lift interference for an outboard engine failure is less than for an inboard engine failure indicates that the outboard engine contributes less to the lift interference than does the inboard engine.

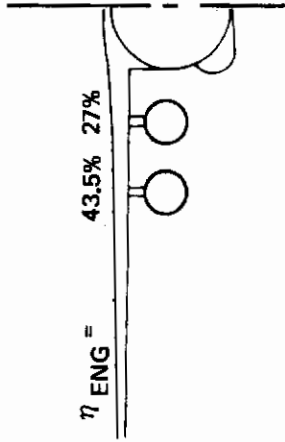
Comparison of the reduction in the unfavorable drag interference for an inboard or outboard engine failure indicates that the outboard engine has a greater influence on drag interference than does the inboard engine.

The positive thrust interference effect on pitching moment is also reduced for either an inboard or outboard engine failure. The results indicate that the outboard engine has less of an influence on pitching moment interference than does the inboard engine.

4.1.1.9 Trailing-Edge Flap Angle

Figure 42 shows that, at $\alpha = 8^\circ$ and 20° , increasing the T.E. flap angle from 20° up to 48° leads to the following effects:

Sweep $\Lambda = 30^\circ$ $\sigma = 60^\circ$ $\alpha = 8^\circ$
 AR = 6.62 $\eta_f = .743$
 $\delta_f = 35^\circ$ $C_{\mu_{LE}} = .06$
 $\delta_{LE} = 70^\circ$
 Free Air Tail Off



Engine Location
 $X/C = 35\%$
 (Nominal)
 $h/c = .371$

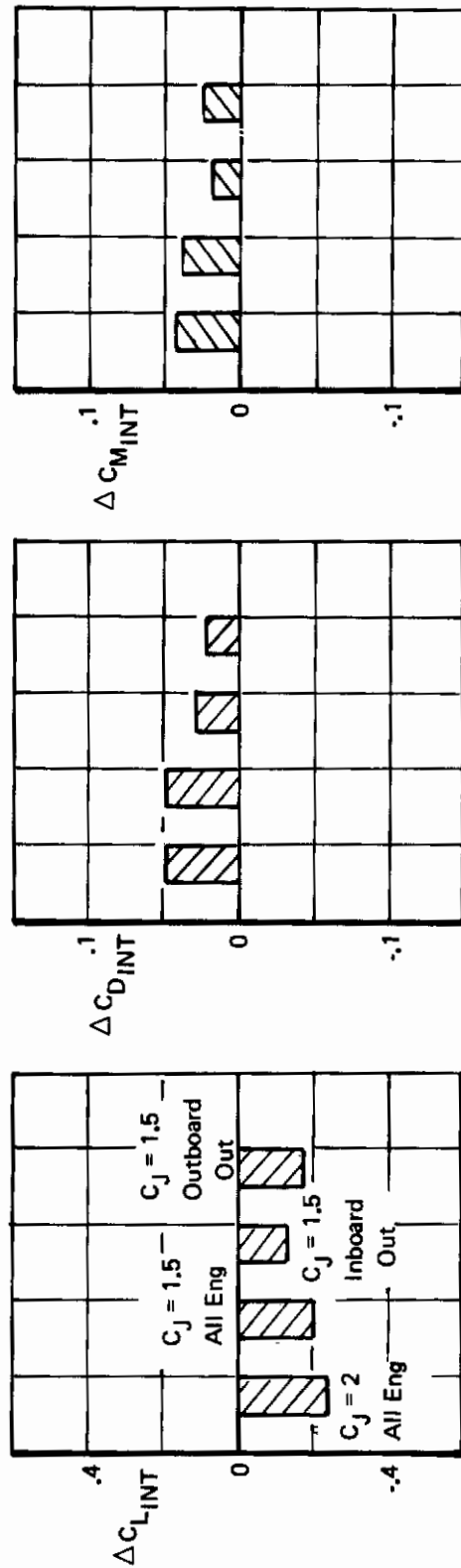
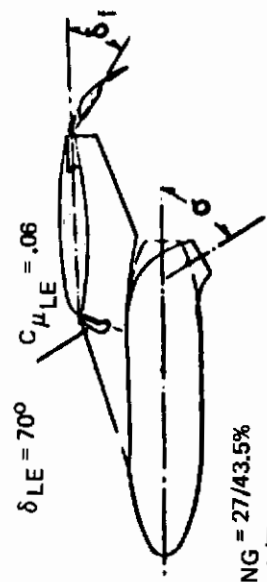


Figure 41: Effect of One Engine Failure on Thrust Interference

$\Lambda = 30^\circ$
 Tail Off
 Free Air
 All Engines Operating
 $C_J = 2$ $\sigma = 30^\circ$
 $AR = 6.62$
 $\eta_{FLAP} = 74.3\%$



$\eta_{ENG} = 27/43.5\%$
 $M\bar{C} = 0.371$
 $X/C = 35\%$ (Nominal)

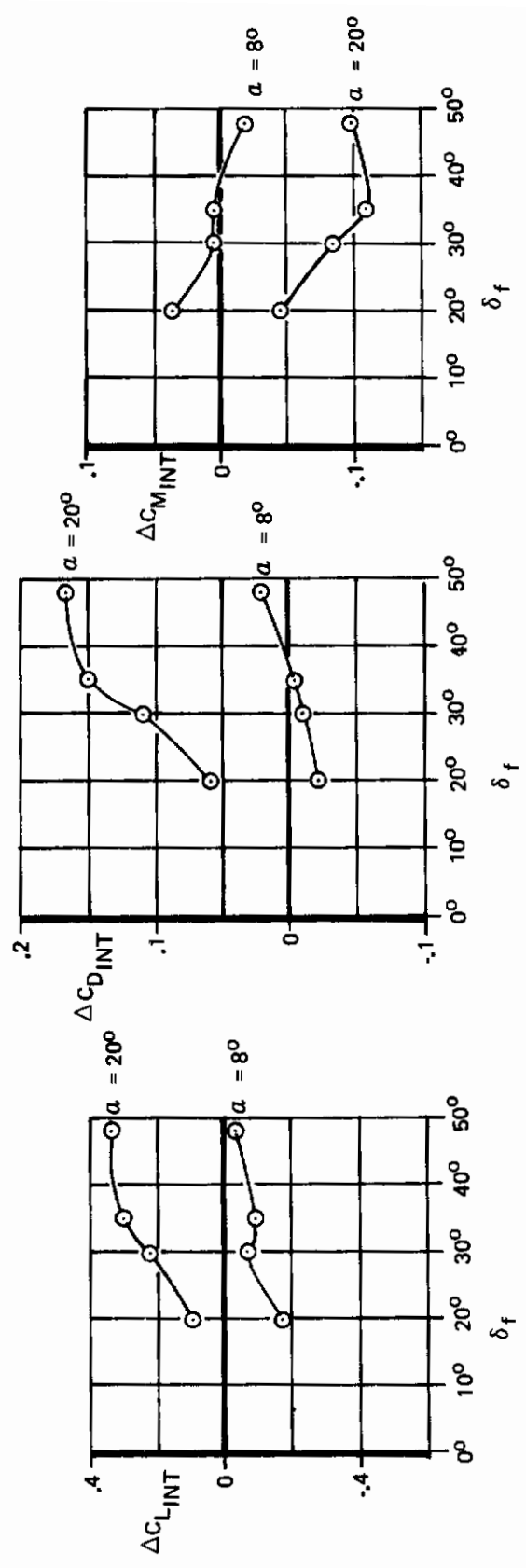


Figure 42: Effect of T.E. Flap Angle on Thrust Interference

Contrails

- o Lift interference becomes more favorable.
- o Drag interference becomes more unfavorable.
- o Pitching moment interference becomes more negative.

Note that these effects are similar to the effects observed when angle of attack is increased for a given flap angle. Indeed, the effect of increasing trailing-edge flap deflection is to create a wing flow field somewhat equivalent to an increase in α .

4.1.1.10 Wing Sweep

Figure 43 shows a comparison of the 30° and 15° wing sweep configuration thrust interference data. The following effects are noteworthy:

- o Lift Interference: At moderate α 's, the 15° sweep data shows more favorable thrust interference than the 30° sweep data. At higher α 's the 15° and 30° sweep data are at about the same level.
- o Drag Interference: The 15° sweep data generally shows more drag interference than 30° sweep at $\alpha = 8^\circ$, while the reverse is true at $\alpha = 20^\circ$.
- o Pitching Moment Interference: The 30° sweep shows a more positive interference at $\alpha = 8^\circ$ at $\sigma = 60^\circ$ and 90° . At $\sigma = 30^\circ$ the reverse is true. The 15° sweep shows a less negative interference than 30° sweep at $\alpha = 20^\circ$. Note that the reduction of the thrust vector from 60° σ to 30° σ shows a much more positive shift in pitching moment interference at 15° sweep than at 30° sweep.

4.1.1.11 Test Conditions

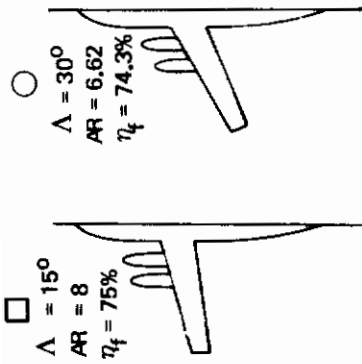
As discussed in Section 2.3, the majority of the vectored thrust testing was conducted at a dynamic pressure (q) = 22 psf which resulted in a freestream Reynolds number per foot (Re_∞/ft) = 0.82×10^6 and a Mach number (M_∞) = 0.12. However, five runs were conducted at $q = 10$ psf which yielded $Re_\infty/ft = 0.55 \times 10^6$ and $M_\infty = 0.08$ which allowed testing C_J up to 6.0. These data are shown in Figures 33 and 34, and also are compared to the $q = 22$ psf data in Figure 44. The other figures in Section IV (unless otherwise noted) are for $q = 22$ psf conditions.

The small change in freestream Mach number associated with the change in dynamic pressure is normally thought to be negligible and, as such, the differences illustrated in Figure 44 would then be due primarily to the change in freestream Reynolds number. However, it should be noted that the change in q also results in a change in the Mach number and Reynolds number of the jet flow. It has been found by many investigations that the main jet trajectory may be correlated with C_J , but the shape of the plume along the trajectory and associated jet mixing is dependent on M_{JET} and Re_{JET} . Therefore, some of the effects shown in

Contrails

Figure 44 are probably due to the change in the jet flow conditions as well as the remote flow. As shown in the figure, an increase in the test dynamic pressure caused:

- o A shift in the unfavorable direction in the lift interference.
- o A decrease in the drag interference for $C_J = 0$ to 1, but an increase in drag interference for C_J 's greater than 1.
- o A shift in the positive pitching moment interference direction.



$C_J = 2$
 Tail Off
 Free Air
 All Engines Operating
 $\delta_{LE} = 70^\circ$ $\eta_{ENG} = 27/43.5\%$
 $\delta_f = 35^\circ$ $M\bar{C} = 0.371$
 $C_{\mu_{LE}} = .06$ $X/C = 35\%$ (Nominal)

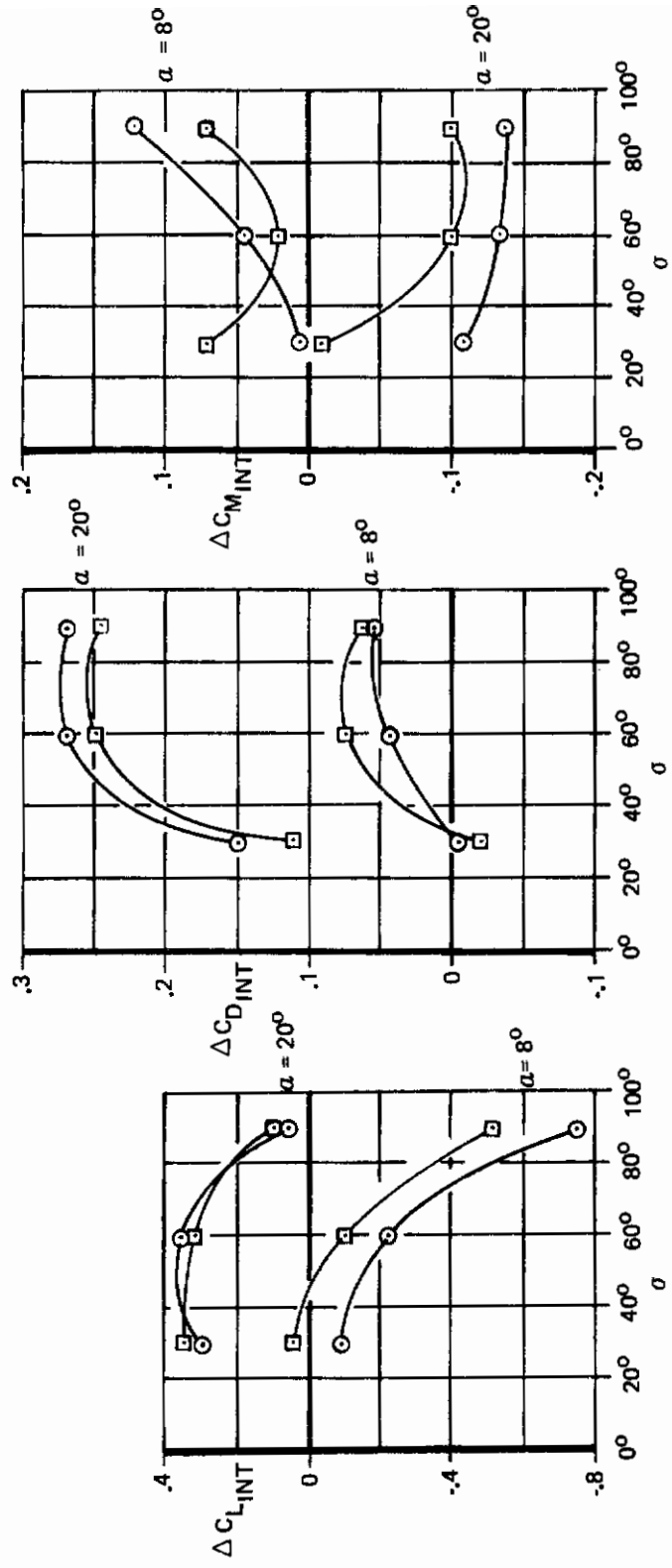


Figure 43: Effect of Sweep on Thrust Interference

$\Lambda = 30^\circ$
 $AR = 6.62$
 $\delta_f = 35^\circ$
 $\delta_{LE} = 70^\circ$
 Free Air

$\sigma = 60^\circ$
 $\eta = 74.3\%$
 $C_{\mu_{LE}} = .06$
 Tail Off
 All Engines Operating

$\eta_{ENG} = 27/43.5\%$
 $h/\bar{c} = 0.371$
 $X/C = 35\%$ (Nominal)

q psf	Re_∞/Ft	M_∞
$\times 10^7$	0.55×10^6	0.08
0.22	0.82×10^6	0.12

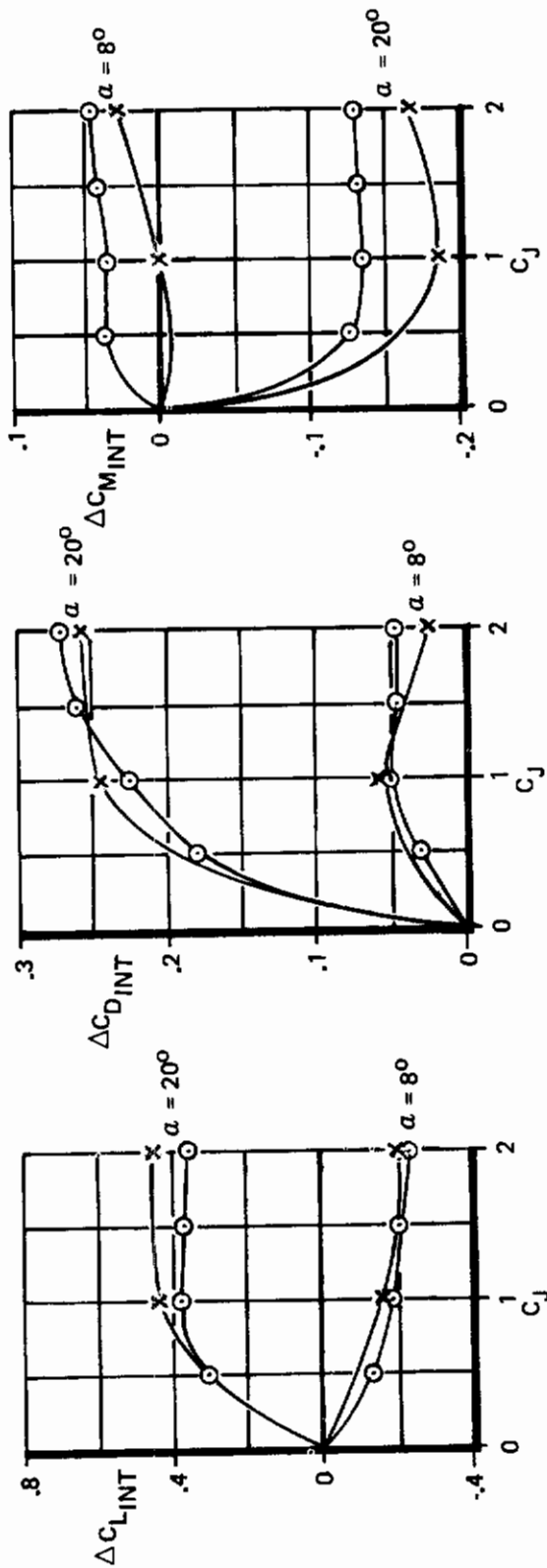


Figure 44: Effect of Test Conditions on Thrust Interference

4.1.2 Thrust Interference in Ground Effect

Table VIII summarizes the influence of ground proximity on the thrust interference terms for each of the principal parameters studied. (Ground effects on the overall longitudinal aerodynamics are discussed separately in Section 4.3.)

Most of the data is shown only at a 4° angle of attack, which represents an average of the range of α 's occurring during takeoff rotation or landing approach near touchdown. Reference 2 contains a complete set of the interference data obtained during the vectored thrust testing.

4.1.2.1 Ground Height

Figure 45 illustrates the change in the thrust interference terms, relative to the free air values, as the ground is approached. Comparison of the data shows the following effects as the airplane height above the ground is decreased from free air to a H/b of 0.24 (at $\alpha = 4^\circ$):

- o The unfavorable lift interference observed in free air becomes less unfavorable.
- o The slightly unfavorable drag interference observed in free air becomes favorable.
- o The positive pitching moment interference observed in free air decreases.

4.1.2.2 Angle of Attack

The influence of increasing the aircraft angle of attack while near the ground, demonstrates trends similar to those observed in free air. However, the effects are smaller in magnitude. (Compare Figure 46 to Figure 34.) Separation occurred on the undersurface of the wing, with flaps down, at angles less than 4° which resulted in large deviations of the data as shown by the $\alpha = 0^\circ$ and 2° data in Figure 46.

Increasing the angle of attack at $C_J = 2$ led to:

- o The unfavorable lift interference becomes less unfavorable.
- o The favorable drag interference becomes less favorable.
- o The positive pitching moment interference reduces.

4.1.2.3 Thrust Coefficient

Figure 46 illustrates the effect of increasing the thrust level at several angles of attack. Figure 45 presents a comparison of the data measured in ground effect versus the free air data at $\alpha = 4^\circ$.

Contrails

Table VIII: Effect of Vecteded Thrust on Thrust Interference in Ground Effect

PARAMETER	FIG.	LIFT INTERFERENCE	DRAG INTERFERENCE	PITCHING MOMENT INTERFERENCE (TAIL-OFF)
Ground Height o As the ground is approached @ α between 4° and 8° , $C_J = 2$	45	Interference is less unfavorable	Interference is less unfavorable	Interference is less positive.
Angle of Attack o Increasing α : @ $C_J = 2$	46	Interference becomes less unfavorable (trend similar to free air)	Interference becomes less favorable (trend similar to free air)	Interference becomes less positive (trend similar to free air)
Thrust Coefficient o Increasing thrust in ground effect: @ $\alpha = 4^\circ$	45 & 46	Unfavorable interference becomes more unfavorable from $C_J = 0$ to 1, less to 2. (Interference in ground than free air but trend is similar.)	Unfavorable interference increases from $C_J = 0$ to 0.5, then decreases to a favorable value at $C_J = 2$. (Interference in ground effect is less unfavorable than free air but trend is similar.)	Positive interference increases. (Interference in ground effect is less positive than free air but trend is similar.)
Thrust Vector Angle o Increasing σ : @ $\alpha = 4^\circ$ $C_J = 2$	47	In-ground-effect interference is less unfavorable (free air interference rapidly more unfavorable).	Interference is more unfavorable. (Trend similar to free air)	Positive interference increases (trend similar to free air)
Nacelle Location: @ $C_J = 2$ o Chordwise (moving nacelles aft):	48	Less unfavorable interference (trend similar to free air)	At low α 's aft nacelle is more favorable than mid nacelle. At $\alpha = 6^\circ$ and 8° both locations have same interference. (Aft location is more unfavorable in free air)	Mid nacelle has more positive interference than aft nacelle. (Trend similar to free air)
Type of Nacelles: o Single Pods vs Dual Pods (inboard mounted nacelles) @ $\alpha = 4^\circ$ $\sigma = 60^\circ$	49	Dual more favorable than single (Reverse trend in free air)	Dual has more drag than single (trend similar to free air)	Same. (Trend similar to free air)
One Engine Inoperative ($\alpha = 4^\circ$, $\sigma = 60^\circ$) (Also see Section 4.2)	50	Interference becomes less unfavorable. More unfavorable for outboard-out than inboard-out. (Trend similar to free air)	Favorable interference decreases slightly for inboard-out and increases for outboard-out. (Different than in free air)	Interference becomes less positive. More positive for outboard-out than inboard-out. (Trend similar to free air)
I.E. Flap Deflection o Increasing δ_f : @ $\alpha = 4^\circ$ $C_J = 2$	51	Interference becomes less unfavorable. (Similar to free air)	Interference becomes less favorable. (Similar to free air)	Interference becomes less positive. (Similar to free air)
Wing Sweep o Increasing Sweep from 15° to 30° : @ $\alpha = 4^\circ$ $C_J = 2$ $\sigma = 60^\circ$	52	Interference becomes more unfavorable. (Trend similar to free air)	Interference becomes more favorable. (Trend similar to free air)	No Change. (Free air interference more positive)

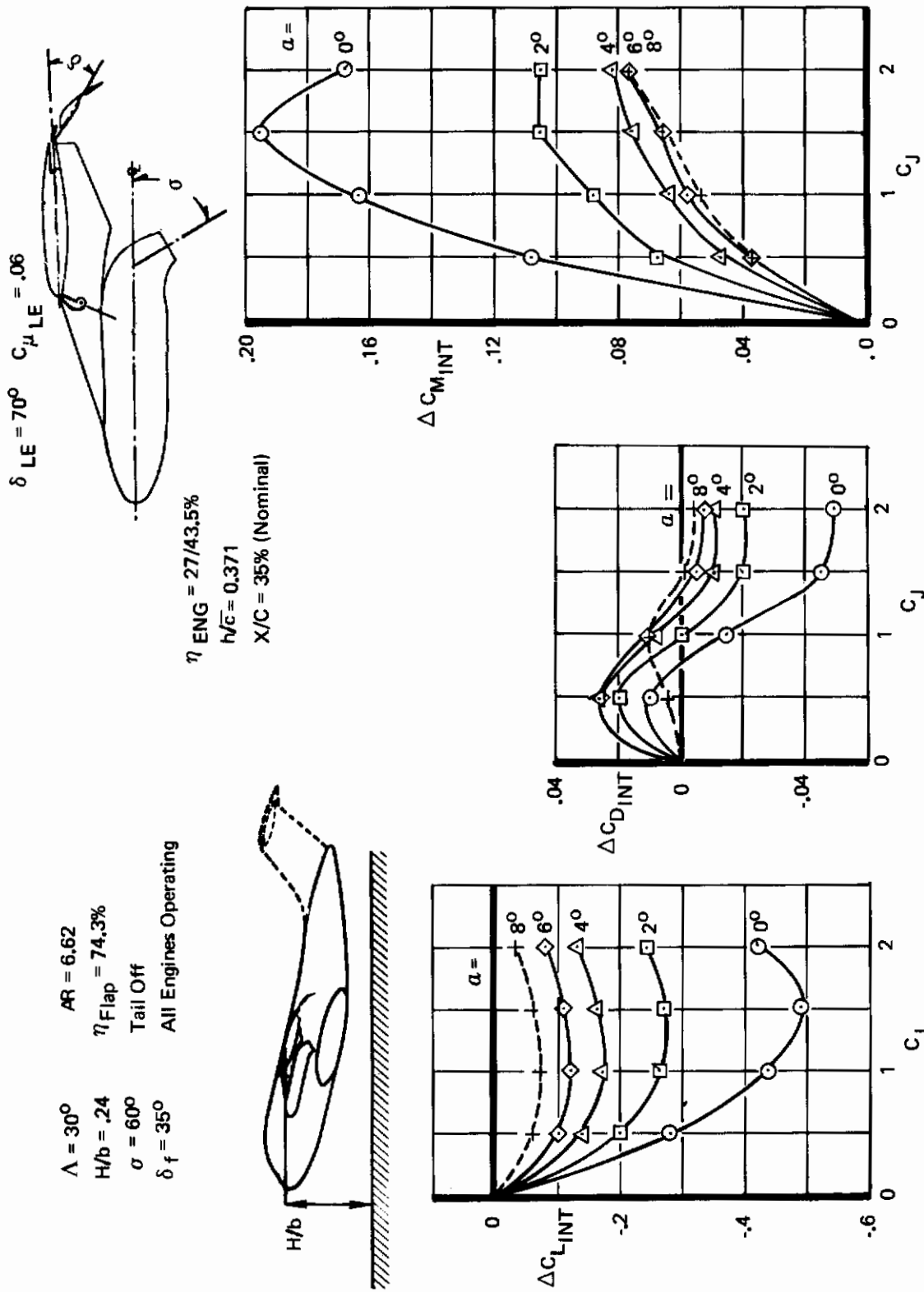


Figure 46: Effect of Thrust Coefficient on Thrust Interference in Ground Effect

As shown, the lift interference becomes more unfavorable as C_J increases at $\alpha = 4^\circ$. However, the in-ground-effect data reaches a minimum level near $C_J = 1.0$ while the free-air data continues in the unfavorable direction.

The $\alpha = 4^\circ$ drag interference shows a maximum unfavorable level at $C_J = 0.5$ and then reduces for both free-air and in-ground-effect data. However, the in-ground-effect data is less unfavorable at $C_J = 0.5$ and then reduces to a favorable level at $C_J = 2.0$ while the free air data interference is still unfavorable at $C_J = 2$.

The pitching moment interference trends at $\alpha = 4^\circ$ are quite similar (in ground effect vs. free air) but the in-ground-effect data reaches a less positive value at $C_J = 2$ than the free air value.

4.1.2.4 Thrust Vector Angle

The influence of rotating the thrust vector angle from 30° to 90° is illustrated in Figure 47. At $\sigma = 30^\circ$, the magnitudes of the lift, drag and pitching moment interference terms were similar for both the free air and the in-ground-effect condition. However, as σ increases to 90° , the unfavorable in-ground-effect lift interference reduces to zero while the unfavorable free-air lift interference becomes much more unfavorable.

The large difference between the in-ground-effect and the free-air data at large σ is due to the fact that the jet trajectory is quite different in ground effect compared to the trajectory in free air. At $\sigma = 60^\circ$, the jet impingement on the ground causes the jet to turn sooner than in free air. At $\sigma = 90^\circ$, some of the jet air was observed to actually move upstream along the ground plane for some distance (almost to the nose of the model). The favorable (negative) drag interference became unfavorable at $\sigma = 60^\circ$ in free air, while the in-ground-effect drag interference changed only slightly. However, at $\sigma = 90^\circ$, the in-ground-effect interference was more positive than the corresponding free-air data.

The positive pitching moment interference became more positive as σ increased in a similar manner for both free air and in ground effect conditions.

4.1.2.5 Nacelle Chordwise Location

Figure 48 illustrates the effect of moving the nacelles aft from the 35%c (mid) to the 70%c (aft) location. As shown, the aft location leads to more favorable lift and drag interference than the mid nacelle location. Pitching moment interference becomes less positive as the nacelles move aft.

4.1.2.6 Single Pods vs Dual Pods

Figure 49 presents a data comparison between the inboard dual pod configuration and the single pods in the inboard location. The following notes summarize the effects shown:

$\Lambda = 30^\circ$ $\delta_f = 35^\circ$
 $C_J = 2$
 $\alpha = 4^\circ$

AR = 6.62
 $\eta_{Flap} = 74.3\%$
 Tail Off
 All Engines Operating

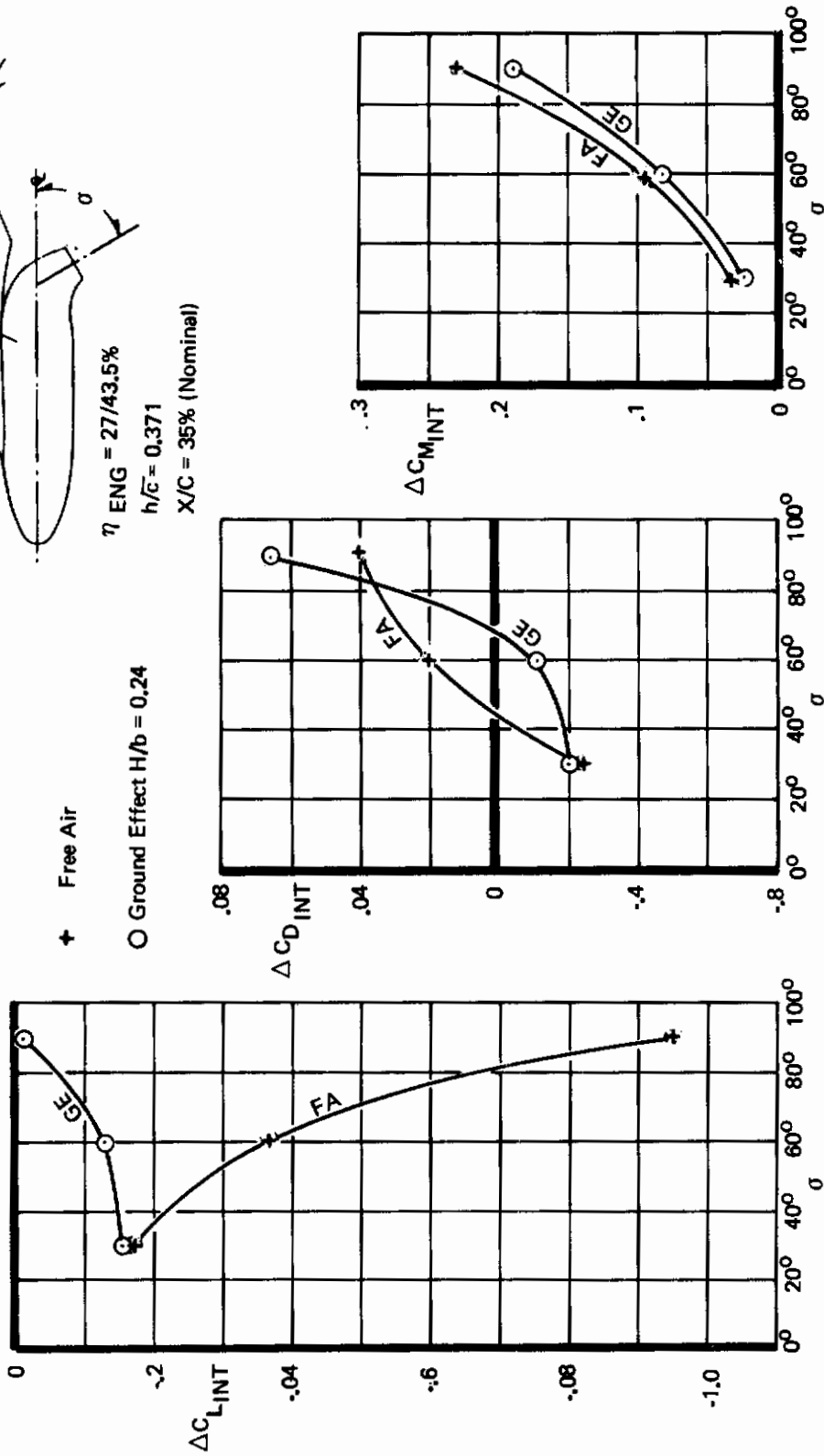
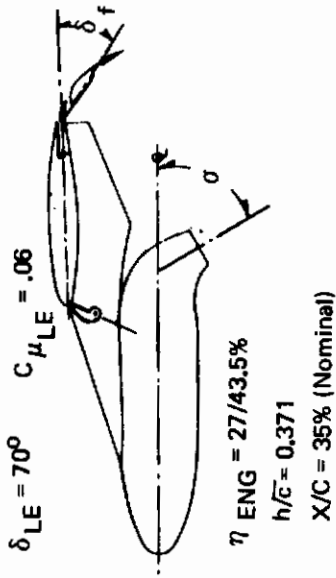
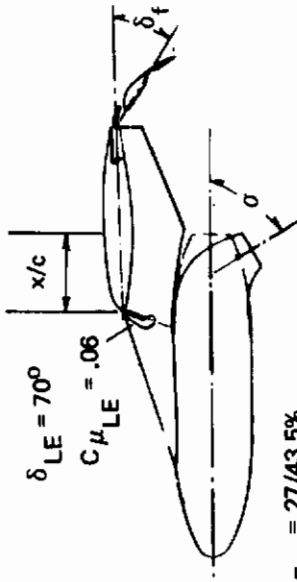


Figure 47: Effect of Thrust Vector Angle on Thrust Interference in Ground Effect versus Free Air



$\Lambda = 30^\circ$
 $AR = 6.62$
 $C_J = 2$
 $\eta_{Flap} = 74.3\%$
 Tail Off
 All Engines Operating

$\eta_{Eng} = 27/43.5\%$
 $h/c = 0.371$

$x/c \begin{cases} \bigcirc = 35\% \text{ (Mid)} \\ \square = 70\% \text{ (Aft)} \end{cases}$

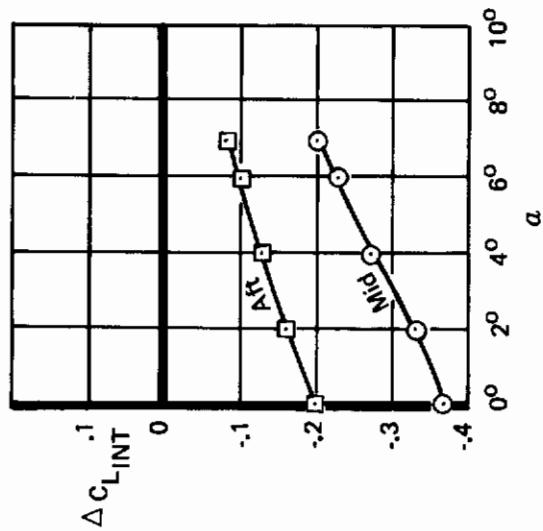
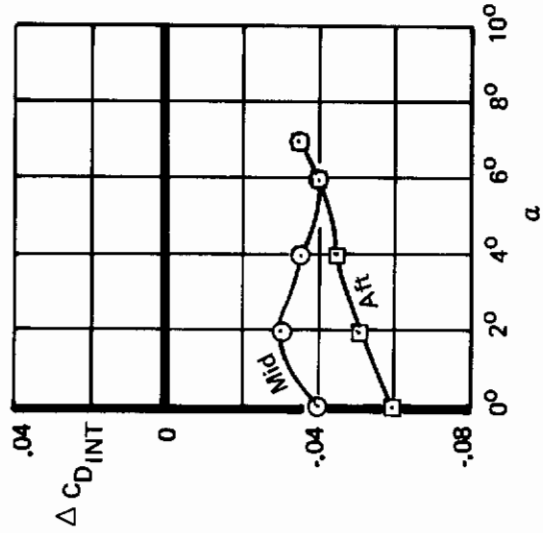
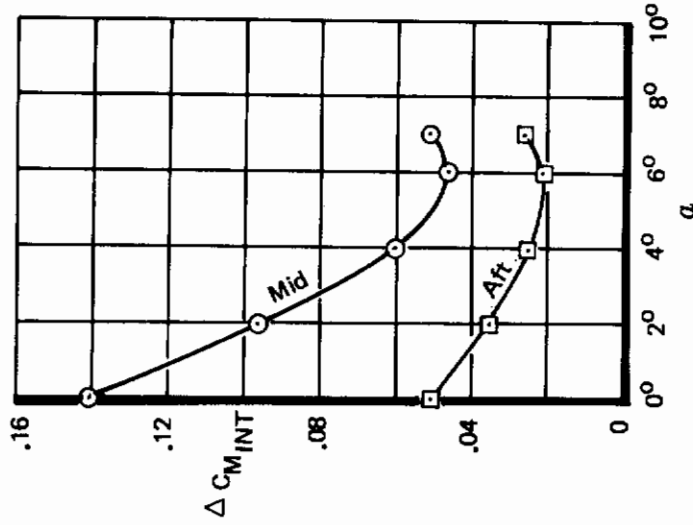
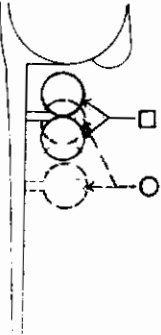


Figure 48: Effect of Nacelle Chordwise Location on Thrust Interference in Ground Effect

$\delta_{LE} = 70^\circ$ $C_{\mu_{LE}} = .06$

$\Lambda = 15^\circ$ $\delta_f = 35^\circ$
 $C_J = 2$ $\eta_{Flap} = 74.3\%$
 $\alpha = 4^\circ$ Tail Off
 $H/b = .21$ All Engines Operating



$x/c = 35\%$ (Nominal)

$h/\bar{c} = 0.406$

□ Dual Pods $\eta = 27\%$

○ Single Pods $\eta = 27/43.5\%$

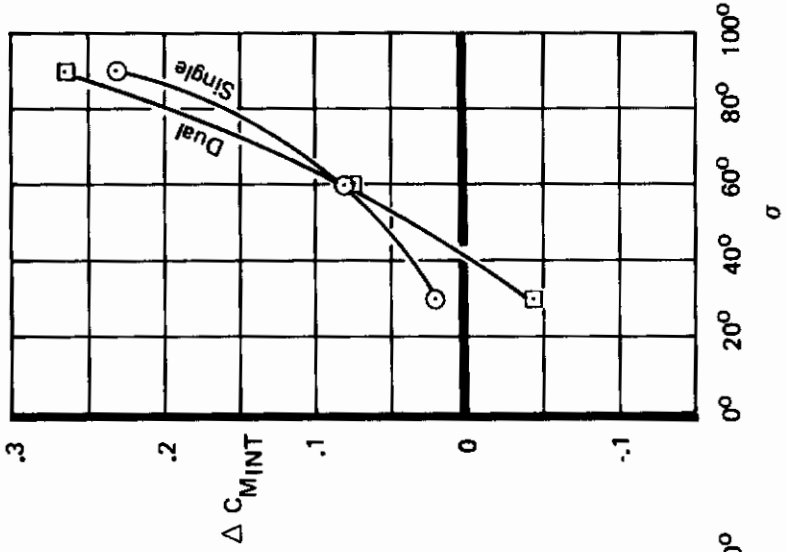
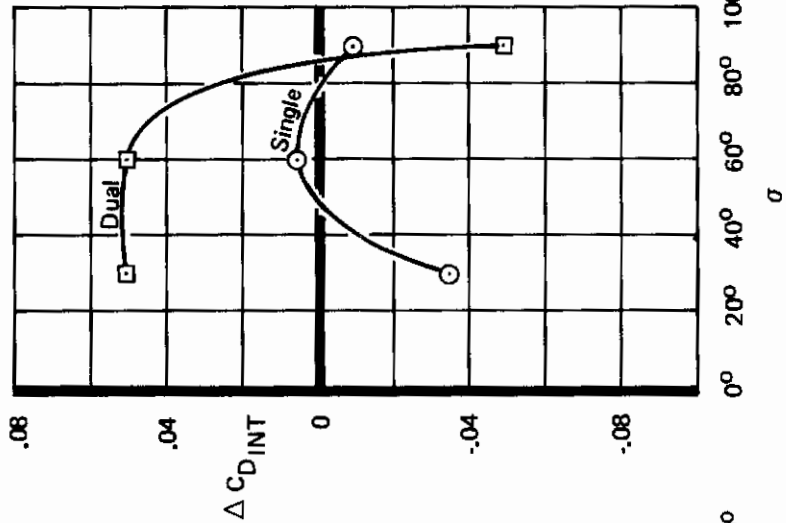
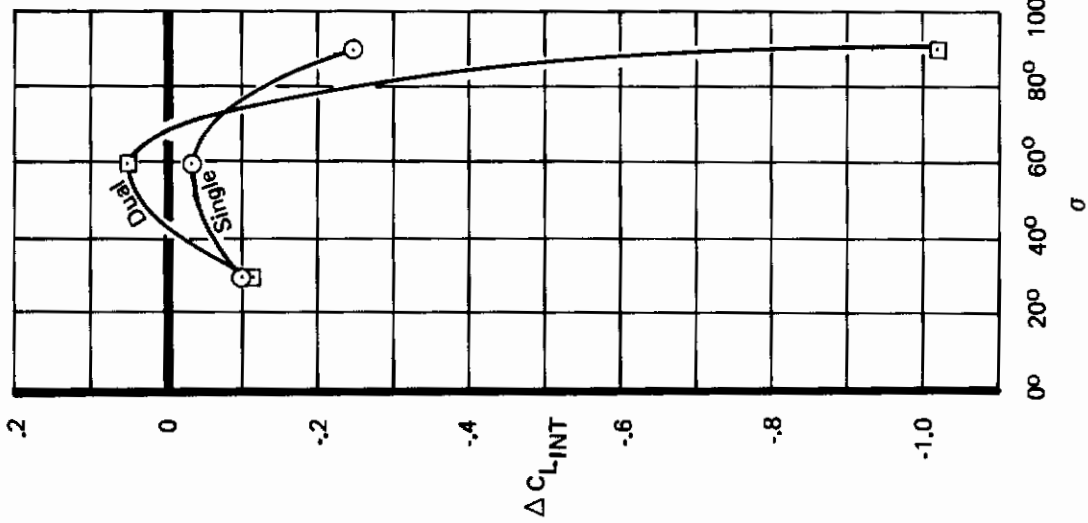


Figure 49: Single Pods versus Dual Pods, Thrust Interference in Ground Effect

At $\sigma = 30^\circ$

- o Lift interference is the same (unfavorable) for the single and dual pods.
- o Drag interference is unfavorable for the dual pods but favorable for the single pods.
- o Pitching moment interference is slightly positive for the single pods but slightly negative for the dual pods.

At $\sigma = 60^\circ$

- o Lift interference is slightly favorable for the dual pods but slightly unfavorable for the single pods.
- o Drag interference is more unfavorable for the dual pods than for the single pods.
- o Pitching moment interference is the same positive value for both pod configurations.

At $\sigma = 90^\circ$

- o Lift interference is much more unfavorable for the inboard dual pods than for the single pods.
- o Drag interference is more favorable for the dual pods than for the single pods.
- o Pitching moment interference is slightly more positive for the dual pods than for the single pods.

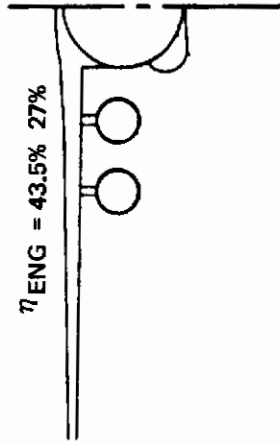
4.1.2.7 One Engine Inoperative

Figure 50 shows the effects of an engine failure on the longitudinal thrust interference in ground effect. As discussed in Section 4.1.1.8, the reduction in thrust interference is due to the loss of both the thrust interference induced by the engine which failed and the mutual interference experienced by two engines when operating side by side.

As is also indicated in free air (Section 4.1.1.8), the outboard engine has a greater influence on drag than does the inboard engine, but has less of an influence on lift and pitching moment.

4.1.2.8 Trailing-Edge Flap Angle

The influence of increasing the T.E. flap angle from $\delta_f = 20^\circ$ to $\delta_f = 48^\circ$ is presented in Figure 51. As shown, the difference between the in-ground-effect data and the free-air data is small.



$\alpha = 4^\circ$

$\sigma = 60^\circ$
 $\eta_f = 74.3\%$
 $C_{\mu_{LE}} = .06$
 Tail Off

Sweep $\Lambda = 30^\circ$
 $AR = 6.62$
 $\delta_f = 35^\circ$
 $\delta_{LE} = 70^\circ$
 $H/b = .24$

Engine Location
 $x/c = 35\%$ (Nominal)
 $h/c = .371$

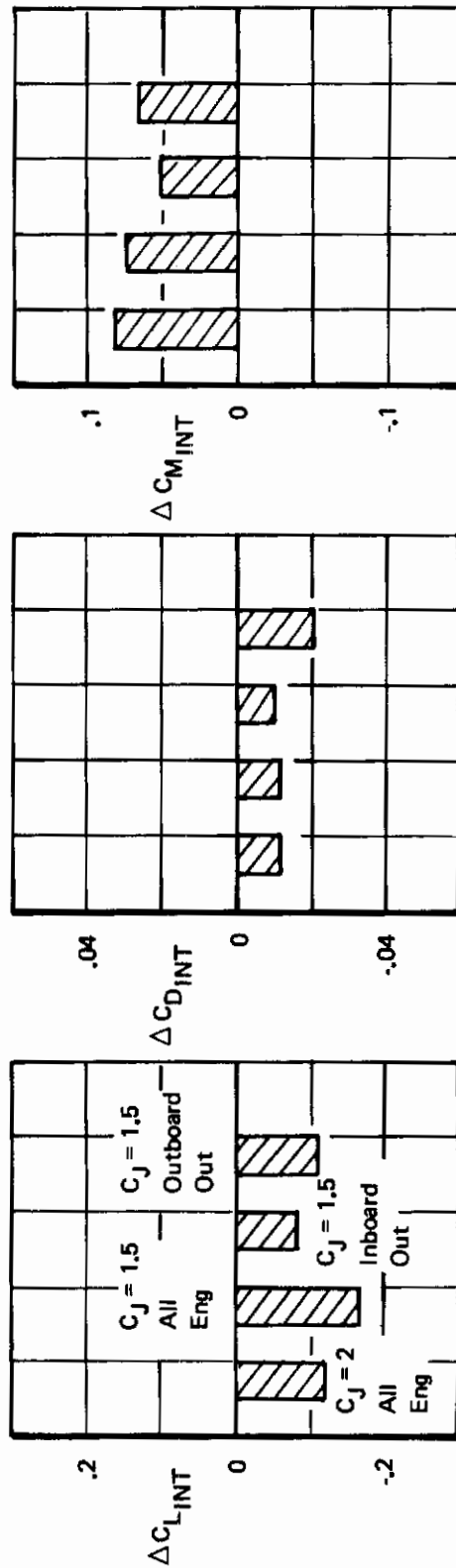
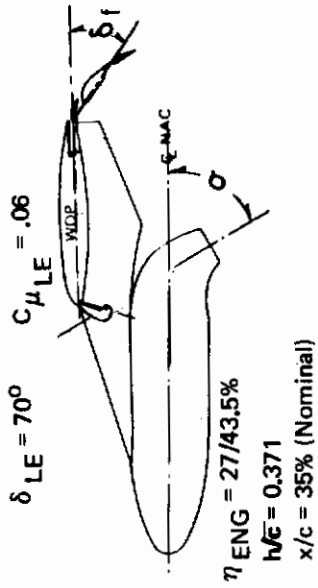


Figure 50: Effect of One Engine Failure on Thrust Interference in Ground Effect

$\Lambda = 30^\circ$
 $C_J = 2$
 $\alpha = 4^\circ$
 $\sigma = 30^\circ$

AR = 6.62
 $\eta_{Flap} = 74.3\%$
 Tail Off
 All Engines Operating



x Free Air
o Ground Effect $H/b = 0.24$

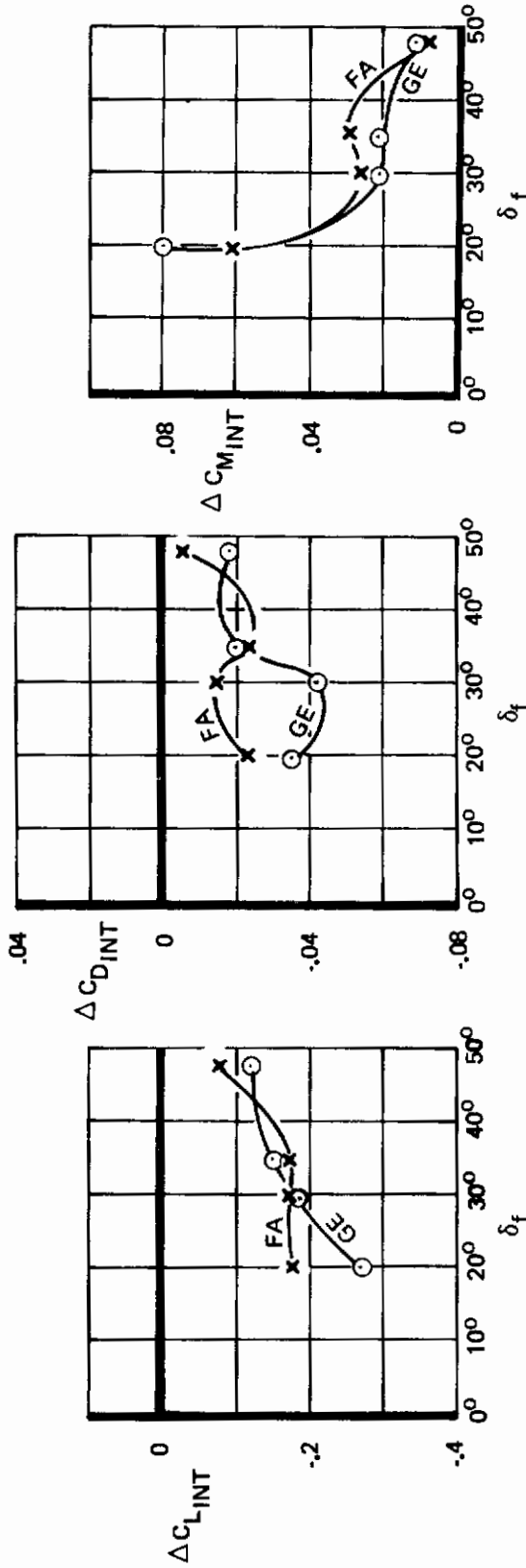


Figure 51: Effect of T.E. Flap Angle on Thrust Interference in Ground Effect versus Free Air

Increasing the flap deflection shows:

- o Less unfavorable lift interference.
- o Less favorable drag interference.
- o Less positive pitching moment interference.

4.1.2.9 Wing Sweep

Figure 52 shows a comparison of the data for the 30° and 15° wing sweep configurations.

- o Lift interference is more unfavorable for the 30° sweep than for the 15° sweep (both free-air and in-ground-effect) except at $\sigma = 90^\circ$. The jet impingement on the ground apparently influences the 15° sweep configuration differently than the 30° sweep.
- o Drag interference is more favorable for 30° sweep (at $\sigma = 60^\circ$) than for 15° sweep. At $\sigma = 30^\circ$ and 90° , the reverse occurs. These statements apply to both free-air and in-ground-effect conditions. The differences are small except at $\sigma = 90^\circ$ with 15° sweep.
- o Pitching Moment interference is generally the same for both sweeps in and out of ground effect.

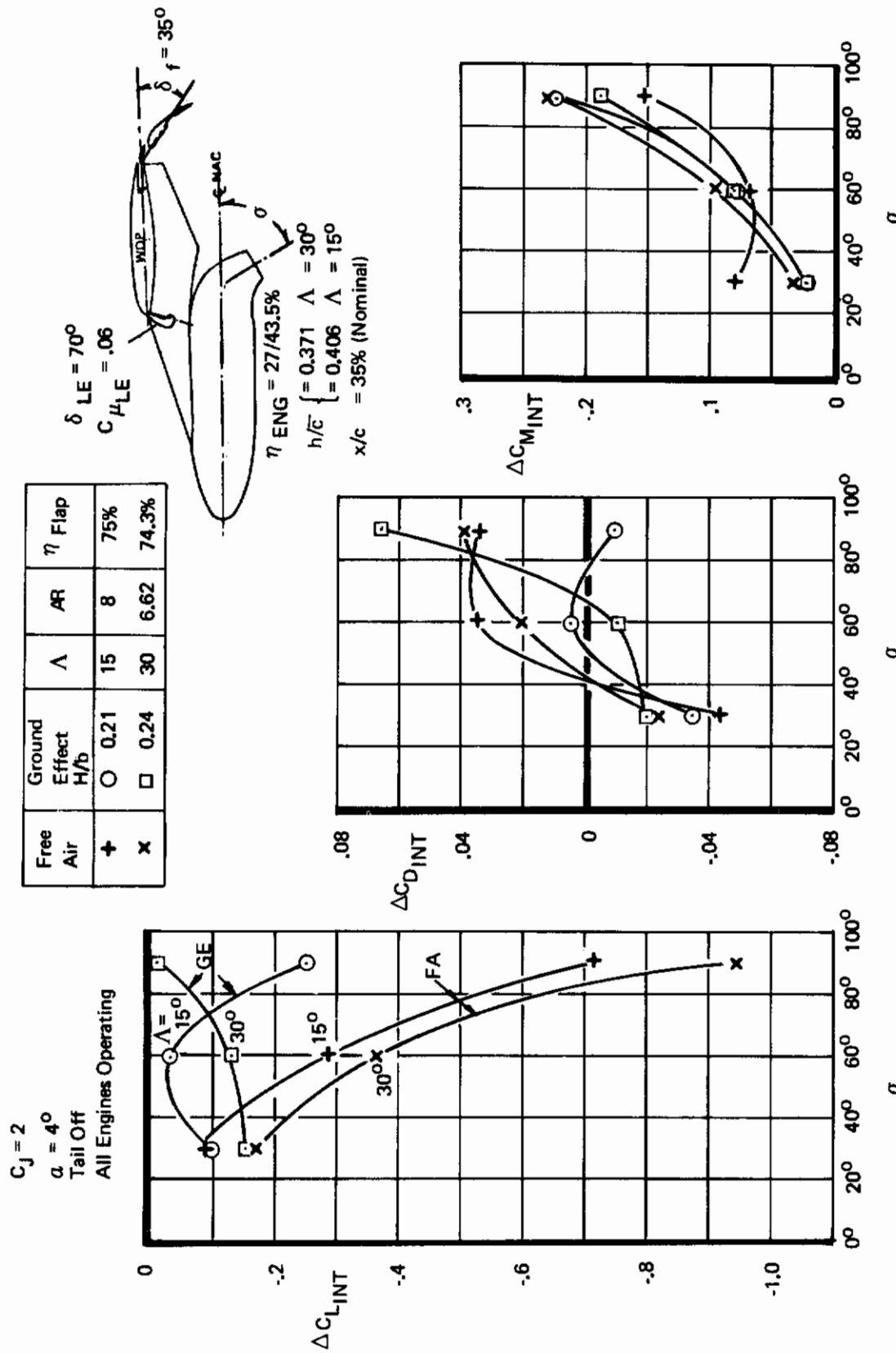


Figure 52: Effect of Sweep on Thrust Interference in Ground Effect versus Free Air

4.2 Engine-Out Thrust Interference

To evaluate control requirements due to engine failure, a series of tests were performed with the left-hand inboard or outboard engine inoperative. As noted in Section 4.1, the thrust interference effects on the aircraft are significant. This section analyzes the effects of the following variables on the thrust interference effects due to an engine failure:

- o Wing angle of attack
- o Thrust vector angle
- o Nacelle spanwise location
- o Trailing-edge flap angle
- o Wing sweep
- o Height above ground plane

Before continuing with this section, it is important that the concept of engine-out thrust interference effects be carefully defined. For example, assume the number one engine of a four-engine airplane has failed. We then speak of the interference effects due to a failed engine. Actually, however, the interference is due to the number four engine which continues to operate. The crucial point is that thrust interference must be caused by an engine developing thrust. So then, when thrust interference due to a failed engine is mentioned, remember that the effect is produced by the opposite engine which remains operative.

A summary of the thrust interference effects, engine out, is presented in Table IX.

4.2.1 Analysis Method

The aircraft response to an engine failure is mainly due to the rolling and yawing moments produced by the vectored thrust of the remaining operative engines. Additional moments occur, however, due to the aerodynamic forces induced on the aircraft by the vectored thrust (thrust interference forces).

Table IX: Effect of Airplane Variables on Engine-Out Thrust Interference

(Results apply to inboard or outboard engine failure, except as noted)

PARAMETER	FIG.	LIFT INTERFERENCE (One Engine)	DRAG INTERFERENCE (One Engine)	PITCHING MOMENT INTERFERENCE (One Engine)
Angle of Attack ($\sigma = 60^\circ$)	56,58	Unfavorable (negative) at low α . Favorable (positive) at high α . More favorable with increasing α .	Unfavorable (positive) at all α . More unfavorable with increasing α .	Positive at 102 α . Negative at high α . More negative with increasing α .
Increasing Thrust Vector Angle	56,58	$\alpha = 8^\circ$: Unfavorable interference becomes more unfavorable $\alpha = 20^\circ$: Favorable interference decreases	Inboard out: $\alpha = 8^\circ$ and 20° : Unfavorable interference increases from $\sigma = 30^\circ$ to 60° and decreases from $\sigma = 60^\circ$ to 90° Outboard out: $\alpha = 8^\circ$ and 20° : Unfavorable interference increases	$\alpha = 8^\circ$ Positive interference increases $\alpha = 20^\circ$ Negative interference becomes more positive from $\sigma = 30^\circ$ to 60° and more negative from $\sigma = 60^\circ$ to 90°
Nacelle Spanwise Location: As location of engine failure moves inboard ($\alpha = 8^\circ$):	60	Unfavorable interference becomes more unfavorable.	Unfavorable interference remains unchanged at $\sigma = 60^\circ$; at $\sigma = 30^\circ$ and 90° the unfavorable interference decreases.	Positive interference increases.
T.E. Flap Deflection: at $\alpha = 8^\circ$, as flap angle increases:	62	Unfavorable interference becomes more favorable.	Unfavorable interference increases.	Positive interference decreases.
Wing Sweep: Sweeping wing from 15° to 30° at $\alpha = 8^\circ$, $\sigma = 60^\circ$:	64,66	Becomes more unfavorable.	Unfavorable interference decreases.	Positive interference increases.
Ground Effect ($\alpha = 4^\circ$, $\sigma = 60^\circ$)	68,70	Unfavorable interference becomes more favorable in ground effect.	Unfavorable interference decreases slightly in ground effect.	Positive interference decreases slightly in ground effect.

Contrails

LATERAL-DIRECTIONAL THRUST INTERFERENCE

NOTE: A. Results apply to left wing inboard or outboard engine failure.

B. Favorable interference reduces engine out moments.

PARAMETER	FIG.	ROLLING MOMENT INTERFERENCE	YAWING MOMENT INTERFERENCE	SIDE FORCE INTERFERENCE
Angle of Attack, $\sigma = 60^\circ$	57,59	Favorable interference becomes unfavorable at high α .	Favorable interference increases with increasing α .	Unchanged by increasing α .
Increasing Thrust Vector Angle	57,59	$\alpha = 8^\circ$: Favorable interference increases $\alpha = 20^\circ$: Unfavorable interference becomes more favorable	$\alpha = 8^\circ$: Interference becomes more favorable $\alpha = 20^\circ$: Favorable interference increases	$\alpha = 8^\circ$ and 20° : Interference becomes more positive.
Nacelle Spanwise Location: As location of engine failure moves inboard ($\alpha = 8^\circ$):	61	Favorable interference increases	Interference relatively unchanged	At $\sigma = 30^\circ$, interference becomes more negative At $\sigma = 60^\circ$ and 90° , interference becomes more positive
T.E. Flap Deflection: At $\alpha = 8^\circ$, as flap angle increases:	63	Favorable interference decreases slightly	Unfavorable interference becomes more favorable	Positive interference decreases
Wing Sweep: Sweeping wing from 15° to 30° at $\alpha = 8^\circ$, $\sigma = 60^\circ$:	65, 67	Favorable interference increases slightly	Favorable interference decreases	Positive interference increases slightly
Ground Effect ($\alpha = 4^\circ$, $\sigma = 60^\circ$)	69,71	Favorable rolling moment decreases in ground effect	Unfavorable yawing moment becomes more unfavorable in ground effect	Positive interference increases in ground effect

Contrails

The equations below were used to determine the interference effects of a single engine. The quantities so defined must be subtracted from the all-engines operating interference to obtain the three-engines operating (OEI) values.

Longitudinal:

$$\Delta C_{L_{INT}}^{\text{One Engine}} = \Delta C_{L_{INT}}^{\text{All Engines Operating}} - \Delta C_{L_{INT}}^{\text{Three Engines Operating}}$$

$$\Delta C_{D_{INT}}^{\text{One Engine}} = \Delta C_{D_{INT}}^{\text{All Engines Operating}} - \Delta C_{D_{INT}}^{\text{Three Engines Operating}}$$

$$\Delta C_{M_{INT}}^{\text{One Engine}} = \Delta C_{M_{INT}}^{\text{All Engines Operating}} - \Delta C_{M_{INT}}^{\text{Three Engines Operating}}$$

Lateral-Directional:

$$\Delta C_{\ell_{INT}}^{\text{One Engine}} = \left[C_{\ell_{Gross}}^{\text{One Engine Out}} + \sum_{i=1}^4 C_{J_i} \cdot \sin(\alpha + \sigma) \cdot \frac{Y_i}{b} \right] - C_{\ell_{Gross}}^{\text{All Engines}}$$

$$\Delta C_{n_{INT}}^{\text{One Engine}} = \left[C_{n_{Gross}}^{\text{One Engine Out}} + \sum_{i=1}^4 C_{J_i} \cdot \cos(\alpha + \sigma) \cdot \frac{Y_i}{b} \right] - C_{n_{Gross}}^{\text{All Engines}}$$

$$\Delta C_{Y_{INT}}^{\text{One Engine}} = \left[C_{Y_{Gross}}^{\text{One Engine Out}} \right] - C_{Y_{All}}^{\text{Engines}}$$

Contrails

The bracketed terms [] are the net components and the Y dimension refers to the location of the nozzle thrust vector (of each of the four nacelles) with respect to the moment reference center. The dimension is listed in Section 2.2, Table IV, for each of the nacelle configurations tested. The all-engine thrust interference terms were determined as shown in Section 4.1.

For the rolling moment, yawing moment, and side force coefficients, the gross coefficients for all engines operating (which should be zero) are subtracted in order to account for unsymmetrical model or tunnel characteristics.

The lift interference for all engines operating is

$$\begin{aligned} \Delta C_{L_{INT}} &= \Delta C_{L_{INT}1} + \Delta C_{L_{INT}1,2} + \Delta C_{L_{INT}2} + \Delta C_{L_{INT}3} + \Delta C_{L_{INT}3,4} \\ \text{All} & \\ \text{Eng} & \\ & + \Delta C_{L_{INT}4} \end{aligned}$$

where,

$$\begin{aligned} \Delta C_{L_{INT}} &= \text{Interference lift induced on the model by the} \\ \text{All} & \quad \text{vectored thrust with all engines operating} \\ \text{Eng} & \end{aligned}$$

$$\begin{aligned} \Delta C_{L_{INT}} &= \text{The lift interference caused by an engine} \\ \text{i=1} \rightarrow \text{4} & \quad \text{as if operating alone} \end{aligned}$$

$$\begin{aligned} \Delta C_{L_{INT}} &= \text{The change in lift interference when two engines} \\ \text{1,2} & \quad \text{operate side by side (mutual interference) compared} \\ \text{3,4} & \quad \text{to the sum of each operating alone} \end{aligned}$$

Now, with the left wing outboard engine inoperative, the lift interference caused by that engine and the mutual interference between the two left wing engines are absent. Thus, the lift interference of the remaining three engines is:

$$\begin{aligned} \Delta C_{L_{INT}} &= \Delta C_{L_{INT}2} + \Delta C_{L_{INT}3} + \Delta C_{L_{INT}3,4} + \Delta C_{L_{INT}4} \\ \text{\#1 Engine} & \\ \text{Out} & \end{aligned}$$

Thus, the reduction in lift interference which occurs when Number 1 engine becomes inoperative is obtained by subtracting the three-engine interference from the all-engine interference:

Contrails

$$\begin{aligned} \Delta C_{L_{INT}} &= \Delta C_{L_{INT}} - \Delta C_{L_{INT}} \\ \text{One Engine} & \quad \text{All Engines} \quad \quad \text{\#1 Engine Out} \\ \text{(\#1 Engine out)} & & & \\ &= \Delta C_{L_{INT_1}} + \Delta C_{L_{INT_{1,2}}} \end{aligned}$$

Now, assuming symmetry, the lift interference for the left and right wing outboard engines are identical as is the mutual interference between the engines on the left and right wings. Thus,

$$\begin{aligned} \Delta C_{L_{INT}} &= \Delta C_{L_{INT_4}} + \Delta C_{L_{INT_{3,4}}} \\ \text{One Engine} & & & \\ \text{(\#1 Engine Out)} & & & \end{aligned}$$

The rolling moment thus obtained, shown schematically in Figure 53, is

$$\begin{aligned} \Delta C_{\ell_{INT}} &= -\Delta C_{L_{INT_{3,4}}} \cdot \frac{Y_{3,4}}{b} - \Delta C_{L_{INT_4}} \cdot \frac{Y_4}{b} \\ \text{One Engine} & & & \\ \text{(\#1 Engine Out)} & & & \end{aligned}$$

where,

Y = the effective moment arm measured positive out the right wing

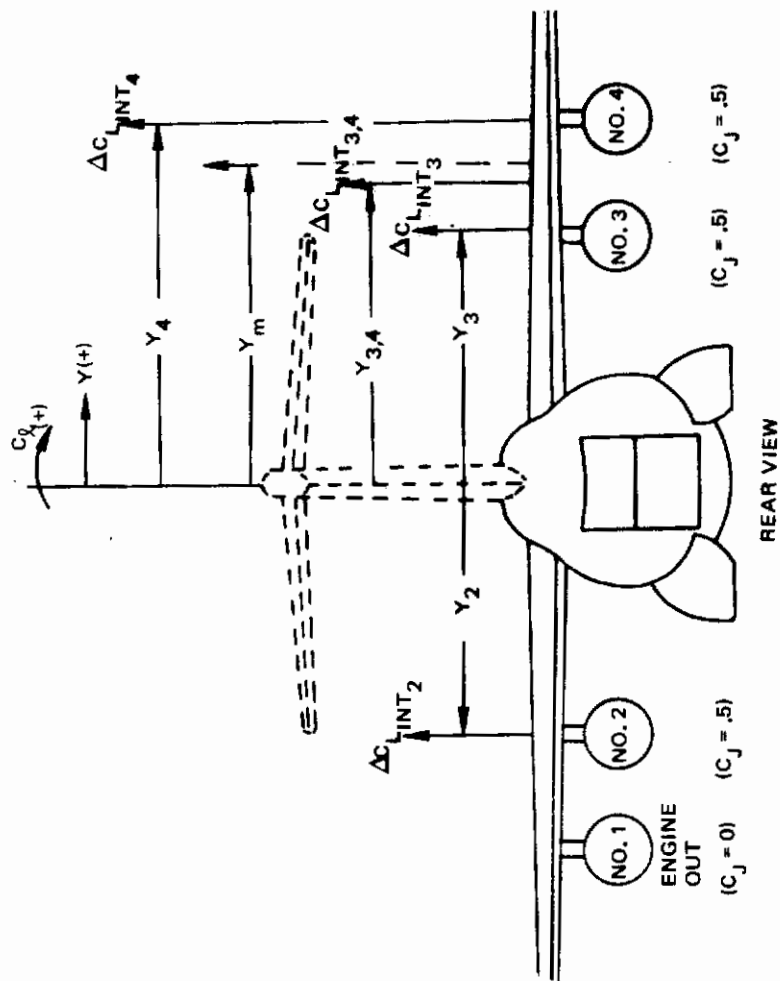
b = wing span

Similarly, the single engine lift interference and rolling moment obtained for a left wing inboard engine out are as follows,

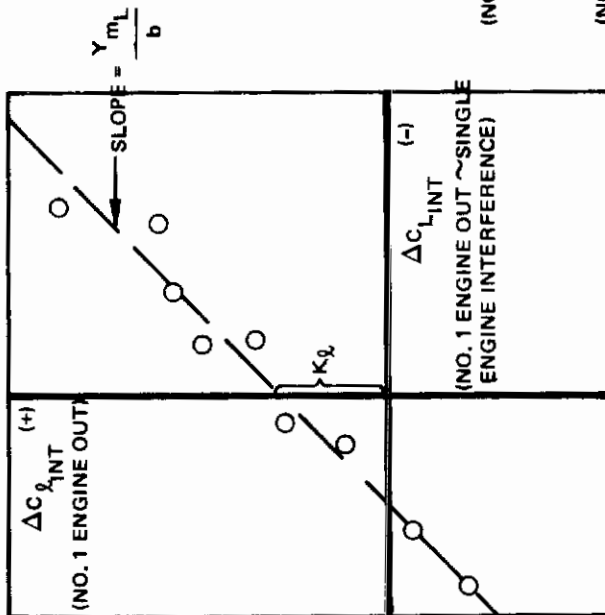
$$\begin{aligned} \Delta C_{L_{INT}} &= \Delta C_{L_{INT_3}} + \Delta C_{L_{INT_{3,4}}} \\ \text{One Engine} & & & \\ \text{(\#2 Engine Out)} & & & \end{aligned}$$

and

$$\begin{aligned} \Delta C_{\ell_{INT}} &= -\Delta C_{L_{INT_{3,4}}} \cdot \frac{Y_{3,4}}{b} - \Delta C_{L_{INT_3}} \cdot \frac{Y_3}{b} \\ \text{One Engine} & & & \\ \text{(\#2 Engine Out)} & & & \end{aligned}$$



REAR VIEW



$$K_{\phi} = \Delta C_{L_{INT_{3,4}}} \cdot \left(\frac{Y_4 - Y_{3,4}}{b} \right)$$

$$\Delta C_{\phi_{INT}} = -\Delta C_{L_{INT_4}} \cdot Y_4 - \Delta C_{L_{INT_{3,4}}} \cdot Y_{3,4}$$

(NO. 1 ENGINE OUT)

$$\Delta C_{L_{INT}} = \Delta C_{L_{INT_4}} + \Delta C_{L_{INT_{3,4}}}$$

(NO. 1 ENGINE OUT)

Figure 53: Rolling Moment Due to Lift Interference

Contrails

It should be emphasized that comparison of the all-engine thrust interference data in Section 4.1 with the engine-out data in this section for a single engine shows that the summation of the single engine interference data does not equal the all-engine interference:

$$\begin{array}{rcc} \Delta C_{L_{INT}} & \neq 2 \cdot (\Delta C_{L_{INT}}) & +2 \cdot (\Delta C_{L_{INT}}) \\ \text{All} & \text{Single Engine} & \text{Single Engine} \\ \text{Eng} & \text{Inboard Out} & \text{Outboard Out} \end{array}$$

This is due to the fact that the single engine thrust interference data defined herein includes the mutual interference terms for two engines operating side by side. In fact, the difference between the right and left hand sides of the above equation divided by two yields the mutual interference term:

$$\begin{array}{rcc} \Delta C_{L_{INT}} & = -\frac{1}{2} [\Delta C_{L_{INT}} & - (2 \cdot \Delta C_{L_{INT}} & + 2 \cdot \Delta C_{L_{INT}})] \\ \text{Mutual} & \text{All} & \text{Single Eng} & \text{Single Eng} \\ \text{Interference} & \text{Eng} & \text{Inboard Out} & \text{Outboard Out} \end{array}$$

Inspection of some of the test data has shown that the magnitude of the mutual interference term is on the order of +.02 to -.06 (for moderate angles of attack) for $\sigma = 30^\circ$ and 60° , respectively. A typical value for total lift interference for all engines operating is $\Delta C_{L_{INT}} = 0.0$ to $-.30$.

As shown schematically in Figure 53, the slope of a straight line faired through the data yields an effective moment arm through which the thrust interference on lift acts. Thus,

$$\begin{array}{rcc} \Delta C_{L_{INT}} & = -(\Delta C_{L_{INT}} & \frac{Y_{mL}}{b}) + K_{\ell} \\ \text{Engine Out} & \text{Engine Out} & \end{array}$$

In Figure 54, the engine-out rolling moment is plotted versus the engine-out lift interference for left wing inboard or outboard engine out. The small offset, K_{ℓ} , shown in Figure 53 and also noted in the test data in Figure 54 at $\Delta C_{L_{INT}} = 0$ is caused by the mutual interference between two engines operating side by side. The mutual interference also causes the nonlinearity in the test results.

Similarly, in Figure 55, the thrust interference on drag with an engine out is compared with the yawing moment. As shown, the slope of the line faired through the data yields the effective moment arm through which the interference drag acts. The resulting yawing moment is,

$$\Delta C_{n_{INT}} = (\Delta C_{D_{INT}} \cdot \frac{Y_{mD}}{b}) + K_n$$

	σ at $\alpha = 4^\circ, 8^\circ, 12^\circ, 16^\circ, 20^\circ, 24^\circ$
○	30°
□	60°
◇	90°

$\Lambda = 30^\circ$
 Tail Off
 Free Air
 $AR = 6.62$
 $\eta_{Flap} = 74.3\%$
 $\eta_{Eng} = 27/43.5\%$

$h/c = 0.371$
 $x/c = 35\%$ (Nominal)
 $\delta_{LE} = 70^\circ$
 $C_{\mu_{LE}} = .06$
 $\delta_{TE} = 35^\circ$

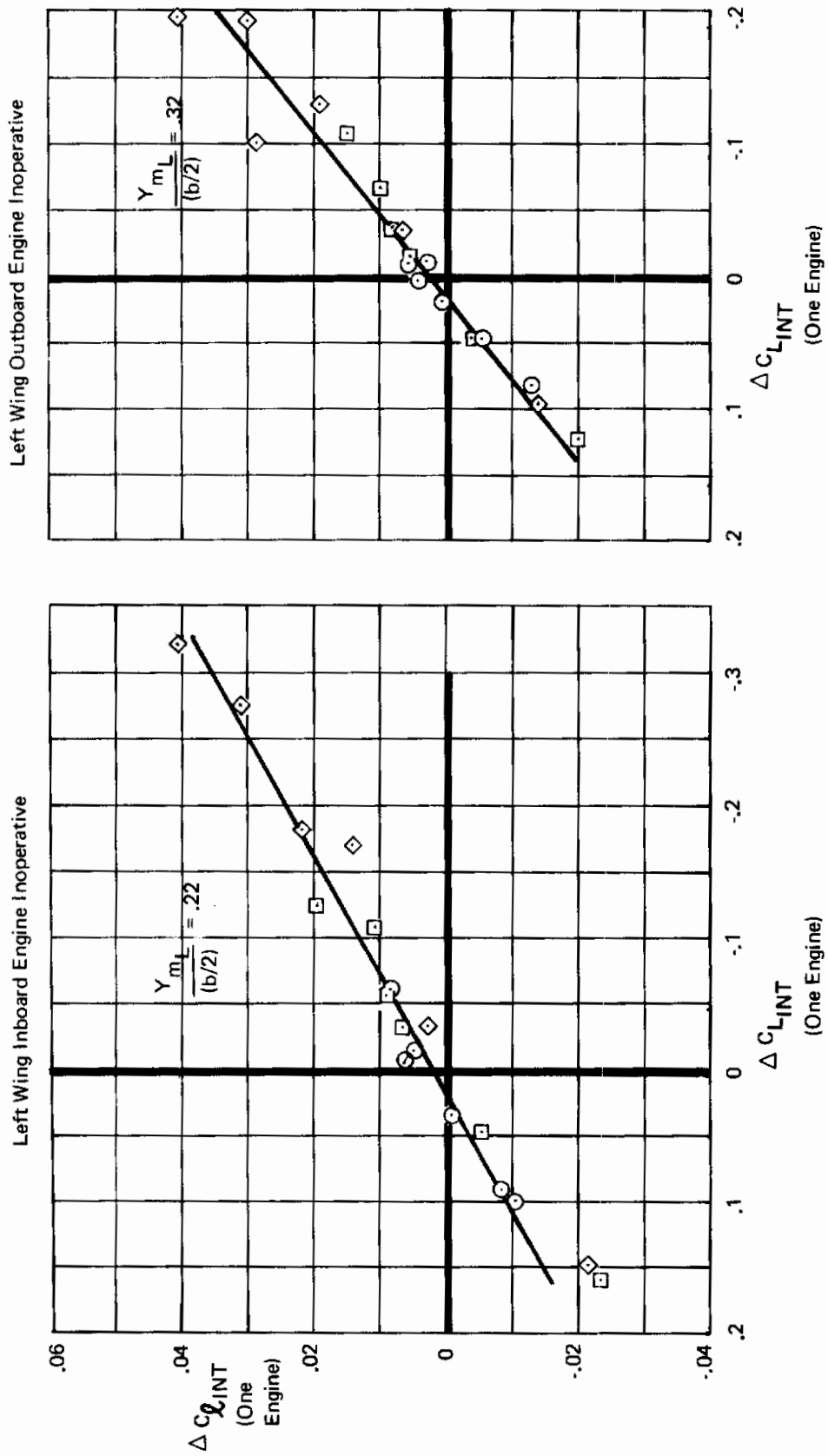


Figure 54 : Comparison of Rolling Moment and Lift Thrust Interference

$\Lambda = 30^\circ$
 Tail Off
 Free Air
 $AR = 6.62$
 $\eta_{Flap} = 74.3\%$
 $\eta_{Eng} = 27/43.5\%$
 $h/\bar{c} = 0.371$
 $x/c = 35\%$ (Nominal)
 $\delta_{LE} = 70^\circ$
 $C_{\mu LE} = .06$
 $\delta_{TE} = 35^\circ$

SYMBOLS	σ AT $\alpha =$
○	$4^\circ, 8^\circ, 12^\circ$ $16^\circ, 20^\circ, 24^\circ$
□	30
◇	60
	90°

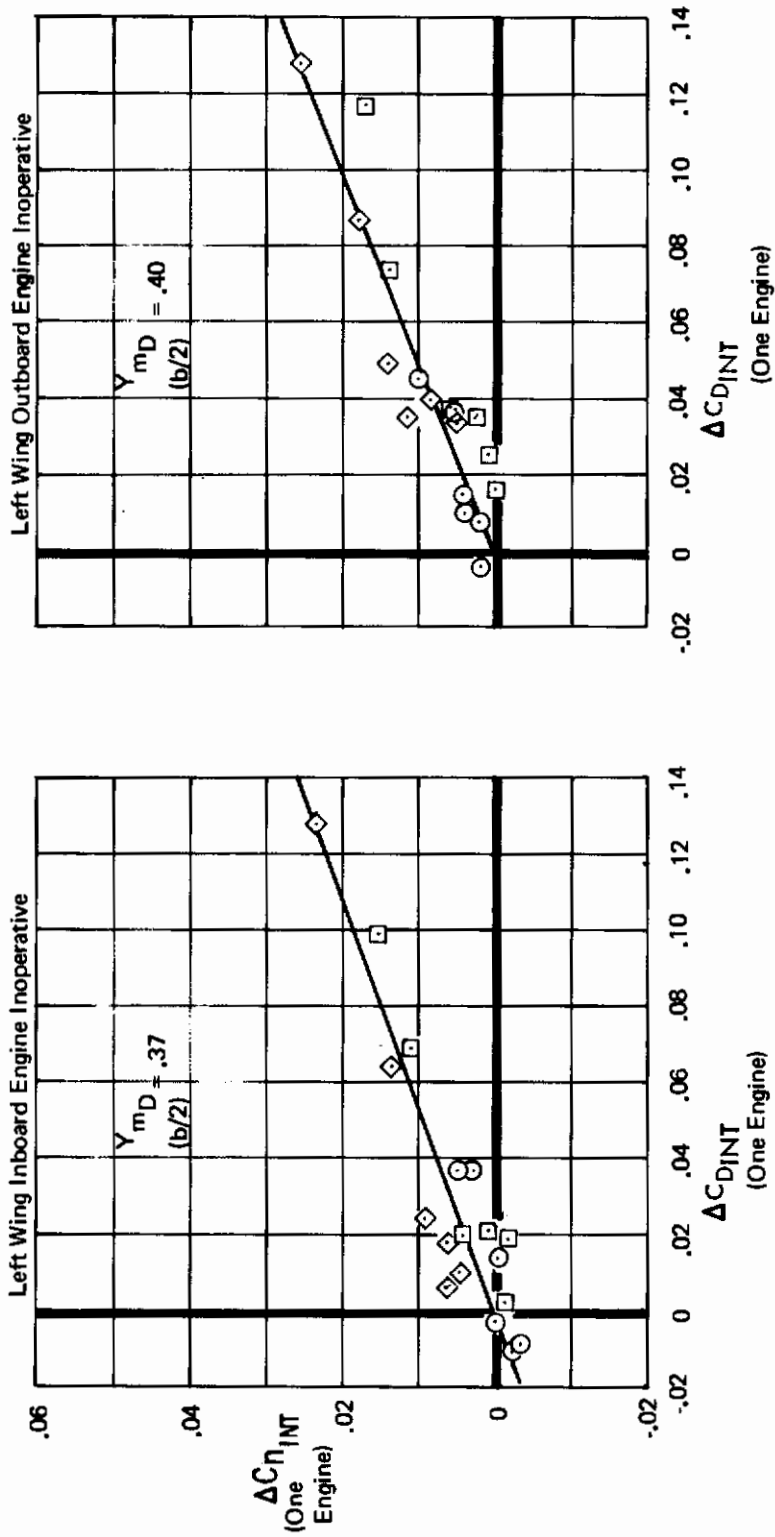


Figure 55: Comparison of Yawing Moment and Drag Thrust Interference

Contrails

The effective moment arms shown in Figures 54 and 55 were determined utilizing the engine-out test results with the engines located at 27% and 43.5% of the wing semi-span. In order to relate the center of the lift interference to the actual engine locations, the effective moment arms must be related to the wing semi-span as follows,

$$\text{SLOPE} = \frac{Y_{m_L}}{b}$$

and

$$2 \cdot (\text{SLOPE}) = Y_{m_L} / (b/2)$$

Thus, for an inboard engine failure (located at $.27 b/2$), the centers of the lift interference and drag interference are at $.22$ and $.37 b/2$, respectively. For an outboard engine failure (located at $.435 b/2$), the centers of the lift interference and drag interference are at $.32$ and $.40 b/2$, respectively.

4.2.2 Engine-Out Test Results

The effects of the principal variables on the thrust interference terms are presented in this section. As discussed in the previous section, the interference forces presented are the single engine thrust interference terms. In the case of lift, drag and pitching moment, these terms were obtained by subtracting the thrust interference with three engines operating from the thrust interference with all engines operating. Most of the test data are presented at $\alpha = 8^\circ$ representing a normal landing approach condition.

In the previous section, the analyses showed that the rolling moment and yawing moments were a direct function of lift and drag, respectively. Therefore, in this section emphasis will be placed on the lift and drag interference forces.

4.2.2.1 Thrust Vector Angle and Angle of Attack

Figures 56 through 59 illustrate the effects of angle of attack and thrust vector angle on the thrust interference terms. The inoperative engine is on the left wing.

For an inboard engine out (Figures 56 and 57), the lift interference becomes more positive at the higher angles of attack resulting in rolling moments which add to the moment due to vectored thrust alone.

The increase in drag at the higher angles of attack is partially due to the induced drag caused by the increased lift interference. The yawing moment follows the same trends as the drag and produces moments at the higher angles of attack which oppose the yawing moment due to thrust.

$\Lambda = 30^\circ$
 Tail Off
 Free Air
 $AR = 6.62$
 $\eta_{Eng} = 27/43.5\%$
 $h/\bar{c} = 0.371$
 $x/c = 35\%$ (Nominal)
 $\delta_{LE} = 70^\circ$
 $C_{\mu_{LE}} = .06$
 $\delta_{TE} = 35^\circ$

Left Wing Inboard Engine Inoperative
(Single Engine Thrust Interference)

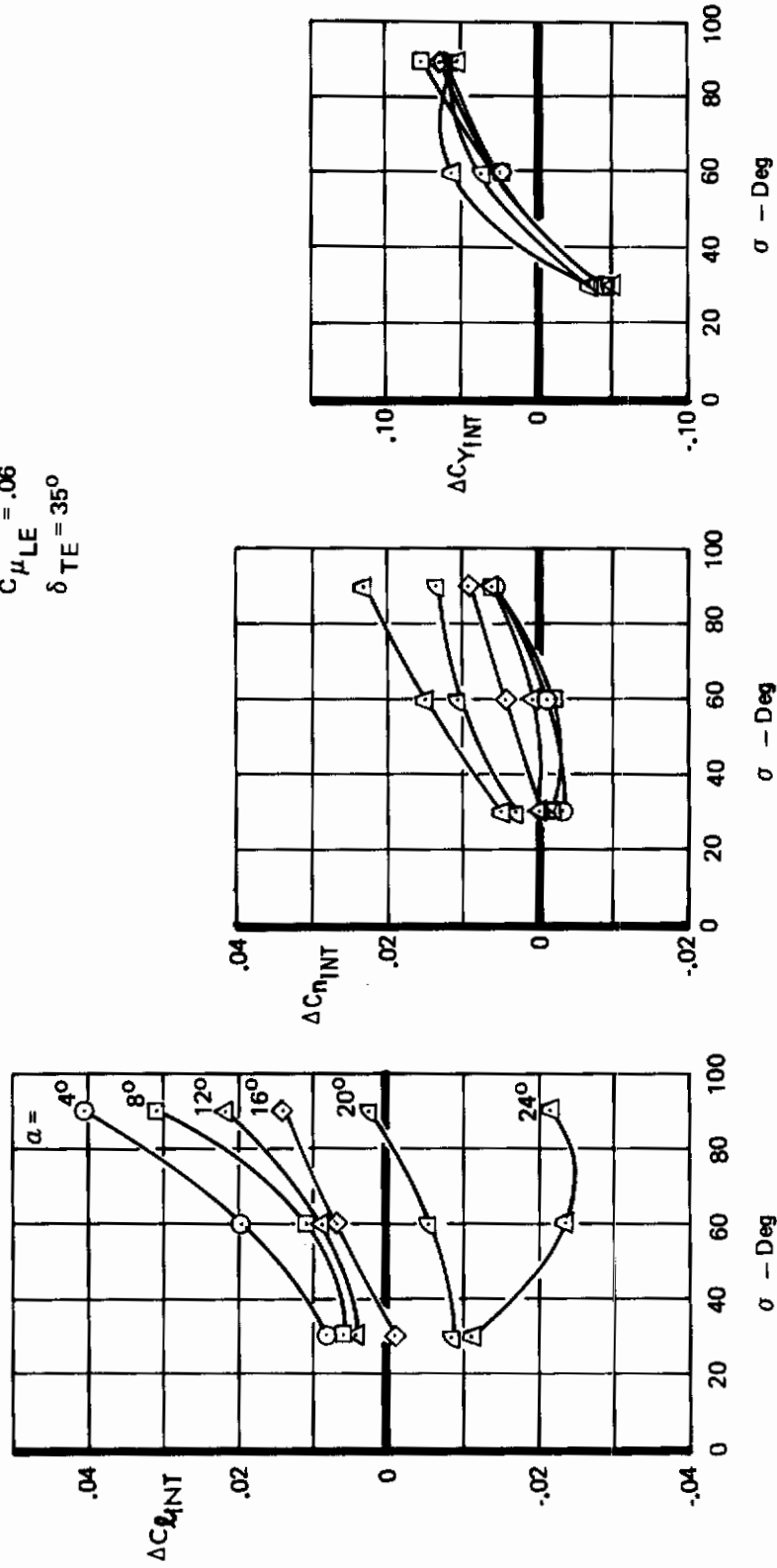
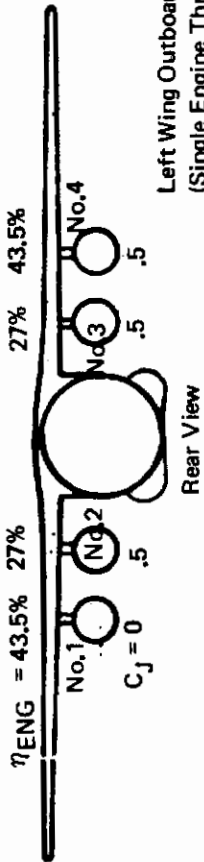


Figure 57: Lateral-Directional Thrust Interference, Effect of Q and σ , Inboard Engine Out

$\Lambda = 30^\circ$
 Tail Off
 Free Air
 $AR = 6.62$
 $\eta_{Flap} = 74.3\%$
 $h/c = 0.371$
 $x/c = 35\%$ (Nominal)
 $\delta_{LE} = 70^\circ$
 $C_{\mu_{LE}} = .06$
 $\delta_{TE} = 35^\circ$



Left Wing Outboard Engine Inoperative
(Single Engine Thrust Interference)

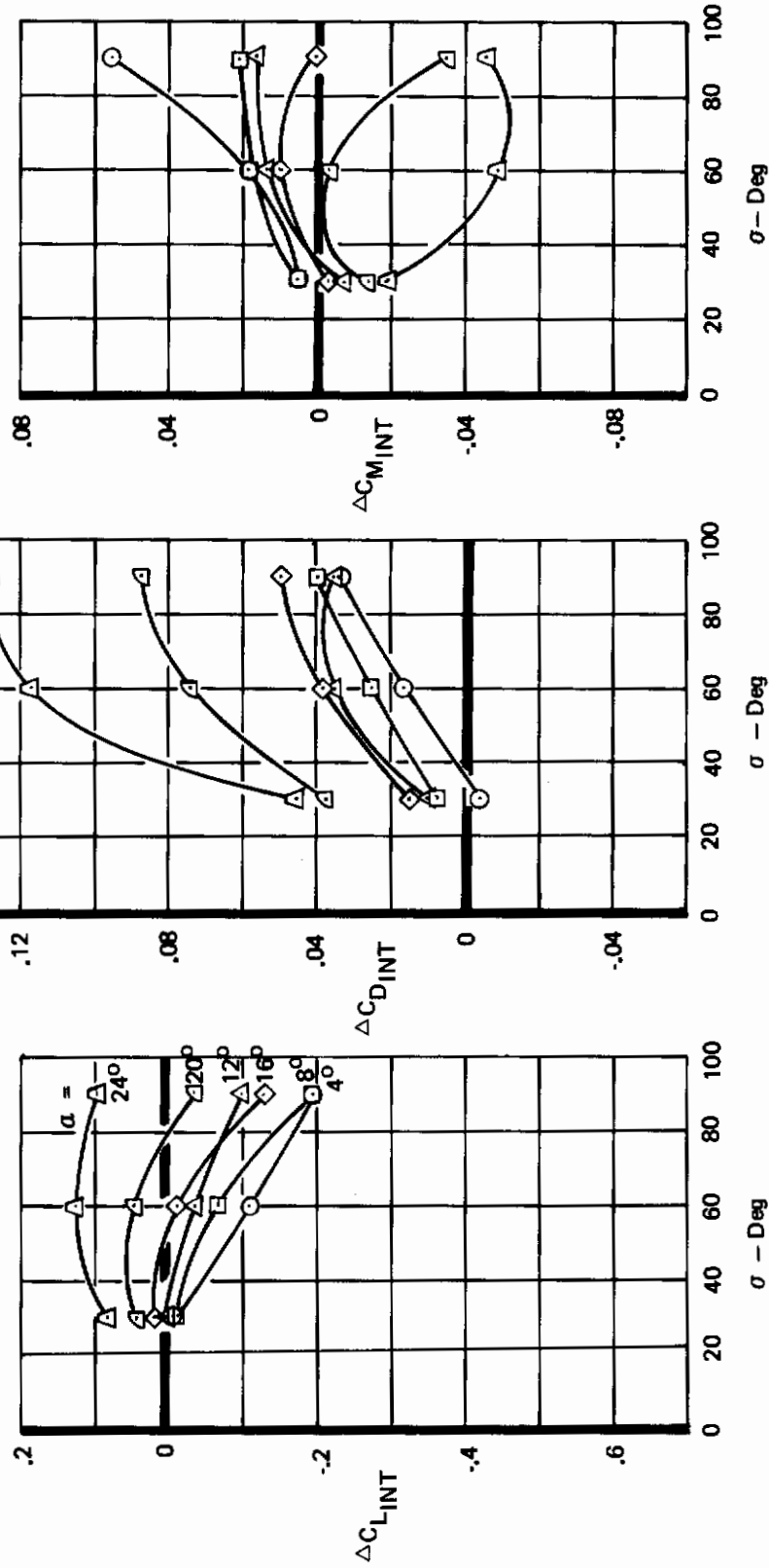


Figure 58: Longitudinal Thrust Interference, Effect of α and σ , Outboard Engine Out

$\Lambda = 30^\circ$
 Tail Off
 Free Air
 $AR = 6.62$
 $\eta_{Flap} = 74.3\%$
 $\eta_{Eng} = 27/43.5\%$
 $h/c = 0.371$
 $x/c = 35\%$ (Nominal)
 $\delta_{LE} = 70^\circ$
 $C_{\mu_{LE}} = .06$
 $\delta_{TE} = 35^\circ$

Left Wing Outboard Engine Inoperative
(Single Engine Thrust Interference)

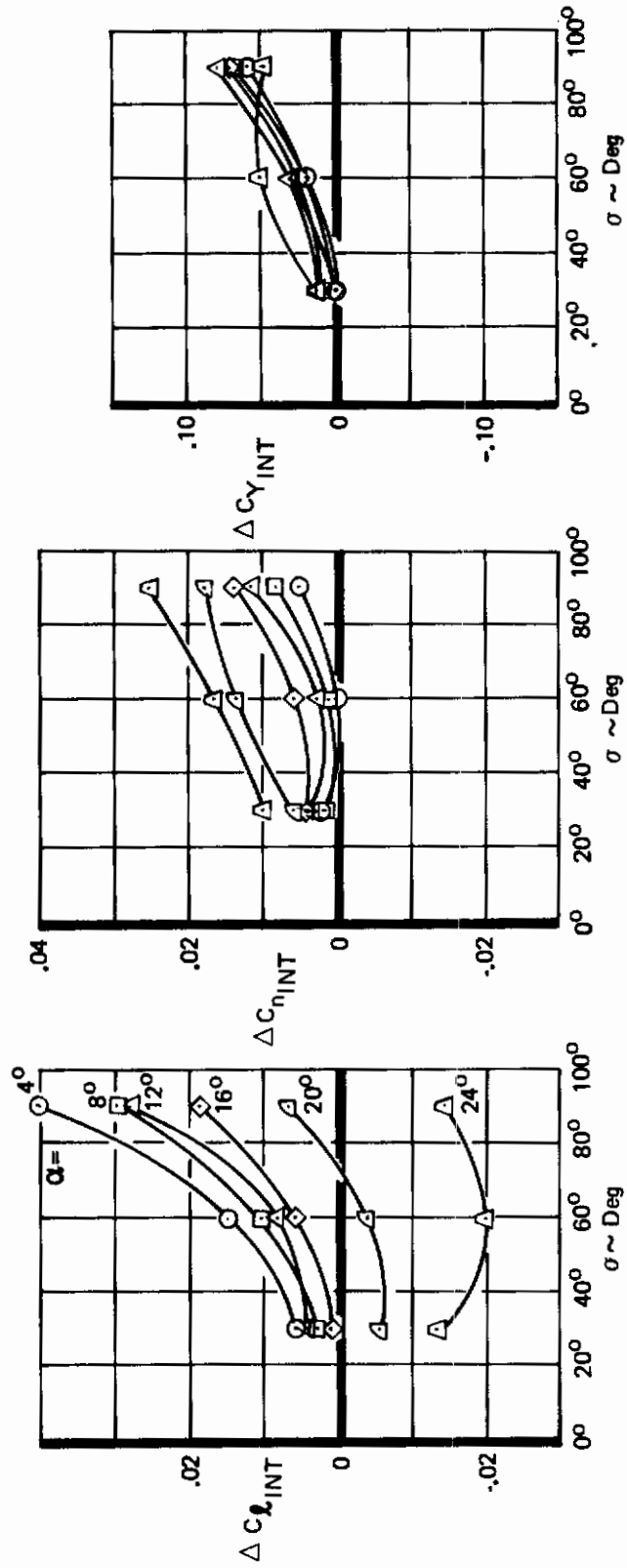


Figure 59: Lateral-Directional Thrust Interference, Effect of α and σ , Outboard Engine Out

The pitching moment is stabilizing at the higher angles of attack and destabilizing at the lower angles. The side force interference terms appear to be independent of angle of attack but significantly affected by thrust vector angle.

All of the thrust interference terms are functions of thrust vector angle. Increasing the thrust vector angle generally produces the following results:

- o Lift interference decreases
- o Drag interference increases
- o Pitching moment interference is variable, becoming more positive at medium vector angles and more negative at high vector angles.
- o Rolling moment, yawing moment, and side force become more positive.

For an outboard engine out (Figures 58 and 59), the thrust interference terms follow the same trends as for the inboard engine-out test results.

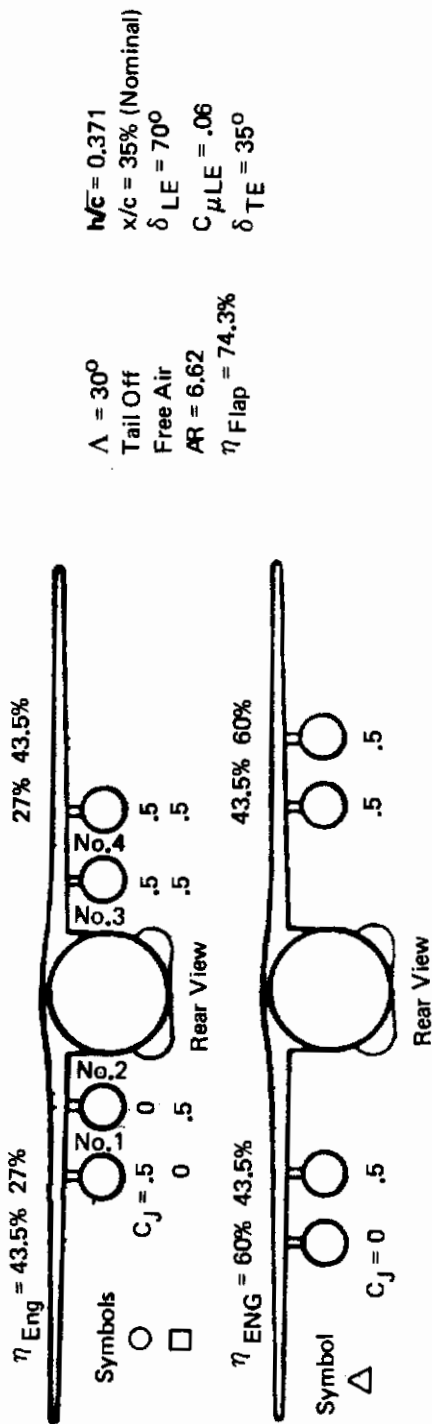
4.2.2.2 Nacelle Spanwise Location

Figures 60 and 61 show the effect of nacelle spanwise location on the single engine thrust interference data. As the location of the inoperative engine moves toward the wing tip, the following results are indicated:

- o Lift interference becomes less unfavorable, resulting in less favorable rolling moments.
- o Drag becomes more positive moving from inboard to mid position. Drag reduces moving from mid to outboard position.
- o Pitching moment decreases.
- o Rolling moment decreases.
- o Yawing moment trends are similar to the drag trends.
- o Side force interference becomes more positive at $\sigma = 30^\circ$ and becomes more negative at $\sigma = 60^\circ$ and 90° .

4.2.2.3 Effect of Flap Deflection

Figures 62 and 63 show the effect of increasing the trailing-edge flap deflection on the thrust interference data. The lift, yawing moment, rolling moment and side force results are, in general, only slightly affected by the flap angle for an inboard or outboard engine out. The interference drag increases with flap setting and the pitching moment becomes more negative.



$\Lambda = 30^\circ$
 Tail Off
 Free Air
 $AR = 6.62$
 $\eta_{Flap} = 74.3\%$
 $M\bar{c} = 0.371$
 $x/c = 35\%$ (Nominal)
 $\delta_{LE} = 70^\circ$
 $C_{\mu LE} = .06$
 $\delta_{TE} = 35^\circ$

Single Engine Thrust Interference $\alpha = 8^\circ$

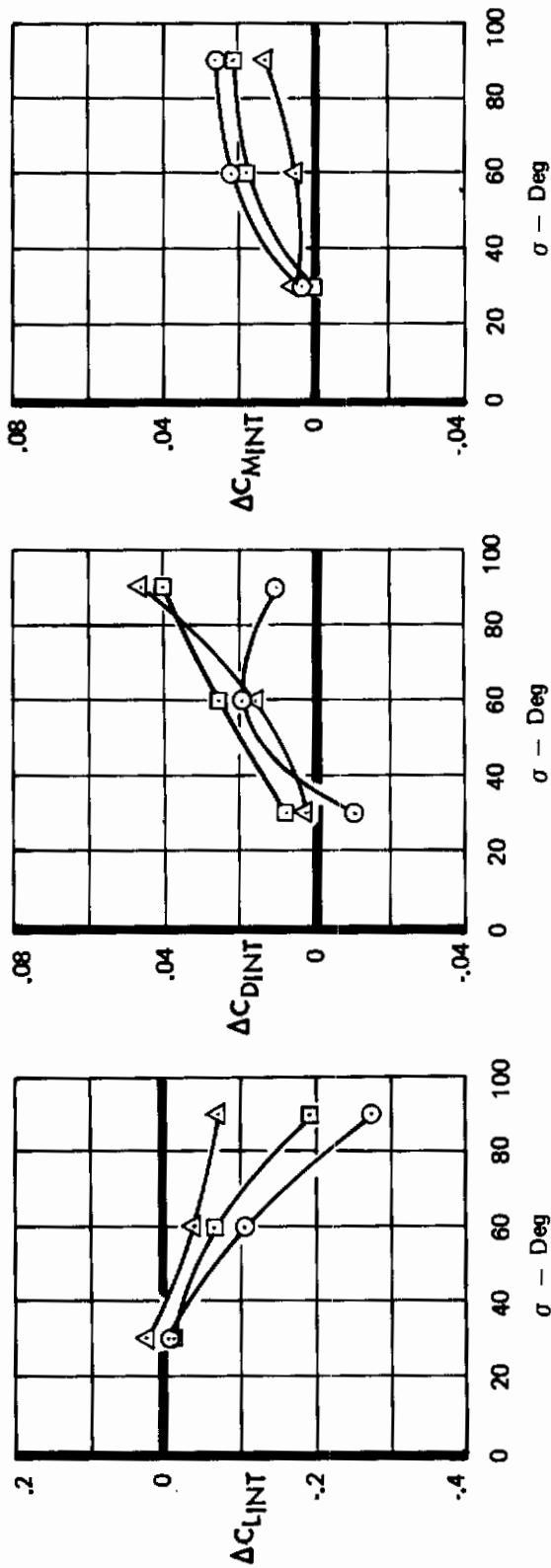
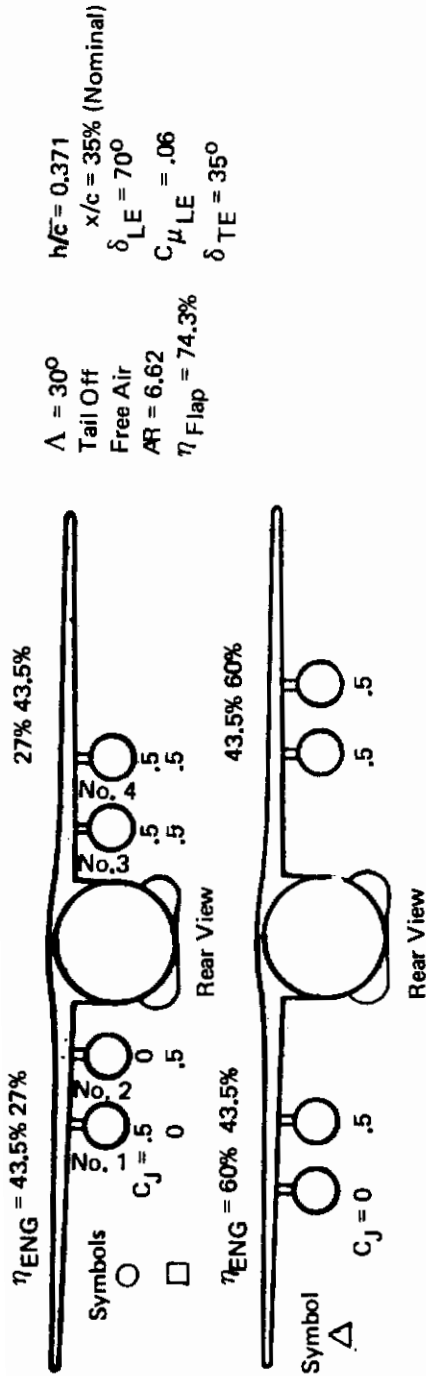


Figure 60: Longitudinal Thrust Interference, Effect of Nacelle Spanwise Location



$\Lambda = 30^\circ$
 Tail Off
 Free Air
 $AR = 6.62$
 $\eta_{Flap} = 74.3\%$
 $h/c = 0.371$
 $x/c = 35\%$ (Nominal)
 $\delta_{LE} = 70^\circ$
 $C_{\mu LE} = .06$
 $\delta_{TE} = 35^\circ$

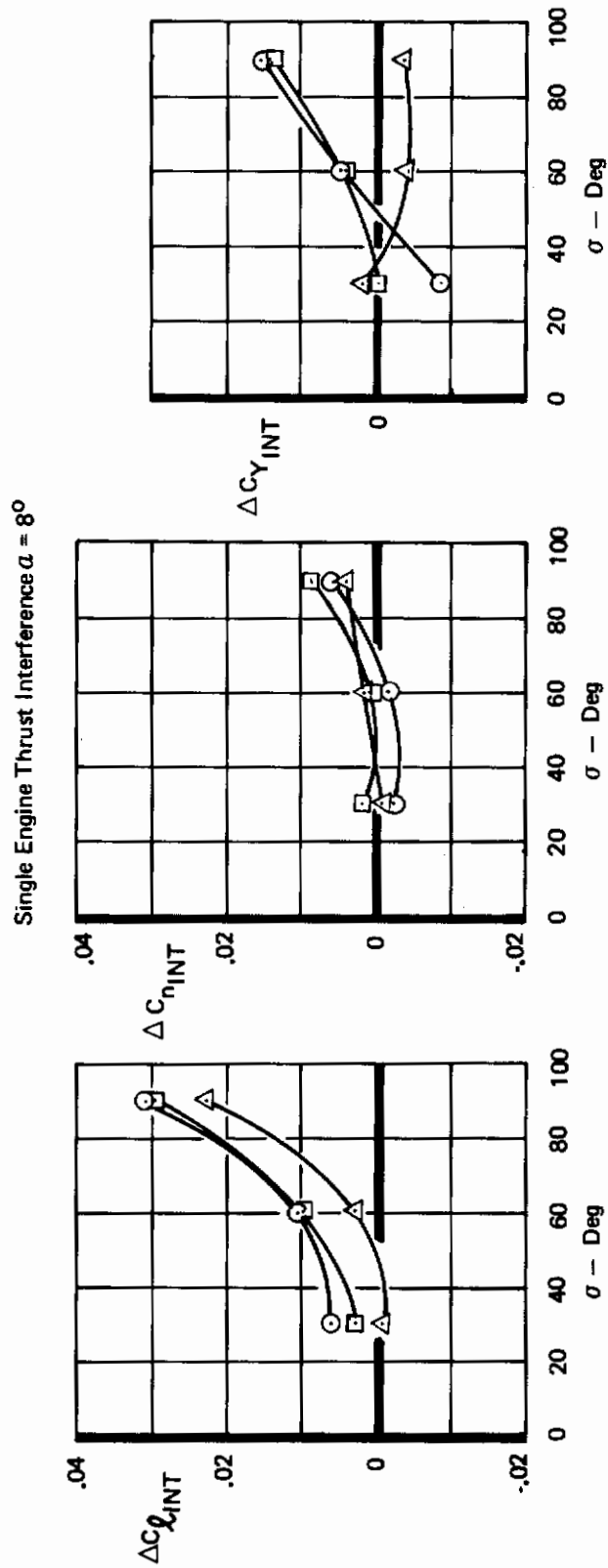
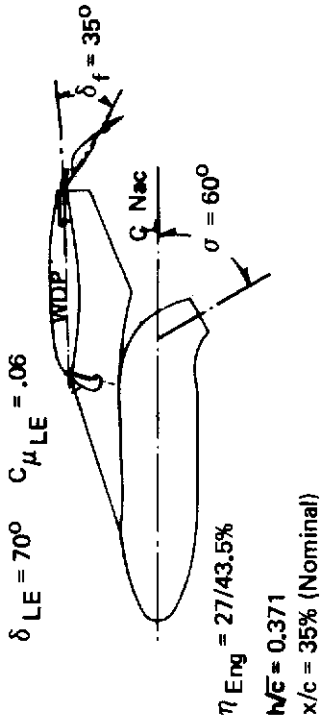


Figure 61: Lateral-Directional Thrust Interference, Effect of Nacelle Spanwise Location



$\Lambda = 30^\circ$
 Tail Off
 Free Air
 $AR = 6.62$
 $\eta_{Flap} = 74.3\%$

⊙	Left Wing Inboard Engine Out
⊠	Left Wing Outboard Engine Out

Single Engine Thrust Interference $\alpha = 8^\circ$

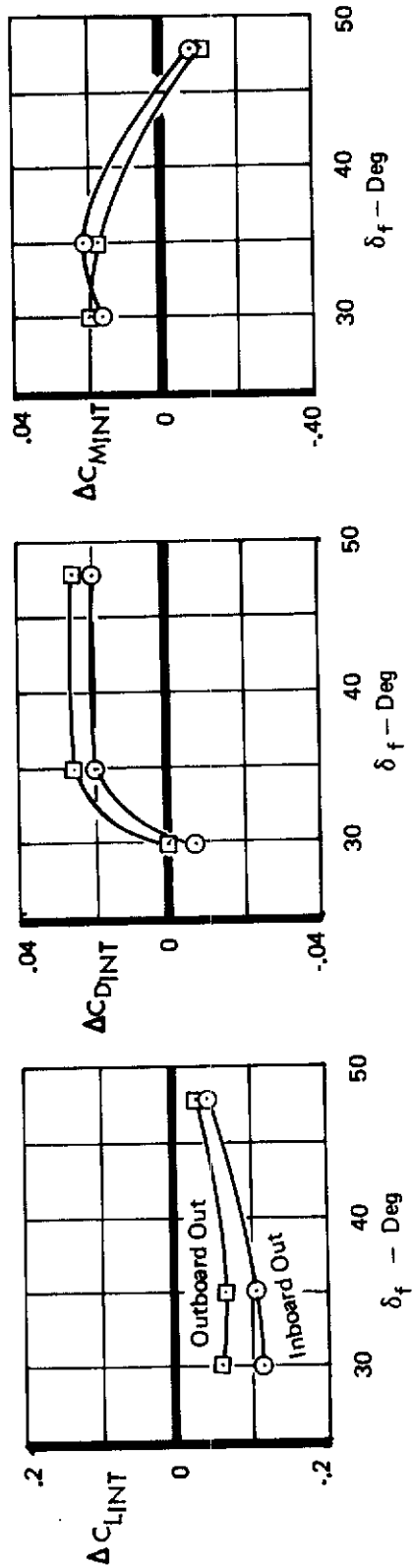
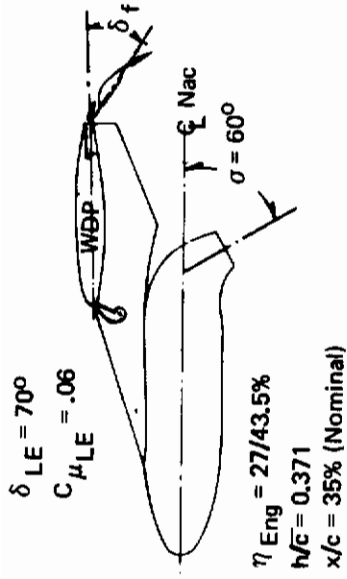


Figure 62: Longitudinal Thrust Interference, Effect of Trailing Edge Flap Angle



$\Lambda = 30^\circ$
 Tail Off
 Free Air
 $AR = 6.62$
 $\eta_{Flap} = 74.3\%$

○	Left Wing Inboard Engine Out
□	Left Wing Outboard Engine Out

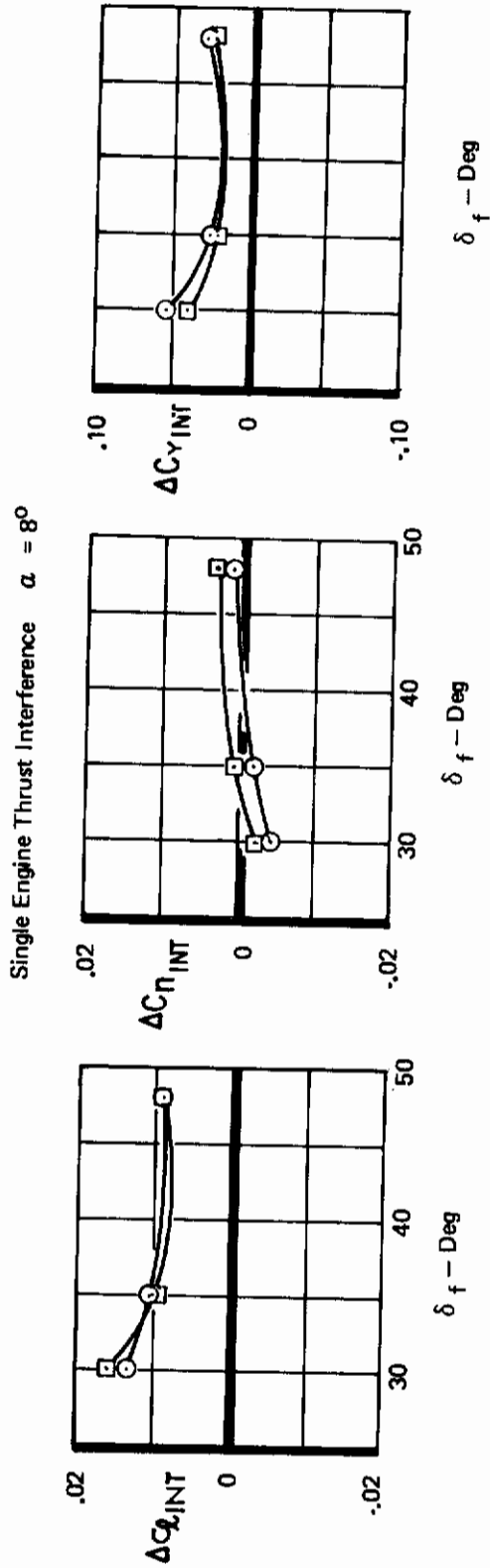


Figure 63: Lateral-Directional Thrust Interference, Effect of Trailing Edge Flap Angle

4.2.2.4 Effect of Wing Sweep

Figures 64 through 67 show the effects of wing sweep on the thrust interference for an inoperative inboard or outboard engine. In general, increasing the wing sweep from 15° to 30° , produces the following results for an inboard or outboard engine out:

- o Lift interference becomes more negative producing more favorable rolling moments.
- o Drag interference is reduced resulting in less favorable yawing moments.
- o Pitching moment increases (except at $\sigma = 30^\circ$) and side force generally increases slightly.

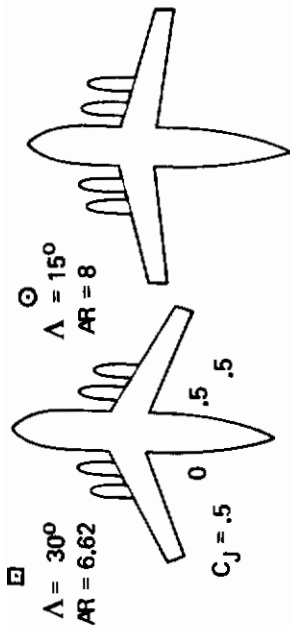
Thrust vector angle has, in general, the same effects on the thrust interference at the two wing sweeps.

4.2.2.5 Thrust Interference in Ground Effect

Figures 68 through 71 show the effects of ground proximity on the thrust interference results for an inboard or outboard engine out. The results are shown for an angle of attack of 4° representing the configuration just prior to touchdown. In ground effect, the following results were obtained for an inboard or outboard engine out. As the ground is approached:

- o Lift interference becomes more positive resulting in a decrease in the rolling moment.
- o Drag interference tends to increase slightly.
- o Yawing moment tends to reduce slightly.
- o Pitching moment decreases at the higher thrust vector angles with no change at the lower vector angles.
- o Side force interference becomes more positive for an inboard engine out and is relatively unaffected for an outboard engine out for moderate σ .

In ground effect for the inboard engine out, the lift interference becomes positive at $\sigma = 90^\circ$ and the rolling moment should become negative. However, the rolling moment remains positive indicating that in the proximity of the ground, the jet impingement on the ground may cross under the fuselage from the right wing and produce the positive rolling moment noted. The same effect was not obtained for the left wing outboard engine out indicating that the two operating inboard engines prevent flow from crossing under the fuselage.



Tail Off
 Free Air
 $\eta_{Flap} = 74.3\%$
 $\eta_{Eng} = 27/43.5\%$
 $x/c = 35\%$ (Nominal)
 $\delta_{LE} = 70^\circ$
 $C_{\mu_{LE}} = .06$
 $\delta_{TE} = 35^\circ$

Left Wing Inboard Engine Inoperative $\alpha = 8^\circ$
(Single Engine Thrust Interference)

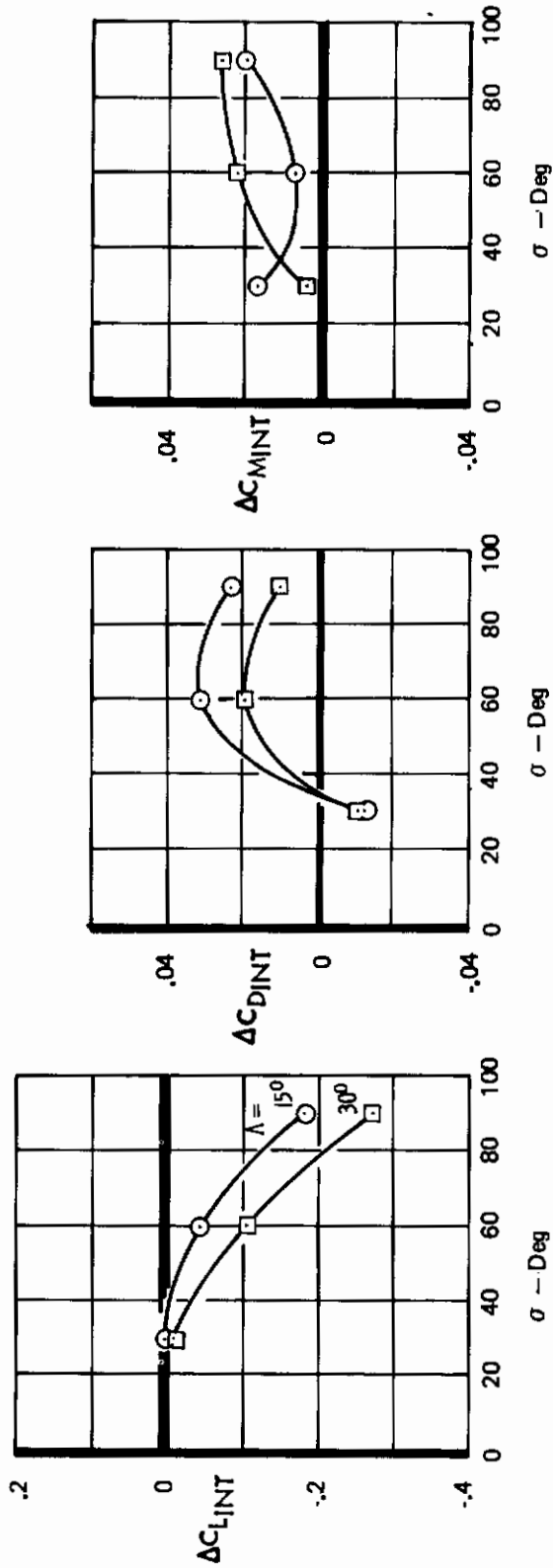
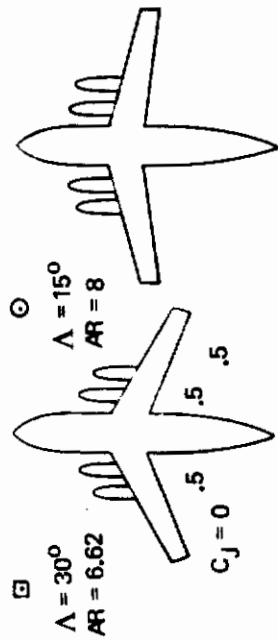


Figure 64: Longitudinal Thrust Interference, Effect of Wing Sweep, Inboard Engine Out



$x/c = 35\%$ (Nominal)
 $\delta_{LE} = 70^\circ$
 $C_{\mu_{LE}} = .06$
 $\delta_{TE} = 35^\circ$

Tail Off
 Free Air
 $\eta_{Flap} = 74.3\%$
 $\eta_{Eng} = 27/43.5\%$

Left Wing Outboard Engine Inoperative $\alpha = 8^\circ$
(Single Engine Thrust Interference)

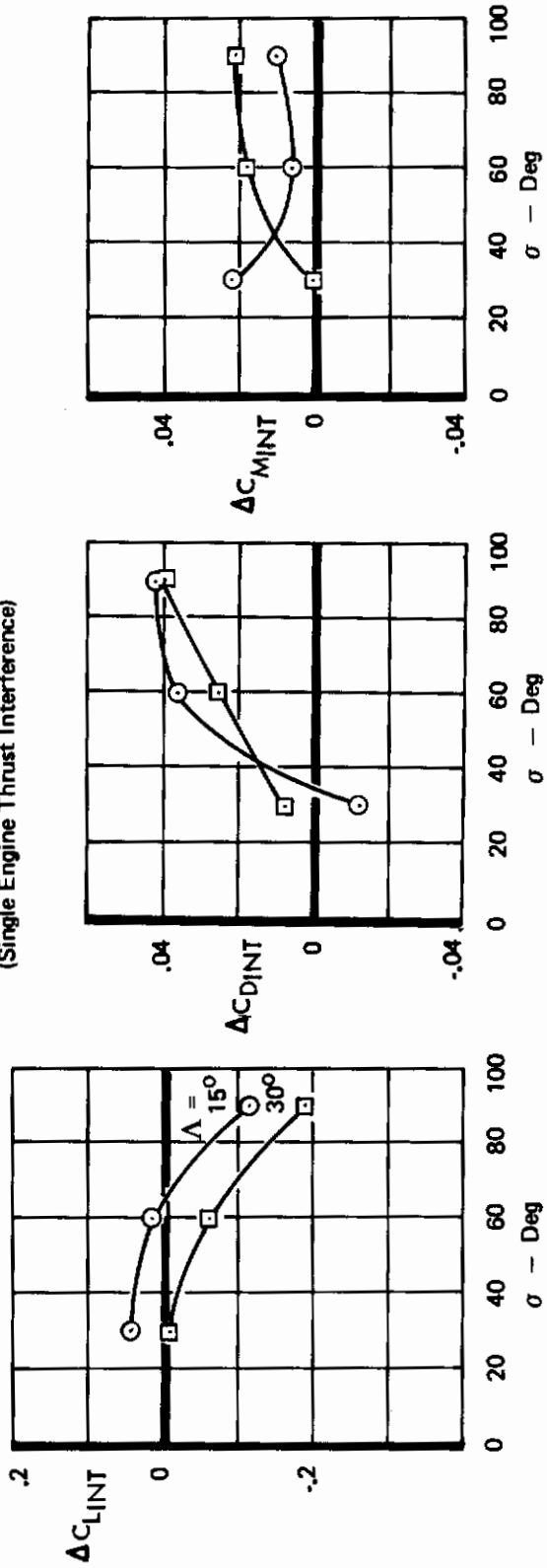


Figure 66: Longitudinal Thrust Interference, Effect of Wing Sweep, Outboard Engine Out

$\Lambda = 15^\circ$
 $AR = 8$
 $h/\bar{c} = 0.406$
 $\eta_{Flap} = 75\%$

$\Lambda = 30^\circ$
 $AR = 6.62$
 $h/\bar{c} = 0.371$
 $\eta_{Flap} = 74.3\%$

Tail Off
 Free Air
 $\eta_{Eng} = 27/43.5\%$
 $\delta_{LE} = 70^\circ$
 $C_{\mu_{LE}} = .06$
 $\delta_{TE} = 35^\circ$

Left Wing Outboard Engine Inoperative $\alpha = 8^\circ$
(Single Engine Thrust Interference)

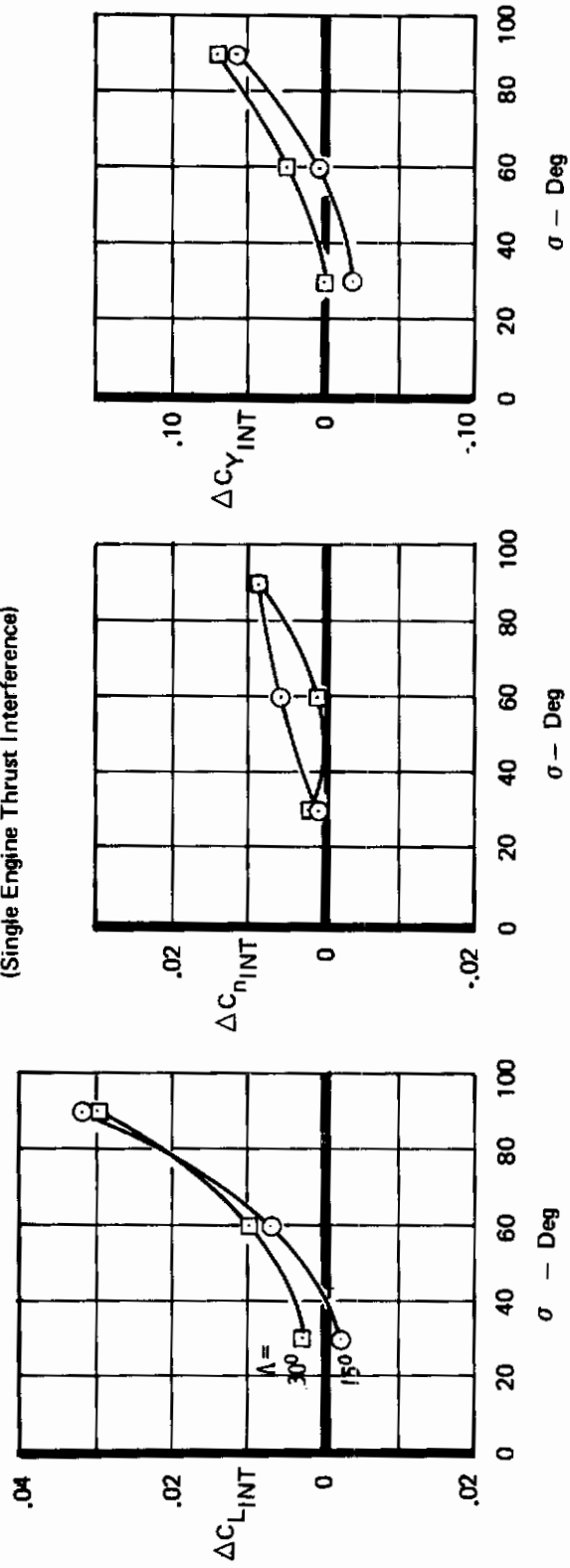
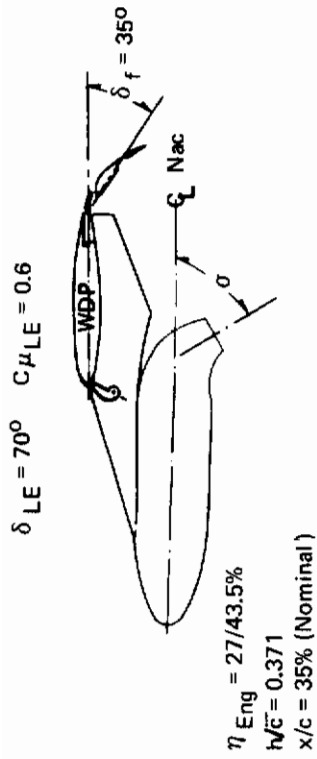


Figure 67: Lateral-Directional Thrust Interference, Effect of Wing Sweep, Outboard Engine Out



$\Lambda = 30^\circ$
 Tail Off.
 $AR = 6.62$
 $\eta_{Flap} = 74.3\%$

Left Wing Inboard Engine Inoperative $\alpha = 4^\circ$
 (Single Engine Thrust Interference)

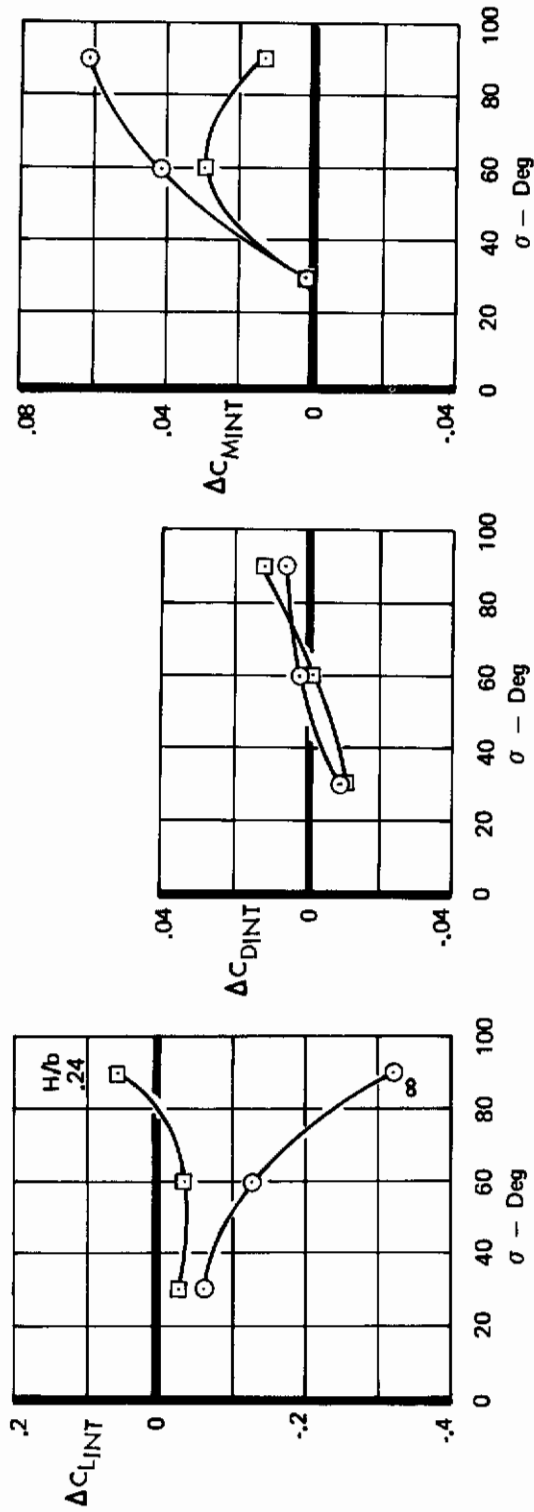


Figure 68: Longitudinal Thrust Interference, Effect of Ground Height, Inboard Engine Out

$\Lambda = 30^\circ$
 Tail Off
 $AR = 6.62$
 $\eta_{Flap} = 74.3\%$
 $\eta_{Eng} = 27/43.5\%$
 $\overline{h/c} = 0.371$
 $x/c = 35\%$ (Nominal)
 $\delta_{LE} = 70^\circ$
 $C_{\mu_{LE}} = .06$
 $\delta_{TE} = 35^\circ$

Left Wing Inboard Engine Inoperative $\alpha = 4^\circ$
 (Single Engine Thrust Interference)

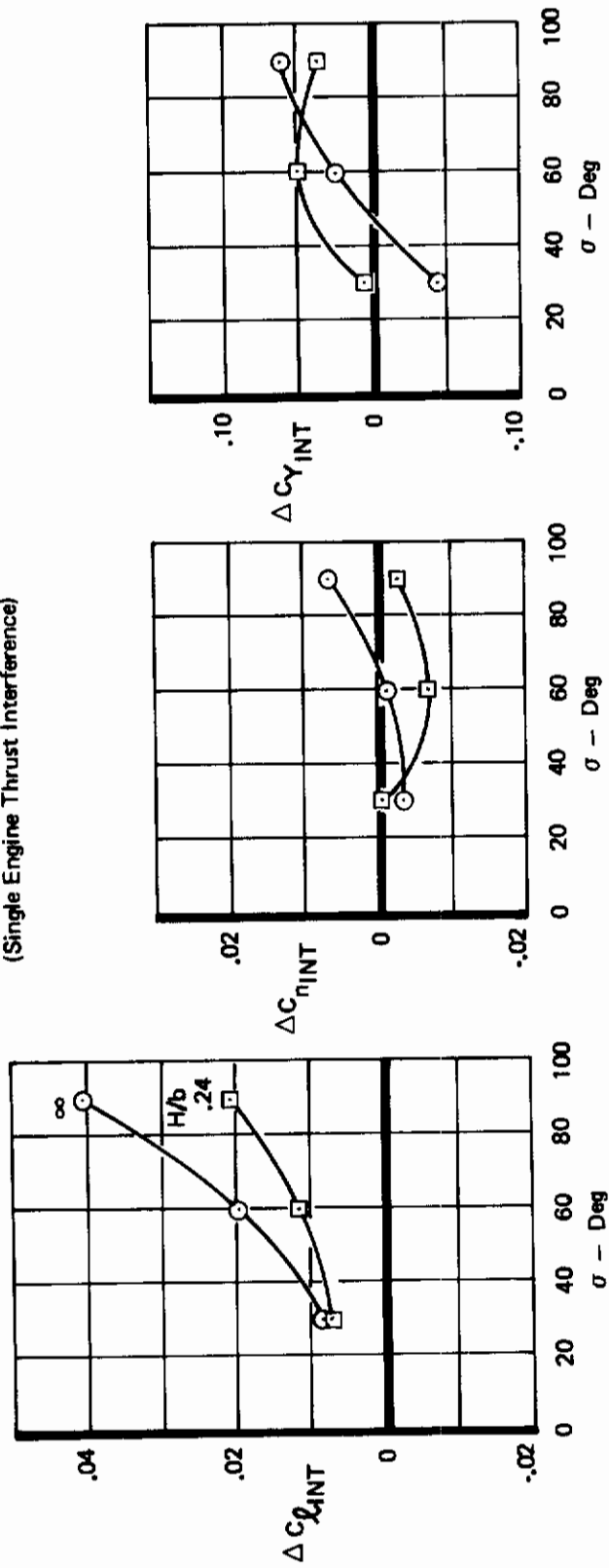
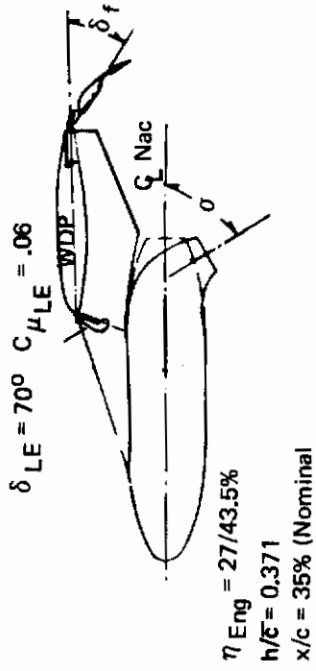


Figure 69: Lateral-Directional Thrust Interference, Effect of Ground Height, Inboard Engine Out

$\Lambda = 30^\circ$
 Tail Off
 $AR = 6.62$
 $\eta_{Flap} = 74.3\%$
 $\eta_{Eng} = 27/43.5\%$



Left Wing Outboard Engine Inoperative $\alpha = 4^\circ$
(Single Engine Thrust Interference)

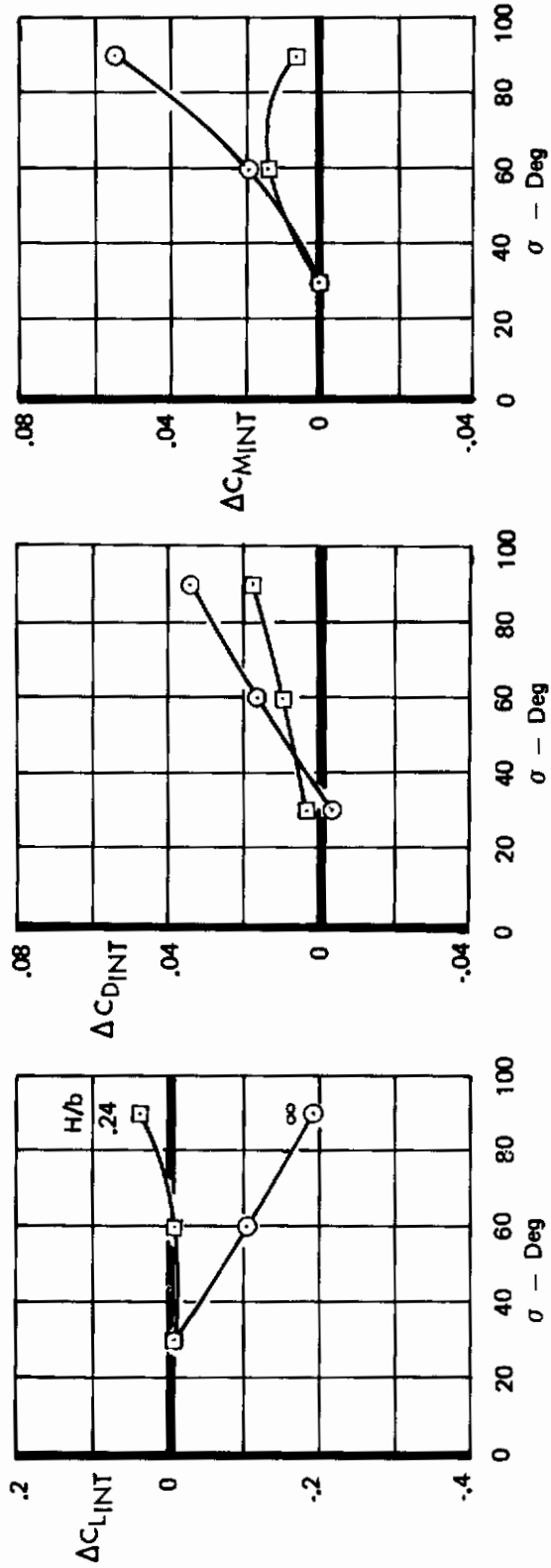


Figure 70: Longitudinal Thrust Interference, Effect of Ground Height, Outboard Engine Out

$\Lambda = 30^\circ$
 Tail Off
 $AR = 6.62$
 $\eta_{Flap} = 74.3\%$
 $\eta_{Eng} = 27/43.5\%$
 $M/\bar{c} = 0.371$
 $x/c = 35\%$ (Nominal)
 $\delta_{LE} = 70^\circ$
 $C_{\mu_{LE}} = .06$
 $\delta_{TE} = 35^\circ$

Left Wing Outboard Engine Inoperative $\alpha = 4^\circ$
 (Single Engine Thrust Interference)

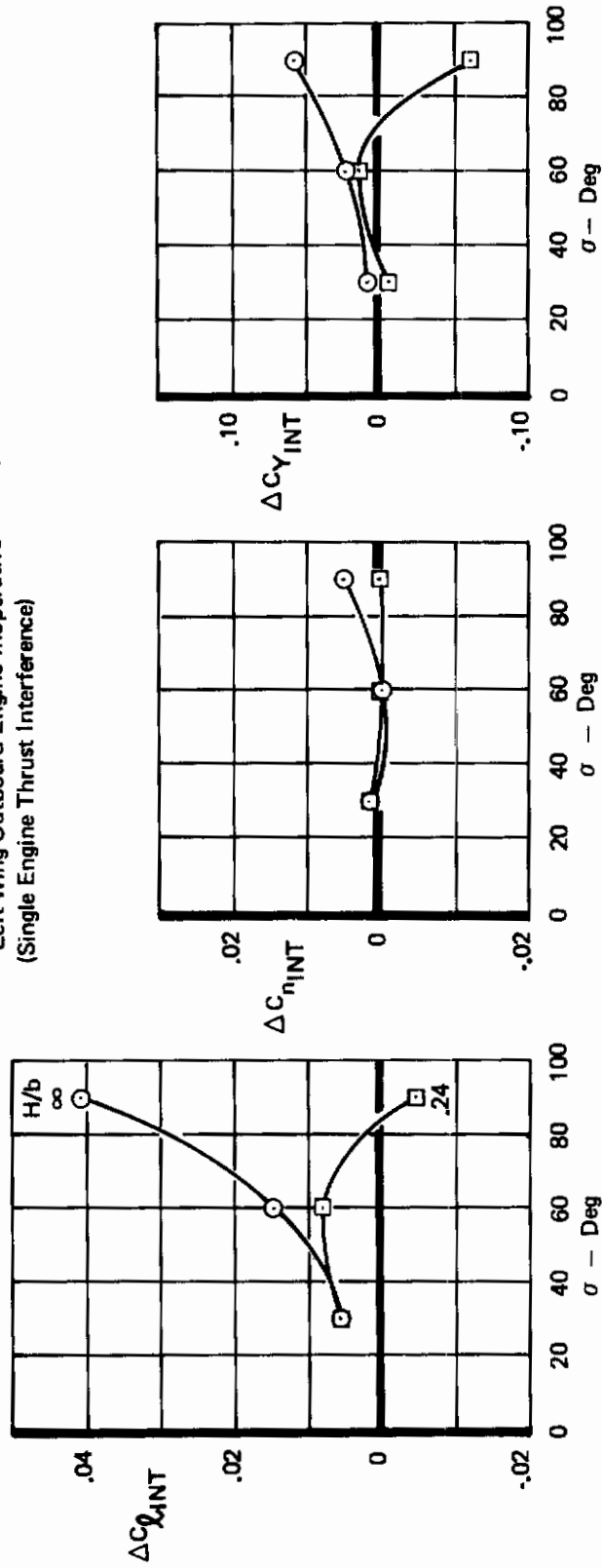


Figure 71: Lateral-Directional Thrust Interference, Effect of Ground Height, Outboard Engine Out

4.3 Ground Effect on Gross Forces and Moments

Table X and the following discussion present ground effect on the total force experienced by the airplane. While this information could to some extent be inferred from the interference data already given (together with procedures given in the design compendium, Ref. 6), it was felt that this subject demanded more extensive and explicit treatment.

In this section, the coefficients for lift, drag and pitching moment in ground effect are presented as a total increment relative to the corresponding free air values at a given angle of attack.

For example:

$$\Delta C_{X_{G.E.}} = C_{X_{G.E.}} - C_{X_{F.A.}}$$

where,

X = Lift, drag or pitching moment

$\Delta C_{X_{G.E.}}$ = Increment in coefficient due to ground effect

$C_{X_{G.E.}}$ = Net (or Gross) coefficient in ground effect

and $C_{X_{F.A.}}$ = Net (or Gross) coefficient in free air

all at a given angle of attack and power-setting.

The increments then represent the forces which tend to disturb the equilibrium of the airplane as it approaches the proximity of the ground.

It must be emphasized that only a portion of the total increments shown is due to the change in thrust interference between the free air thrust interference and the thrust interference in ground effect. This can be demonstrated by inspecting the lift increment as an example:

$$\Delta C_{L_{G.E.}} = C_{L_{GROSS_{G.E.}}} - C_{L_{GROSS_{F.A.}}} = C_{L_{NET_{G.E.}}} - C_{L_{NET_{F.A.}}} \quad (\text{POWER-ON})$$

but

$$C_{L_{NET}} = C_{L_{C_J=0}} + \Delta C_{L_{INT}}$$

Contrails

Table X: Ground Effect on Gross Forces

INCREMENT DUE TO GROUND EFFECT AT VARYING ANGLES OF ATTACK

PARAMETER	FIG.	LIFT	DRAG	PITCHING MOMENT (Tail-Off)
Ground Height (power-off, H/b = .24)	72	At high angles of attack, ground proximity reduces both $C_{L_{max}}$ and stall angle. At moderate α 's C_L increases.	At moderate angles of attack, ground proximity reduces drag.	At moderate angles of attack, ground proximity induces a more positive pitching moment.
(power-on, H/b = .21)	73	Similar to above except C_L increases even more at moderate α 's.	Same influence as above but a greater reduction is achieved.	Same influence as above but a more positive shift is shown.
(power-on, varying H/b) As the ground is approached:	74	At constant moderate α , the favorable lift increment (due to ground effect) increases rapidly as ground height decreases below H/b = 0.3.	At constant moderate α , the drag reduction (due to ground effect) becomes steadily larger below H/b = 0.6.	At constant moderate α , the pitching moment increment (due to ground effect) increases more positively below H/b = 0.5.
Angle of Attack (power-on)	75	Favorable lift increment decreases with increasing α .	Favorable drag increment becomes more favorable with increasing α .	Pitching moment increment becomes more positive with increasing α .

INCREMENT DUE TO GROUND EFFECT AT CONSTANT ANGLE OF ATTACK, $\alpha = 4^\circ$

PARAMETER	FIG.	FAVORABLE LIFT INCREMENT	FAVORABLE DRAG INCREMENT	POSITIVE PITCHING MOMENT INCREMENT (Tail-Off)
Thrust Coefficient	75	Increment increases with thrust.	Increment more favorable with thrust.	Increment decreases with thrust.
Thrust Vector Angle	76	Increment increases with σ for power-on and is constant for power-off.	Increment reduces between $\sigma = 30^\circ$ and 60° but between $\sigma = 60^\circ$ and 90° , increment increases power-on. Drag essentially constant power-off.	Increment reduces between $\sigma = 30^\circ$ and 60° but increases between $\sigma = 60^\circ$ and 90° power-on and power-off.
Nacelle Location Chordwise (moving nacelle aft)	77	Less favorable increment.	Increment more favorable.	Increases.
Spanwise (moving pods out-board)	78	Less favorable increment.	Negligible change.	Increases.
Height (lowering nacelles)	78	Less favorable increment.	Negligible change.	Increases.
Single Pods vs Dual Pods (inboard nacelles)	79	Dual pods show a greater increment increase than single pods at $\sigma = 30^\circ$ and 60° . At $\sigma = 90^\circ$ the reverse occurs.	Small changes in increment except dual pods are more negative at $\sigma = 90^\circ$.	At $\sigma = 30^\circ$ and 90° the dual pods show a more positive increment than the single pods. The reverse occurs at $\sigma = 60^\circ$.
One Engine Inoperative	80	More loss with inboard engine out than with outboard engine out.	Increment less with outboard engine out than with inboard engine out.	More positive with inboard engine out than with outboard engine out.
T.E. Flap Deflection	81	Increment increases, power-on.	Increment is more favorable.	Increment increases.
Wing Sweep (sweeping wing from 15° to 30°)	82	Increment increases at $\sigma = 30^\circ$ and 90° while at $\sigma = 60^\circ$, increment is nearly the same for both sweeps.	Increment is less favorable.	Increment decreases.

Contrails

Contrails

therefore

$$\Delta C_{L_{G.E.}} = (C_{L_{C_{J=0}}} + \Delta C_{L_{INT}}) - (C_{L_{C_{J=0}}} + \Delta C_{L_{INT}})$$

G.E. G.E. F.A. F.A.

finally

$$\Delta C_{L_{G.E.}} = (C_{L_{C_{J=0}}} - C_{L_{C_{J=0}}}) + (\Delta C_{L_{INT}} - \Delta C_{L_{INT}})$$

POWER-OFF G.E. F.A. G.E. F.A.

"a" "b"

Therefore, as can be seen above, the total increments with power on are represented by the sum of "a" (the increment due to ground effect, power-off) and "b" (the change in thrust interference between free air and in ground effect). This fact must be borne in mind, particularly if the following Table X and charts are compared to Table VIII and charts of Section 4.1.2 "Thrust Interference in Ground Effect."

4.3.1 Introduction

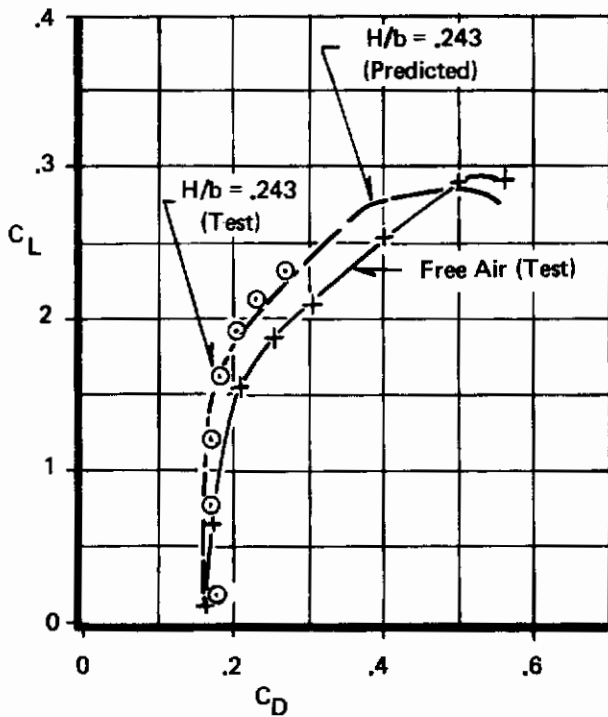
The effects generally observed as the ground is approached for moderate angles of attack are:

- o Lift is increased.
- o Drag is reduced.
- o The wing-body contribution to pitching moment becomes more positive.

At higher angles of attack, the maximum lift and associated stall angle are reduced.

Figure 72 shows the calculated characteristics in ground effect for 30° sweep, power-off, using the prediction method presented in Reference 6. The predicted curve agrees well with the data at moderate angles of attack and, assuming the method works as well at higher angles of attack, illustrates the reduction in $C_{L_{max}}$ due to ground effect. The data obtained in ground effect during this test were limited to fairly low angles of attack due to the wind tunnel model support sting interfering with the moving ground belt.

Ground effects on "net" forces may be analyzed in terms of the velocities induced by the images of the wing's bound and trailing vortices. The image trailing vortices reduce the downwash, increasing α and C_L while reducing C_D . The image bound vortex induces a tail wind, reducing all forces by lowering q . The latter effect is proportional to C_L^2 , and usually is masked by the α change except at very high C_L 's, which leads to the reduction in $C_{L_{max}}$. (A detailed discussion of this subject is provided in Ref. 6.)



$\Lambda = 30^\circ$ $\delta_f = 35^\circ$
 $C_J = 0$ $\sigma = 60^\circ$

Tail Off
 All Engines Operating $\delta_{LE} = 70^\circ$
 $AR = 6.62$ $C_{\mu_{LE}} = .06$
 $\eta_{Flap} = 74.3\%$

$\eta_{Eng} = 27/43.5\%$
 $h/c = 0.371$
 $x/c = 35\%$ (Nominal)

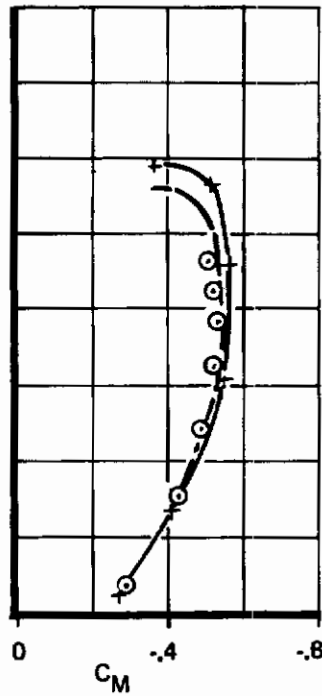
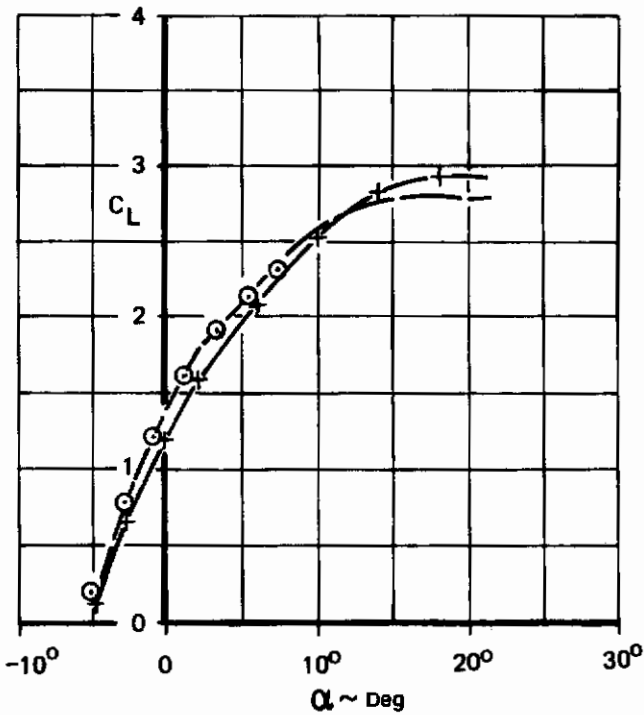
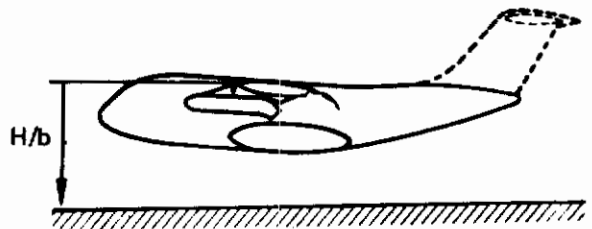


Figure 72: Comparison of Free Air and Ground Effect Characteristics, Power-Off

Ground effects on thrust interference are more complex. In the first place, the velocities induced by jet entrainment are reduced by the images of the jets. Secondly, the jets themselves have different paths near the ground. This sometimes causes very irregular behavior of the interference forces. For example, at high values of σ , the jet sometimes goes upstream along the ground plane, separating from it well forward of the wing.

Figure 73 compares the net longitudinal characteristics in ground effect with the corresponding free air values, power-on, at 15° sweep. The changes due to ground effect with power-on are similar to those observed with power-off; however, the ground effects are more pronounced power-on. This is partly due to the impingement of the jet on the ground.

The following discussion and figures illustrate the ground effect increments for each of the principal parameters studied.

4.3.2 Ground Height

Figure 74 shows the change of the longitudinal characteristics with ground height varying for a given value of angle of attack, power-on. Again, the general trends of ground effect (increasing lift, drag reduction, and more positive pitching moment as the ground is approached) are demonstrated for moderate angles of attack. At $\alpha = 0^\circ$, flow separation occurred on the wing undersurface in the flaps-down configuration which caused considerable data deviation from the usual observed (attached flow) trends.

4.3.3 Thrust Level and Angle of Attack

Figure 75 demonstrates the effect of thrust coefficient on ground effect at several angles of attack. The major effect of increasing power near the ground is generally to emphasize the ground effects. As shown in the figure, as C_J increases, the lift increase and drag reduction due to ground effect becomes more pronounced. However, the pitching moment increment due to ground effect at moderate angles of attack ($\alpha = 4^\circ$ to 8°) shows little change as power increases. Again, at low angles of attack ($\alpha = 0^\circ$ and 2°), the undersurface flow separation caused nonlinear effects which were emphasized as C_J increased.

4.3.4 Thrust Vector Angle

The influence of the thrust vector angle on the ground effects is shown in Figure 76. The effect of σ with power-off is relatively small, as one might expect. However, the additional lift due to ground effect with power-on is increased quite dramatically as the thrust vector angle increases from 30° to 90° , largely because of the impingement of the nozzle jet on the ground. The jet impingement and resulting distortion to the flow field is particularly noticeable in the data at $\sigma = 90^\circ$. At this thrust angle, some of the jet air actually was observed to move forward along the moving ground belt. Then, near the nose of the model, the jet air began to recirculate.

Contrails

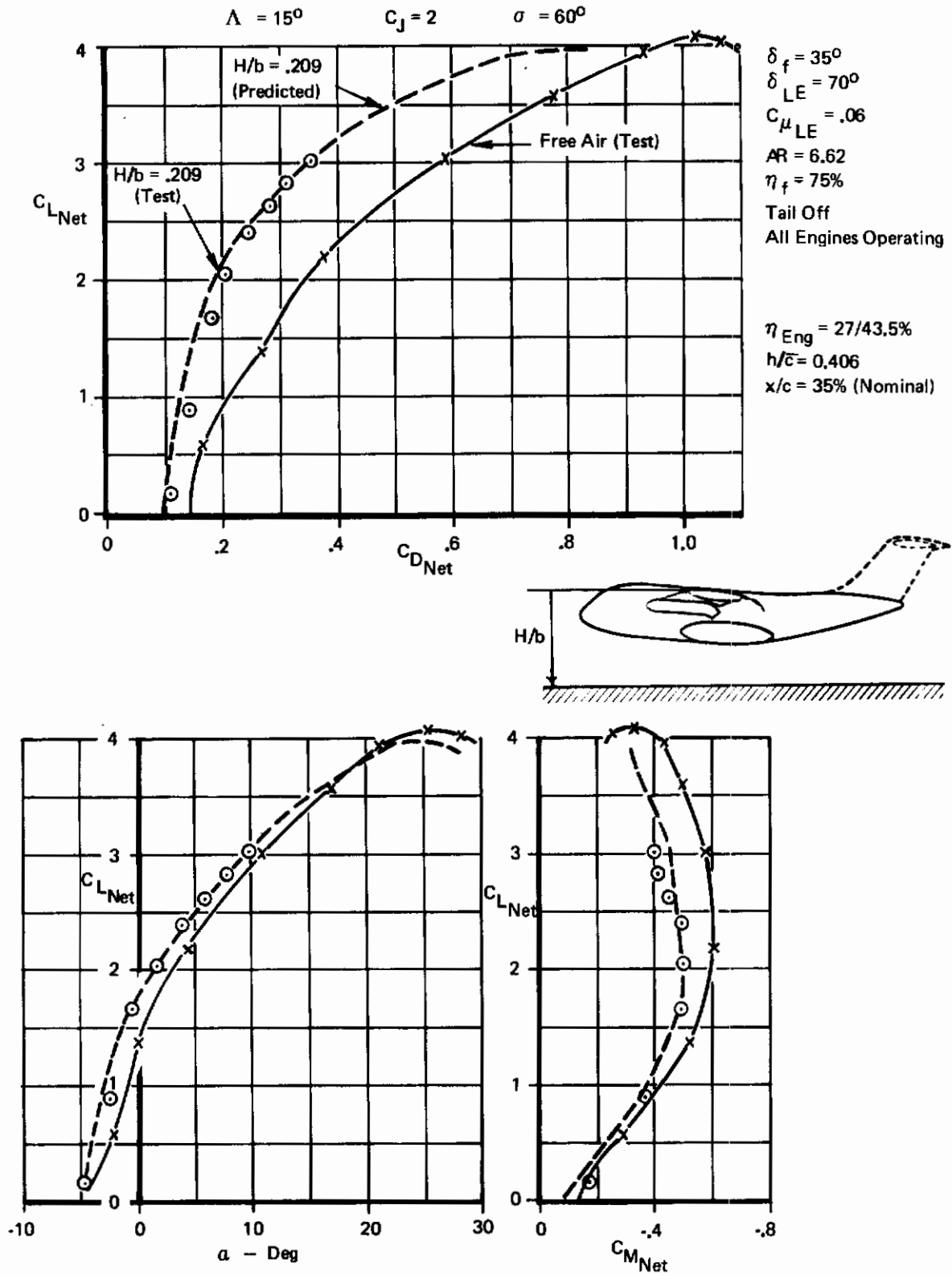
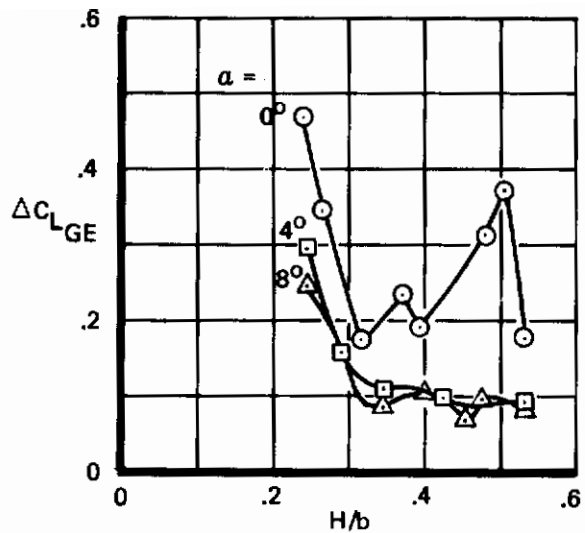


Figure 73: Comparison of Free Air and Ground Effect Characteristics, Power-On



$\Lambda = 30^\circ$ $C_J = 2$
 $AR = 6.62$ $\sigma = 60^\circ$
 $\delta_f = 35^\circ$ $\eta_f = 74.3\%$
 $\delta_{LE} = 70^\circ$ $C_{\mu_{LE}} = .06$

$\eta_{Eng} = 27/43.5\%$
 Tail Off $h/\bar{c} = 0.371$
 All Engines Operating $x/c = 35\%$ (Nominal)

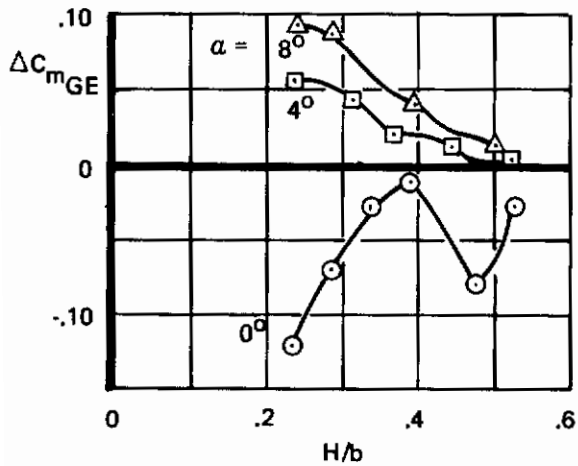
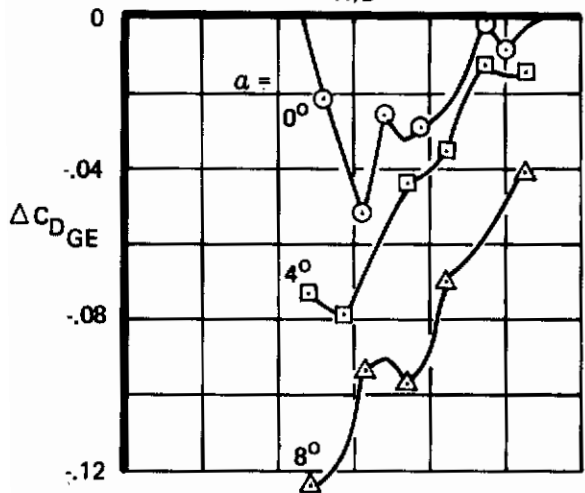
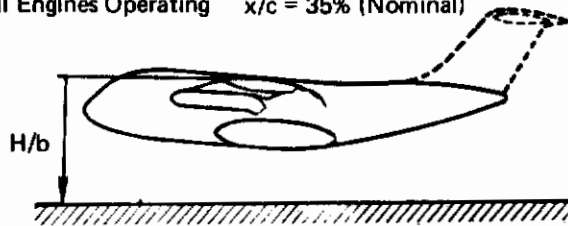


Figure 74: Effect of Ground Height on Longitudinal Characteristics

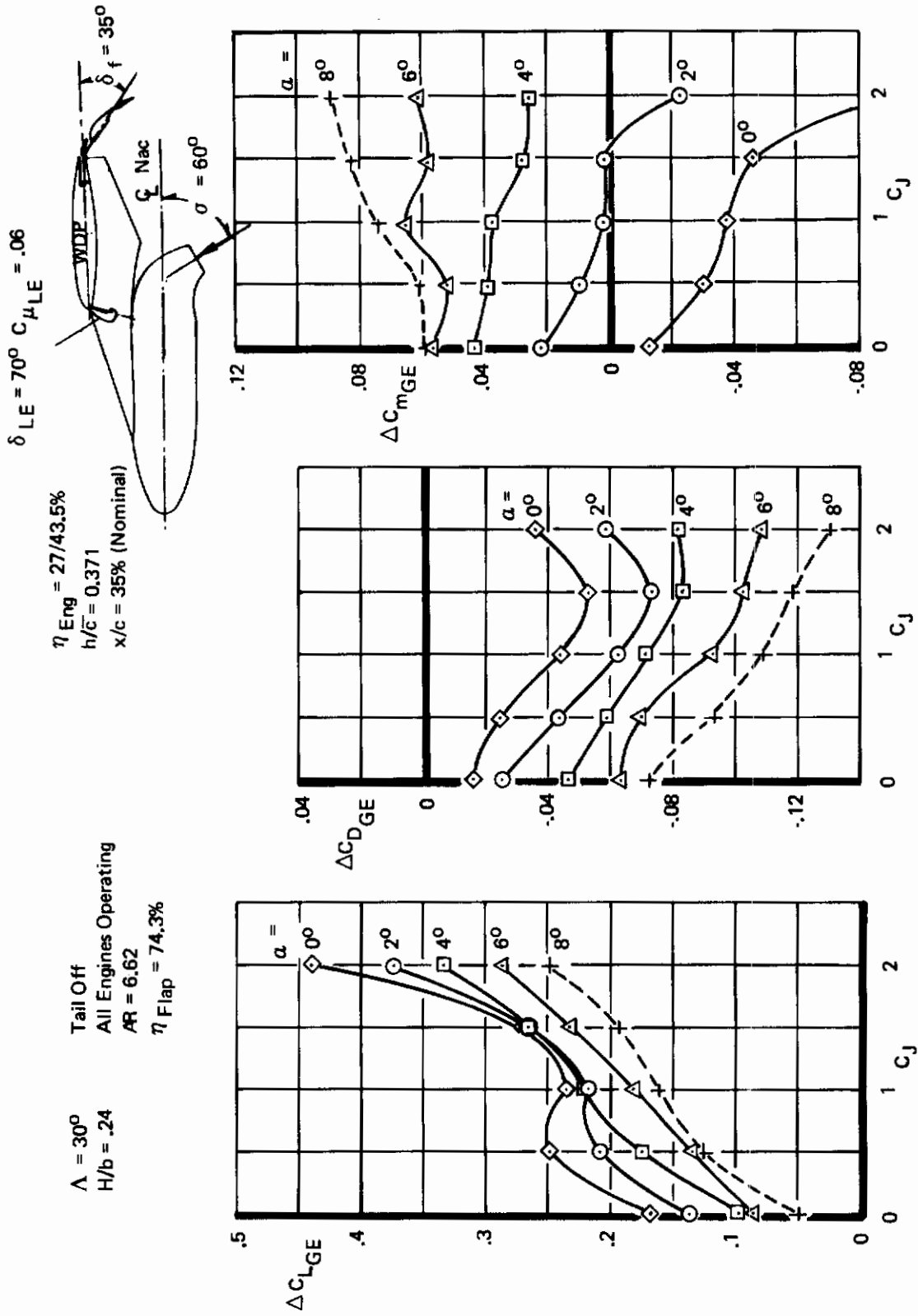
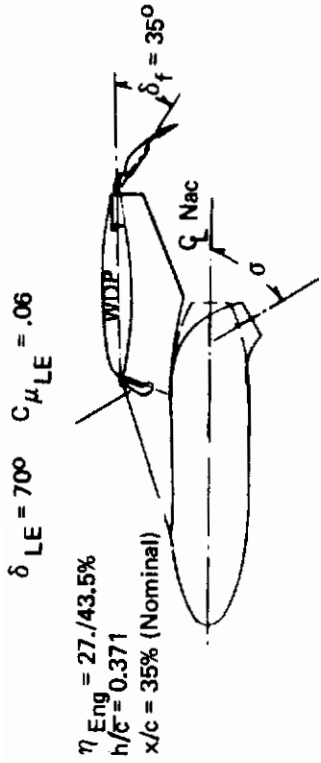


Figure 75: Effect of Thrust Coefficient and Angle of Attack on Ground Effect



Tail Off
 All Engines Operating
 $AR = 6.62$
 $\eta_{Flap} = 74.3\%$

$\Lambda = 30^\circ$
 $C_J = 0 \text{ \& } 2$
 $\alpha = 4^\circ$
 $H/b = .24$

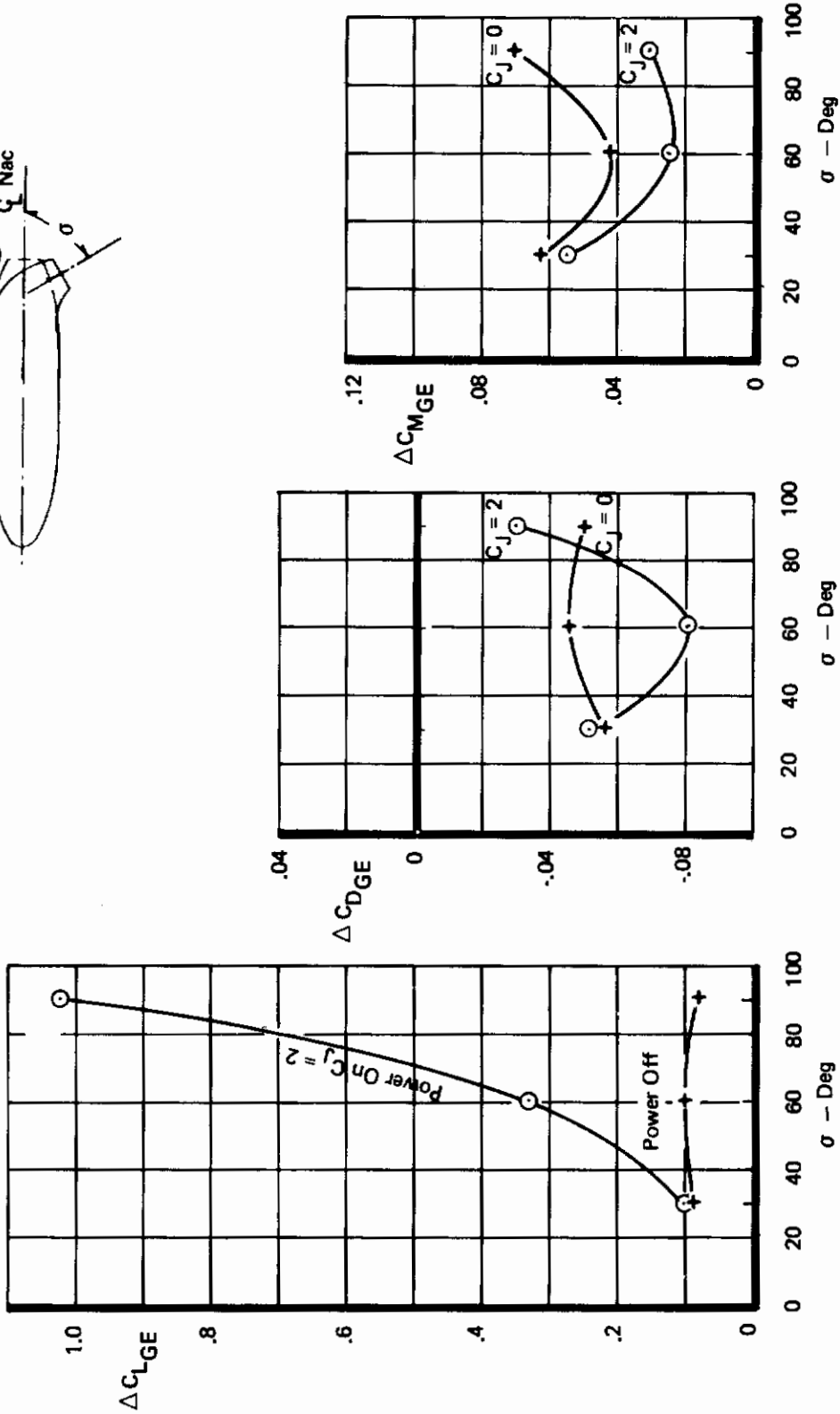


Figure 76: Effect of Thrust Vector Angle on Ground Effect

Note that the difference between the power-on and the power-off increments shown in Figure 76 is equal to the difference between the thrust interference in ground effect and the thrust interference in free air shown in Figure 47. This is demonstrated by the final equation on page 139 (last paragraph of Section 4.3).

4.3.5 Nacelle Location

Figure 77 through 79 summarize the ground effects for several nacelle locations including chordwise, spanwise, and height variations as well as a comparison of the single pods versus the dual pod installation.

4.3.6 Nacelle Chordwise Position

The effects of chordwise movement of the nacelles are shown in Figure 77. In general, the effect of moving the nacelle aft from 0% c to 70% c (with power on, $C_J = 2$) is to:

- o Reduce the lift increase due to ground effect.
- o Emphasize the drag reduction due to ground effect.
- o Increase the positive pitching moment increment due to ground effect.

Note that the 90° thrust deflection angle data again shows the recirculation effects discussed (4.3.4) above, particularly when the nozzle is at 0% x/c.

4.3.7 Nacelle Spanwise Position

Figure 78 illustrates that the influence of moving the single-pods outboard with power-on ($C_J = 2$) is to:

- o Reduce the lift increase due to ground effect.
- o Slightly emphasize the drag reduction due to ground effect.
- o Show an increase in the positive pitching moment increment due to ground effect at $\sigma = 60^\circ$, but no change was observed at $\sigma = 30^\circ$ and 90° .

4.3.8 Nacelle Height

Figure 78 also shows that the effect of lowering the nacelle from $h/\bar{c} = 0.371$ to 0.452 is to:

- o Reduce the lift increase due to ground effect.
- o Show only small changes in the drag.
- o Increase the positive pitching moment increment due to ground effect.

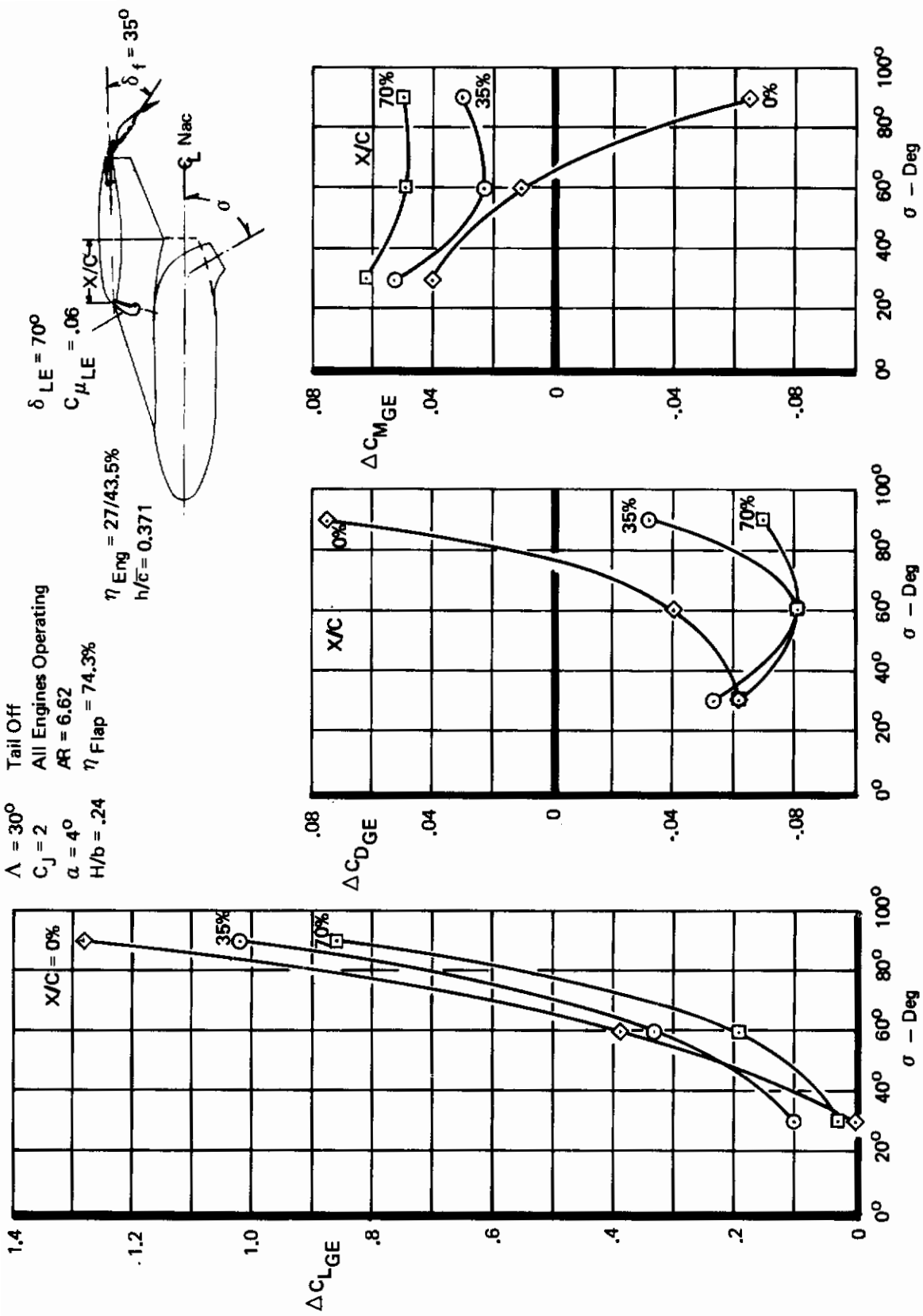


Figure 77: Effect of Nacelle Chordwise Location on Ground Effect

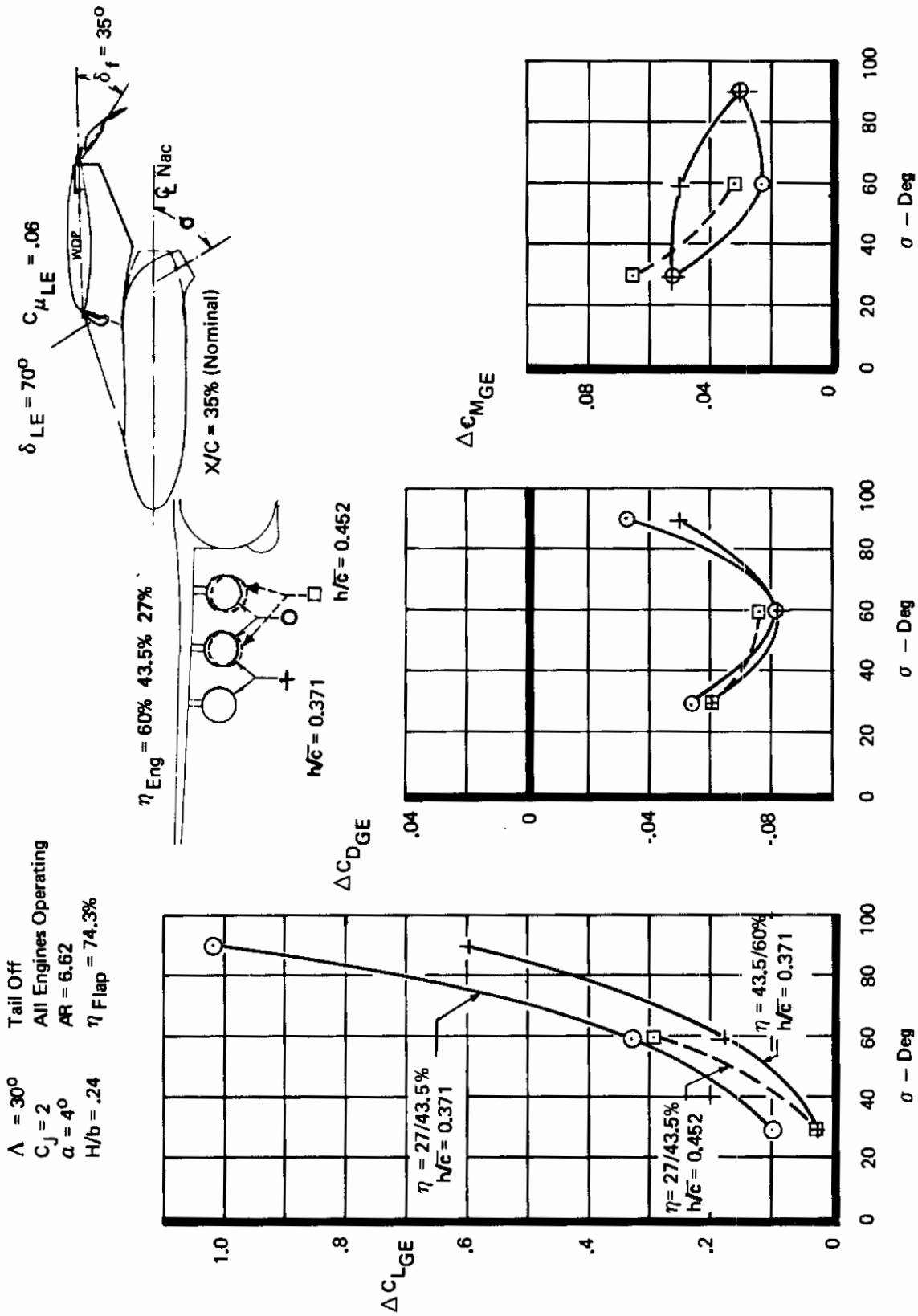


Figure 78: Effect of Nacelle Height and Spanwise Location on Ground Effect

4.3.9 Single Pods versus Dual Pods

A comparison of the single pods versus the dual pods located inboard is shown in Figure 79. The 30° and 60° thrust vector angle data show the following effects in changing from the single pod to the dual pod configuration:

- o The lift increment due to the ground is increased.
- o Little change in drag due to ground effect is present.
- o Pitching moment increment due to ground shows no change going from 30° to 60° for the dual pods, but an increase is observed for the single pods going from 30° to 60°

The 90° vector angle data shows a large difference compared to the above trends in that:

- o The lift increase due to ground goes to zero for the dual pods while the single pods show a continuing increase.
- o The drag reduction and pitching moment increase is emphasized for the dual pods compared to the single pods.

4.3.10 One Engine Inoperative

The effects of the failure of one engine are shown in Figure 80. Note that the ground effect trends are similar for all the power-on runs and are relatively independent of whether the power (total $C_J = 1.5$) is distributed over three engines or four, except for the small effects noted below. The failure of the inboard engine instead of the outboard engine shows:

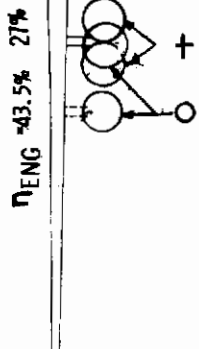
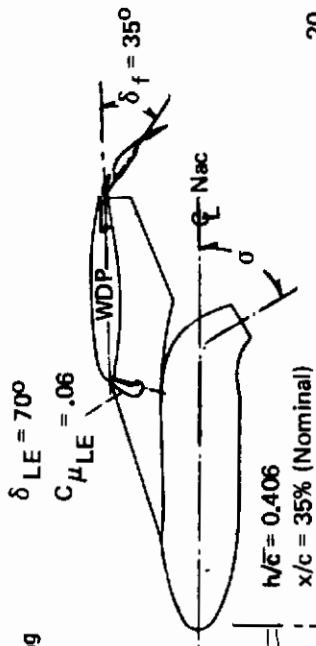
- o Slightly less lift increase due to ground effect.
- o More drag reduction due to ground effect.
- o More of a pitching moment increment due to ground effect.

4.3.11 Trailing-Edge Flap Angle

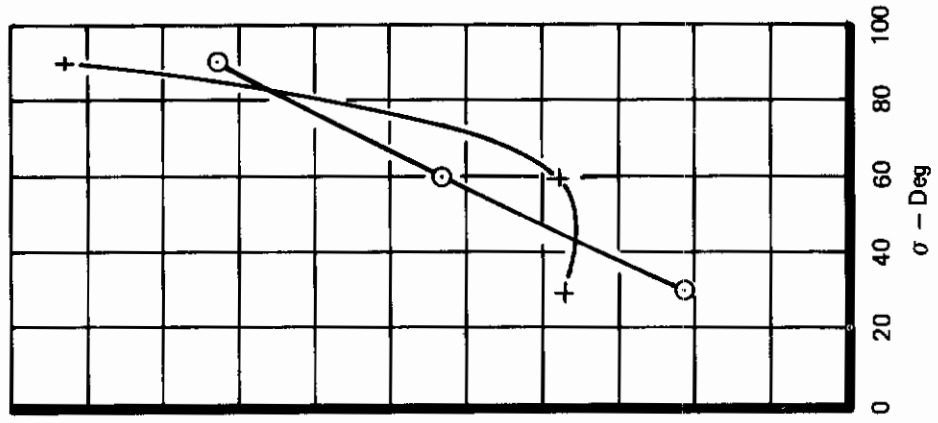
The influence of the trailing-edge flap angle is illustrated in Figure 81. In general, the effects are small. As the flap angle is increased:

- o The lift increase due to ground effect increases with power-on, but shows a decrease with power-off except at $\delta_f = 48^\circ$.
- o The drag reduction due to ground effect is emphasized both power-on and power-off.

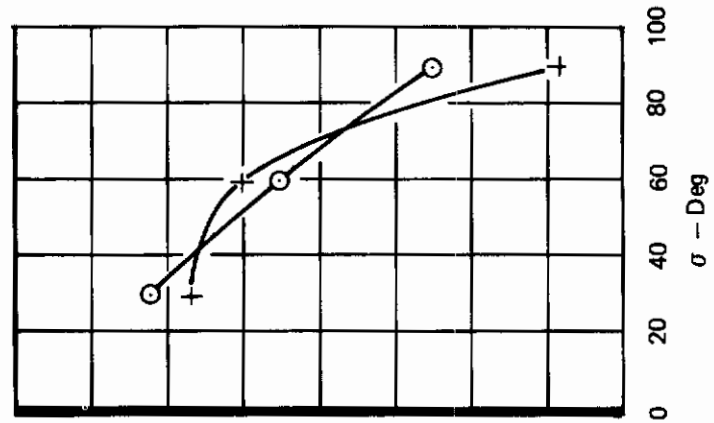
$\Lambda = 15^\circ$
 $C_J = 2$
 $\alpha = 4^\circ$
 $H/b = .24$
 Tail Off
 All Engines Operating
 $AR = 8$
 $\eta_{Flap} = 75\%$



ΔC_{MGE}



ΔC_{DGE}



ΔC_{LGE}

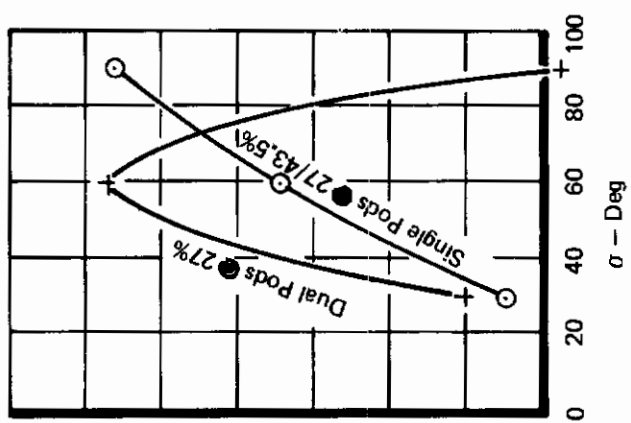
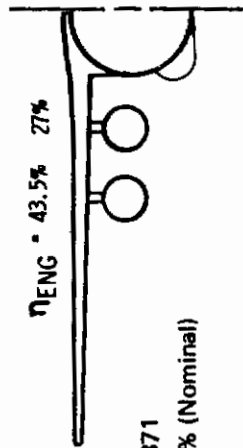


Figure 79: Effect of Nacelle Type on Ground Effect

Contrails

$\Lambda = 30^\circ$
 $AR = 6.62$
 $\alpha = 4^\circ$
 $H/b = .24$
 $\delta_f = 35^\circ$
 $\delta_{LE} = 70^\circ$
 $\eta_{Flap} = 74.3\%$
 $C_{\mu_{LE}} = .06$



$h/\bar{c} = 0.371$
 $x/c = 35\% \text{ (Nominal)}$

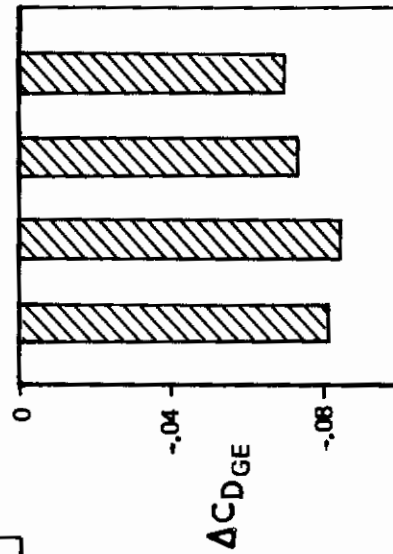
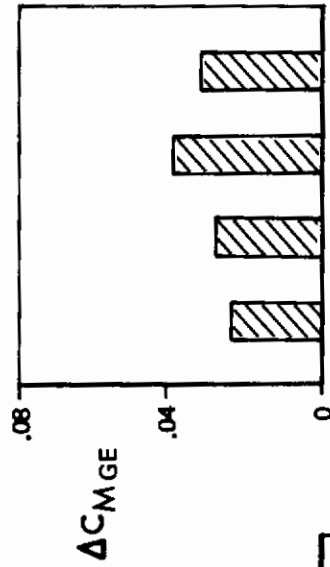
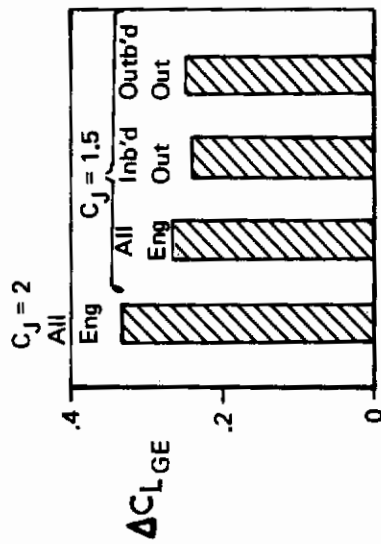


Figure 80: Effect of an Engine Failure on Ground Effect

$\Lambda = 30^\circ$ Tail Off
 $C_J = 0 \text{ \& } 2$ All Engines Operating
 $\alpha = 4^\circ$ AR = 6.62
 $H/b = .24$ η Flap = 74.3%

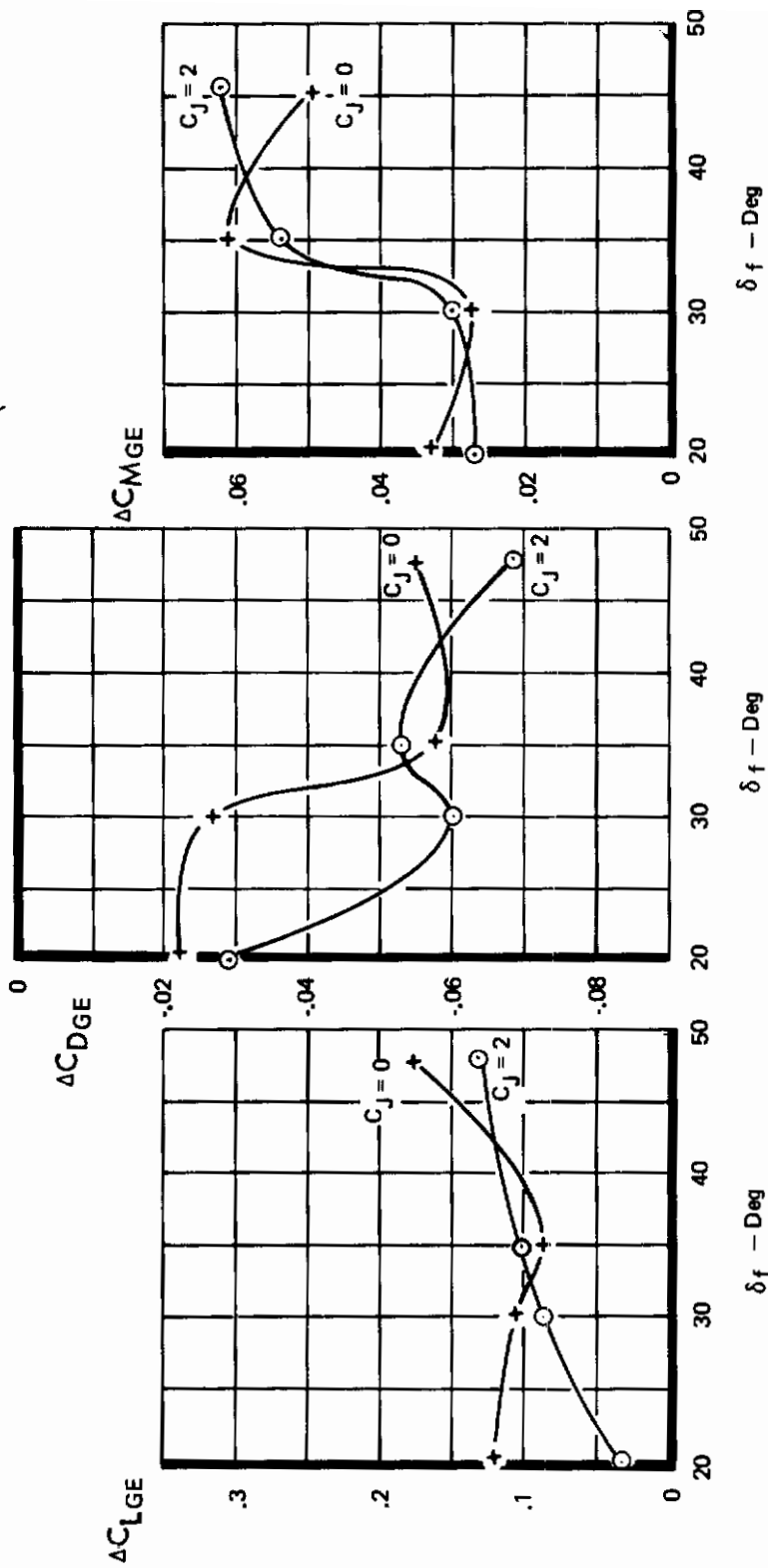
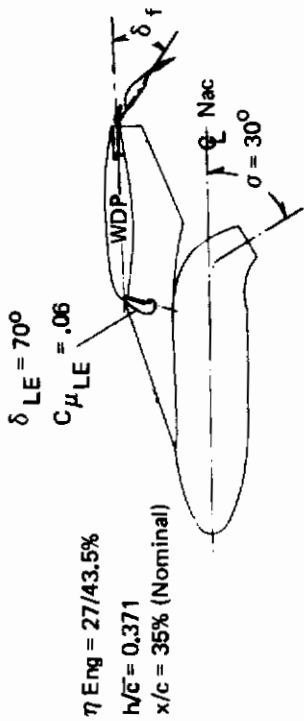


Figure 81: Effect of Flap Angle on Ground Effect

- o The pitching moment increase due to ground effect shows approximately an 0.03 increase when the flap setting is increased from 30° to 35° both power-on and power-off. There is essentially no change going from 20° to 30° δ_f and in going from 35° to 48° δ_f .

4.3.12 Wing Sweep

Figure 82 shows a comparison of the ground effect increments obtained on the 15° versus the 30° wing sweep configurations. The following items are noteworthy:

- o The lift increase due to ground effect is similar for both configurations although the 30° sweep data shows more lift increase (power-on) at $\sigma = 90^\circ$ than the corresponding 15° sweep data.
- o The drag reduction due to ground effect is more for the 15° sweep configuration than for the 30° sweep configuration.
- o The positive pitching moment increase due to ground effect, with power-on, shows a steep increase as σ increases for the 15° sweep. The 30° sweep configuration shows a decrease as σ increases from 30° to 60°, and an increase as σ increases from 60° to 90°.

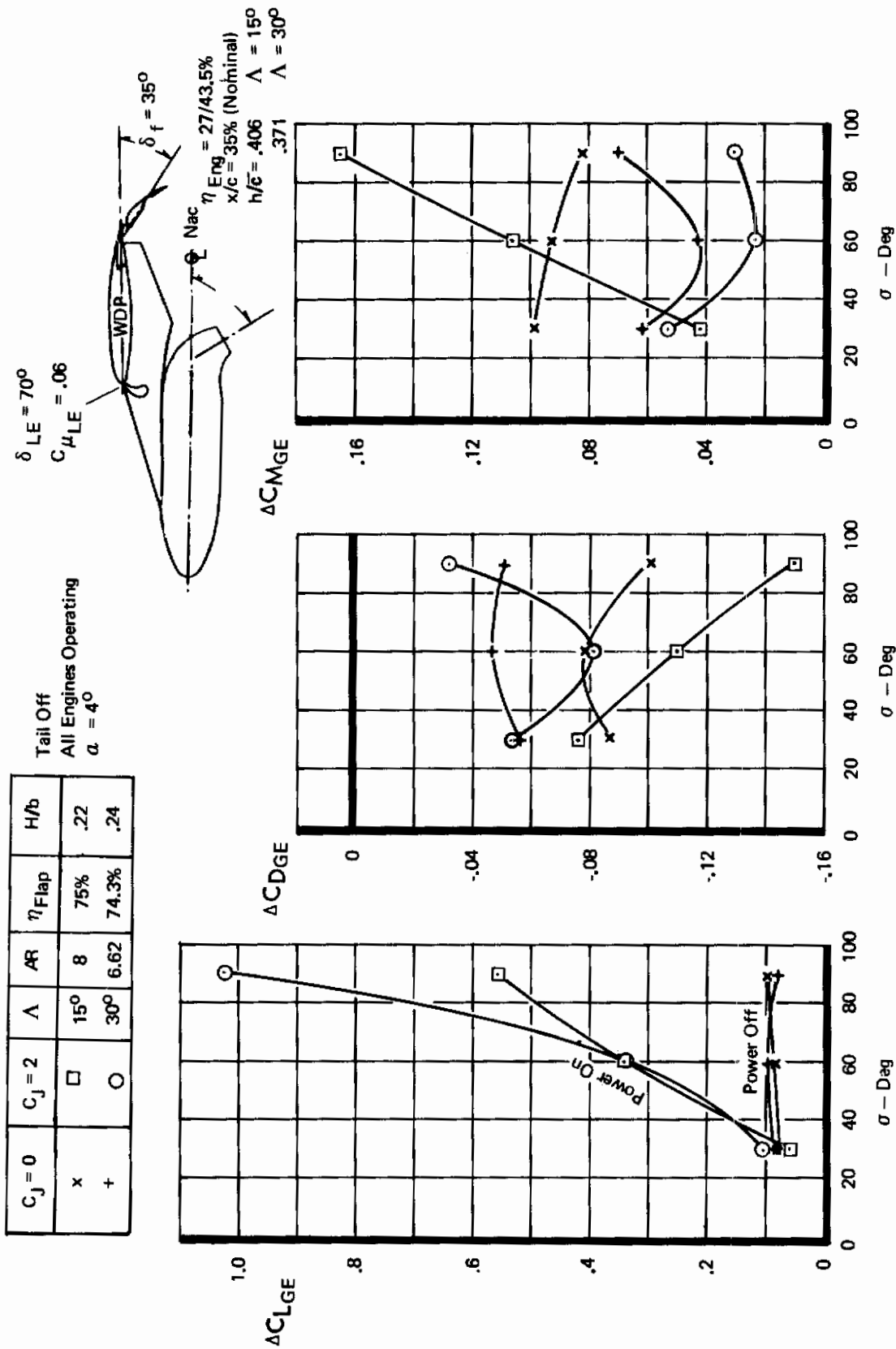


Figure 82: Effect of Sweep Angle on Ground Effect

4.4 Maximum Lift

This section discusses how maximum lift is affected by vectored thrust. The following table presents a brief summary of the trends obtained.

TABLE XI EFFECT OF VECTORED THRUST ON MAXIMUM LIFT

PARAMETER	FIG.	EFFECT
Thrust Coefficient	83	$C_{L_{max}}$ and stall angle increase with thrust. Favorable lift interference increases with thrust.
Thrust Vector Angle	84	60° vector angle gives highest $C_{L_{max}}$.
Nacelle Location		
o Chordwise	84	$C_{L_{max}}$ improves as nacelle moves aft for 60° and 90° vector angle.
o Spanwise	85	Inboard mounted nacelle gives slightly better $C_{L_{max}}$.
o Height	86	Lower nacelle showed slight increase in $C_{L_{max}}$.
Nacelle Type	85	Dual pod gives slightly lower $C_{L_{max}}$ than single pods.
One Engine Inoperative	87	One engine out decreases favorable lift thrust interference by 25 to 40%.
T.E. Flap Deflection	88	T.E. flap deflection slightly increases the favorable thrust interference on $C_{L_{max}}$.
L.E. Flap	89	L.E. flap increases power-on $C_{L_{max}}$ by 0.7 and α stall by 8.5°.
Wing Sweep	90	Reducing wing sweep increases $C_{L_{max}}$ power-on and power-off. Lift interference at $C_{L_{max}}$ shows essentially no change.
Stall Characteristics	91	15° wing sweep has a more definitive stall than 30° wing sweep for both power-on and power-off.
Ground Effect	92	Ground effect reduces both $C_{L_{max}}$ and stall angle.
Reynolds Number	93	An increase in Reynolds number slightly increases $C_{L_{max}}$ both power-on and power-off.

4.4.1 Thrust Coefficient

Figure 83 illustrates the effect of power on a typical lift curve and shows, in particular, the favorable thrust interference which exists at $C_{L_{max}}$. For example, $C_{L_{max}}$ due to thrust interference is as high as 0.7 at $C_J = 2.0$, flaps down. Note that the angle of attack at which $C_{L_{max}}$ occurs generally increases as C_J increases indicating the jet sink effect (see Section 4.1.1.1). Typically, the increase in angle was 11° for a C_J of 2.0 with flaps down. The stall characteristics of this model exhibited no large, abrupt loss of lift when the stall angles were exceeded.

4.4.2 Thrust Vector Angle

Figure 84 presents the results of varying the thrust vector angle from 30° to 90° for several chordwise nacelle positions. The highest power-on $C_{L_{max}}$ occurs near 60° thrust vector angle for the range of nacelle chordwise locations tested. The most favorable thrust interference at $C_{L_{max}}$ also occurs near $\sigma = 60^\circ$. (The effect of thrust vector angle is small for power-off.)

4.4.3 Nacelle Location

The effects of various nacelle locations are discussed below, including variations in chordwise, spanwise and height positions. A comparison of the single pods to dual pods is also made.

4.4.4 Nacelle Chordwise Position

Figure 84 also illustrates the nacelle chordwise effects at several vector angles.

For $\sigma = 30^\circ$, the highest power-on $C_{L_{max}}$ occurs at the forward nacelle location ($x/c = 0\%$) while for a $\sigma = 60^\circ$ and 90° , the most aft nacelle location is best.

4.4.5 Nacelle Spanwise Position

Figure 85 illustrates the influence of locating the nacelles at various spanwise locations. As shown, the inboard position is slightly more favorable than the outboard position for the 15° sweep, $60^\circ \sigma$ configuration shown. However, the data in Ref. 2 shows that the nacelles should be more outboard as σ increases, particularly for the 30° sweep condition.

4.4.6 Nacelle Height

Data shown in Figure 86 illustrates that the influence of lowering the nacelle $\Delta h/\bar{c} = .08$ (at $\Lambda = 30^\circ$) showed only a slight (.07) increase in $C_{L_{max}}$ for most configurations tested.

$\eta_{Eng} = 27/43.5\%$ $\Lambda = 30^\circ$
 $h/c = 0.371$ Tail Off
 Nominal Nozzle Location Free Air
 $x/c = 35\%$ All Engines Operating

$AR = 6.62$
 $\eta_f = 74.3\%$

Note: $q = 10$.psf

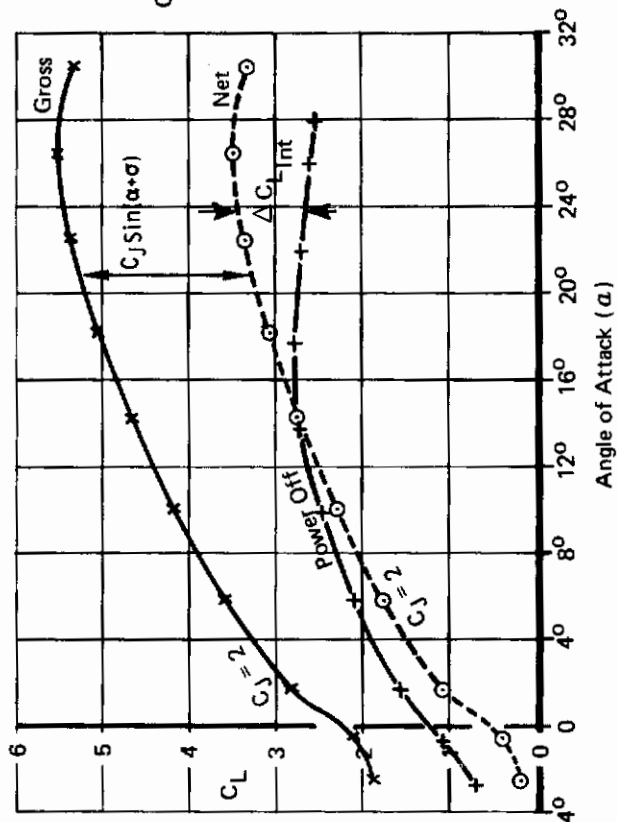
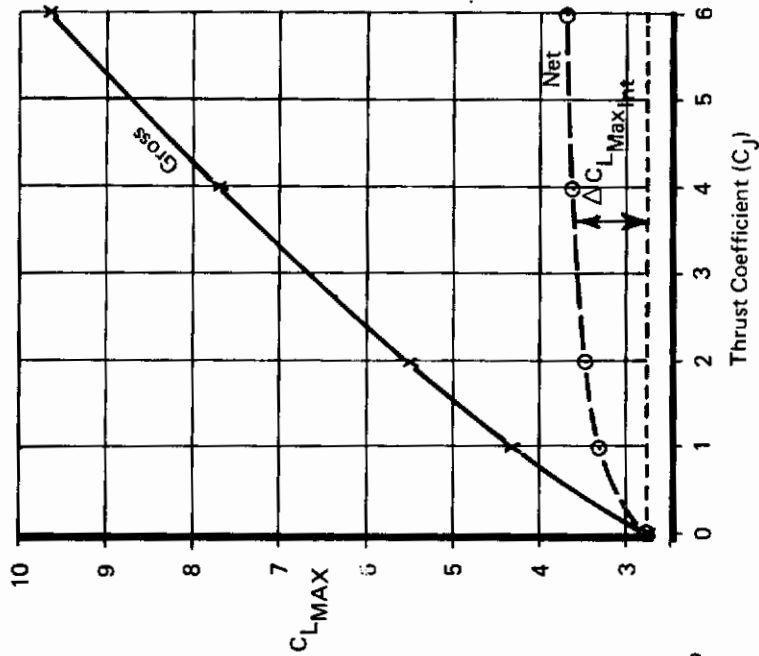
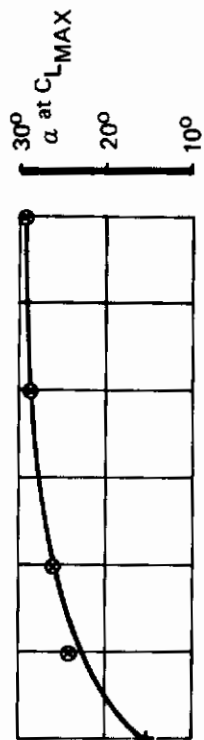
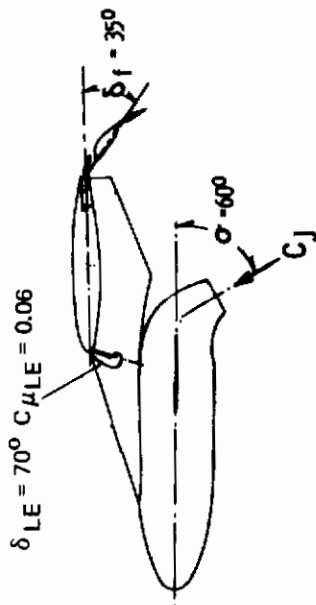
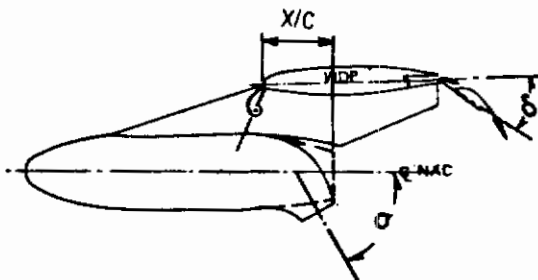


Figure 83: Effect of Thrust Coefficient on $C_{L\text{Max}}$

Contrails

$\Lambda = 30^\circ$
 $\delta_f = 35^\circ$
 Tail Off
 Free Air
 $\delta_{LE} = 70^\circ$
 $AR = 6.62$
 $\eta_{Eng.} = 27/43.5\%$
 $h/\bar{c} = 0.371$
 $\eta_f = 74.3\%$
 $C_{\mu_{LE}} = 0.06$



All Engines Operating

$C_J = 2$

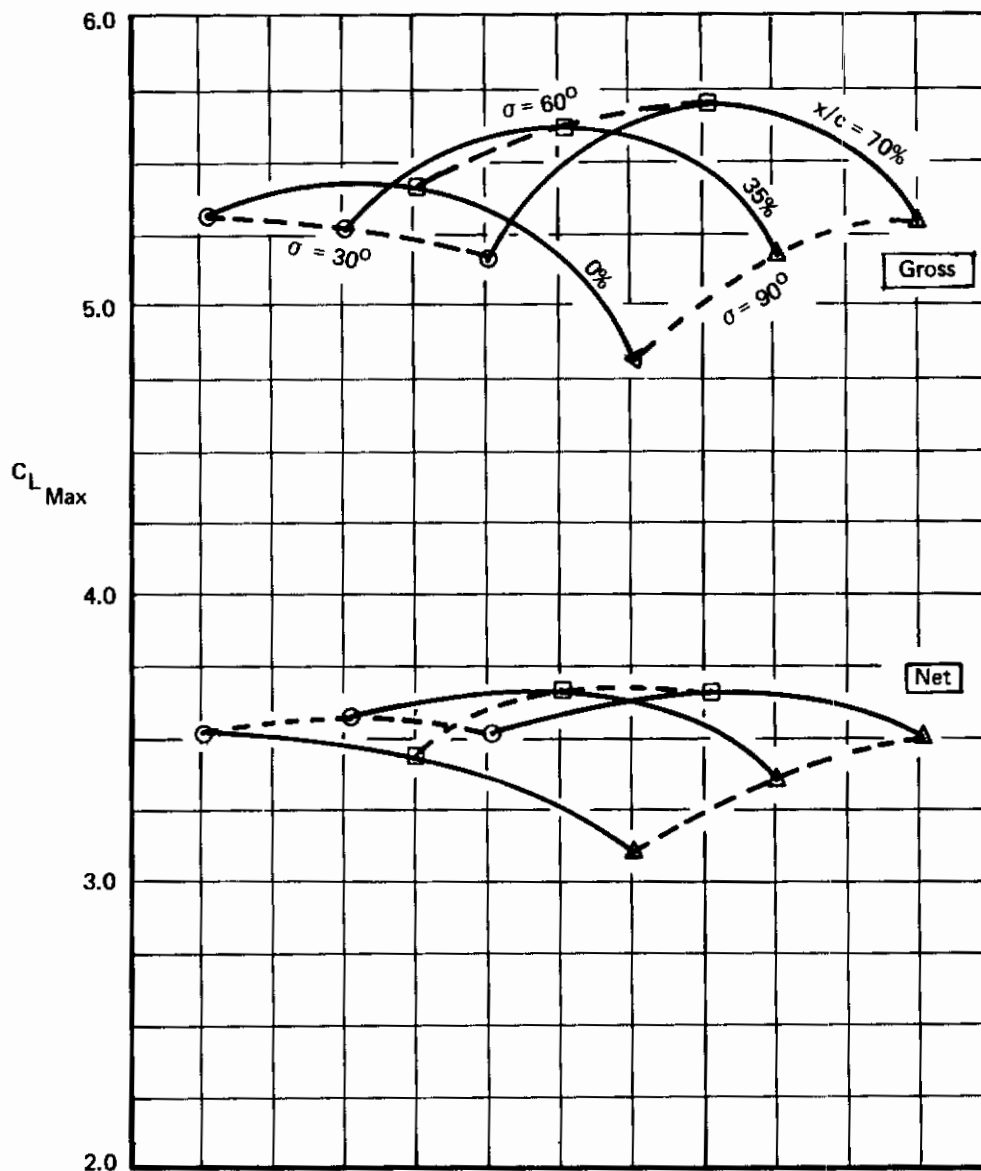


Figure 84: Effect of Thrust Vector and Nacelle Chordwise Location on $C_{L_{Max}}$

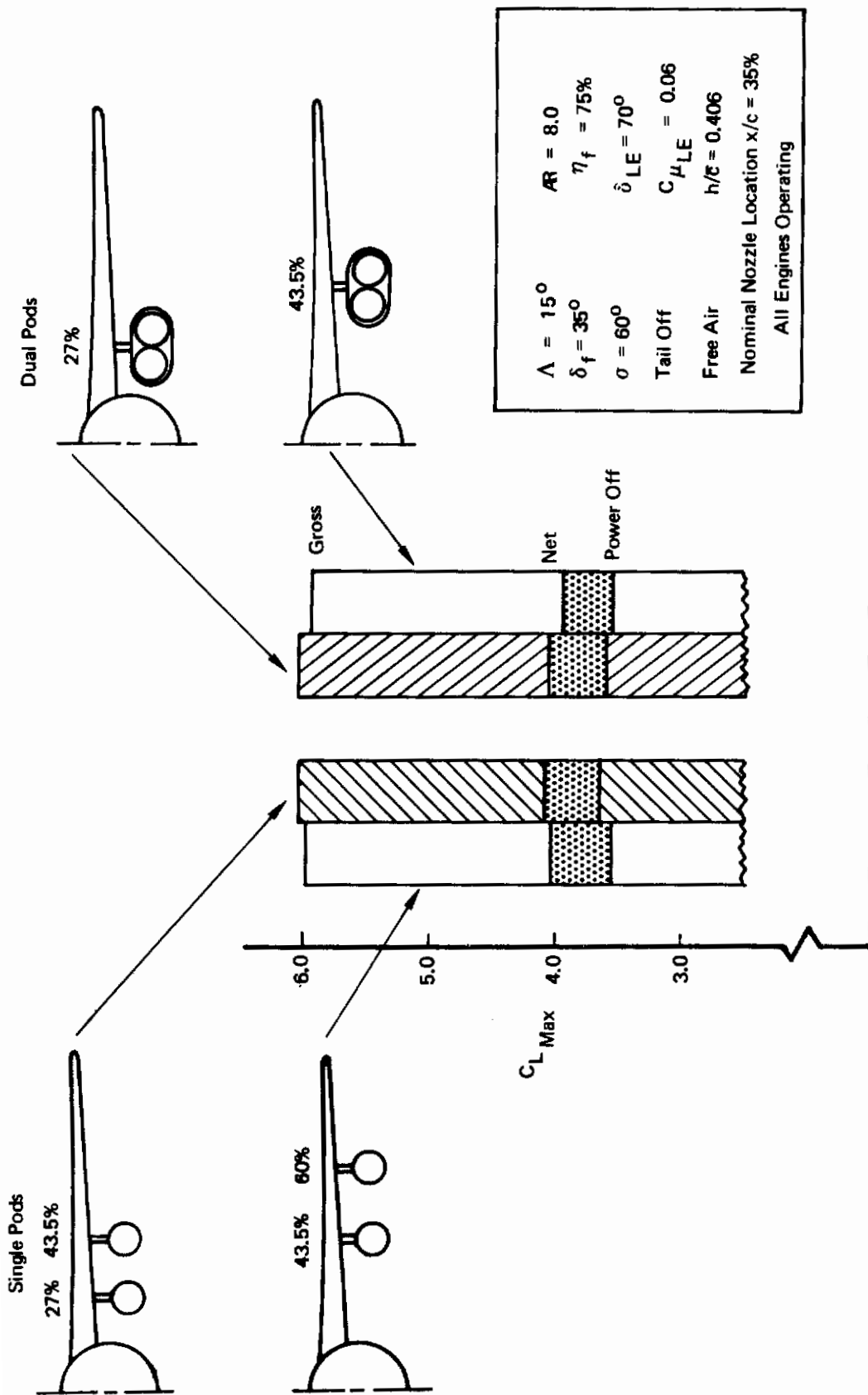


Figure 85: Effect of Nacelle Spanwise Location and Nacelle Type on C_L Max

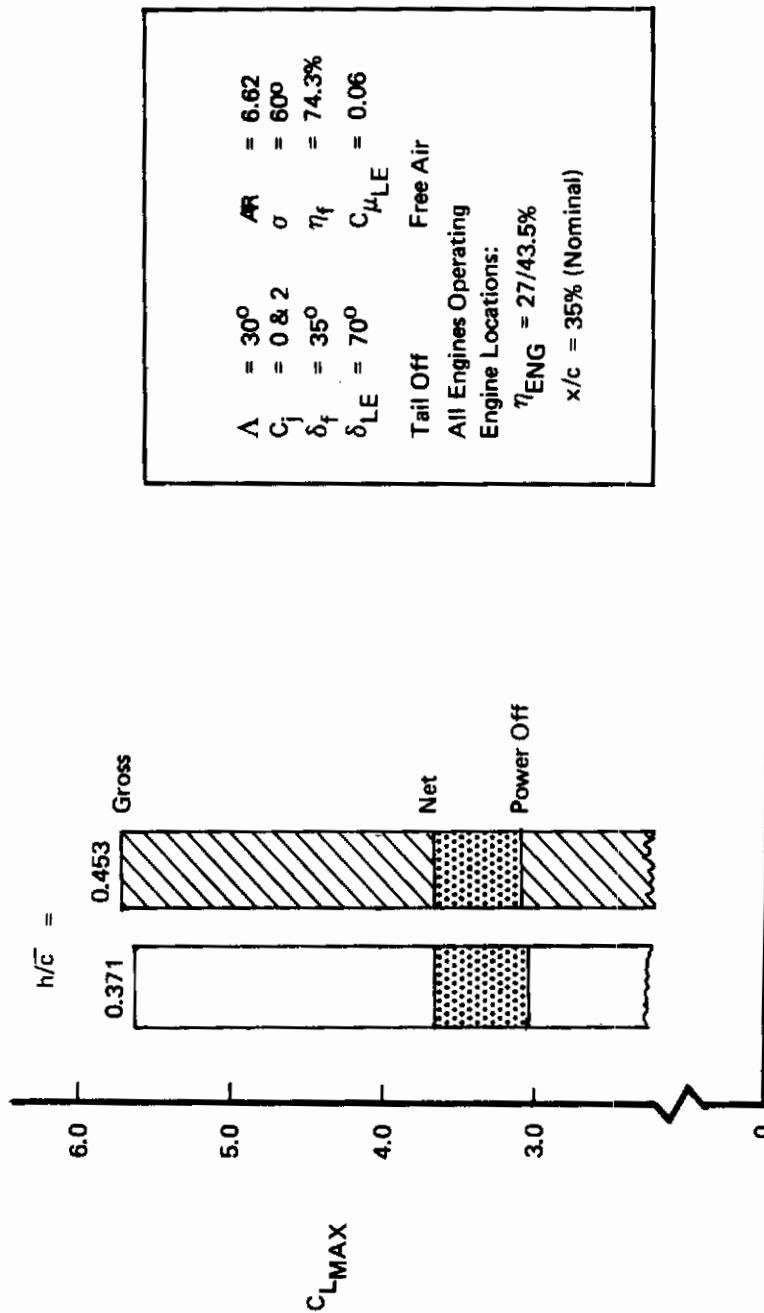
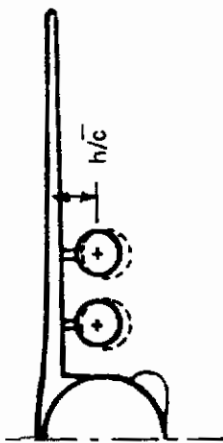


Figure 86: Effect of Nacelle Height on C_{LMAX}

4.4.7 Single Pods vs Dual Pods

Figure 85 compares the dual pods and single pods and shows very little difference in $C_{L_{max}}$ level at $\sigma = 60^\circ$. The data in Ref. 2 shows a slight trend for the $C_{L_{max}}$ of the dual pod configuration to deteriorate compared to the configuration with single pods as σ increases.

4.4.8 One Engine Inoperative

It was found that the failure of any one of the four engines reduced the favorable lift thrust interference at $C_{L_{max}}$ by 25 to 40% for $\sigma = 60^\circ$. Compare Figure 87(a) to (c) and (d). Reduction of the all-engine thrust to give a change of thrust equivalent to an engine-out condition reduced the favorable interference, by comparison, only 15%. Compare Figure 87(a) to (b). This dependence of the lift change on the thrust distribution is partly explained by the curve of lift interference versus thrust shown in Figure 83, which shows that a total loss of thrust gives a much larger loss of lift compared to a small change of thrust at the higher thrust levels. Similar results were obtained at $\sigma = 30^\circ$ and 90° .

4.4.9 Trailing-Edge Flap Deflection

The effect of trailing-edge flaps, power-off, is discussed in Section III. The influence of trailing-edge flap deflection comparing power-on and power-off $C_{L_{max}}$ is demonstrated in Figure 88. $C_{L_{max}}$ is the highest power-off between δ_f 30° and 35° . The highest power-on $C_{L_{max}}$ lies between δ_f of 35° and 48° . For both power-on and power-off, only a small increase in $C_{L_{max}}$ (0.09 and 0.06, respectively) occurs from $\delta_f = 20^\circ$ to 35° . The favorable thrust interference at $C_{L_{max}}$ increases from essentially zero, flaps-up (see Ref. 2) to an increment of $0.5 \Delta C_{L_{INT}}$ at 48° flaps, with most of the increase occurring between flaps-up and $\delta_f = 20^\circ$.

4.4.10 Leading-Edge Flap

Figure 89 presents the effect of the leading-edge flap for power-on and power-off conditions. As shown, the $\Delta C_{L_{max}}$ due to leading flap is 0.40 and 0.70 for $G_J = 0$ and $C_J = 2.0$, respectively. The stall angle of attack increases approximately 8.5° in both cases. Note that, for this comparison, the leading-edge blowing was operating even with the leading-edge removed. With no leading-edge blowing in the flaps-up case, the $C_{L_{max}}$ increment due to L.E. flap, power-off, was 1.0 (shown in Section III).

4.4.11 Wing Sweep

Figure 90 shows that an increase of wing sweep decreases $C_{L_{max}}$ substantially. (Note that aspect ratio changes simultaneously.) This effect is also shown with power-off in Section III. The decrease of $C_{L_{max}}$ with increasing sweep, power-on, is less than that shown with power-off. This implies that the thrust interference is more favorable for the 30° sweep wing than for the 15° at $C_{L_{max}}$. Data in 4.1.1.12 shows that thrust interference on lift was generally more favorable for 15° sweep than 30° sweep with the above case being the exception rather than the rule (see Figure 43).

Contrails

$\Lambda = 15^\circ$	$AR = 8.0$
$\delta_f = 35^\circ$	$\eta_f = 75\%$
$\sigma = 60^\circ$	$\delta_{LE} = 70^\circ$
Tail Off	$C_{\mu_{LE}} = 0.06$
Free Air	$h/c = 0.406$
Nominal Nozzle Location $x/c = 35\%$	

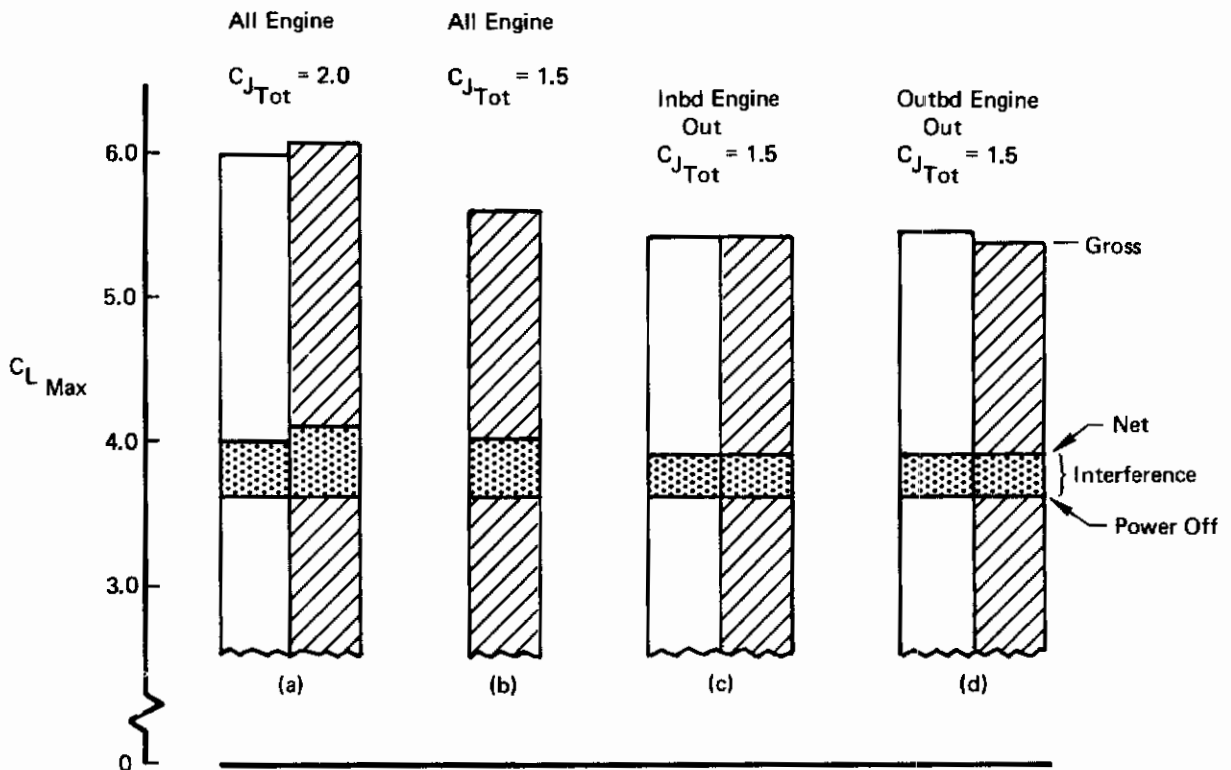
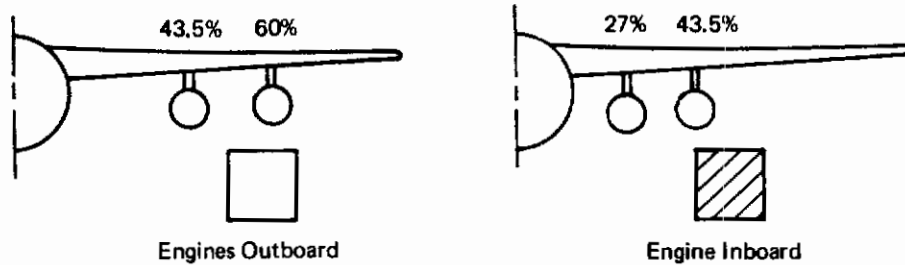


Figure 87: Effect of an Engine Failure on $C_{L_{Max}}$

Contrails

$\Lambda = 30^\circ$ $AR = 6.62$
 Tail Off $\eta_f = 74.3\%$
 Free Air $\delta_{LE} = 70^\circ$
 $\eta_{Eng} = 27/43.5\%$ $C_{\mu_{LE}} = 0.06$
 $h/\bar{c} = 0.371$ $\sigma = 30^\circ$
 Nominal Nozzle Location $x/c = 35\%$
 All Engines Operating

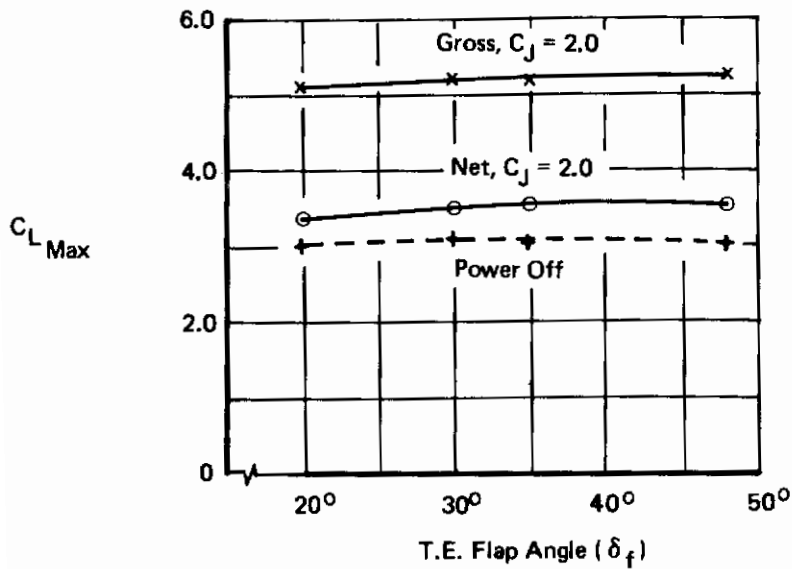
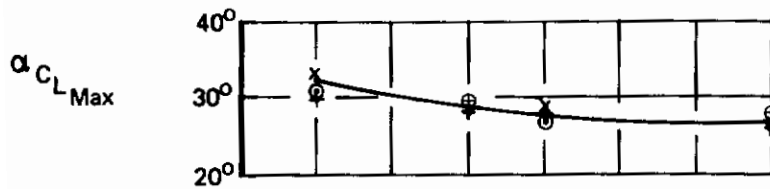
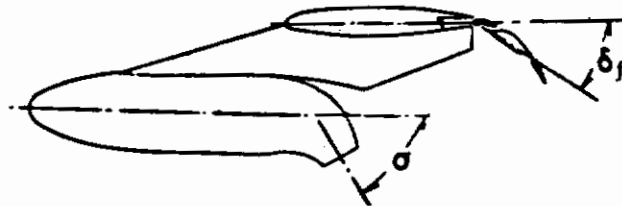


Figure 88: Effect of Flap Angle On $C_{L Max}$

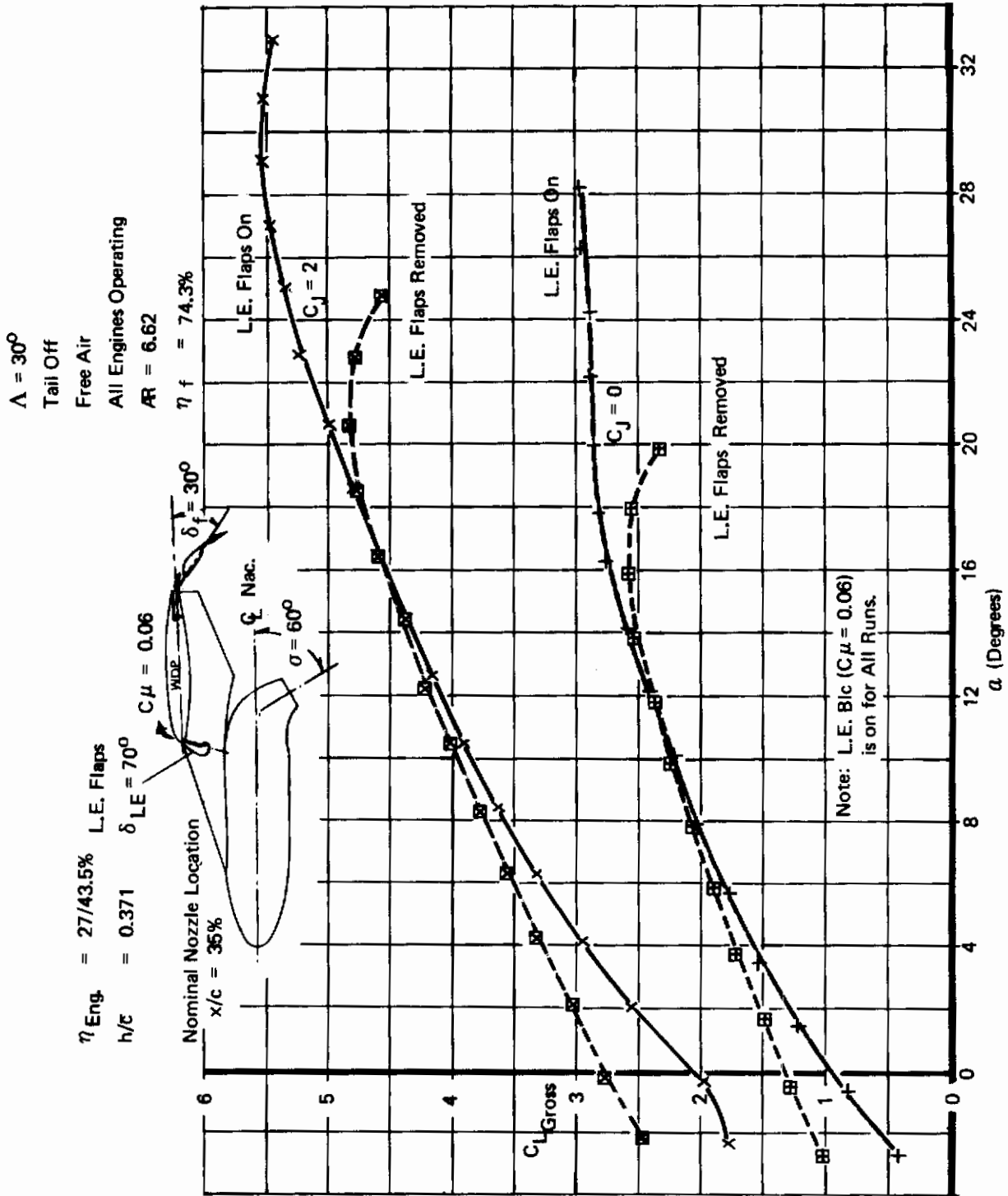


Figure 89 : Effect of L.E. Flap on $C_{L\text{ Max}}$

Contrails

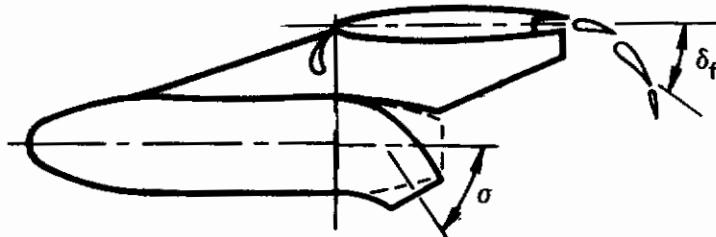
Tail Off $\eta_{Eng.} = 27/43.5\%$

Free Air $\delta_{LE} = 70^\circ$

$\delta_f = 35\%$ $C_{\mu_{LE}} = 0.06$

$\sigma = 60^\circ$

Nominal Nozzle Location $x/c = 35\%$
ALL ENGINES OPERATING



Sweep Λ	Aspect Ratio AR	Flap Span η_f	h/\bar{c}
15°	8	75%	0.406
30°	6.62	74.3%	0.371

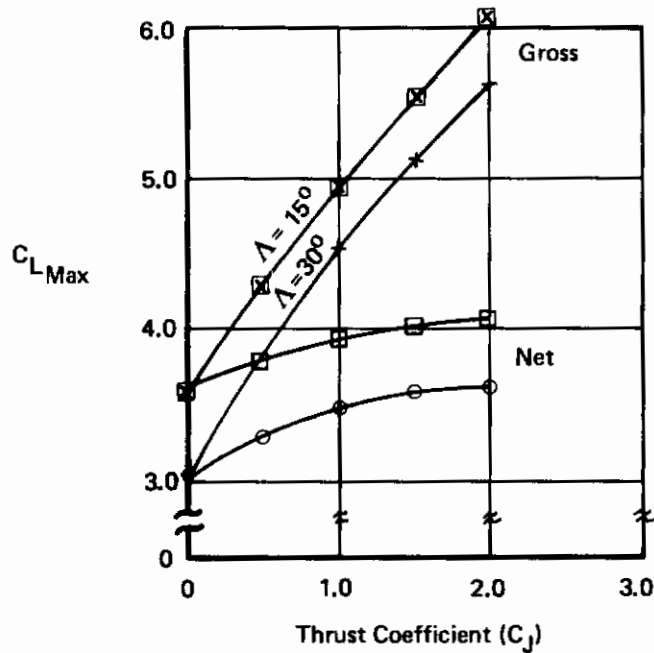


Figure 90: Comparison of $C_{L_{Max}}$ for 15° and 30° Wing Sweep

4.4.12 Stall Characteristics

Figure 83 shows that for flaps-down, power-off C_L is relatively constant for increasing angle of attack above the initial stall. This is also shown on Figure 7, Section III. Figure 83 also shows flaps-down power-on effects. With power-on, both $C_{L_{max}}$ and the stall angle increase. Power-on also gives a more definite, yet mild stall, as compared to the power-off data.

Figure 91 compares lift for two wing sweeps for the flaps-up configuration. Both the power-on and power-off data show that the 15° wing sweep has a more definite stall compared to 30° wing sweep. Note that, at 30° wing sweep, the lift continues to increase to the highest angle of attack tested (32°) both power-on and power-off. The same result occurs for the power-off flaps-up data shown in Figure 16, Section III.

4.4.13 Ground Effect

As discussed in Section 4.3, the angle of attack range was restricted while in the proximity of the moving belt ground plane. However, as shown in Figure 92, a semi-empirical method (Ref. 6) was used to extrapolate the test data to higher α 's in ground effect. The prediction shows that the effect of the ground is to reduce $C_{L_{max}}$ and the corresponding stall angle. For example at $H/b = .209$, the stall angle is reduced by 3.5° and $C_{L_{max}}$ is reduced by .22, power-off.

Note that the predicted reduction in $C_{L_{max}}$ is smaller power-on than for power-off. This is because the prediction method assumes that the favorable effect of the ground on the lift-thrust interference observed at moderate angles of attack (see Section 4.1.2) also occurs at high angles of attack.

4.4.14 Reynolds Number

Figure 93 illustrates that the effect of an increase in the flow velocity in the wind tunnel test section led to an increase in $C_{L_{max}}$. The most influential parameter, in the case of $C_{L_{max}}$, is the freestream Reynolds Number. As shown, an increase of about 0.2 in $C_{L_{max}}$ was observed, both power-on and power-off, when freestream Re/ft increased from 0.55×10^6 to 0.82×10^6 . This change matches unpublished data measured on other high-lift configurations.

At the very high C_L 's attainable with modern high-lift systems, local pressures on the wing surface, particularly near the leading edge, fall to very low values. Locally, the flow velocity can become a significant fraction of the speed of sound. Compressibility effects can thus affect maximum lift. Unpublished Boeing data for wings similar to the one discussed in this report show that beyond $M = .15$, further increases in freestream Mach Number will result in declining $C_{L_{max}}$.

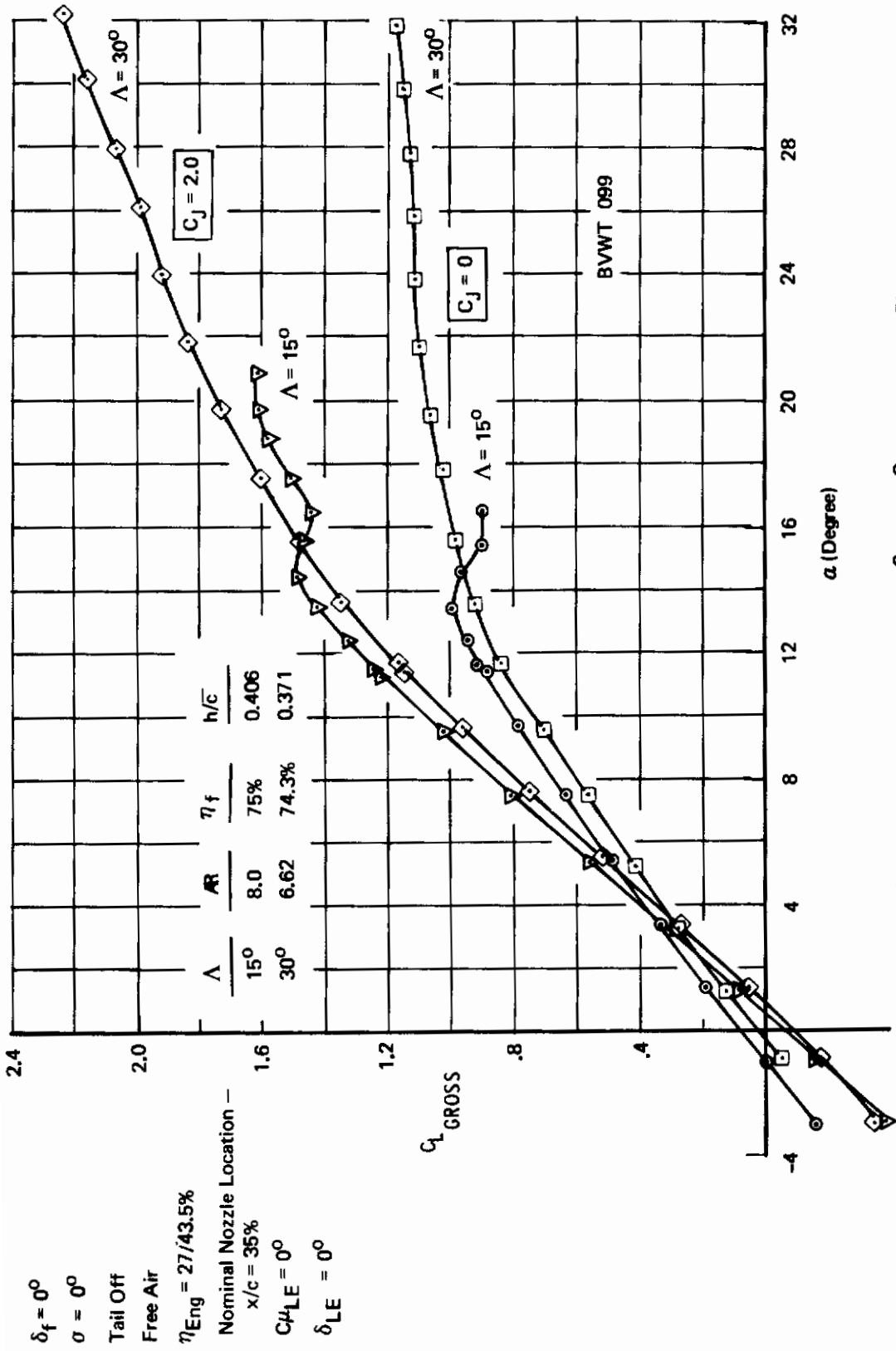


Figure 91: Comparison of Lift for 15° and 30° Wing Sweep, Flaps Up

$\Lambda = 15^\circ$ $AR = 8.0$
 $\delta_f = 35^\circ$ $\eta_{Eng} = 27/43.5\%$
 $\sigma = 60^\circ$ $\eta_f = 75\%$
 $\delta_{LE} = 70^\circ$ $h/c = 0.406$
 $C_{\mu LE} = .06$ TAIL OFF

Nominal Nozzle Location $x/c = 35\%$

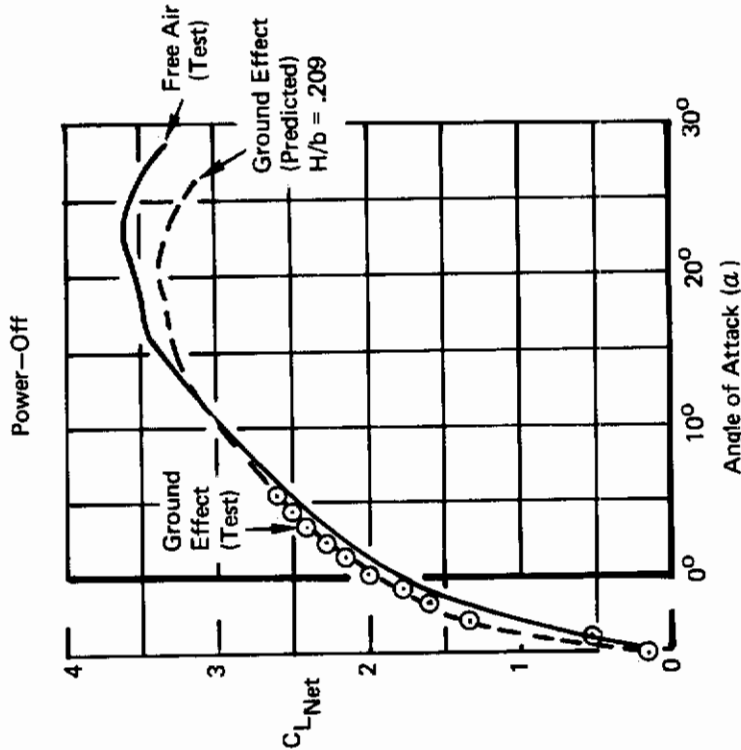
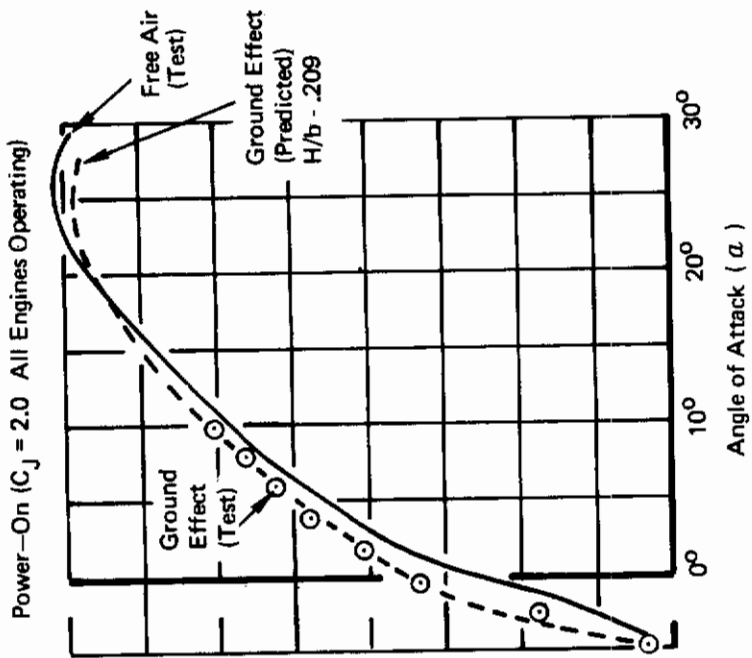
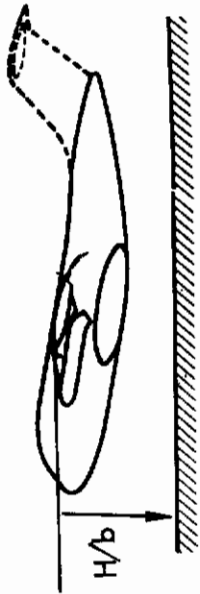


Figure 92: Effect of Ground Proximity on $C_{L\text{Max}}$

Contrails

$\Lambda = 30^\circ$

$AR = 6.62$

Tail Off

Free Air

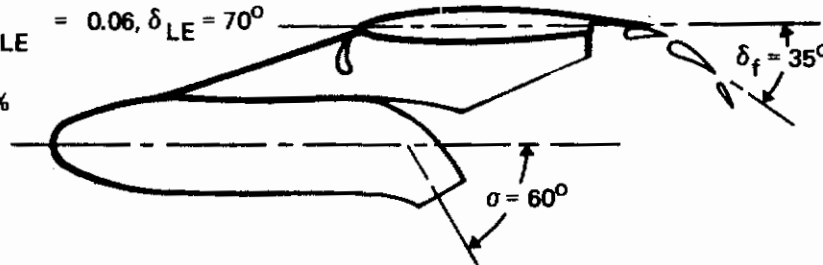
All Engines Operating
Nominal Nozzle $x/c = 35\%$

$\eta_f = 74.3\%$

$\eta_{Eng} = 27/43.5\%$

$h/c = 0.371$

$C_{\mu LE} = 0.06, \delta_{LE} = 70^\circ$



$\alpha_{C_{L Max}}$

30°
20°
10°

q_{psf}

$Re_{co}/ft.$

M_∞

10

0.55×10^6

0.08

22

0.82×10^6

0.12

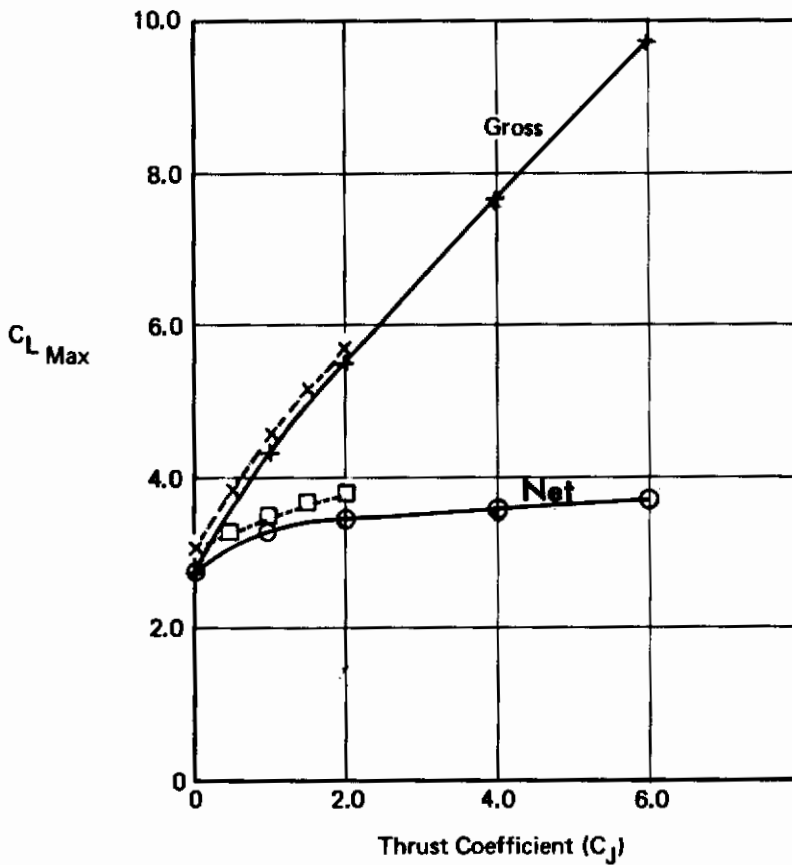


Figure 93: Effect of Reynolds Number on $C_{L Max}$

4.5 Longitudinal Stability

The effects of various vectored thrust parameters and air-plane variables are analyzed herein with respect to their impact on longitudinal stability derivatives. The more significant effects are summarized in Table XII.

4.5.1 Effect of Vectored Thrust

4.5.1.1 Thrust Coefficient

Net lift and net pitching moment for 30° vector angle are presented on Figure 94. These data are typical of the effects of thrust on longitudinal stability, since the entire family of sweep and thrust vector angles tested exhibited similar characteristics. Vectored thrust also adds a positive increment to the pitching moment curves.

The direct pitching moment (no aerodynamic or interference components) due to vectored thrust is presented on Figure 95. The data indicate that the direct thrust produced pitching moments can exceed the total aerodynamic and interference pitching moment (Figure 94) depending upon the location of the nacelles and nozzles.

The aerodynamic center, lift slope and moment interference were evaluated at an angle of attack equal to 8° to minimize the effect of separation on either the wing upper or lower surfaces. An 8° angle of attack is also representative of the climb-out and approach flight condition. The effect of power on the aerodynamic center, lift slope, and moment interference are presented on Figures 96 and 97. The tail-off aerodynamic center tends to shift from 10 to 30% aft as C_J increases to 2.0. The tail-on aerodynamic center tends to remain fixed or decrease slightly as C_J increases to 2.0. The lift slope increases as C_J increases, either tail-on or tail-off. The pitching moment interference increases with both thrust deflection and thrust coefficient.

4.5.1.2 Thrust Deflection Angle

The effect of thrust deflection angle is presented on Figure 98. When the thrust is deflected from $\sigma = 30$ degrees to $\sigma = 90$ degrees the aerodynamic center shifts aft, depending on C_J . The lift slope increases with thrust deflection and is also dependent upon C_J . The moment interference increases with both thrust level and deflection. The pitching moment interference also increases with sweep as shown on Figure 98.

4.5.1.3 Nacelle Position

The fore and aft nacelle position affects the power-off aerodynamic center position and lift slope level. Moving the nacelles forward moves the aerodynamic center forward and reduces the lift curve slope, as shown in Figures 99 and 100. With power on ($C_J = 2.0$), the variation of aerodynamic center with chordwise position is small (approximately 5%) at all thrust deflections while the lift slope

Table XII: Effect of Vectored Thrust on Longitudinal Stability

PARAMETER	FIG.	PITCHING MOMENT $\alpha = \text{Variable}$	AERODYNAMIC CENTER $\alpha = 8^\circ$	LIFT SLOPE $\alpha = 8^\circ$	MOMENT INTERFERENCE $\alpha = 8^\circ$
Thrust Coefficient	94 96 97	Increases C_m . (Figure 94)	Thrust moves a.c. aft tail-off, tail-on a.c. unaffected. (Figures 96 and 97)	Thrust increases the lift slope. (Figures 96 and 97)	Thrust increases pitching moment interference. (Figures 96 and 97)
Thrust Deflection	98		Deflection moves the a.c. aft.	Deflection increases the lift slope.	Deflection increases the moment interference.
Nacelle Position Chordwise	99 100		Power-off the a.c. shifts forward with the nacelle. Power-on small effect.	Moving nacelle aft decreases $C_{L\alpha}$ power-on, increases $C_{L\alpha}$ power-off.	Moment interference max. at mid (35% chord) position.
Spanwise	101		The a.c. shifts aft power-off and forward power-on as the nacelle moves outboard.	The lift slope decreases as the nacelle moves outboard except at $\lambda = 15^\circ$ power-on.	The moment interference decreases as the nacelles move outboard.
One Engine Inoperative	102				Effect is small ($\pm 0.015 \Delta C_{mINT}$)

EFFECT OF AIRPLANE VARIABLES ON LONGITUDINAL STABILITY

Wing Sweep	103		Increasing sweep shifts the a.c. aft.	Increasing sweep increases lift slope.	Sweep increases moment interference.
T. E. Flap	104		T. E. flap deflection has little effect.	T. E. flap deflection decreases $C_{L\alpha}$ slightly.	T. E. flap deflection has slight effect.
Angle of Attack	105	Increasing α causes non-linearities and pitch-up.			Over the normal range $\Delta C_{mINT} = \pm 1$ or less.
Ground Effect	106				Moment interference due to ground height greatest at $\sigma = 30^\circ$.

EFFECT OF THRUST ON DOWNWASH

Thrust Coefficient	107	Increasing thrust increases downwash, and linearizes ϵ versus α .			
Thrust Deflection Angle	107	Increasing thrust deflection angle increases downwash.			
One Engine Inoperative	108	One engine out equivalent to operating at .75 C_J , all engines operating.			
T-Tail Vs. Body Mounted Tail	107	Downwash 10 degrees greater for body mounted tail.			
Ground Effect	109	Ground effect reduces downwash.			

Nacelle Location $\eta = 27/43.5\%$ Span
 $h/\bar{c} = .371$
 Nozzle Location 35% Chord
 TE Flap 35°
 Sweep 15°
 Thrust Deflection 30°
 Free Air

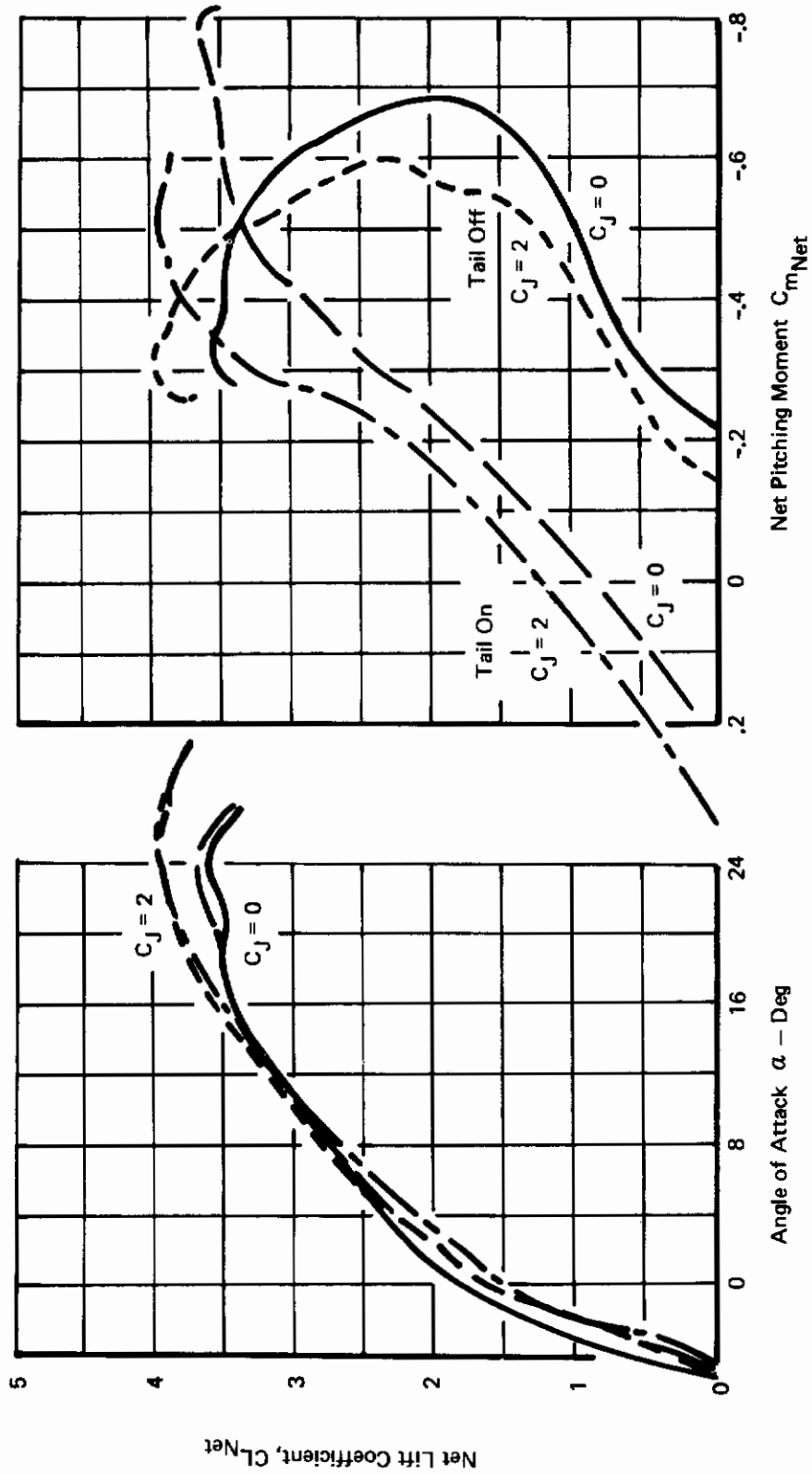


Figure 94 : Effect of Thrust on Longitudinal Stability

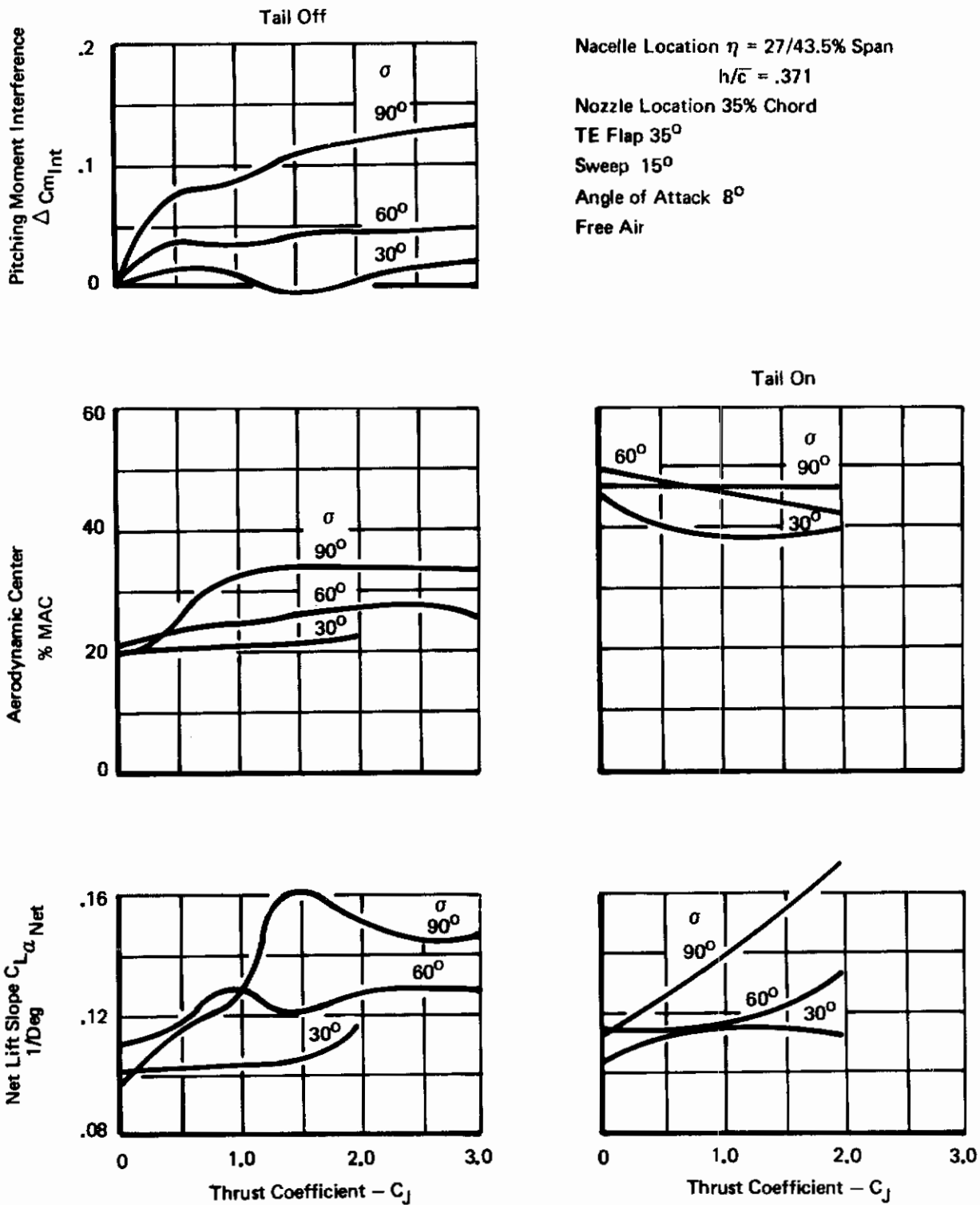


Figure 97: Effect of Thrust on Longitudinal Stability
 $\Lambda = 30^\circ$

Nacelle Location $\eta = 27/43.5\%$ Span

$h/\bar{c} = .371$

Nozzle Location 35% Chord

Angle of Attack 8°

TE Flap 35°

Free Air

Tail Off

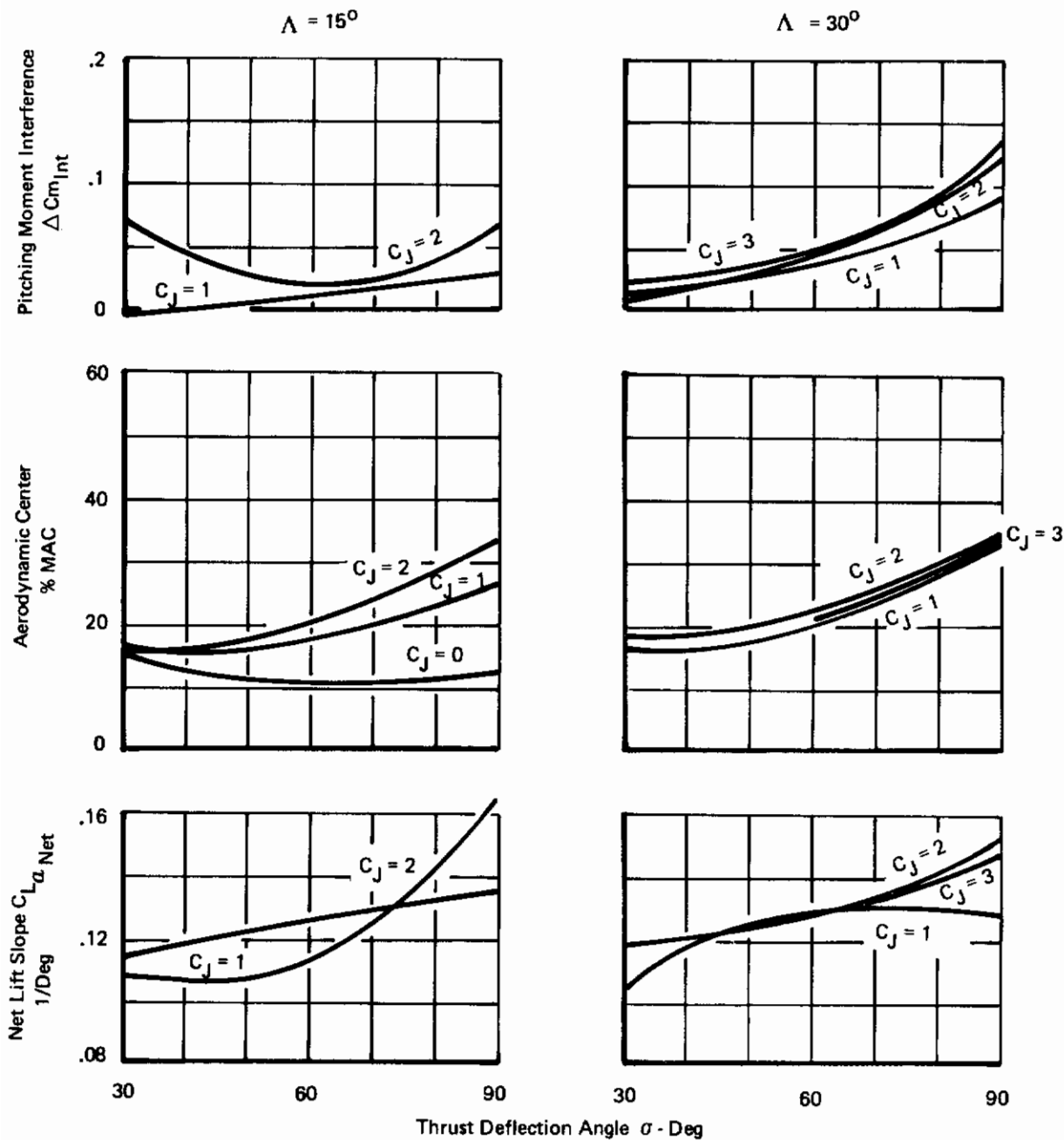


Figure 98: Effect of Thrust Deflection Angle on Longitudinal Stability

Nozzle Location $\eta = 27/43.5\%$ Span
 $h/\bar{c} = .371$

TE Flap 35°
 Tail Off
 Sweep 15°

Angle of Attack 8°

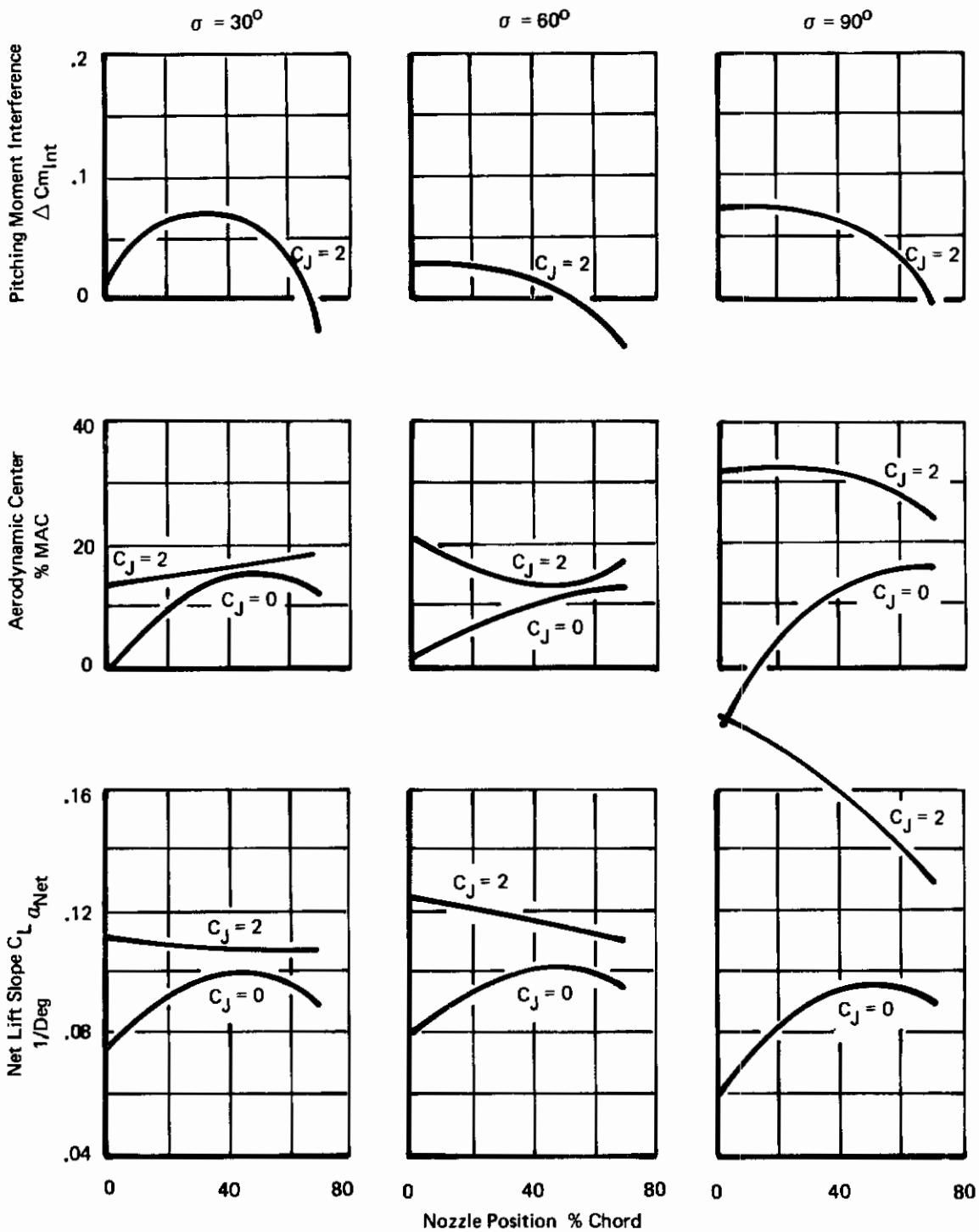


Figure 99: Effect of Nozzle Chordwise Position on Longitudinal Stability
 $\Lambda = 15^\circ$

Nacelle Location $\eta = 27/43.5\%$ Span
 $h/\bar{c} = .371$
 Angle of Attack 8°

TE Flap 35°
 Tail Off
 Sweep 15°

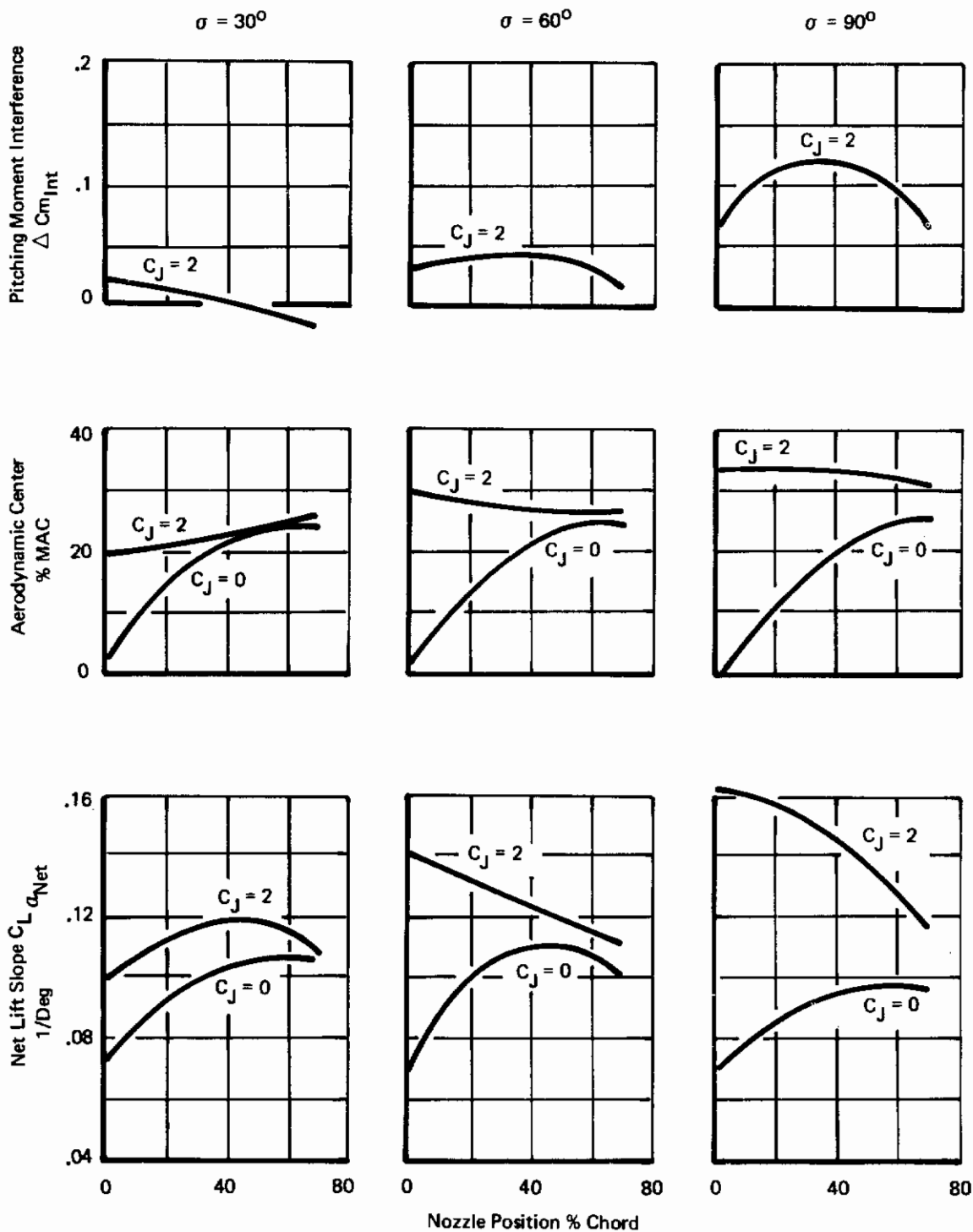


Figure 100: Effect of Nozzle Chordwise Position on Longitudinal Stability
 $\Lambda = 30^\circ$

variation with chordwise nacelle position becomes more exaggerated as the thrust deflection angle increases. The pitching moment interference presented on Figures 99 and 100 varies substantially with nacelle chordwise position, with the minimum occurring at the 70% chord position and the maximum occurring at the 35% chord position. However, the trend is not consistent for changes in sweep and thrust deflection.

The effect of spanwise location is opposite power-on versus power-off as shown on Figure 101. When the nacelles are moved outboard, the aerodynamic center shifts aft up to 5% power-off and forward up to 5% power-on ($C_J = 2.0$). Moving the nacelles outboard decreases the lift slope up to .025 except for $\Lambda = 15^\circ$ power-on, which shows an increase of .016. The pitching moment interference decreases up to .09 as the nacelles move outboard.

4.5.1.4 One Engine Inoperative

The effect of an engine out on longitudinal stability is small. A comparison between all-engine operating power levels and the one-engine inoperative effects is also included in Figure 102. With 15 degree sweep, the moment interference is reduced from .01 to .02 and has the same characteristics as the all-engine configuration operating at a $C_J = 2.0$ (each engine has a $C_J = .5$). With 30 degree sweep, there is very little difference between the all-engine operating data either $C_J = 1.5$ or $C_J = 2.0$. With an outboard engine inoperative, the moment interference increases .015 but with an inboard engine inoperative, the moment interference decreases .015.

4.5.2 Effect of Airplane Variables

4.5.2.1 Wing Sweep

The effect of increasing the wing sweep from 15° to 30° is to reduce the maximum C_L and to increase the pitching moment interference as presented on Figure 103. The aerodynamic center shifts aft about 7 percent. The lift curve slope at an angle of attack of 8° increases about .01 for 30° of sweep. This increase is the result of separation on the underside of the leading-edge device, and is also to be seen on the power-off lift curve (Figure 16, Section III).

4.5.2.2 Trailing Edge Flap Deflection

The effect of flap deflection over the range of 20 to 48 degrees is relatively minor on longitudinal stability as shown on Figure 104. The lift slope tends to decrease while the aerodynamic center remains relatively constant (within 5%). The pitching moment interference decreases approximately .05 at 30 degrees of sweep and increases .04 at 15 degrees of sweep.

4.5.2.3 Angle of Attack

The net lift and net pitching moment coefficients are non-linear with angle of attack due to separation as shown on Figure 94.

TE Flap 35°
 Angle of Attack 8°
 Tail Off
 Free Air

Nacelle Spanwise Locations

η Inboard = 27/43.5% Span $h/\bar{c} = .371$

η Outboard = 43.5/60% Span $h/\bar{c} = .371$

Nozzle Location 35% Chord

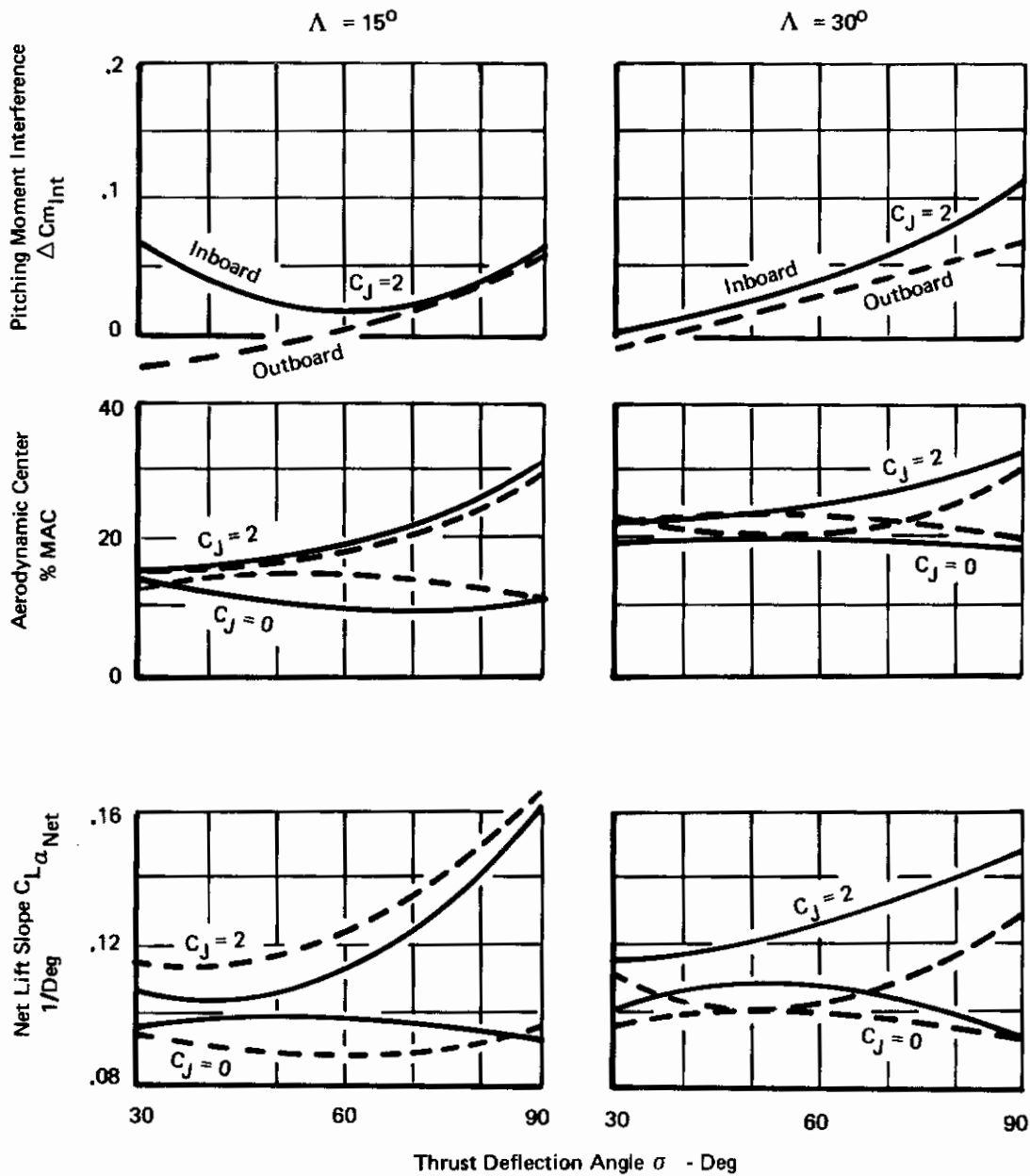


Figure 101: Effect of Nacelle Spanwise Location on Longitudinal Stability

Nacelle Location $\eta = 27/43.5\%$ Span
 $h/\bar{c} = .371$
 Nozzle Location 35% Chord
 TE Flap 35°
 Angle of Attack 8°
 Free Air Tail Off

Total C_j	Eng. Inop.	Line Style
2.0	None	—————
1.5	None	-----
1.5	Inboard	- - - - -
1.5	Outboard	— · — · —

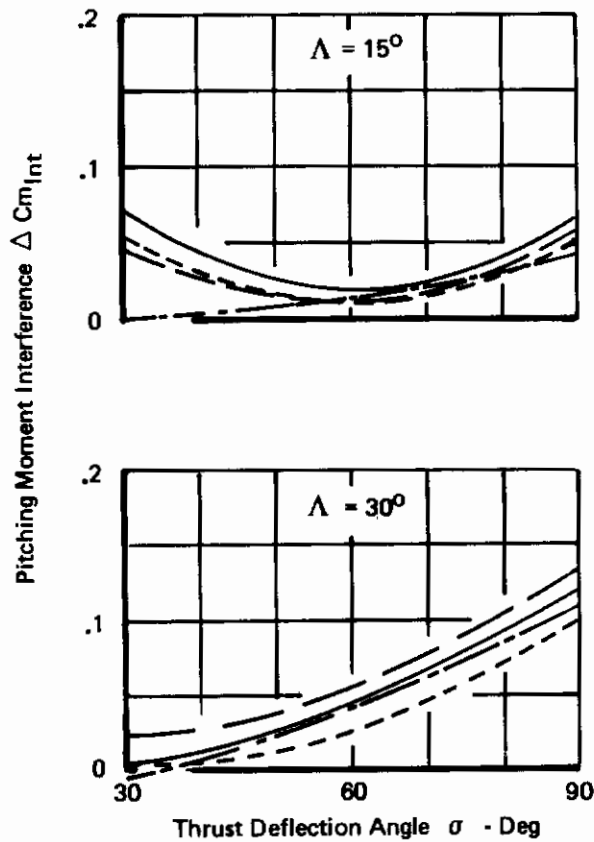


Figure 102: Effect of One Engine Inoperative on Longitudinal Stability

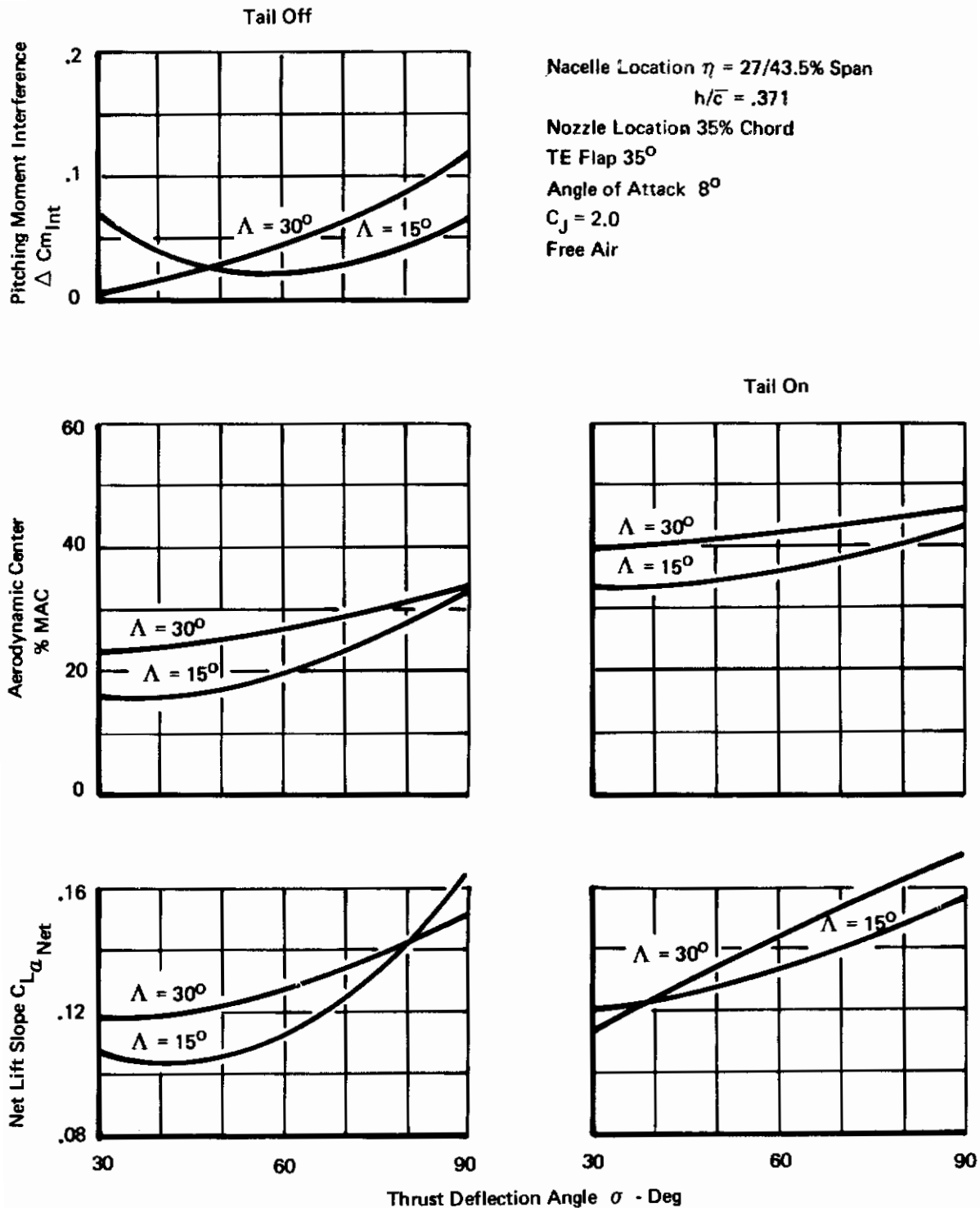


Figure 103: Effect of Sweep on Longitudinal Stability

Nacelle Location $\eta = 27/43.5\%$ Span

$h/\bar{c} = .371$

Nozzle Location 35% Chord

Angle of Attack 8°

Free Air

Tail Off

$C_J = 2.0$

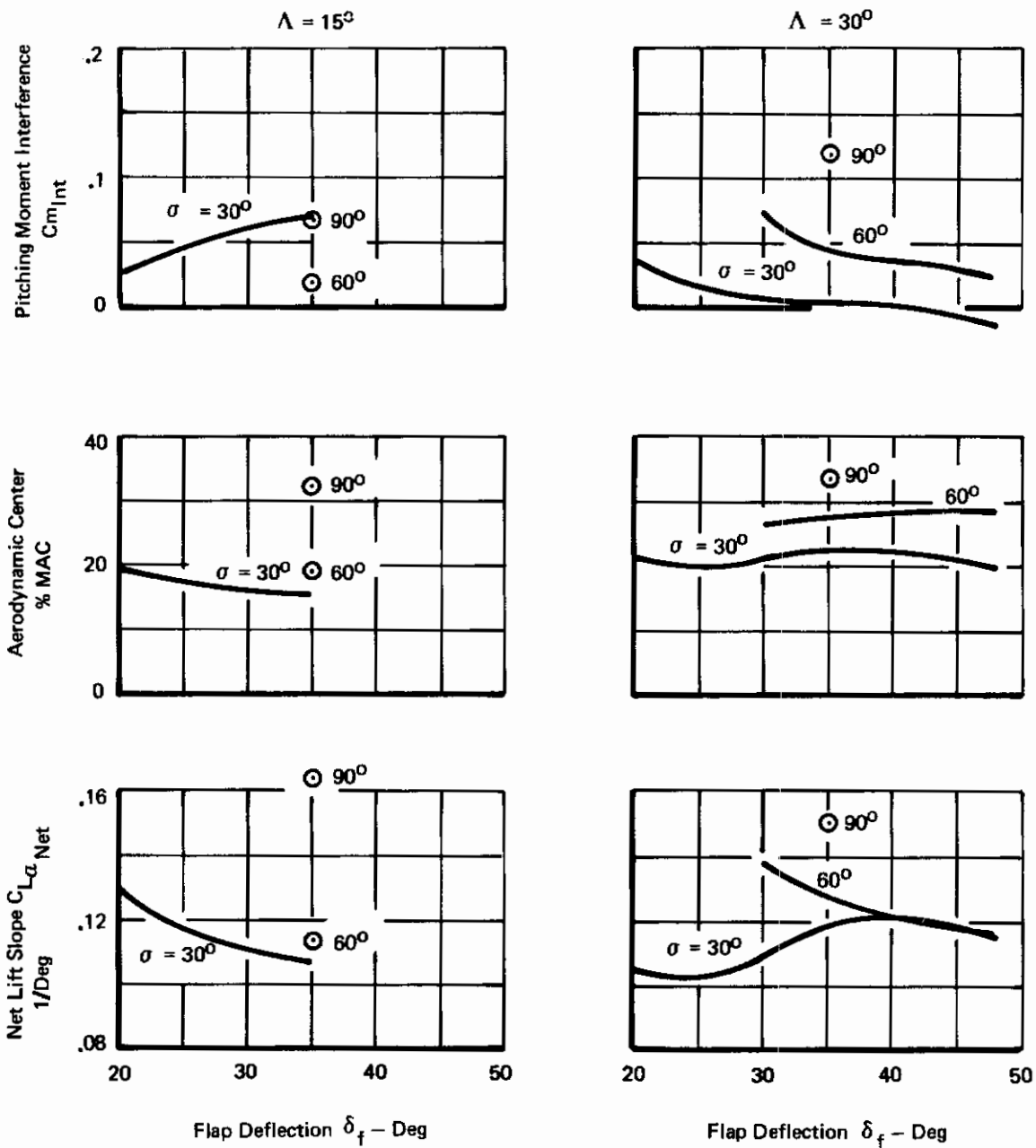


Figure 104: Effect of Flap Deflection on Longitudinal Stability

The separation on the undersurface occurs at angles less than 4° and is caused by the leading-edge devices. The upper surface separation begins at approximately 14° angle of attack. The configurations tested exhibit pitch-up with the tail on and the power off after maximum lift has been exceeded ($\alpha = 26$ to 28°). The pitching moment interference is between $-.1$ and $+.1$ over the normal expected angle of attack range as shown on Figure 105.

4.5.2.4 Ground Effect

The pitching moment interference increases in ground effect with the largest increase (.08) at $\sigma = 30^\circ$, a moderate increase (.02) at $\sigma = 60^\circ$, and plus or minus variation ($\pm .03$) at $\sigma = 90^\circ$ as shown on Figure 106.

4.5.3 Effect of Thrust on Downwash

Increasing the thrust coefficient and thrust deflection angle increases the downwash (ϵ) and the effect becomes more pronounced as the angle of attack increases as shown on Figure 107. The downwash increases 2° when the thrust deflection is increased from 30 to 60° . The downwash is approximately 10° greater at $\alpha = 8^\circ$ for the body mounted tail than it is for the T-tail configuration. For the T-tail and 8° angle of attack, $\partial\epsilon/\partial\alpha$ is $.54$ at $\sigma = 60^\circ$ and $C_J = 0$. With $C_J = 2.0$, $\partial\epsilon/\partial\alpha$ is $.66$. For the body mounted tail and 8° angle of attack $\partial\epsilon/\partial\alpha$ is $.70$ power off ($C_J = 0$) and 1.18 power on ($C_J = 2.0$). The effect of power tends to linearize the change in downwash with changes in angles of attack. The downwash data presented on Figure 107 through 109 were obtained utilizing a wake rake. A comparison between the force derived downwash and the rake data is shown on Figure 107 and indicate good agreement.

The effect of one engine inoperative is equivalent to operating at 75% of the all-engine thrust coefficients ($C_J = 1.5$). With one engine inoperative, the $\partial\epsilon/\partial\alpha$ varies between $.56$ and $.60$ at $\alpha = 8^\circ$ depending on thrust deflection. There is negligible effect with the spanwise location of the engine out, as presented on Figure 108, whereas ground effect reduces the downwash as shown on Figure 109. Due to ground plane shielding, $\partial\epsilon/\partial\alpha$ is reduced to approximately $.2$ at $\alpha = 8^\circ$ for the T-tail, whereas the body mounted tail location is subject to reflection effects power off. Power-on the body mounted location at $\alpha = 8^\circ$ has a $\partial\epsilon/\partial\alpha$ value of $.41$.

Nacelle Location $\eta = 27/43.5\%$ Span

$h/\bar{c} = .371$

Nozzle Location 35% Chord

TE Flap 35°

Sweep 15°

Power On $C_J = 2.0$

Tail Off

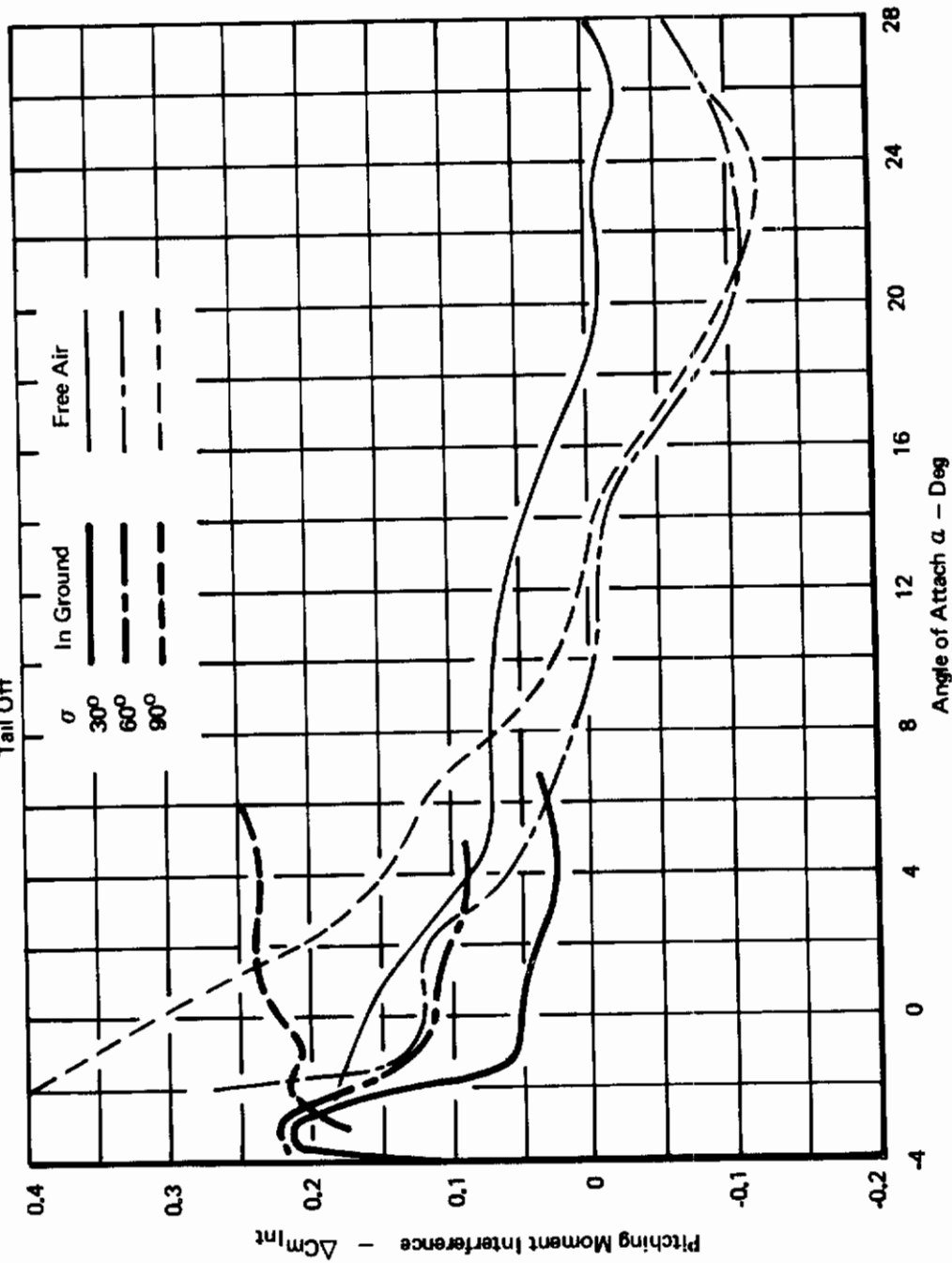


Figure 105: Effect of Angle of Attack on Pitching Moment Interference

Nacelle Location $\eta = 27/43.5\%$ Span
 $h/\bar{c} = .371$
 Nozzle Location 35% Chord
 TE Flap 35°
 Sweep 30°
 Angle of Attack 8°
 Tail Off

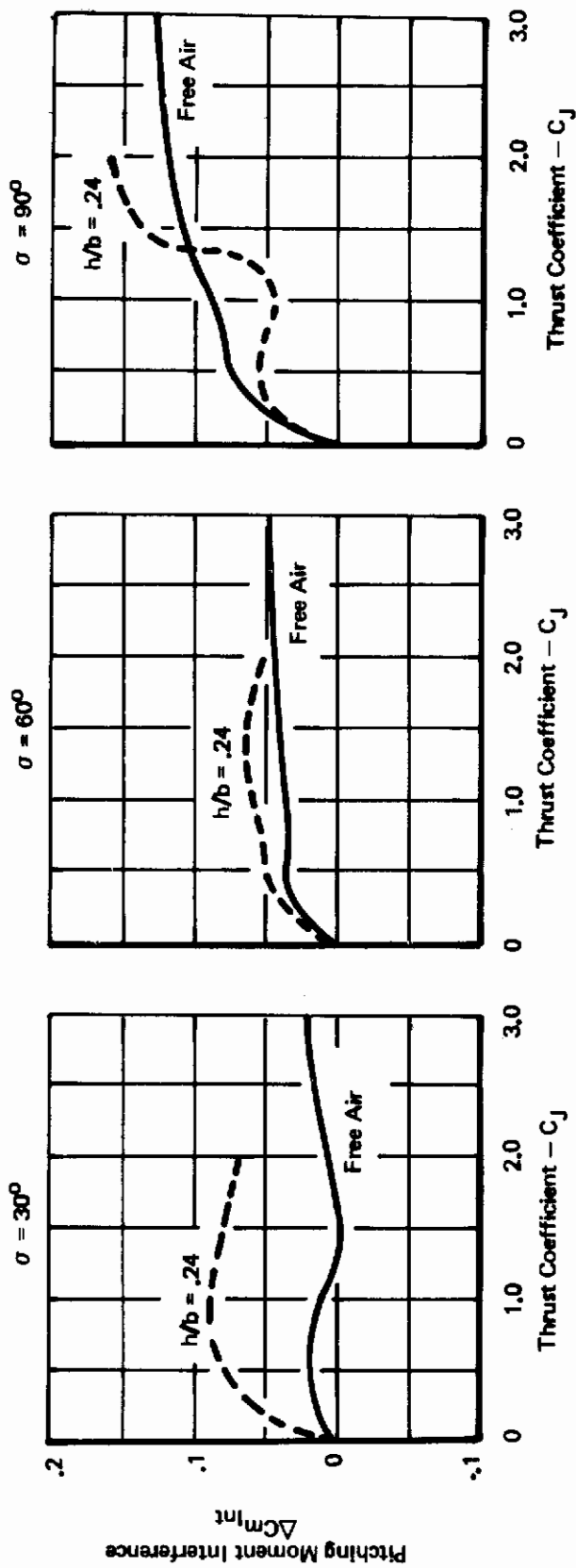


Figure 106: Effect of Ground Height on Longitudinal Stability

Contrails

Nacelle Location $\eta = 27/43.5\%$ Span
 $h/\bar{c} = .371$
 Nozzle Location 35% Chord
 TE Flap 35°
 Sweep 30°
 Free Air Tail Off Thrust Deflection Angle 60°

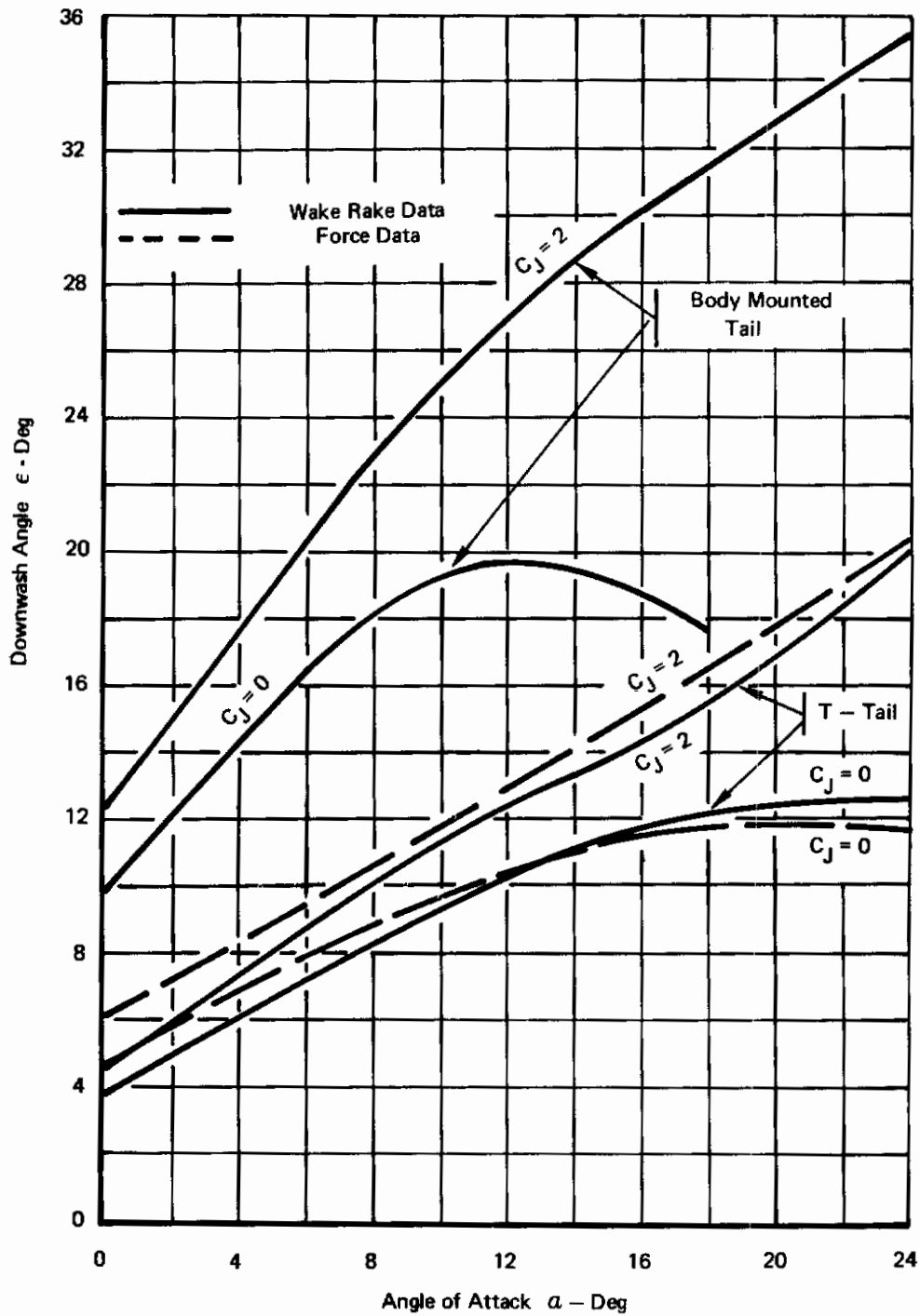


Figure 107: Effect of Vectored Thrust on Downwash at the Horizontal Tail

Contrails

Nacelle Location $\eta = 27/43.5\%$ Span

$h/\bar{c} = .371$

Nozzle Location 35% Chord

TE Flap 35°

Sweep 30°

Tail Off

Free Air

Wake Rake at the T-Tail Location

Total $C_J = 1.5$

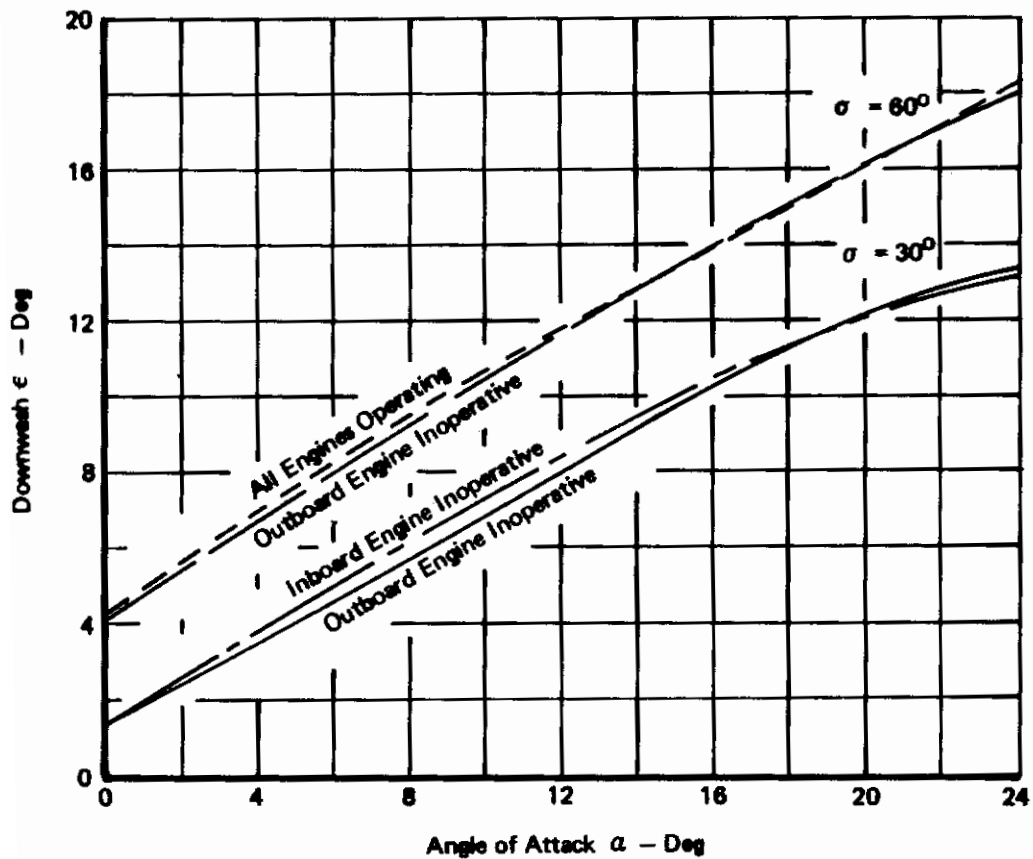


Figure 108: Effect of One Engine Inoperative on Downwash

Nacelle Location $\eta = 27/43.5\%$ Span
 $h/c = .371$
 Nozzle Location 35% Chord
 TE Flap = 35° Wake Rake Installed
 Ground Height $h/b = .24$

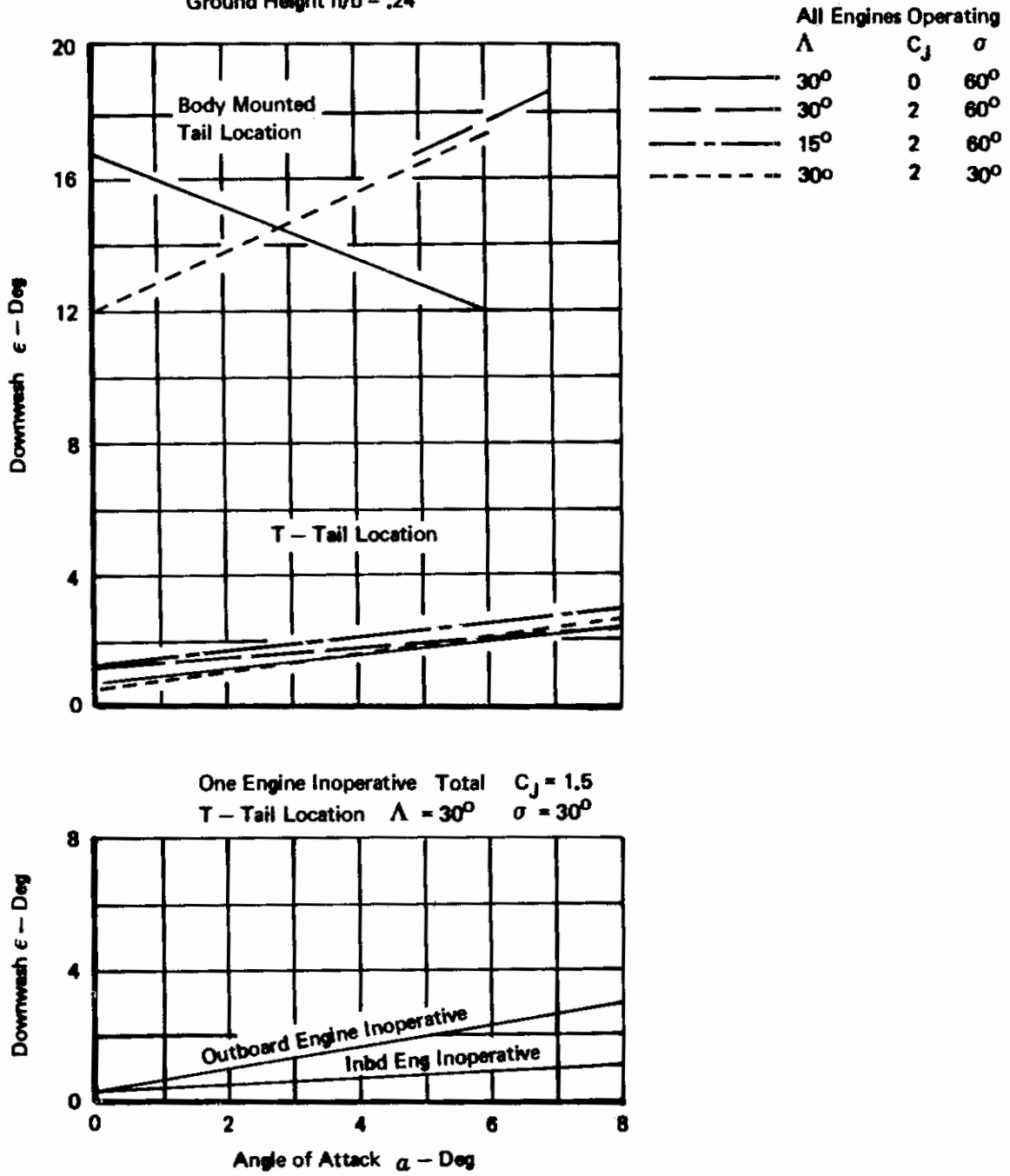


Figure 109: Effect of Ground Height on Downwash

4.6 Lateral Stability

The lateral stability derivatives, in general, do not exhibit a strong dependence on vectored thrust. However, there are some changes which are discussed in the table on the next page.

Free air effects are discussed in Sections 4.6.1 through 4.6.2.3. Ground effects are discussed in Sections 4.6.2.4 and 4.6.3.

Contrails

Table XIII: Sideslip Derivative Behavior

Effect of Thrust

PARAMETER	FIG.	SIDEFORCE	YAWING MOMENT	ROLLING MOMENT	GROUND EFFECT
Thrust Coefficient	110 Thru 113	Thrust has little influence except for inboard mounted nacelles. (Fig. 110, 111)	Thrust has little influence. (Fig. 111, 113)	Thrust has little influence on the rolling moment except at $\alpha = 90^\circ$. (Fig. 112, 113)	
Thrust Deflection Angle	114 Thru 116	$C_{Y\beta}$ increases with thrust deflection. (Fig. 114)	Insignificant effects on $C_{N\beta}$. (Fig. 115)	Outboard nacelle decreases $C_{L\beta}$ with power on. (Fig. 116)	$C_{Y\beta}$ decreases with thrust deflection. Insignificant effects on $C_{N\beta}$ and $C_{Y\beta}$ (Fig. 114, 115, 116)
Nacelle Chordwise Position	117 Thru 119	Movement of nacelle has little effect. (Fig. 117)	Movement of nacelle has little effect. (Fig. 118)	Movement of nacelle has little effect except at $\alpha = 90^\circ$ where $C_{Y\beta}$ decreases as nacelle is aft. (Fig. 119)	Nacelle position in ground effect has little influence on the lateral derivatives. (Fig. 117, 118, 119)
One Engine Inoperative	120 Thru 122	Outboard engine out increases $C_{Y\beta}$ at $\alpha = 60^\circ$ for inboard mounted nacelles. (Fig. 120)	Engine out has little influence. (Fig. 121)	Engine out has little influence. (Fig. 122)	Outboard engine out increases $C_{Y\beta}$ rapidly from $\alpha = 60^\circ$ to 90° for inboard mounted nacelles. (Fig. 120, 121, 122)

Effect of Configuration Variables

Wing Sweep	123	Wing sweep has little influence.	Wing sweep has little influence.	Increasing wing sweep increases rolling moment Derivative as expected.	
T. E. Flap	124	Has little influence.	Insignificant effect on $C_{N\beta}$.	Has little influence.	Has little influence.
Angle of Attack	125 Thru 130	$C_{Y\beta}$ slightly increases with α . $C_{Y\beta}$ for tail input slightly decreases with α . (Fig. 125, 126)	Has little influence. (Fig. 127, 128)	$C_{Y\beta}$ decreases with angle of attack except for $\delta_f = 20^\circ$, $\alpha = 30^\circ$. Tail contribution also decreases with alpha. (Fig. 129, 130)	

Tail Off (Except Where Noted)

4.6.1.1 Thrust Coefficient

The effects of thrust on the sideslip derivatives are shown in Figures 110 - 113. Figures 110 - 112 are for the tail off, while Figure 113 presents the tail contribution.

Figure 110 shows that the outboard nacelle location has essentially no effect of thrust. The inboard nacelles show a moderate increase in $C_{Y\beta}$ at $\sigma = 60^\circ$ and 90° . Figure 113 shows that the vertical tail contribution to $C_{Y\beta}$ increases slightly with thrust.

The yawing moment derivative, shown in Figures 111 and 113, is influenced very little by thrust.

The rolling moment derivative shown in Figure 112 is influenced very little by thrust. For inboard mounted nacelles at $\sigma = 90^\circ$, $C_{L\beta}$ increases somewhat with thrust. Figure 113 shows that the tail contribution to $C_{L\beta}$ varies only slightly with thrust.

4.6.1.2 Thrust Deflection

The influence of thrust deflection on the lateral derivatives is shown in Figure 114 through 116. For the power-on condition, in free air, the side force derivative increases negatively for $\sigma = 30^\circ$ to 60° with inboard single pods. From $\sigma = 60^\circ$ to 90° , $C_{Y\beta}$ becomes less negative. For the outboard mounted nacelle, $C_{Y\beta}$ decreases slightly with thrust deflection.

Thrust deflection has little influence on yawing moment as shown in Figure 115.

Figure 116 shows that the rolling moment derivative becomes less negative with thrust deflection for the outboard mounted nacelles. Thrust deflection has small influence on $C_{L\beta}$ for the inboard mounted nacelles.

4.6.1.3 Nacelle Chordwise Location

Figures 117 through 119 show the influence of moving the nacelle aft. $C_{Y\beta}$ decreases as the nacelle is moved aft except at $\delta_f = 35^\circ$, $\sigma = 90^\circ$ as shown in Figure 117.

Figure 118 shows that chordwise movement has little effect on the yawing moment derivative, power-on or power-off.

With power-on or -off, the rolling moment derivative is influenced very little by chordwise movement as shown in Figure 119.

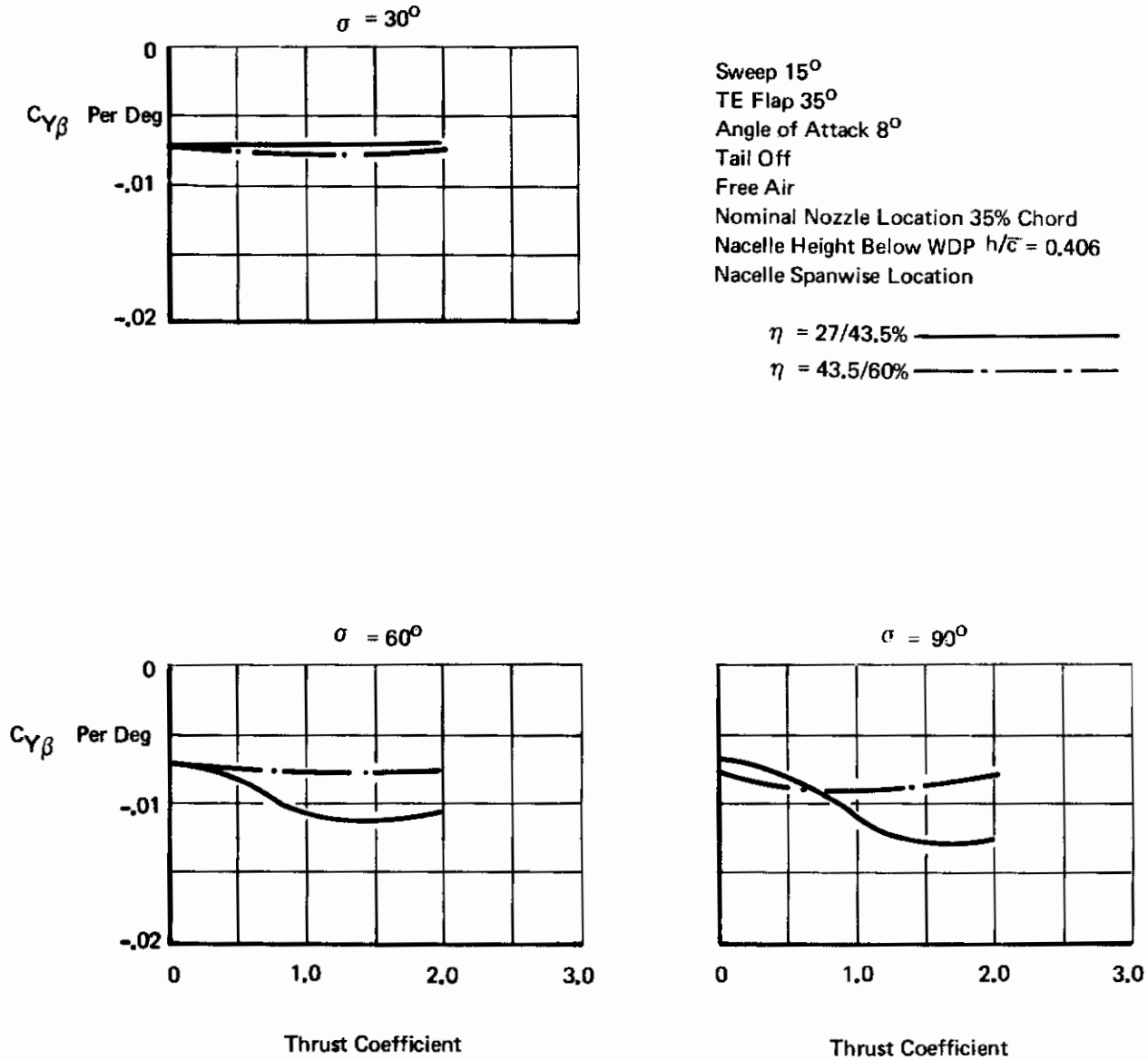


Figure 110: Effect of Thrust on Sideforce Derivative

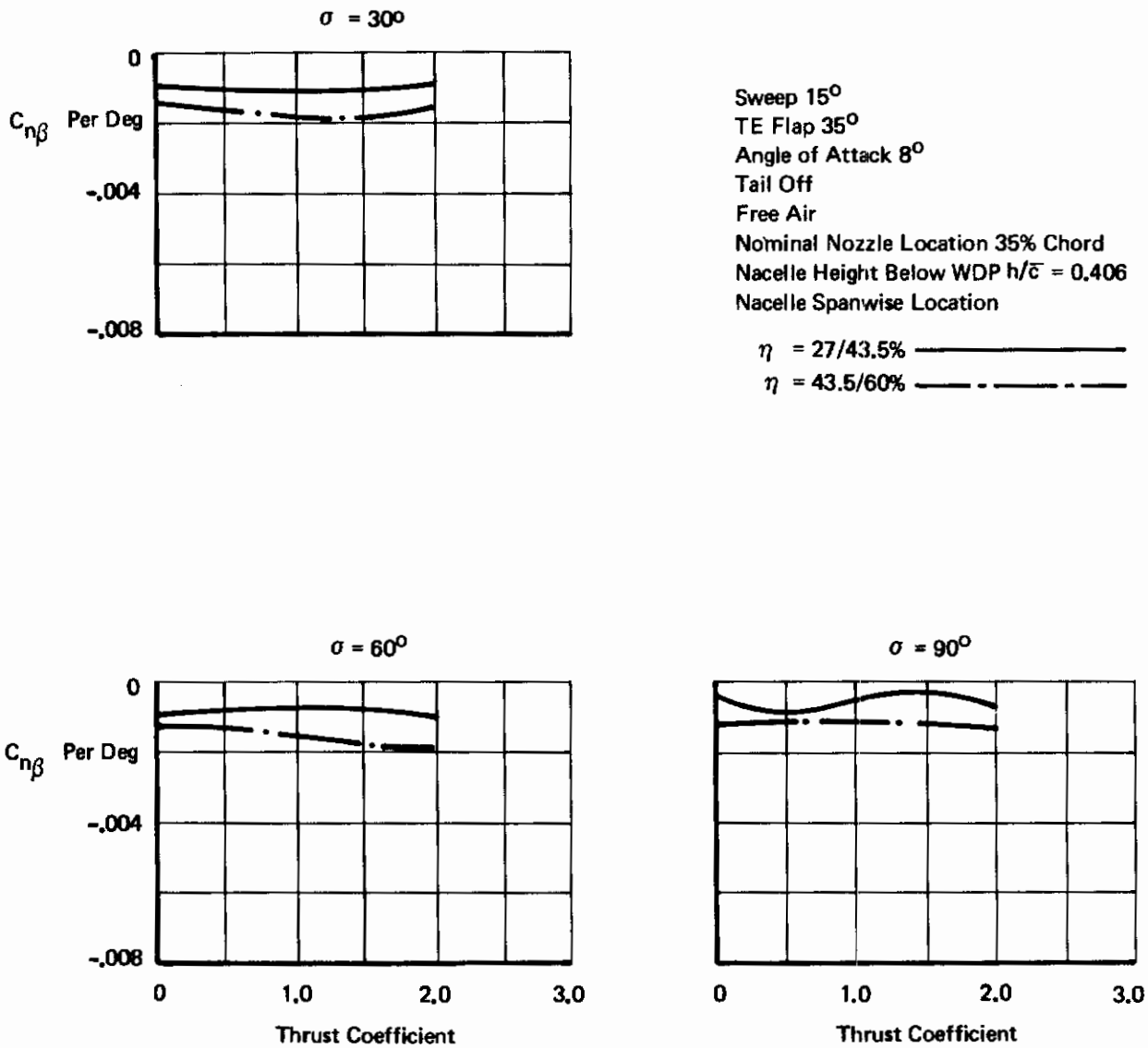


Figure 111 : Effect of Thrust on Yawing Moment Derivative

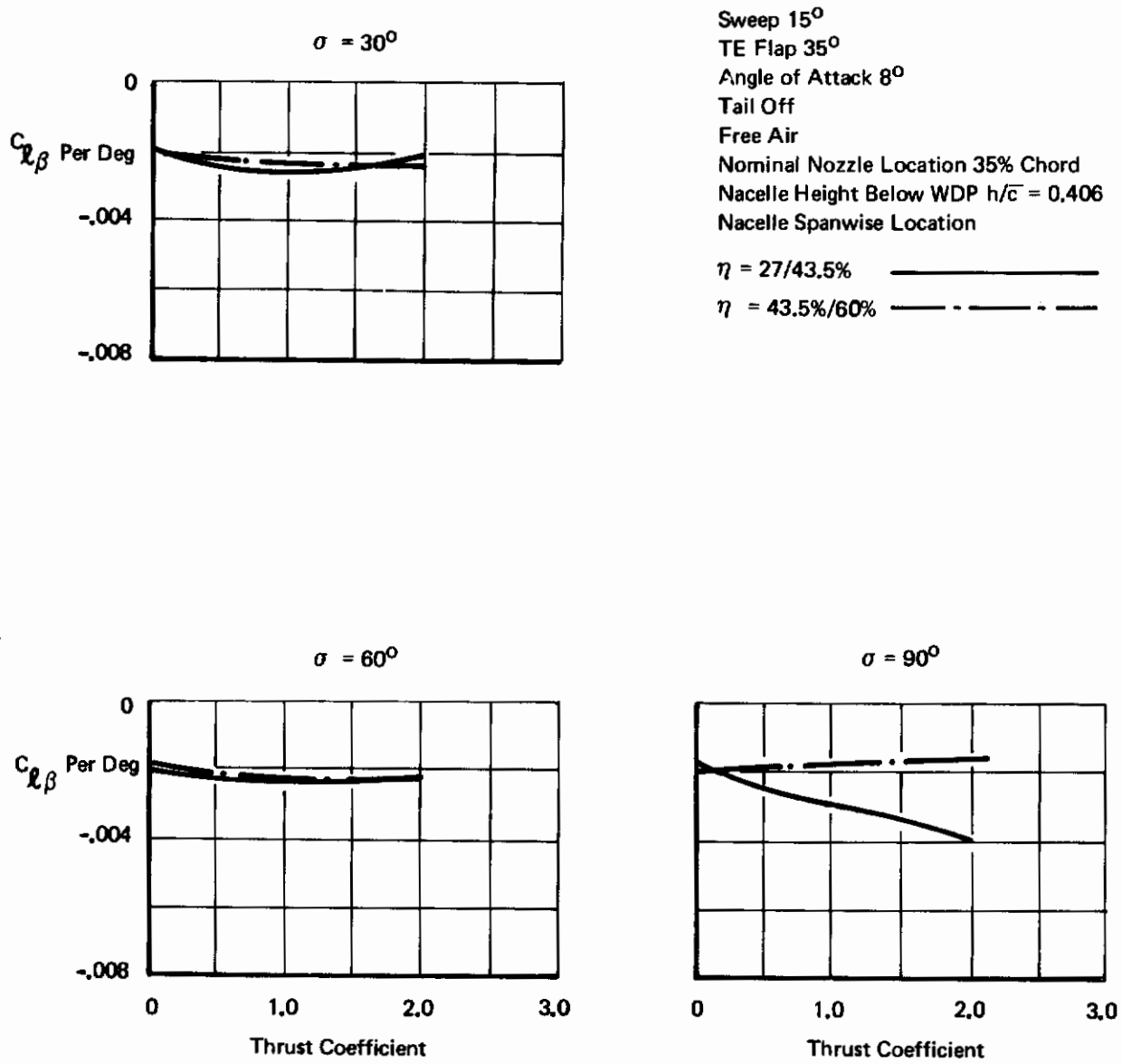


Figure 112: Effect of Thrust on Rolling Moment Derivative

Contrails

Sweep 15°
 Angle of Attack 8°
 Nominal Nozzle Location 35% Chord
 Nacelle Height Below WDP $h/\bar{c} = 0.406$
 Free Air
 Nacelle Spanwise Location
 $\eta = 27/43.5\%$
 $\eta = 43.5\%$ (Dual Pods)
 Thrust Deflection 60°
 TE Flap 35°

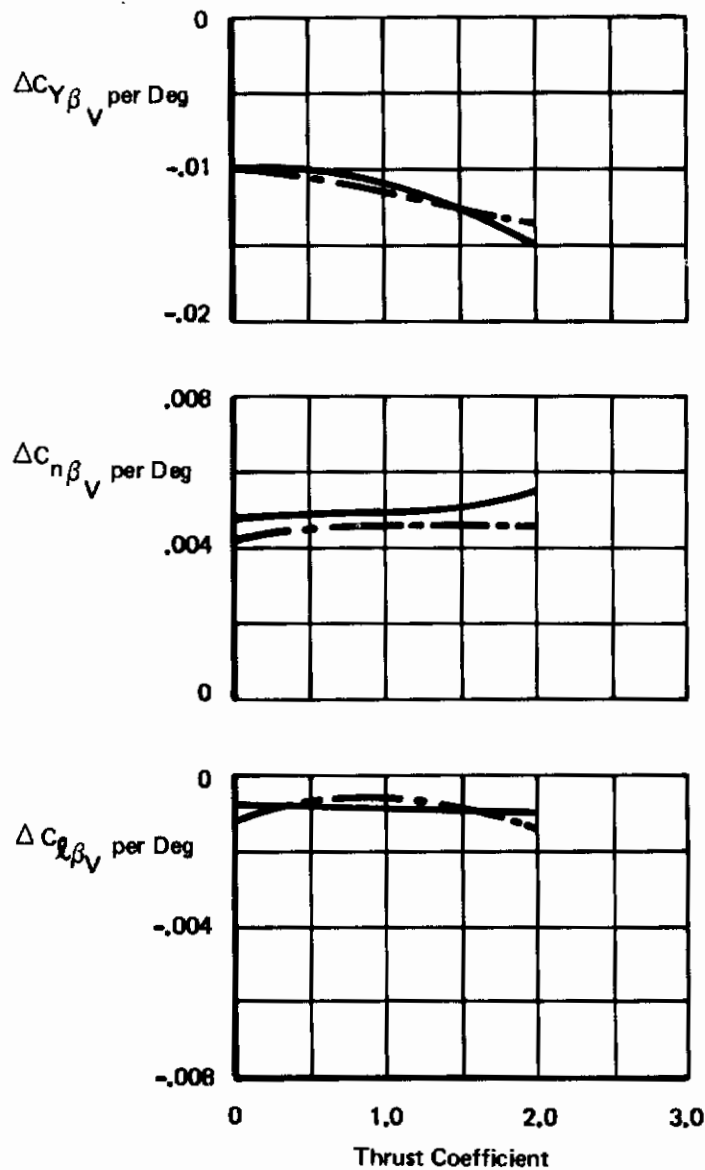


Figure 113: Effect of Thrust on Tail Input to Sideslip Derivatives

Sweep 30°
 Tail Off
 TE Flap 35°
 Nominal Nozzle Location 35% Chord
 Nacelle Height Below WDP $h/c = 0.371$
 Angle of Attack 8°

$C_J = 0$ —————
 $C_J = 2.0$ - - - - -

Nacelle Spanwise Location $\eta = 27/43.5\%$

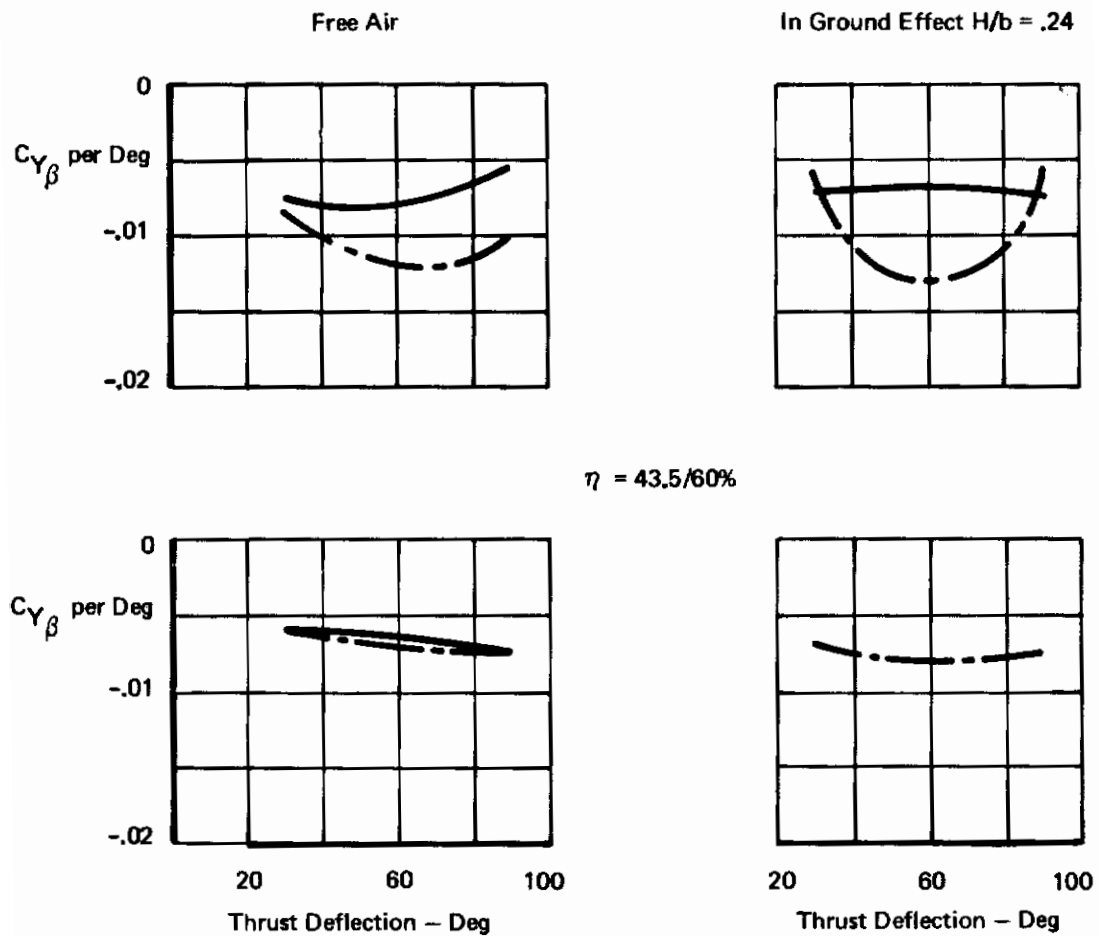


Figure 114 : *Effect of Thrust Deflection Angle on Side Force Derivative*

Sweep 30°
 Tail Off
 TE Flap 35°
 Nominal Nozzle Location 35% Chord
 Nacelle Height Below WDP $h/\bar{c} = 0,371$
 Angle of Attack 8°

$C_J = 0$
 $C_J = 2,0$

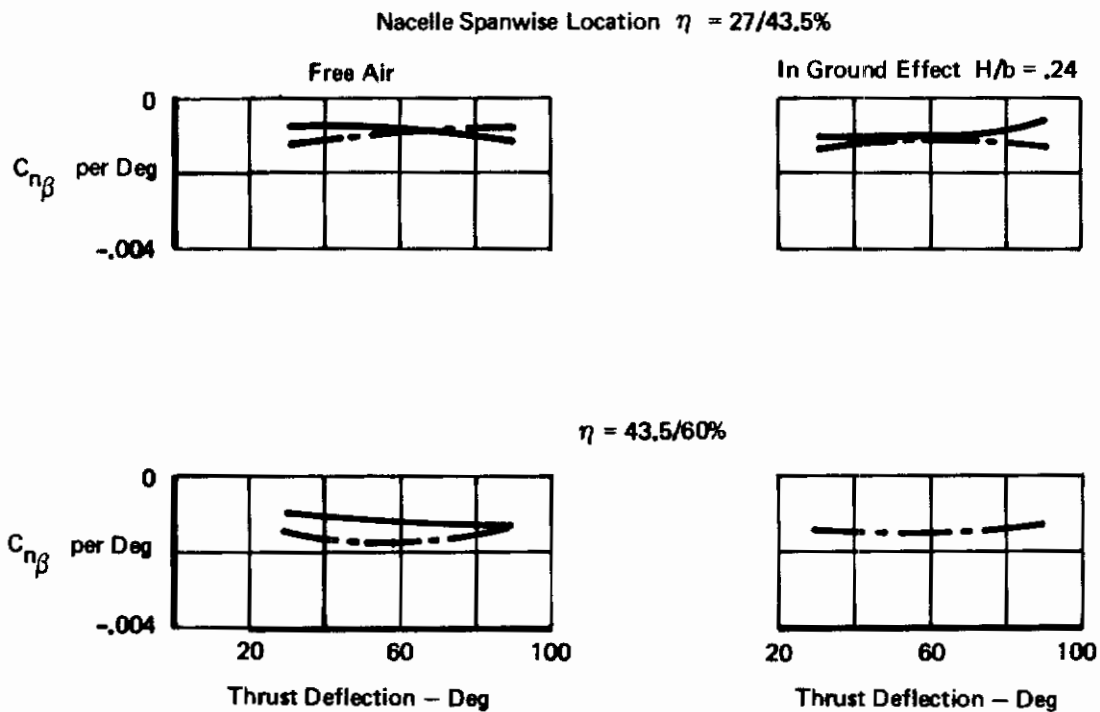




Figure 115: Effect of Thrust Deflection Angle on Yawing Moment Derivative

Sweep 30°
 Tail Off
 TE Flap 35°
 Nominal Nozzle Location 35% Chord
 Nacelle Height Below WDP $h/\bar{c} = 0.371$
 Angle of Attack 8°

$C_J = 0$ 
 $C_J = 2.0$ 

Nacelle Spanwise Location $\eta = 27/43.5\%$

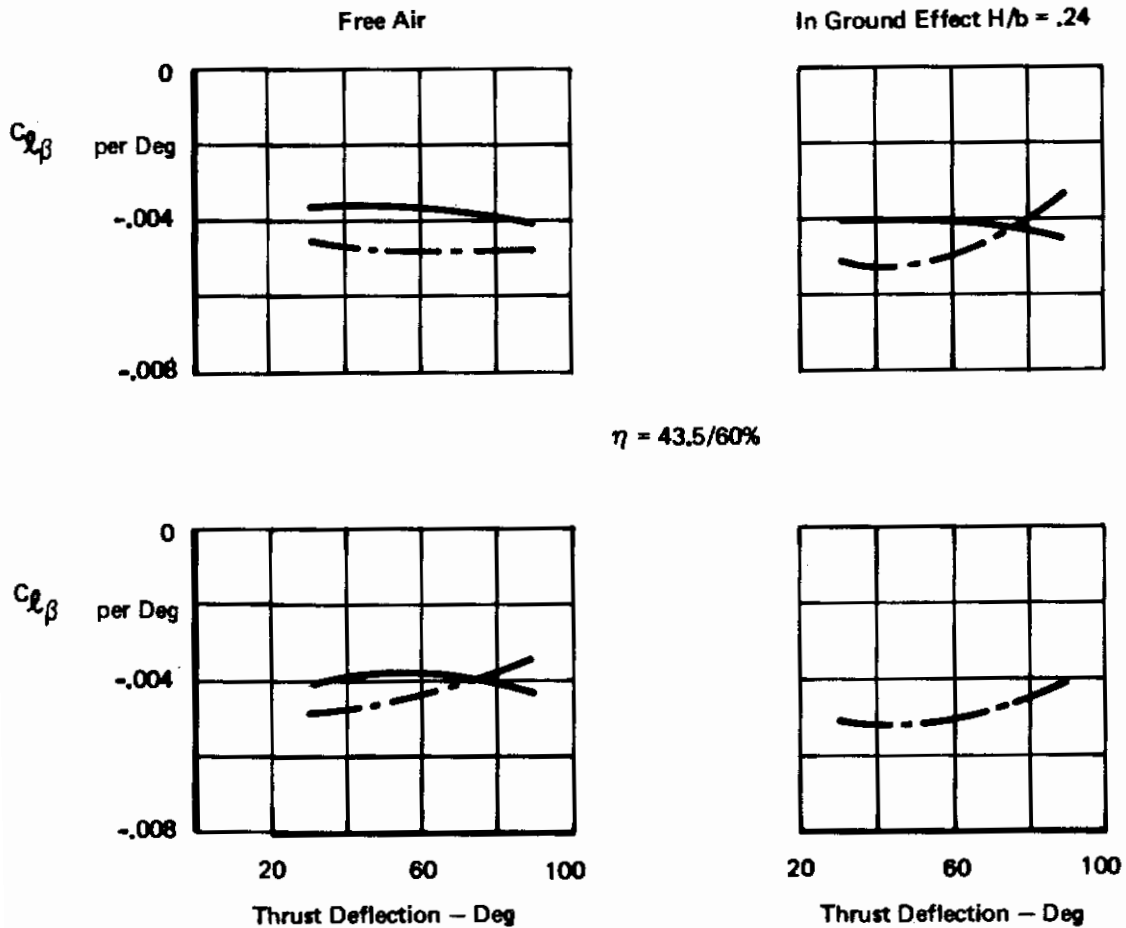


Figure 116: Effect of Thrust Deflection Angle on Rolling Moment Derivative

Sweep 15°
 Tail Off
 Angle of Attack 8°
 Nacelle Spanwise Location $\eta = 27/43.5\%$
 Nacelle Height Below WDP $h/\bar{c} = 0.408$
 Free Air
 $C_J = 0$ —————
 $C_J = 2.0$ - - - - -

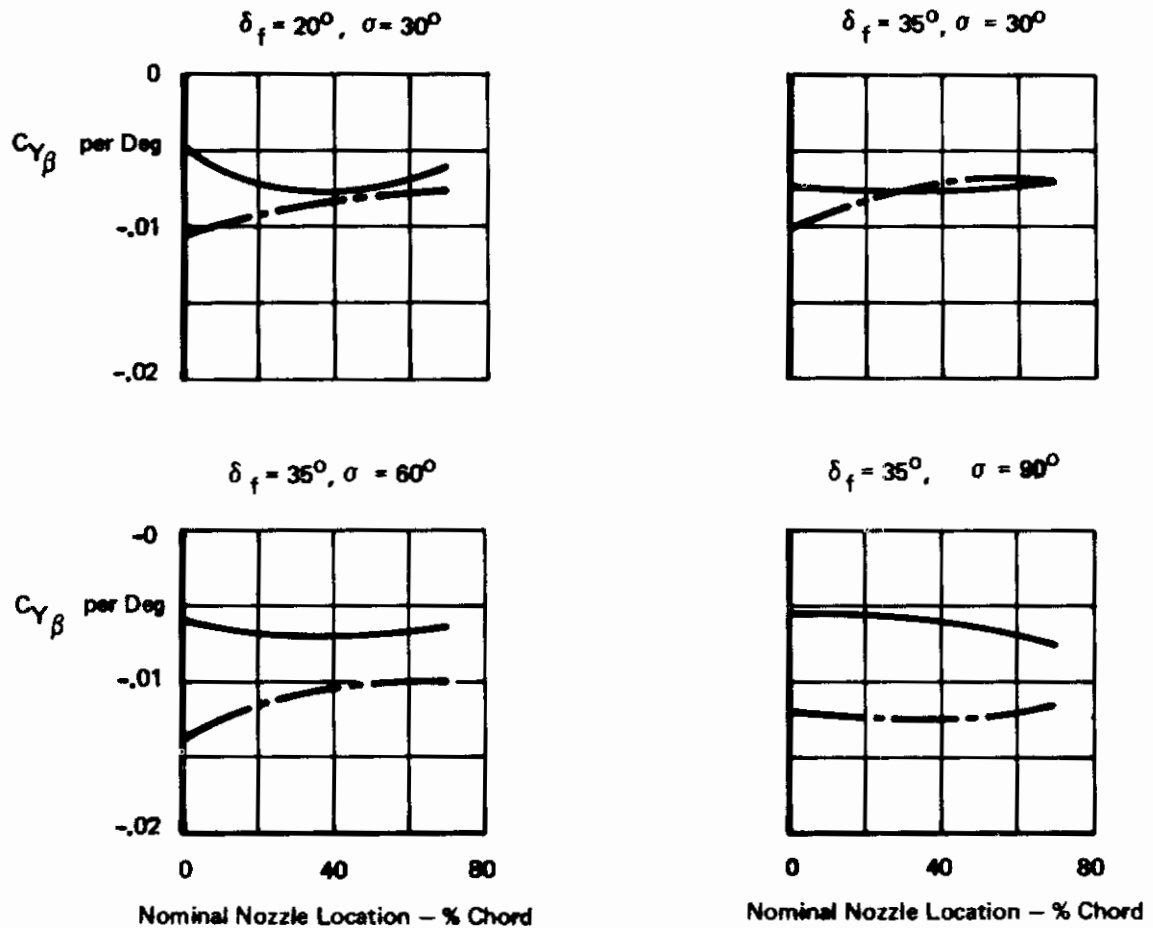


Figure 117: Effect of Nacelle Chordwise Location on Side Force Derivative

Sweep 15°
 Tail Off
 Angle of Attack 8°
 Nacelle Spanwise Location $\eta = 27/43.5\%$
 Nacelle Height Below WDP $h/\bar{c} = 0.406$
 Free Air
 $C_J = 0$ —————
 $C_J = 2.0$ - - - - -

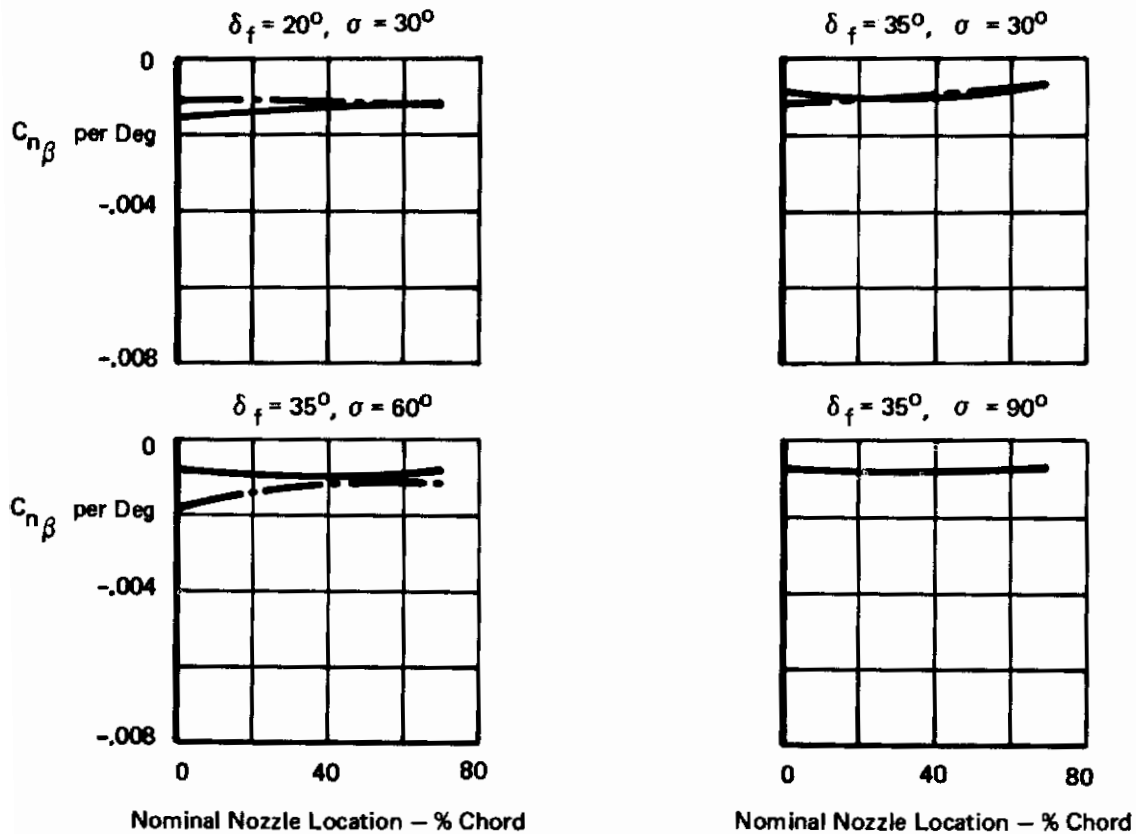


Figure 118: Effect of Nacelle Chordwise Location on Yawing Moment Derivative

Sweep 15°
 Tail Off
 Angle of Attack 8°
 Nacelle Spanwise Location $\eta = 27/43.5\%$
 Nacelle Height Below WDP $h/\bar{c} = 0.406$
 Free Air
 $C_J = 0$ —————
 $C_J = 2.0$ - - - - -

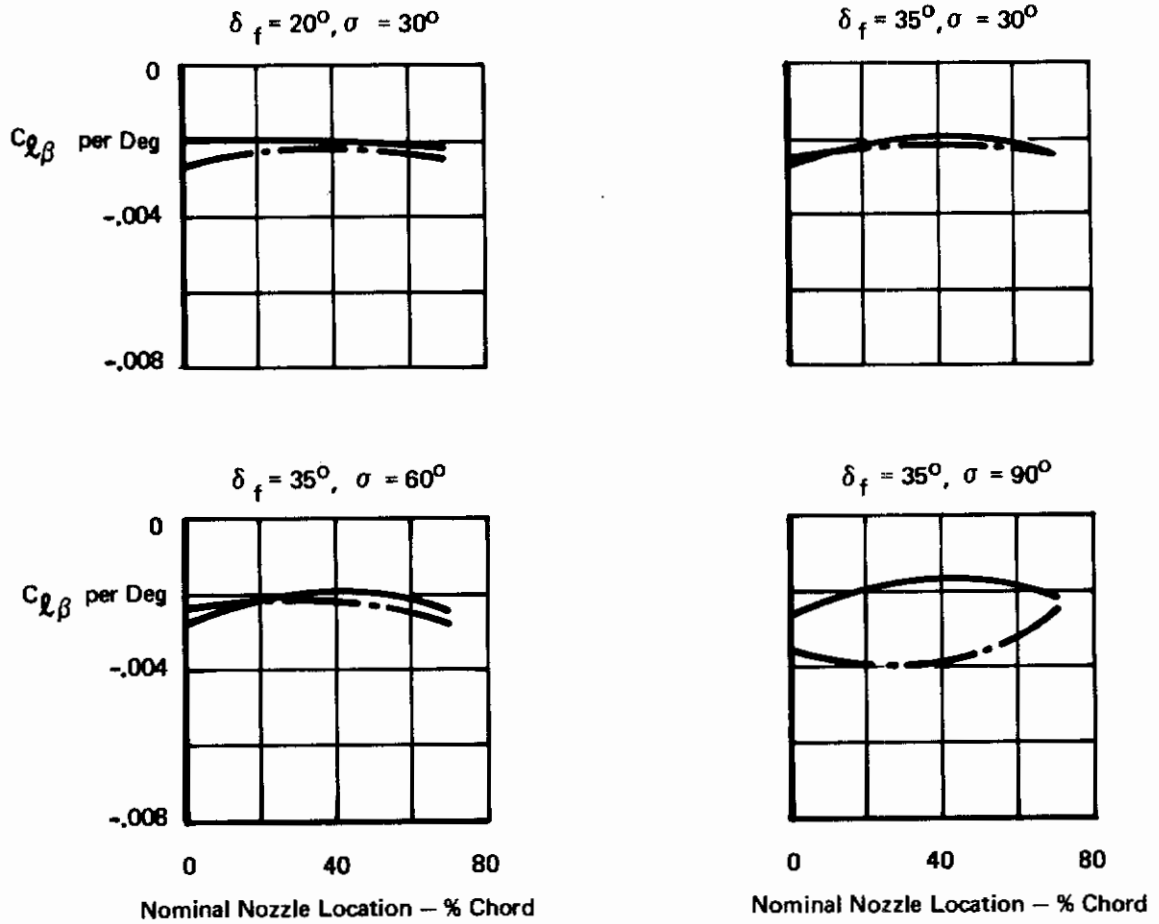


Figure 119: Effect of Nacelle Chordwise Location on Rolling Moment Derivative

4.6.1.4 One Engine Inoperative

Figures 120 through 122 show that thrust deflection has little influence on the derivatives, either inboard engine out or outboard engine out.

4.6.2 Effect of Configuration Variables on Sideslip Derivatives

4.6.2.1 Wing Sweep

Figure 123 shows that sweep has little influence on the side force and yawing moment derivatives. However, increasing sweep increases the rolling moment derivative, which was expected.

4.6.2.2 T.E. Flap Deflection

The influence of T.E. flap deflection on lateral derivatives is small for constant thrust deflection, see Figure 124.

4.6.2.3 Angle of Attack

The effects of angle of attack on the sideslip derivatives are shown in Figures 125 through 130. Figure 125 shows that for the various flap deflections and thrust deflections, the side force derivative increases with angle of attack. Power-on increases $C_{Y\beta}$ except for $\delta_f = 35^\circ$, $\sigma = 30^\circ$. At $\delta_f = 35^\circ$, $\sigma = 90^\circ$, $C_J = 2.0$ $C_{Y\beta}$ rapidly decreases as alpha increases, while at $C_J = 0.0$ and 1.0 the effect is small. Figure 126 shows that the influence of angle of attack on the tail contribution to $C_{Y\beta}$ is small except for $C_J = 2.0$, $\delta_f = 35^\circ$, $\sigma = 90^\circ$ and power-off, $\delta_f = 35^\circ$, $\sigma = 30^\circ$. At these conditions, $C_{Y\beta}$ decreases with alpha.

Yawing moment derivative increases slightly with alpha as shown in Figure 127. Figure 128 shows that the tail input is insensitive to alpha. Adding power has a varying influence on $C_{N\beta}$ (sometimes increasing, sometimes decreasing $C_{N\beta}$).

Rolling moment derivative decreases with alpha except for $\delta_f = 20^\circ$, $\sigma = 30^\circ$ as shown in Figure 129. Adding power increases $C_{l\beta}$.

4.6.2.4 Ground Effect

Ground effects are shown in Figures 114 through 116 and 120 through 122 and Figure 124. Generally, ground effect tends to decrease the side force and rolling moment derivatives. Yawing moment derivatives are influenced only slightly.

4.6.3 Effect of Thrust on Sidewash

Figure 131 shows that the various thrust parameters (C_J , σ , engine inoperative), ground height, and angle of attack have negligible effect on sidewash at the vertical tail.

Sweep 30°
 Tail Off
 TE Flap 35°
 Nominal Nozzle Location 35% Chord
 Nacelle Height Below WDP $h/\bar{c} = 0,371$
 Angle of Attack 8°
 Inbd Engine Out - - - - -
 Outbd Engine Out _ _ _ _ _
 $C_J = 2.0$ Less .5

Nacelle Spanwise Location $\eta = 27/43.5\%$

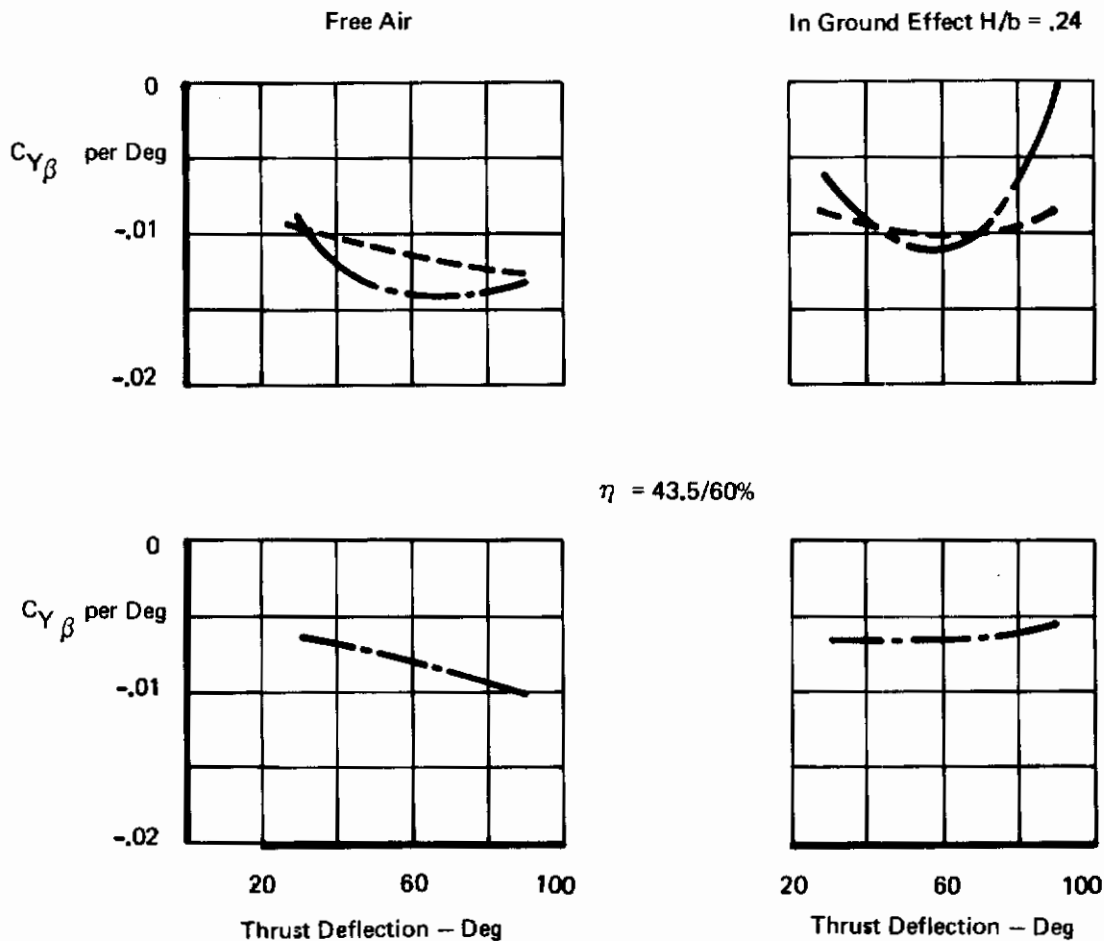


Figure 120: Effect of Thrust Deflection Angle on Side Force Derivative, Engine Out

Sweep 30°
 Tail Off
 TE Flap 35°
 Nominal Nozzle Location 35% Chord
 Nacelle Height Below WDP $h/\bar{c} = 0,371$
 Angle of Attack 8°
 $C_J = 2.0 \text{ Less } .5$

Inboard Engine Out
 Outboard Engine Out

Nacell Spanwise Location $\eta = 27/43,5\%$

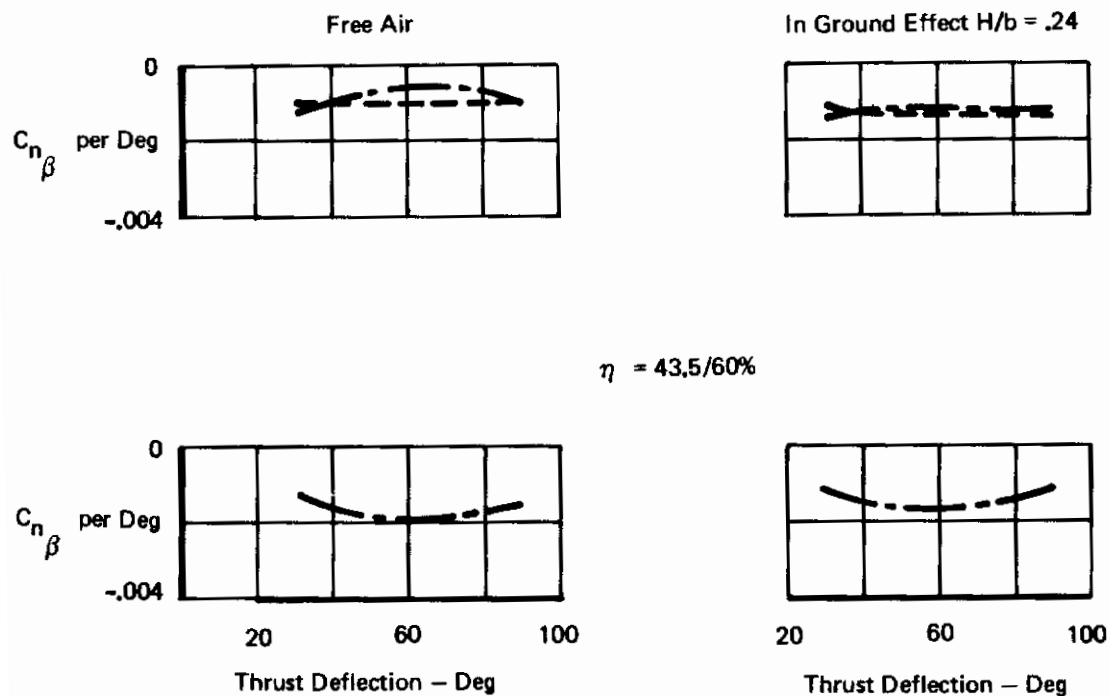


Figure 121 : Effect of Thrust Deflection Angle on Yawing Moment Derivative, Engine Out

Sweep 30°
 Tail Off
 TE Flap 35°
 Nominal Nozzle Location 35% Chord
 Nacelle Height Below WDP $h/\bar{c} = 0,371$
 Angle of Attack 8°

Inboard Engine Out - - - - -
 Outboard Engine Out — — — — —

$C_J = 2,0 \text{ Less } .5$

Nacelle Spanwise Location $\eta = 27/43,5\%$

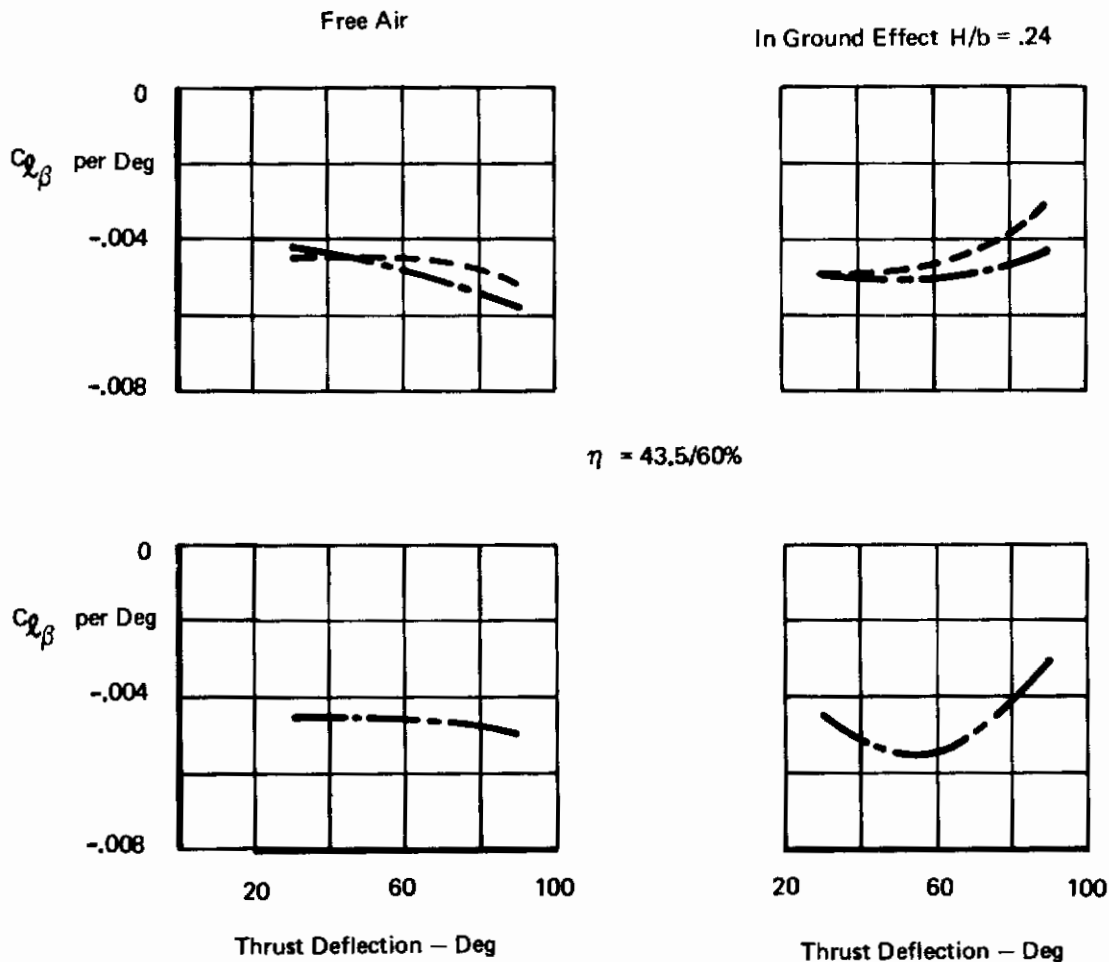


Figure 122: Effect of Thrust Deflection Angle on Rolling Moment Derivative, Engine Out

Thrust Deflection 30°
 TE Flap 35°
 Tail Off
 Angle of Attack 8°
 Nominal Nozzle Location 35% Chord
 Nacelle Spanwise Location $\eta = 27/43,5\%$
 Nacelle Height Below WDP $h/\bar{c} = 0,371$

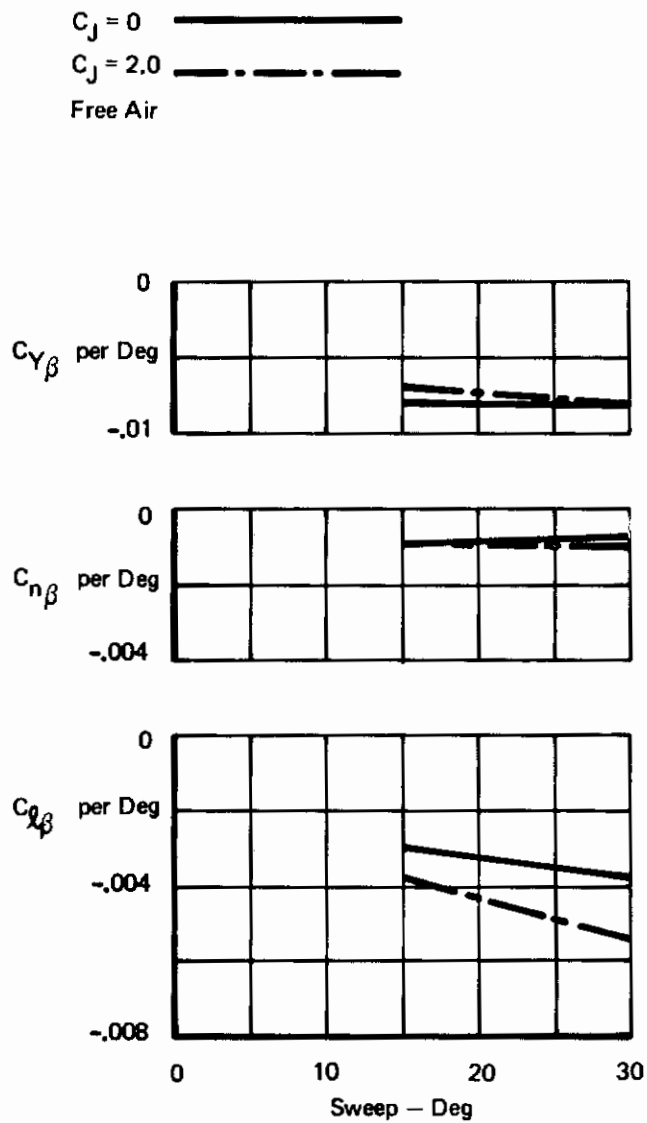


Figure 123: Effect of Wing Sweep on Sideslip Derivatives

Sweep 30°
 Nacelle Spanwise Location $\eta = 27/43.5\%$
 Nominal Nozzle Location 35% Chord
 Nacelle Height Below WDP $h/\bar{c} = 0.371$
 Angle of Attack 8°
 Power On $C_j = 2.0$
 Tail Off
 $\sigma = 30^\circ$ —————
 $\sigma = 60^\circ$ - - - - -

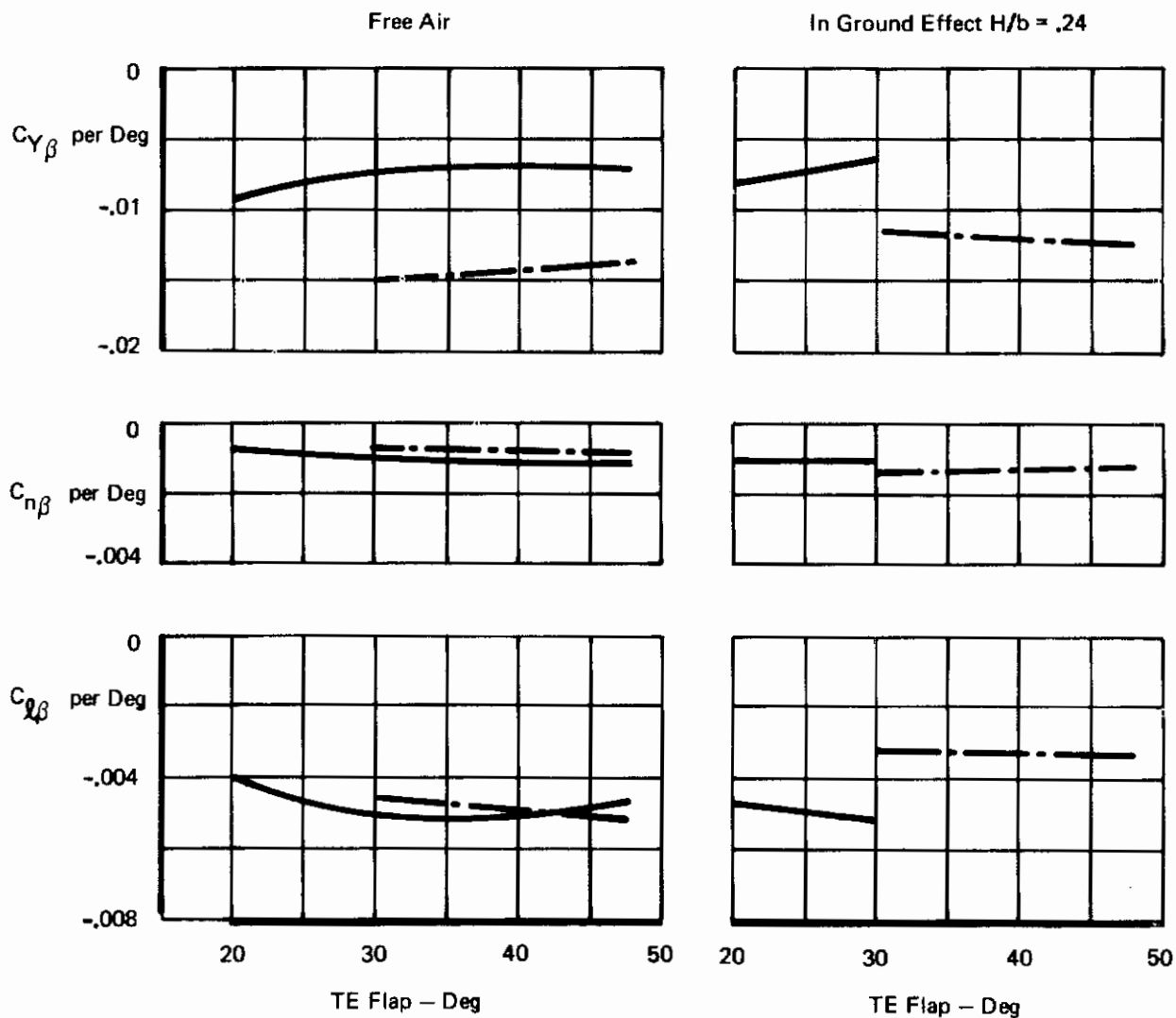


Figure 124: Effect of T.E. Flap Angle on Sideslip Derivatives

Sweep 30°
 Tail Off
 Free Air
 Nominal Nozzle Location 35% Chord
 Nacelle Height Below WDP $h/\bar{c} = 0.371$
 Nacelle Spanwise Location $\eta = 27/43.5\%$

$C_J = 0$ —————
 $C_J = 1.0$ - - - - -
 $C_J = 2.0$ - · - · -

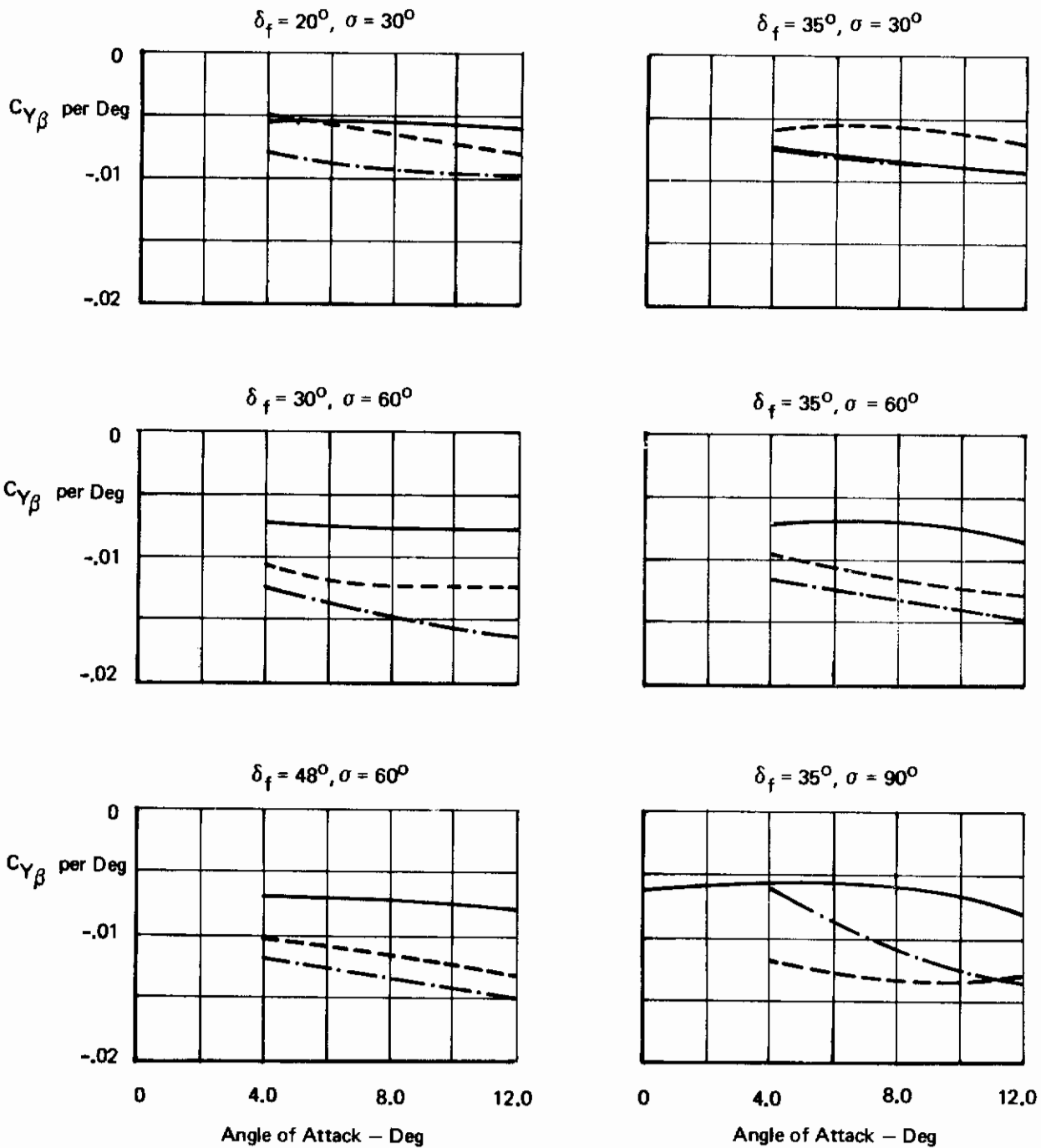


Figure 125: Effect of Angle of Attack on Side Force Derivative

Sweep 30°
 Free Air
 Nominal Nozzle Location 35% Chord
 Nacelle Spanwise Location $\eta = 27/43.5\%$
 Nacelle Height Below WDP $h/\bar{c} = 0.371$

$C_J = 0$ —————
 $C_J = 1.0$ - - - - -
 $C_J = 2.0$ - - - - -

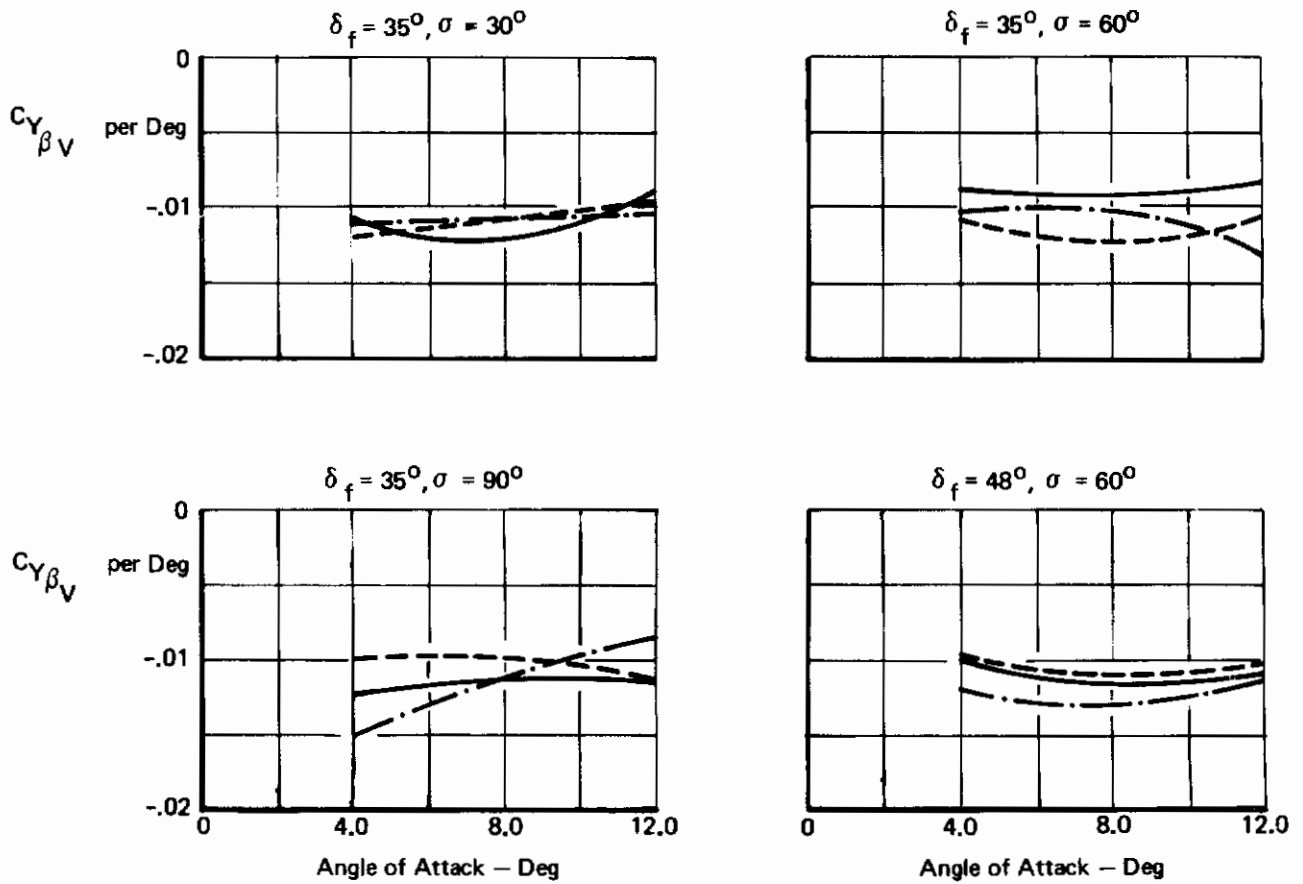


Figure 126: Effect of Angle of Attack on Tail Input to Side Force Derivative

Sweep 30°
 Tail Off
 Free Air
 Nominal Nozzles Location 35% Chord
 Nacelle Spanwise Location $\eta = 27/43.5\%$
 Nacelle Height Below WDP $h/\bar{c} = 0.371$

$C_J = 0$ —————
 $C_J = 1.0$ - - - - -
 $C_J = 2.0$ - · - · - ·

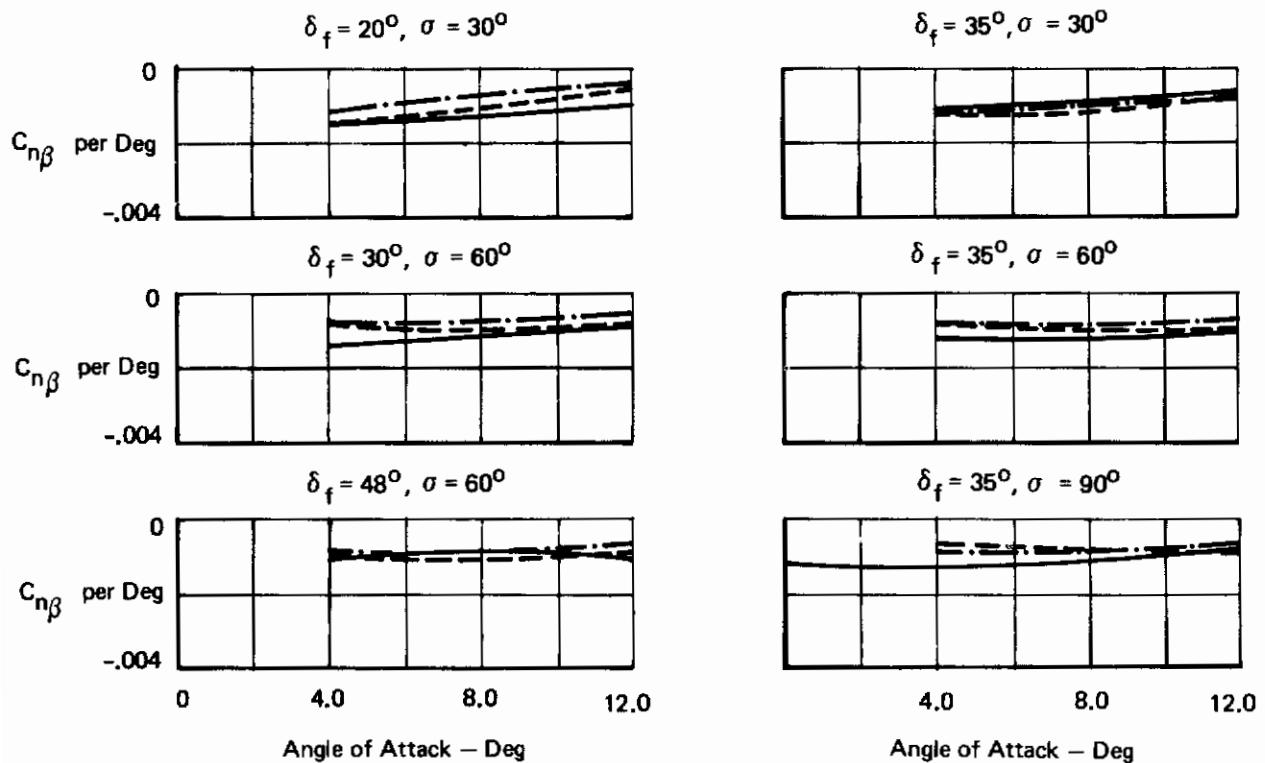


Figure 127: Effect of Angle of Attack on Yawing Moment Derivative

Sweep 30°
 Free Air
 Nominal Nozzle Location 35% Chord
 Nacelle Spanwise Location $\eta = 27/43.5\%$
 Nacelle Height Below WDP $h/\bar{c} = 0.371$

$C_J = 0$ —————
 $C_J = 1.0$ - - - - -
 $C_J = 2.0$ - - - - -

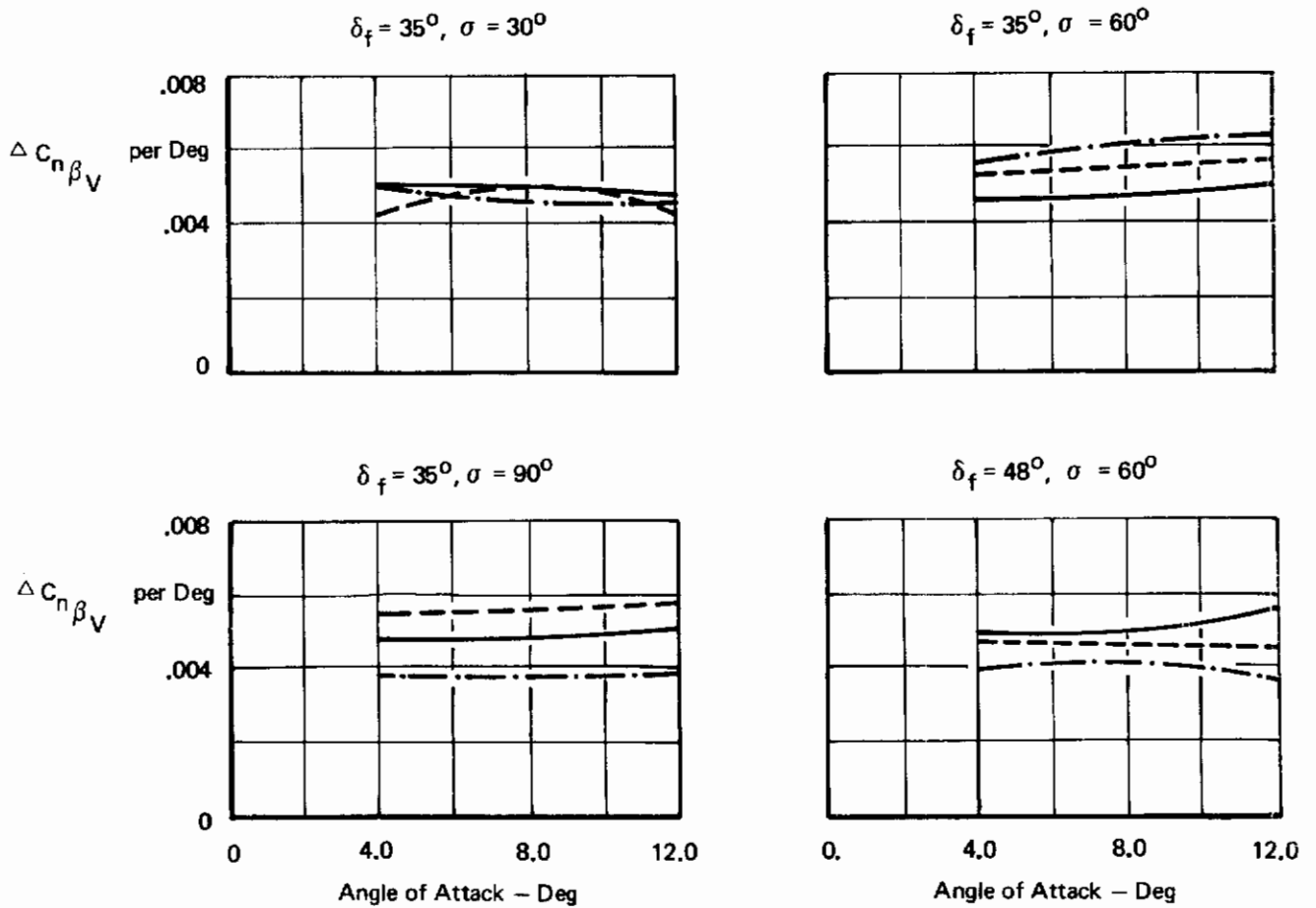


Figure 128 Effect of Angle of Attack on Tail Input to Yawing Moment Derivative

Sweep 30°
 Tail Off
 Free Air
 Nominal Nozzle Location 35% Chord
 Nacelle Height Below WDP $h/\bar{c} = 0.371$
 Nacelle Spanwise Location $\eta = 27/43.5\%$

$C_J = 0$ —————
 $C_J = 1.0$ - - - - -
 $C_J = 2.0$ - - - - -

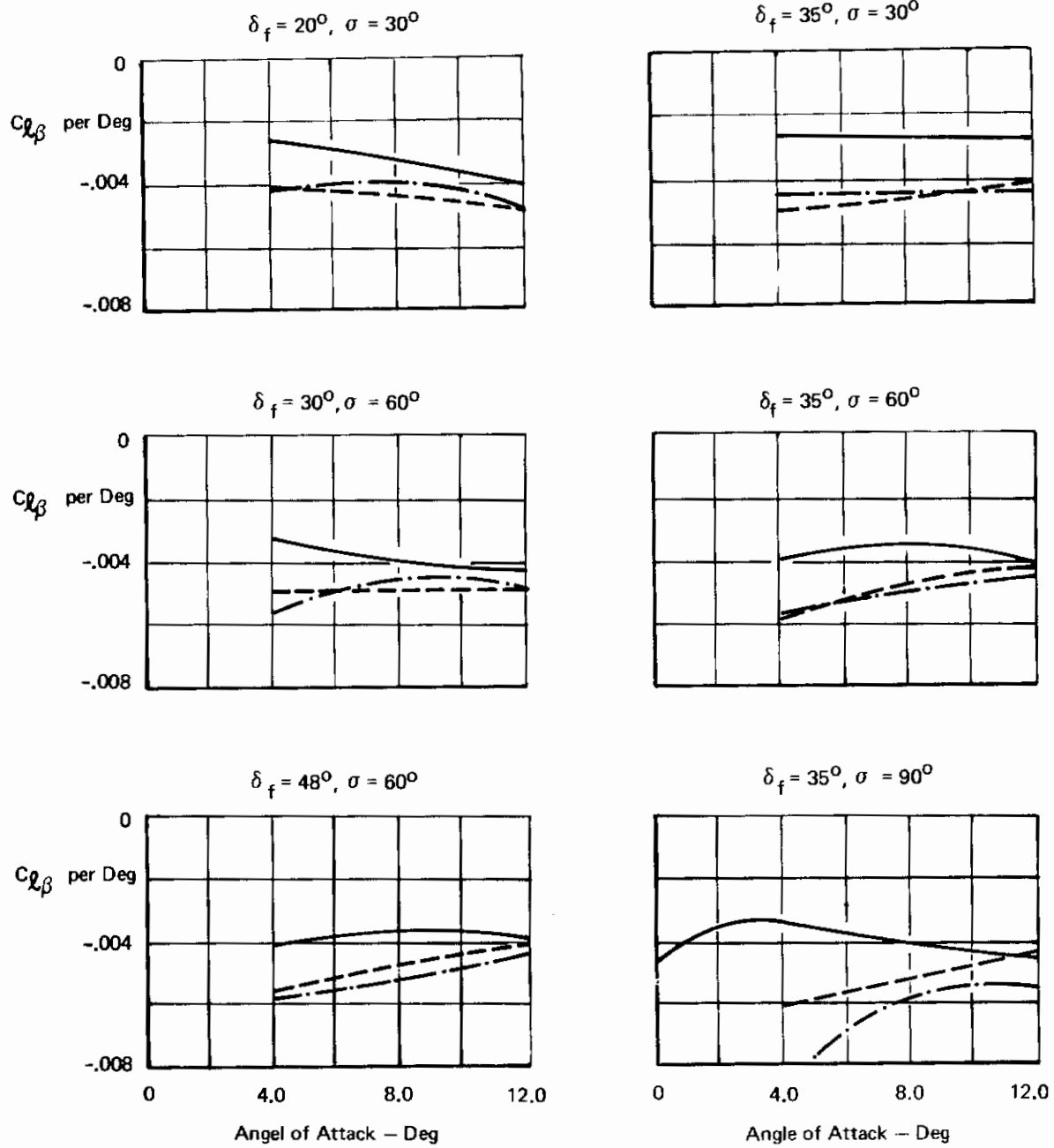


Figure 129: Effect of Angle of Attack on Rolling Moment Derivative

Contrails

Sweep 30°
 Free Air
 Nominal Nozzle Location 35% Chord
 Nacelle Spanwise Location $\eta = 27/43.5\%$
 Nacelle Height Below WDP $h/\bar{c} = 0.371$
 Tail Effectiveness

$C_J = 0$ —————
 $C_J = 1.0$ - - - - -
 $C_J = 2.0$ - · - · - ·

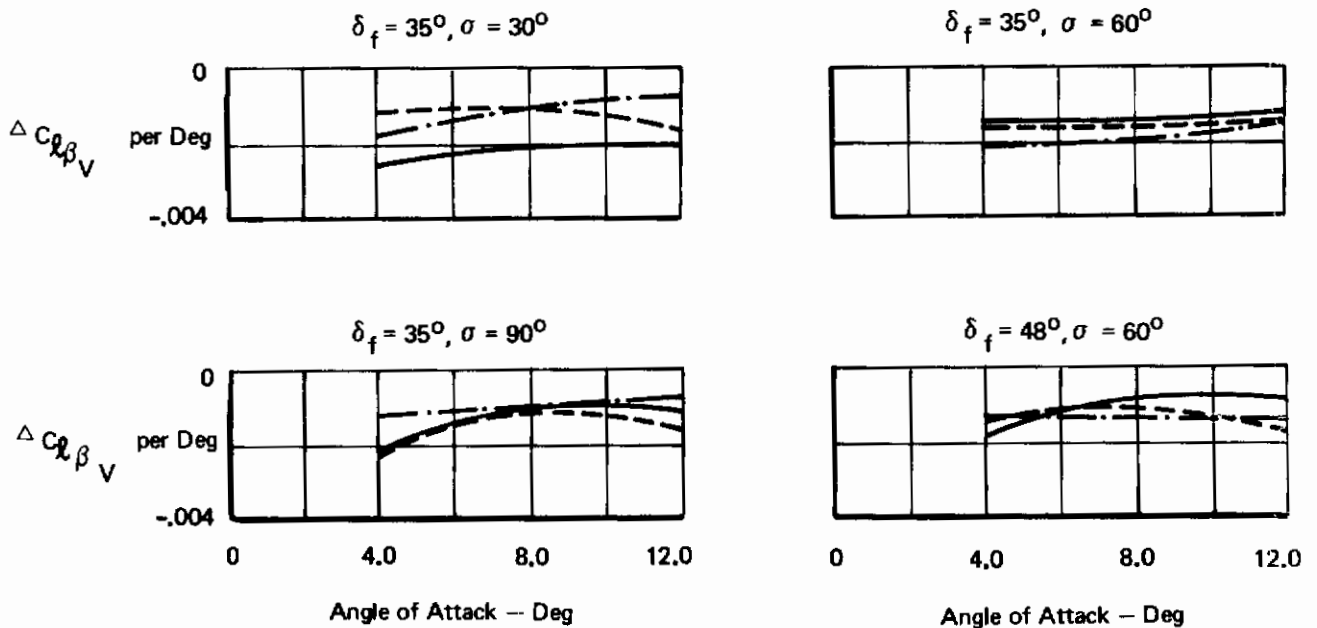


Figure 130: Effect of Angle of Attack on Tail Input to Rolling Moment Derivative

Symbol	α (Deg)	C_J	σ (Deg)	h/b	Run	Engine-Out
○	8.0	.5/.5/0/.5	30	∞	138	Right Inboard
△	8.0	.5/.5/.5/0"	30	∞	139	Right Outboard
□	8.0	2.0	30	∞	140	None
◇	8.0	2.0	30	.242	141	None
○	0	.5/.5/.5/0	30	.242	142	Right Outboard
△	8.0	.5/.5/.5/0	30	.242	142	Right Outboard
△	8.0	.5/.5/0/.5	30	.242	143	Right Inboard
D	8.0	0	60	.242	144	-
△	8.0	2.0	60	.242	145	None
◇	6.0	2.0	30	.242	147	None

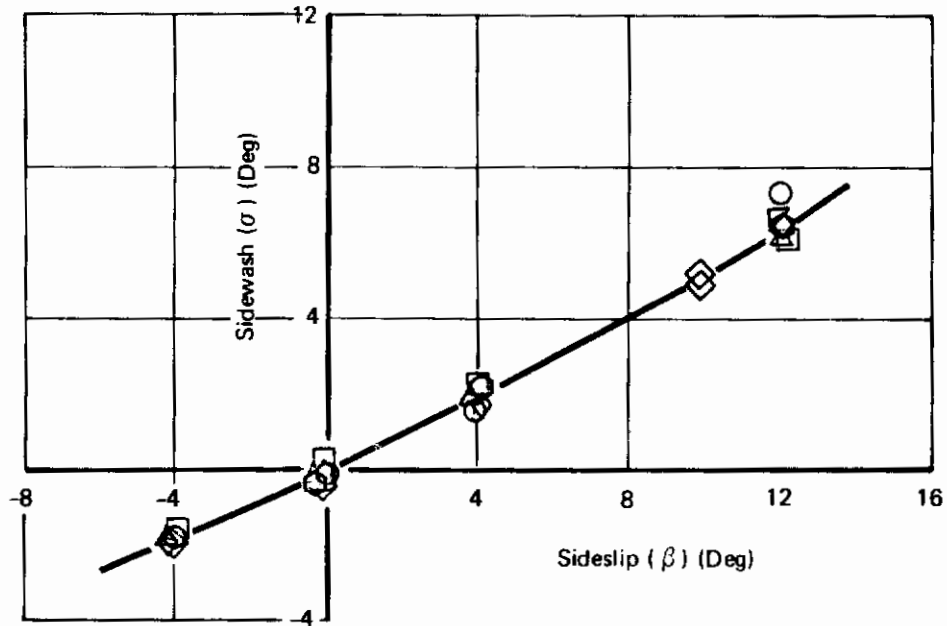


Figure 131: Sidewash at the Vertical Tail

4.7 Control Power

The control power tests evaluated the dependence of control effectiveness on the following variables:

- o Aileron boundary layer control
- o Wing leading edge blowing
- o Engine thrust
- o Engine thrust vector angle
- o Wing sweep
- o Flap setting
- o Angle of attack
- o Sideslip angle

The data on which this analysis is based is given in References 9 and 10.

4.7.1 Lateral Control

4.7.1.1 Aileron Control

Figure 132 shows the effects of aileron boundary layer control (BLC) on downgoing aileron effectiveness, power-off. The maximum aileron deflection angle before aileron stall is greatly increased by increasing the aileron blowing ($C_{\mu Ail}$). The maximum rolling moment attainable is increased by a factor of four to five. The aileron yaw to roll ratio stays approximately constant as the aileron effectiveness improves.

Test results indicated that wing leading edge blowing also increased the downgoing aileron effectiveness. The effects of wing leading edge blowing are shown in Figure 133.

Figure 134 shows that the addition of engine thrust significantly increases the downgoing aileron effectiveness and reduces the amount of aileron blowing required to produce a given rolling moment. Test results indicated that engine thrust had only a slight influence on the upgoing aileron effectiveness. The data also indicated that thrust vector angle influenced the aileron effectiveness only slightly.

4.7.1.2 Spoiler Effectiveness

Figure 135 shows the right wing spoiler effectiveness power on and off. The spoiler effectiveness decreases rapidly beyond $\alpha = 12^\circ$ for power-off. Power-on spoiler effectiveness is significantly greater than power-off beyond $\alpha = 3^\circ$ and does not exhibit the rapid loss of effectiveness at higher angles of attack. At angles of attack below 7° there is a large increase in drag due to spoiler deflection. For angles of attack above 7° , however, the drag with spoiler deflected is lower than for the undeflected case (due to the compensating changes in induced drag). This phenomenon greatly reduces the favorable yawing moment normally associated with a spoiler roll control system.

Contrails

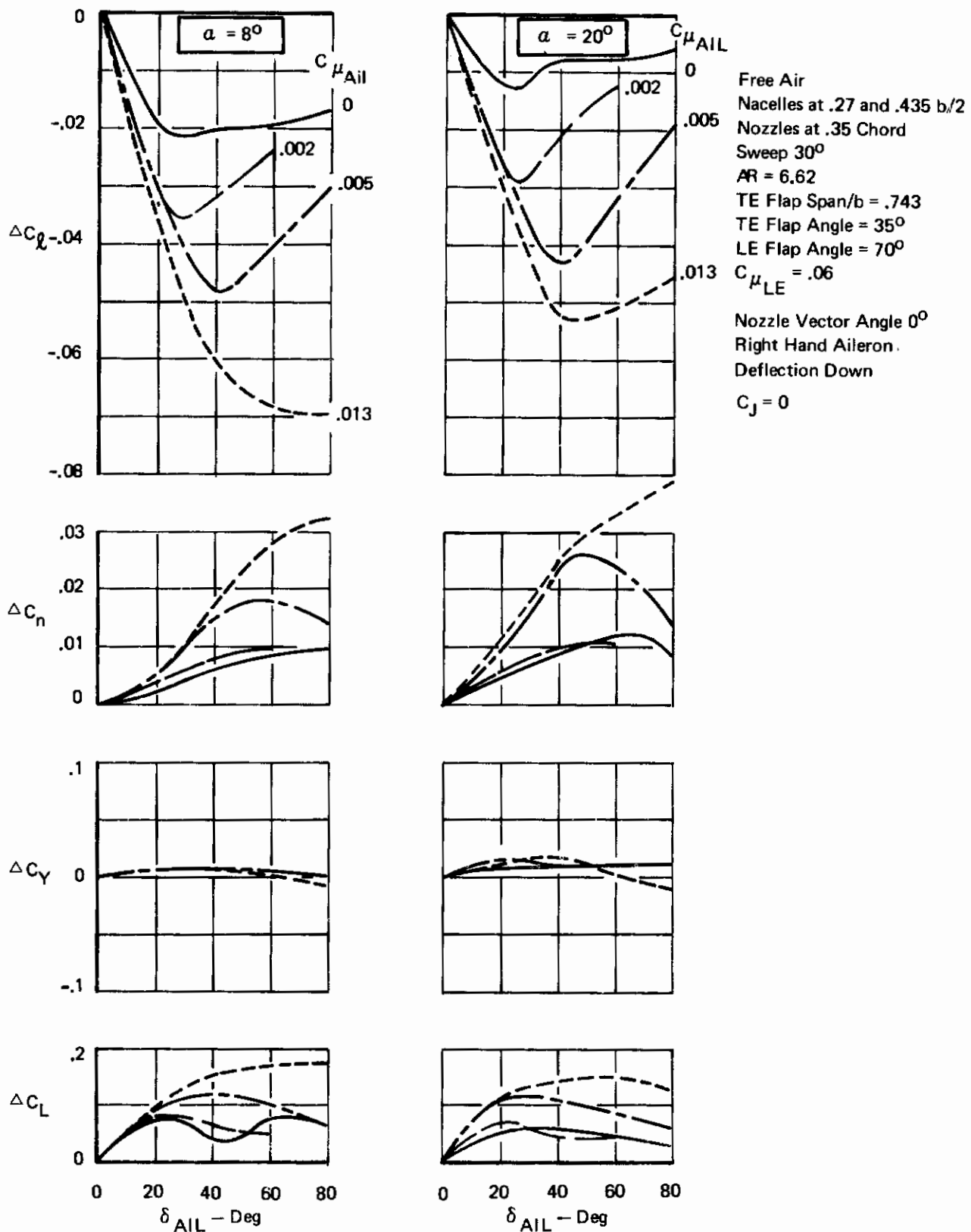
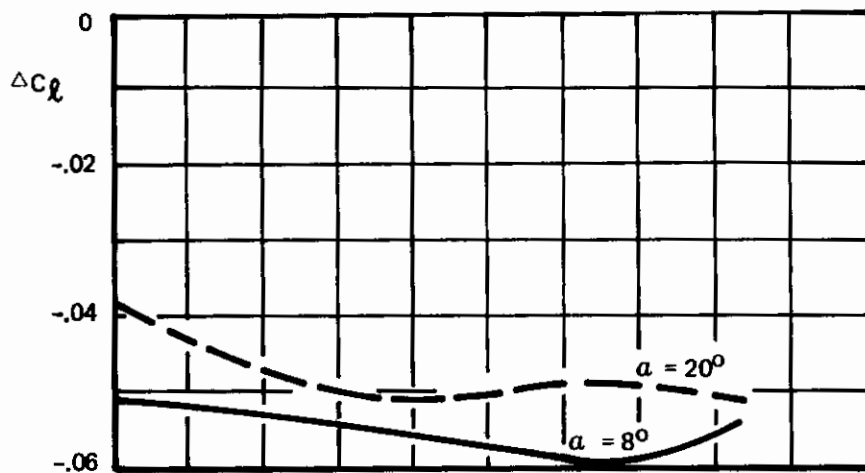


Figure 132: Effect of Aileron Deflection and Blowing on Effectiveness

Contrails



Free Air
 Tail Off
 Nacelles at .27 and .435 b/2
 Nozzles at .35 Chord
 Sweep 30°
 AR = 6.62
 TE Flap Span/b = .743
 TE Flap Angle = 35°
 LE Flap Angle = 70°
 Right Aileron = 40° Dn
 $C_{\mu,Ail} = .005$
 Nozzle Vector Angle = 60°
 $C_J = 2.0$

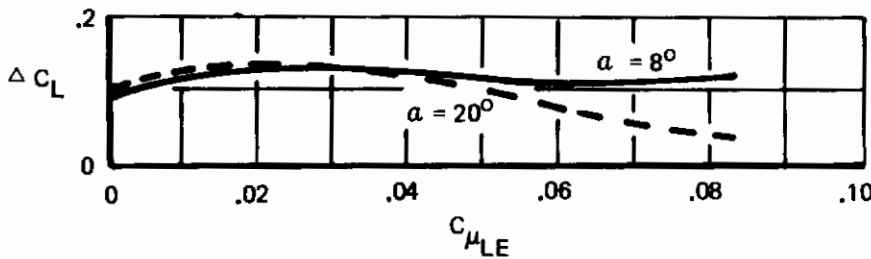
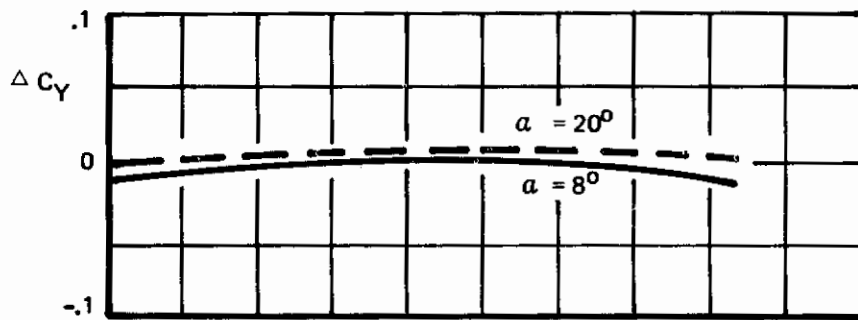
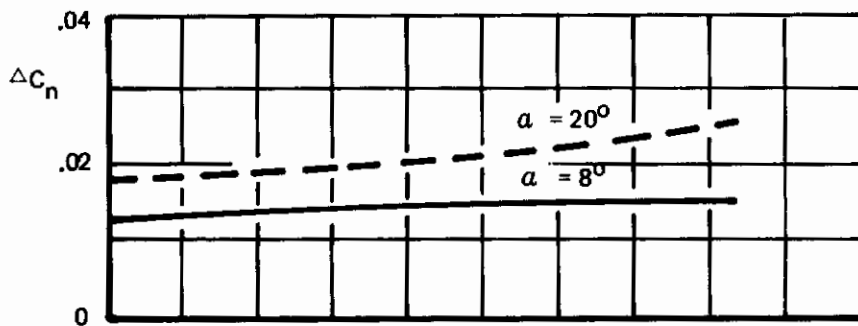


Figure 133: Aileron Effectiveness – Effect of Wing Leading Edge Blowing

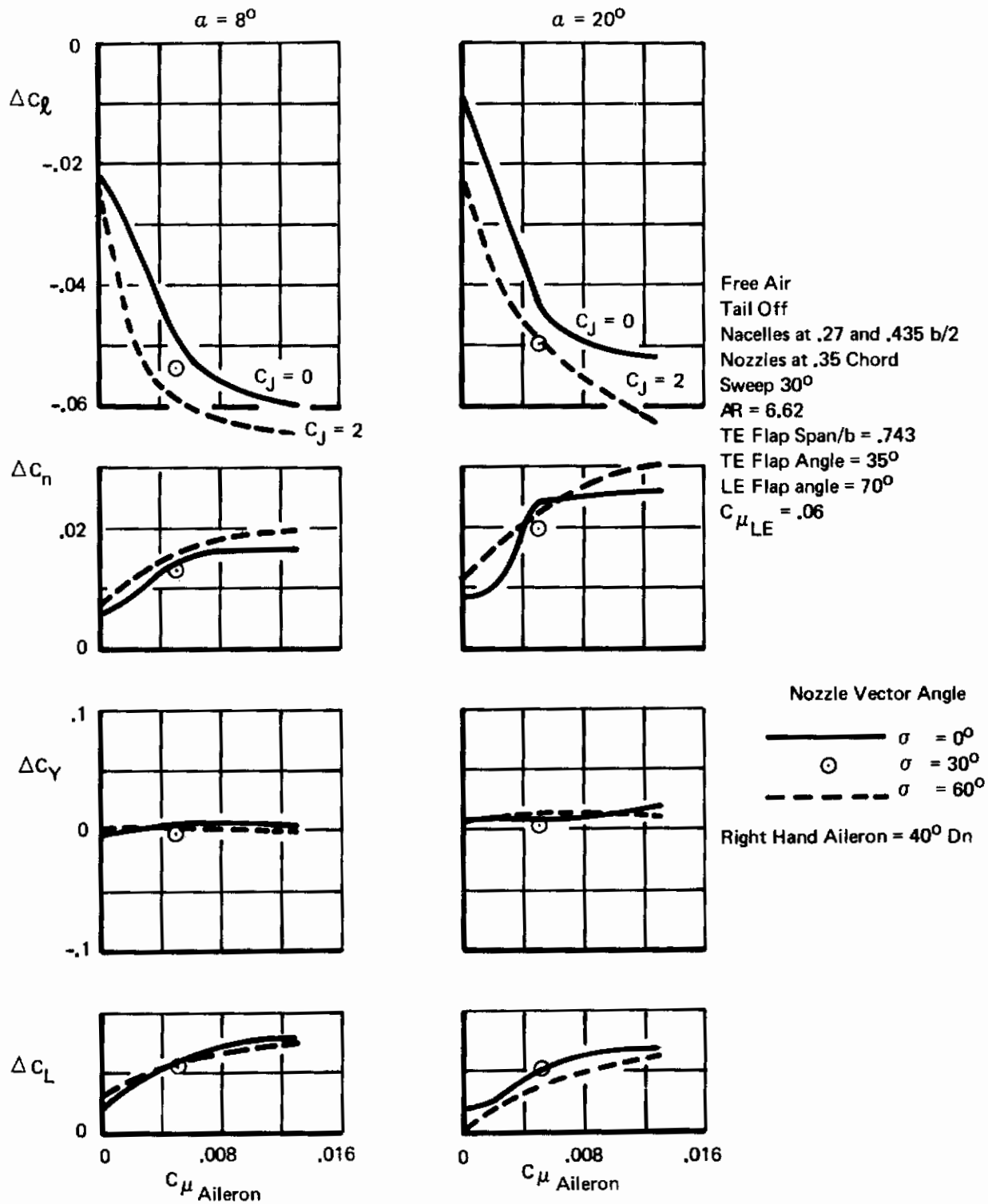
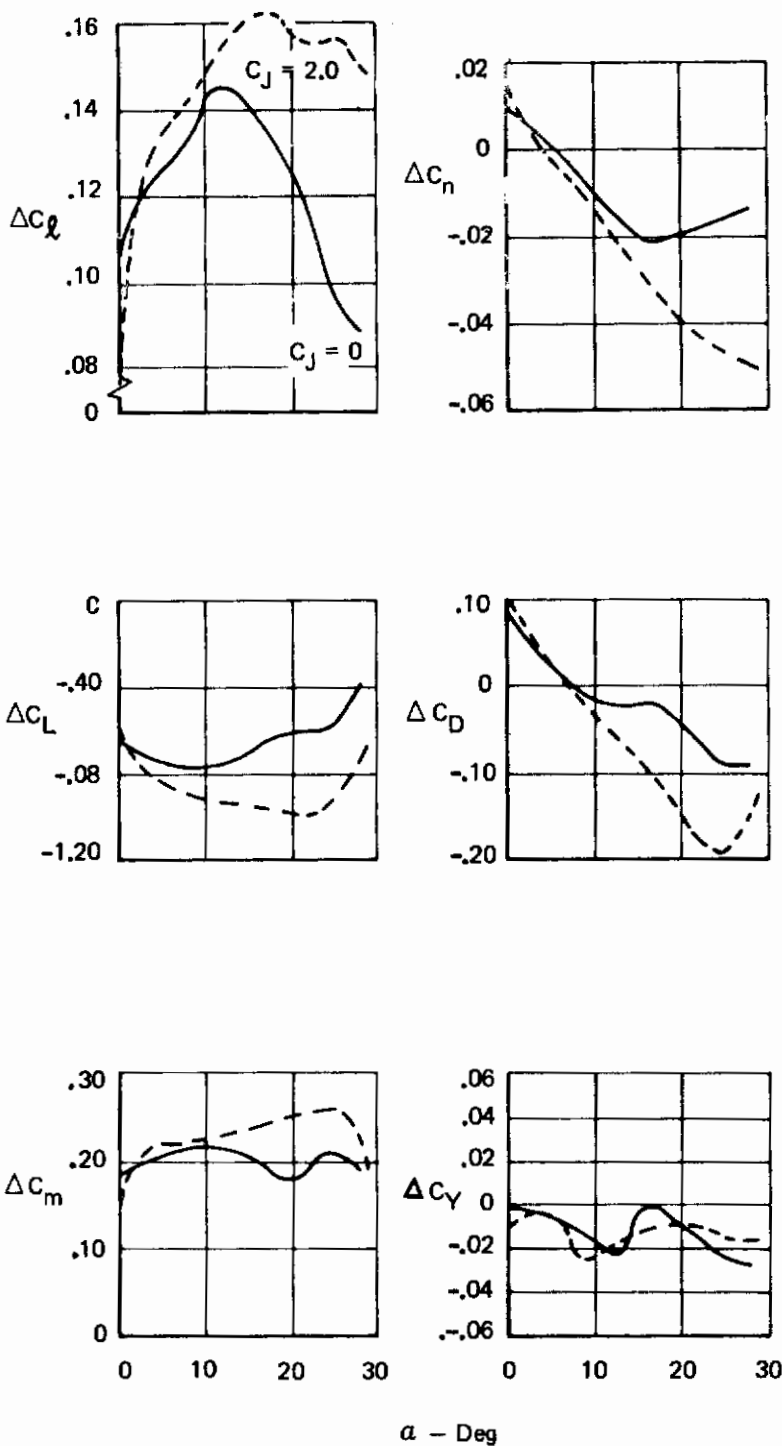


Figure 134: Effect of Aileron Blowing and Engine Thrust on Aileron Effectiveness

δ Spoiler Right = 49°



Free Air
 Tail Off
 Nacelles at .27 and .435 b/2
 Nozzles at .35 Chord
 Sweep 30°
 AR = 6.62
 TE Flap Span/b = .743
 TE Flap Angle = 35°
 LE Flap Angle = 70°
 $C_{\mu_{LE}} = .06$
 $C_{\mu_{AIL}} = 0$
 Nozzle Vector Angle 60°

Figure 135: Spoiler Effectiveness

4.7.1.3 Combined Lateral Control Power

The total lateral control power due to combined aileron and spoiler deflection is shown in Figure 136. The lateral control power due to aileron deflection is approximately constant for positive angles of attack. Addition of roll control due to spoiler deflection increases the lateral control power significantly.

4.7.2 Directional Control

The directional control power test results are shown in Figure 137 for engine power-off. The rudder effectiveness is reduced at the higher angles of attack, power-off, but the addition of engine thrust significantly improved the effectiveness. The thrust effect on rudder power is indicated on Figure 138. Most of the control power testing was conducted with the horizontal tail on. A series of tests conducted with the tail off indicated that the horizontal tail had a favorable influence on the rudder power and increased the effectiveness by 12 percent at the higher angles of attack.

In ground effect, the rudder effectiveness was reduced by 20 percent for both power-on and power-off. Thrust vector angle had only a slight influence on rudder power in free air and in ground effect.

The effect of sideslip on rudder effectiveness is shown in Figure 138. The rudder effectiveness, ΔC_n , is significantly reduced at the larger sideslip angles and produces only 60 percent of the effectiveness at zero sideslip. The addition of engine thrust improves the effectiveness at all sideslip angles tested.

4.7.3 Longitudinal Control

The stabilizer effectiveness shown in Figure 139 was obtained by deflection of the entire horizontal stabilizer surface. The stabilizer longitudinal control power increases with angle of attack until $\alpha = 20^\circ$ and then drops off rapidly. Engine thrust significantly improved the effectiveness at the higher angles of attack. Proximity to the ground plane did not affect the stabilizer power for low angles of attack.

Contrails

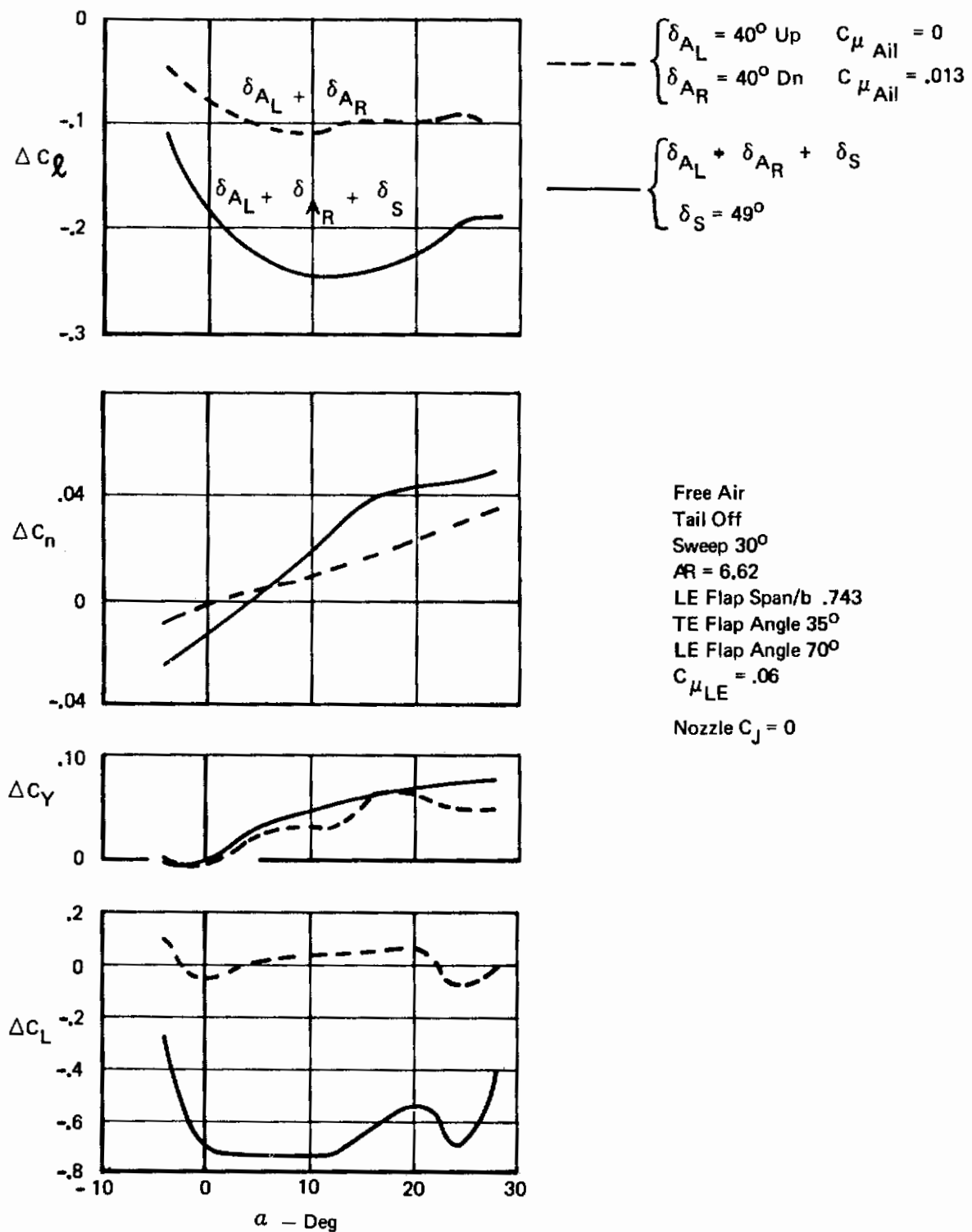
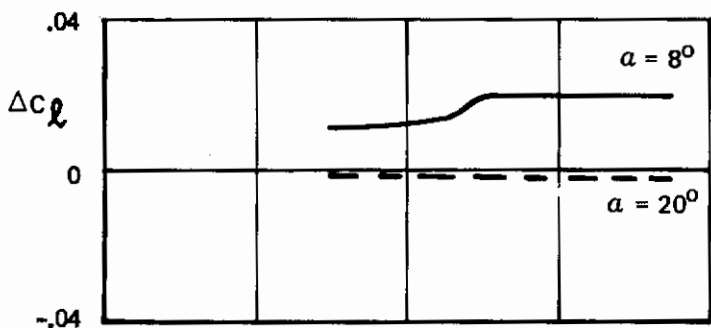
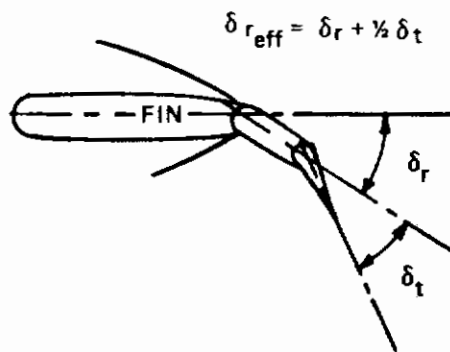
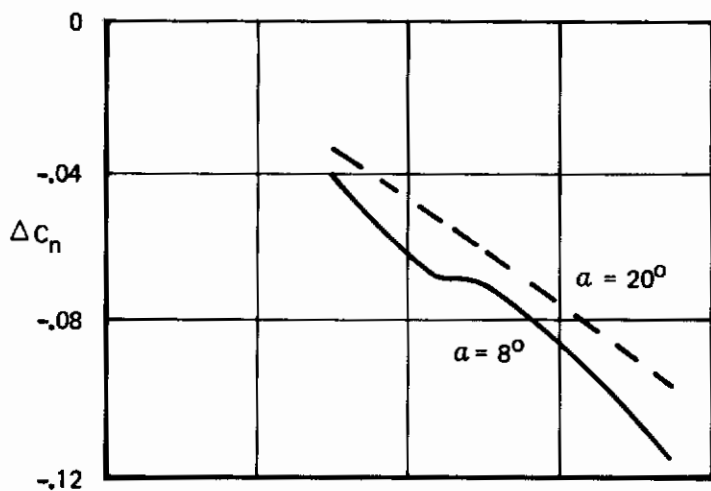


Figure 136: Lateral Control – Combined Aileron and Spoiler

Contrails



Free Air
 Horiz Tail On
 Sweep 30°
 $AR = 6.62$
 TE Flap Span/b = .743
 TE Flap Angle = 35°
 LE Flap angle = 70°
 $C_{\mu_{LE}} = .06$
 Nozzle $C_j = 0$

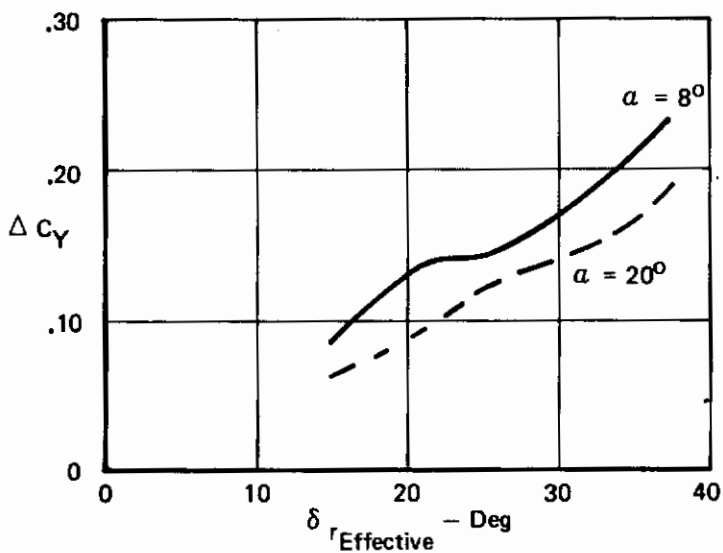
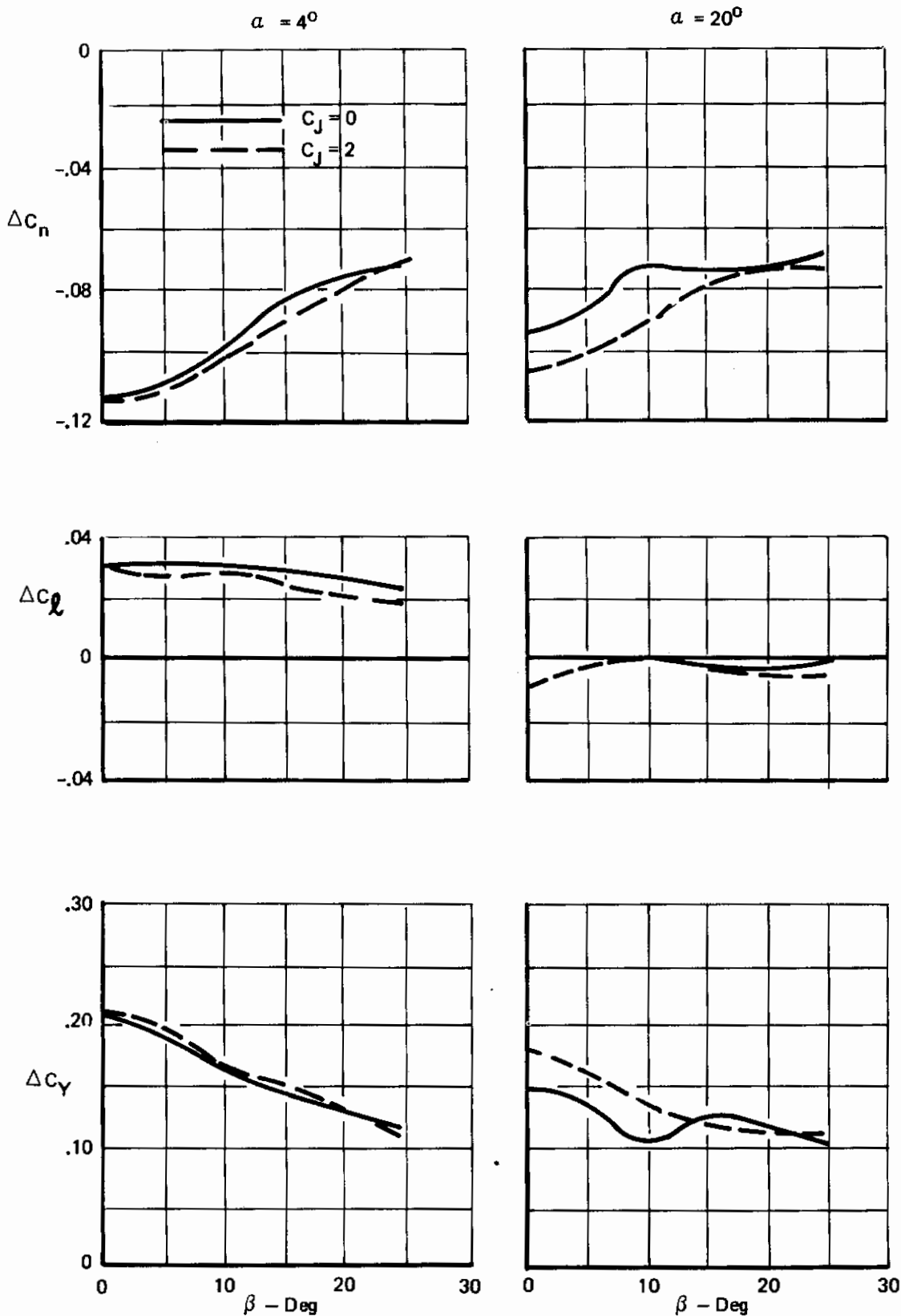


Figure 137: Rudder Effectiveness – Power Off

Contrails



Free Air
 Horiz Tail On
 Nacelles at .27 and .435 b/2
 Nozzles at .35 Chord
 Sweep 30°
 AR = 6.62
 TE Flap Span/b = .743
 TE Flap Angle = 35°
 LE Flap Angle = 70°
 $C_{\mu LE} = .06$
 Nacelle Vector Angle 30°
 Rudder/Tab Angle = $25^\circ/25^\circ$
 $\delta_{\text{Effective}} = 37.5^\circ$

Figure 138: Effect of Sideslip on Rudder Power

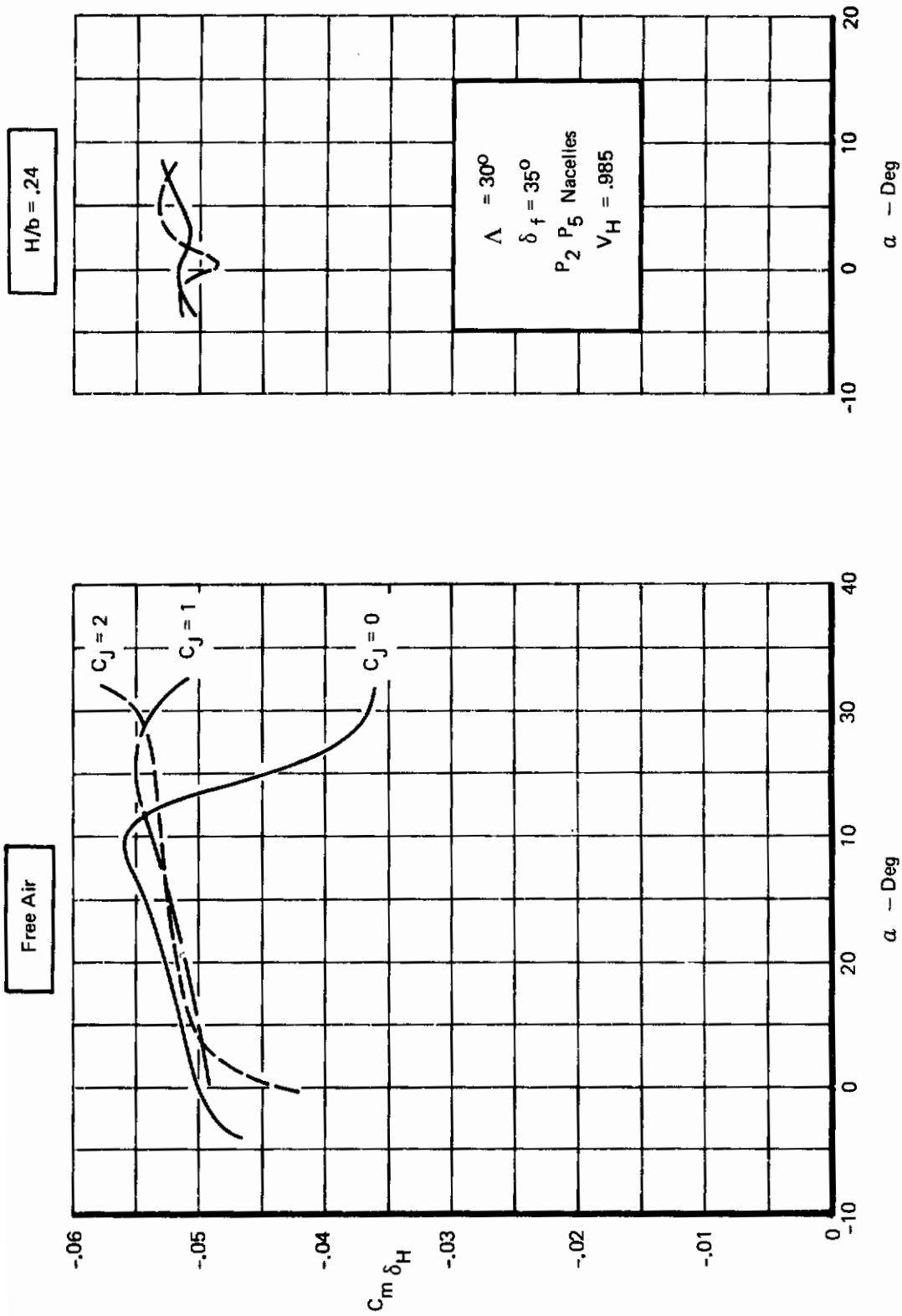


Figure 139: Stabilizer Effectiveness

Contrails

SECTION V

INTERNALLY BLOWN JET FLAP

The Air Force's need to develop STOL transport aircraft focused attention on the inadequacies of the aerodynamic data base for a number of powered lift concepts under investigation. As part of the Boeing Company's portion of the STOL Tactical Aircraft Investigation, a limited wind tunnel test program was performed on the internally blown jet flap concept.

A significant amount of wind tunnel testing has been accomplished in the past on the jet flap concept. This testing, in general, assumed that all of the engine air was ducted into the wing and used to power the jet flap. In a practical airplane application, it is probable that all of the engine airflow would not be ducted to the jet flap. For example, due to temperature limits in the wing, it might be desirable to use only the bypass air from a low or moderate bypass ratio engine to power the jet flap while allowing the hot core jet to exhaust aft or be deflected for additional lift or glide path control. This exhaust jet would produce aerodynamic interference by interacting with the jet flap sheet.

A limited jet flap test program was run with two objectives.

- (1) To provide data for an aerodynamically efficient reference high lift system for comparison with the vectored thrust powered lift concept which was the primary focus of Boeing's STAI investigation.
- (2) To provide an indication of the magnitude of the interference effects due to the interacting of residual nacelle exhaust for conventional underwing engine locations and the jet sheet.

5.1 Aerodynamic Data for Internally Blown Jet Flap and Vectored Thrust

Vectored thrust and internally blown jet flaps were tested on the same model in order to obtain a direct comparison between the two concepts. Testing was accomplished with basic wing, body, nacelle location, and flap span identical in both cases.

This section presents a comparison of aerodynamic data for the two concepts.

5.1.1 Longitudinal Characteristics

Low speed longitudinal aerodynamic characteristics of the model with internally blown jet flaps and vectored thrust at approximately the same jet angles are shown in Figures 140 and 141. Figure 141 shows vectored thrust at 90° deflection angle and the 80° jet flap which had a measured static jet angle of 86°. Figure 140 shows

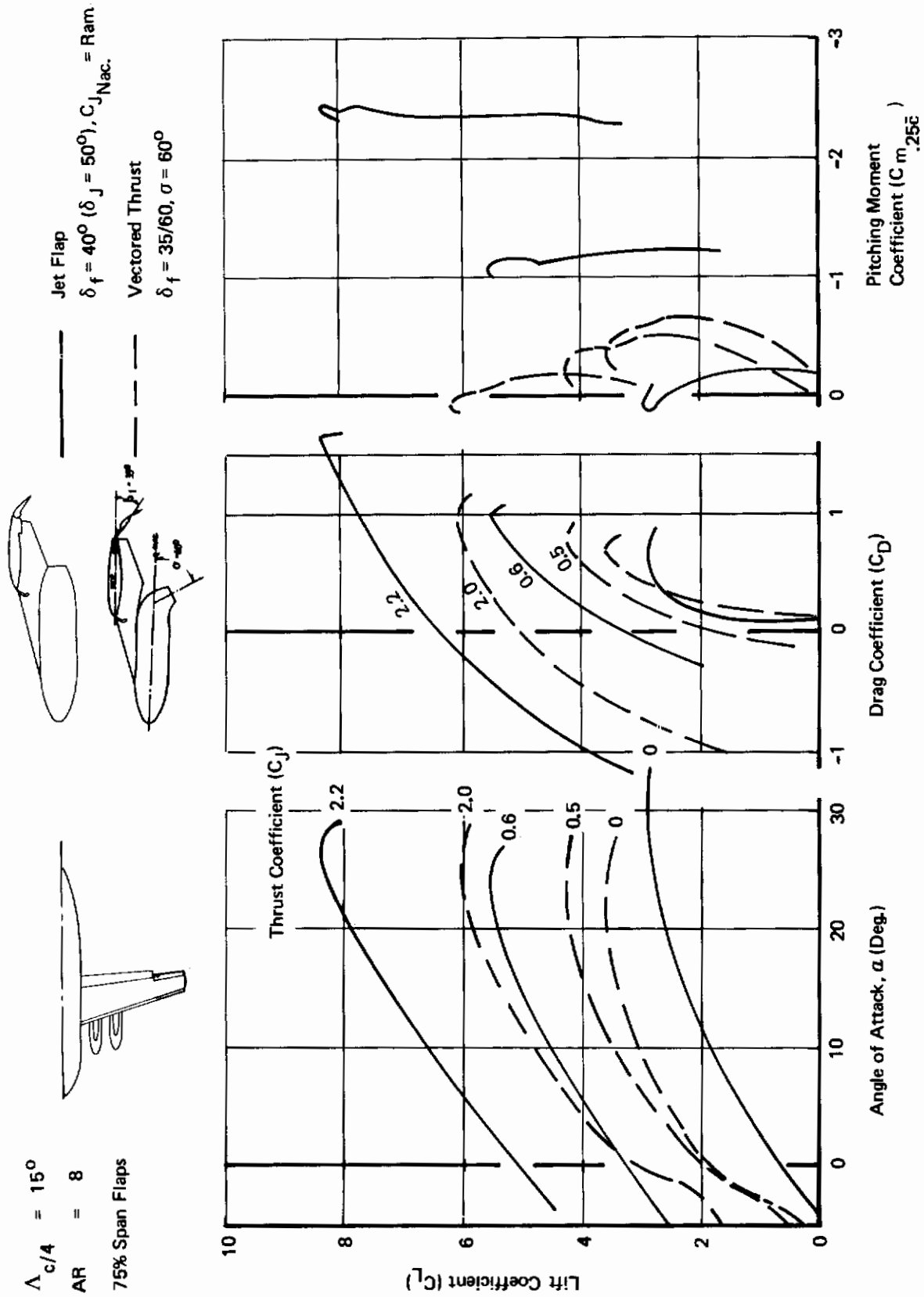


Figure 140: Comparison of Aerodynamic Characteristics of Jet Flap to Vektored Thrust

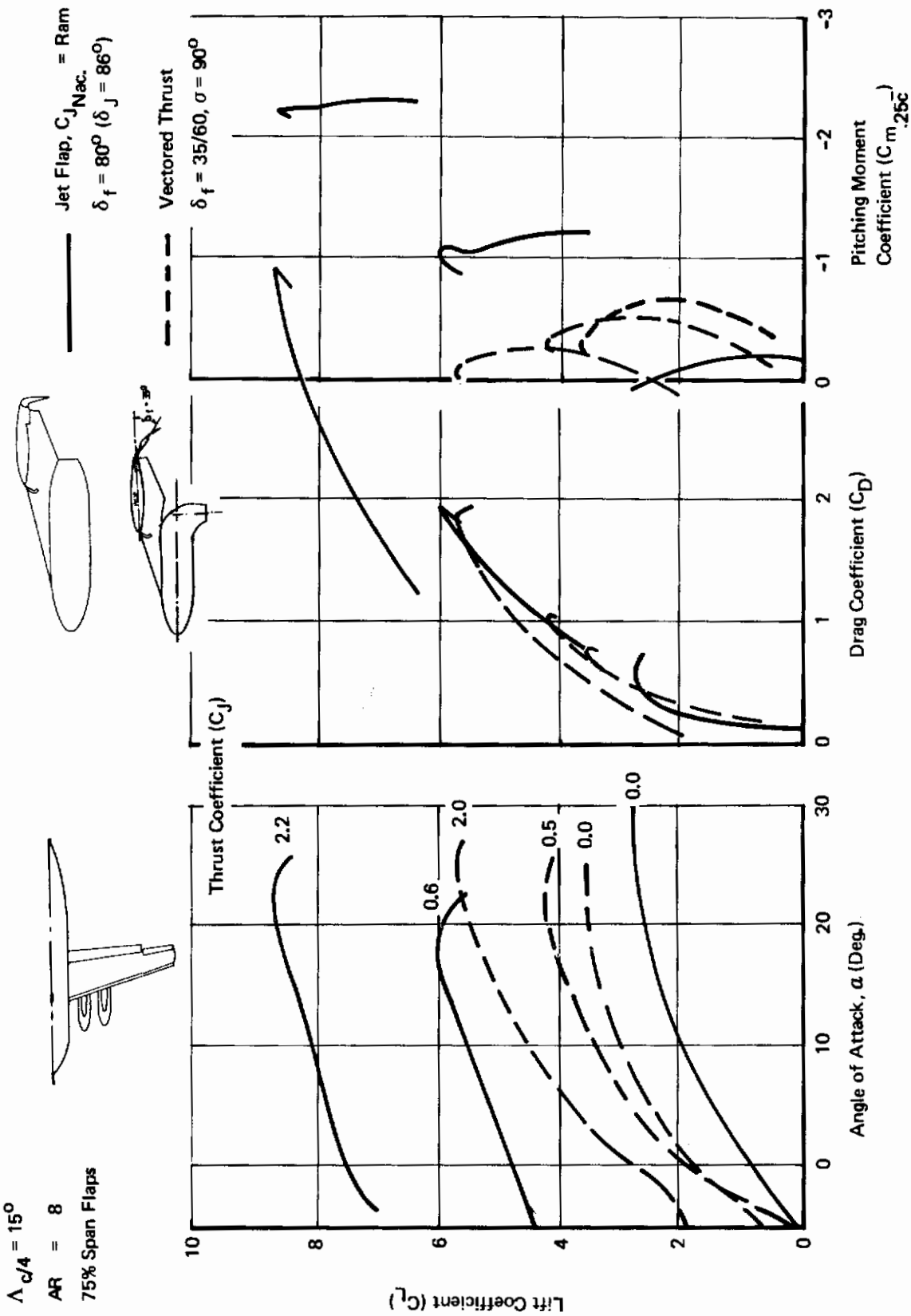


Figure 141: Comparison of Aerodynamic Characteristics of Jet Flap to Vectored Thrust

vectored thrust at 60° and jet flaps at 40° . It can be seen that the IBJF produces considerably more lift for the same amount of thrust, due to the generation of supercirculation lift. However, large pitching moments accompany this lift since it is induced well aft on the wing. For the vectored thrust nozzle location shown, 35% local chord, the pitching moments due to thrust actually decline with increasing thrust coefficient for the vectored thrust/mechanical flap concept.

The variation of maximum lift with thrust coefficient is shown in Figure 142. The vectored thrust has a higher unpowered maximum lift than the jet flap since it has an efficient triple-slotted trailing edge high lift system. This advantage quickly disappears as thrust coefficient is increased since the vectored thrust maximum lift increase with C_J is about equal to C_J while the jet flap enjoys a large amplification factor because of the super-circulation lift associated with jet flaps. Although insufficient data were taken to define the jet flap maximum lift variation between $C_J = 0$ and 0.6, IBJF data typically shows an initial high slope due to boundary layer control effects with a knee which is conventionally denoted as the boundary layer attachment point.

Since both the jet flap and vectored thrust were tested on the same model, for economy the same blown leading edge device was used on both concepts. Figure 143, which shows the effect of leading edge boundary layer control on maximum lift, illustrates that this must be done with caution. Leading edge BLC is only about half as effective for the jet flap configuration as it is for the vectored thrust configuration. This illustrates that the leading-edge high-lift system must be designed for the lift levels achieved by the particular concept under investigation. It is not reasonable to expect that a leading edge designed to have favorable characteristics at one lift level will necessarily behave well at another.

5.1.2 Lateral Stability

A comparison of lateral stability for the two concepts is shown in Figure 144. For the lower jet angle the IBJF has higher stability than the MF + VT. $C_{l\beta}$ decreases with jet flap thrust for the IBJF while MF + VT remains constant. At the 90° jet the IBJF has higher stability at $C_J = 0$ than the jet flap; however, the effects of power are large and in opposite directions for the two concepts. For the jet flap $C_{l\beta}$ decreased substantially with increasing thrust while it increased for the vectored thrust configuration.

5.1.3 Lateral Control

Several alternative methods were investigated to provide lateral control: spoilers, asymmetric jet flap deflection, and asymmetric blowing.

Contrails

$$\Lambda_{c/4} = 15^\circ$$

$$AR = 8$$

75% Span Flaps

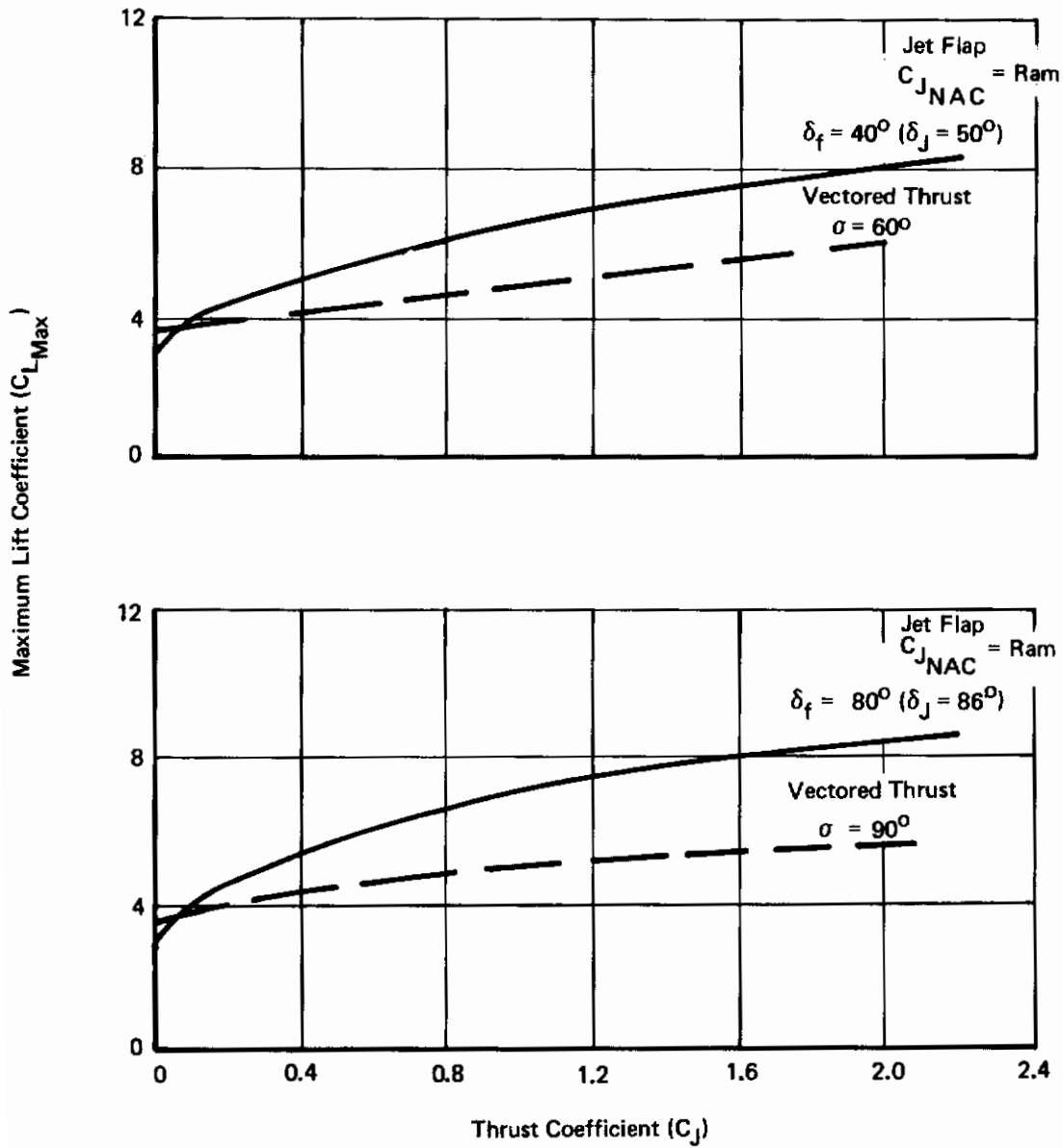


Figure 142: Maximum Lift Comparison

$$\Lambda_{c/4} = 15^\circ$$

$$AR = 8$$

75% Span Flaps

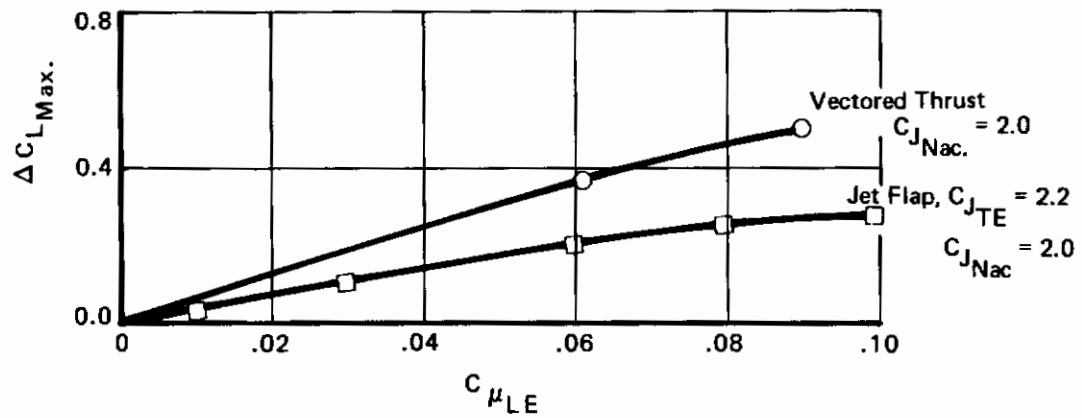
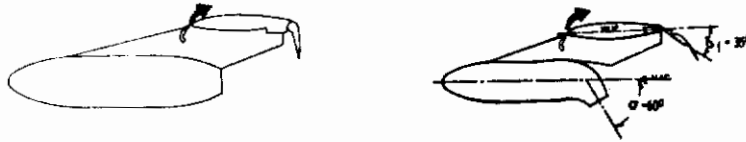
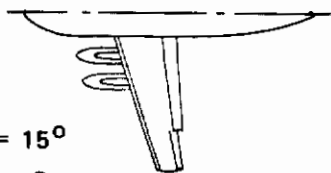


Figure 143: Leading Edge Boundary Layer Control Effectiveness

Contrails



$\Lambda_{C/4} = 15^\circ$

AR = 8

75% Span Flaps

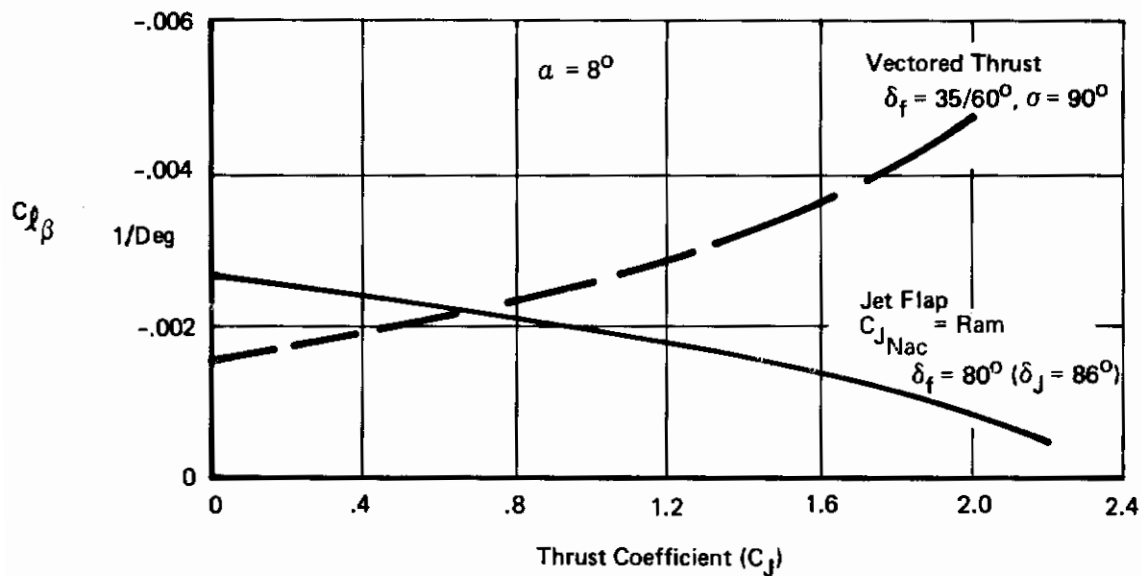
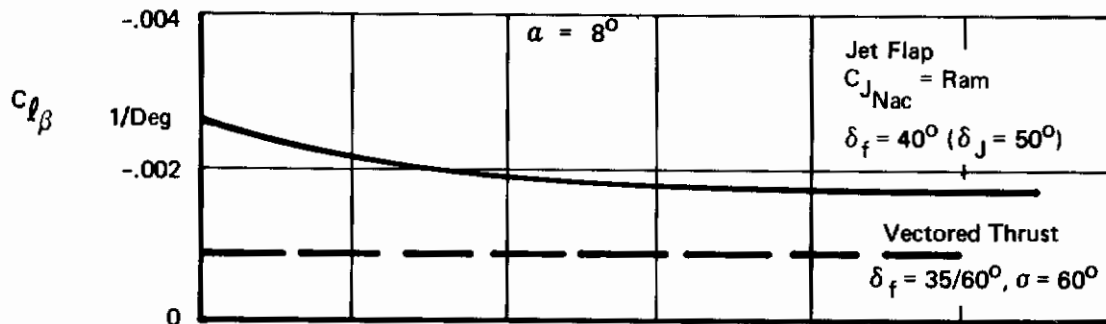


Figure 144: Lateral Stability

5.1.3.1 Spoiler Effectiveness

Spoiler effects for the mechanical flap plus vectored thrust concept were tested only at 30° sweepback so that the comparison presented here cannot be as unambiguous as desired. However, the conclusions reached are still valid.

A comparison of spoiler effects for spoiler deflection of 60° is shown in Figure 145. At $C_J = 0$, the spoilers on the jet flap configuration are less effective than on the vectored thrust configuration. This was to be expected since spoiler effectiveness depends on the effectiveness of the trailing edge flap system behind it. At $C_J = 2.0$ spoiler rolling effectiveness is increased significantly for the vectored thrust configuration and dramatically for the jet flap configuration. Again, this result could be anticipated because of the very high lift levels generated by the jet flap and the rolling moment is accompanied by large lift losses.

5.1.3.2 Asymmetric Jet Flap For Lateral Control

The use of asymmetric outboard jet flap deflection for lateral control was explored briefly. From full span 80° jet flap deflection, the outboard 25% span flap on the right wing was retracted to 40° giving $\delta f_{\text{left}} - \delta f_{\text{right}} = 40^\circ$. The asymmetric flap was 80/40. The data, Figure 146, shows that this is highly effective at low angles of attack but that rolling moment decreases rapidly with increasing angle of attack. Referring back to Figures (140) and (141), the explanation for this is readily apparent. The 80° flap deflection has a higher lift at zero angle of attack than the 40° flap but a much lower lift curve slope. Therefore, the lift difference, and thus rolling moment for the asymmetric flap deflection, decreases as angle of attack increases.

Lateral control could also be obtained by using asymmetric jet flap blowing, perhaps in conjunction with asymmetric flap deflection. Only an extreme case was tested in order to determine the maximum rolling moment such a scheme could generate. From 80° full span flap deflection, the right outboard flap section (25% span) was retracted to zero deflection and the blowing on that segment also eliminated. The results are given in Figure 147. Large rolling moments were generated at the expense of a large lift decrement. Roll effectiveness is nearly independent of angle of attack until 20° where it drops off sharply due to asymmetric wing stall.

5.2 Residual Nacelle Thrust

Traditionally the performance of an airplane with jet flaps has not accounted for the residual thrust, if any, from the jet engines. For engines mounted below the wing, the engine exhaust will interact with the jet sheet to reduce its effective deflection or to effectively create a part span cut-out in the sheet. The majority of the testing accomplished on the jet flap model was to determine the magnitude of the aerodynamic interference effects due to exhausting the residual jet

Contrails

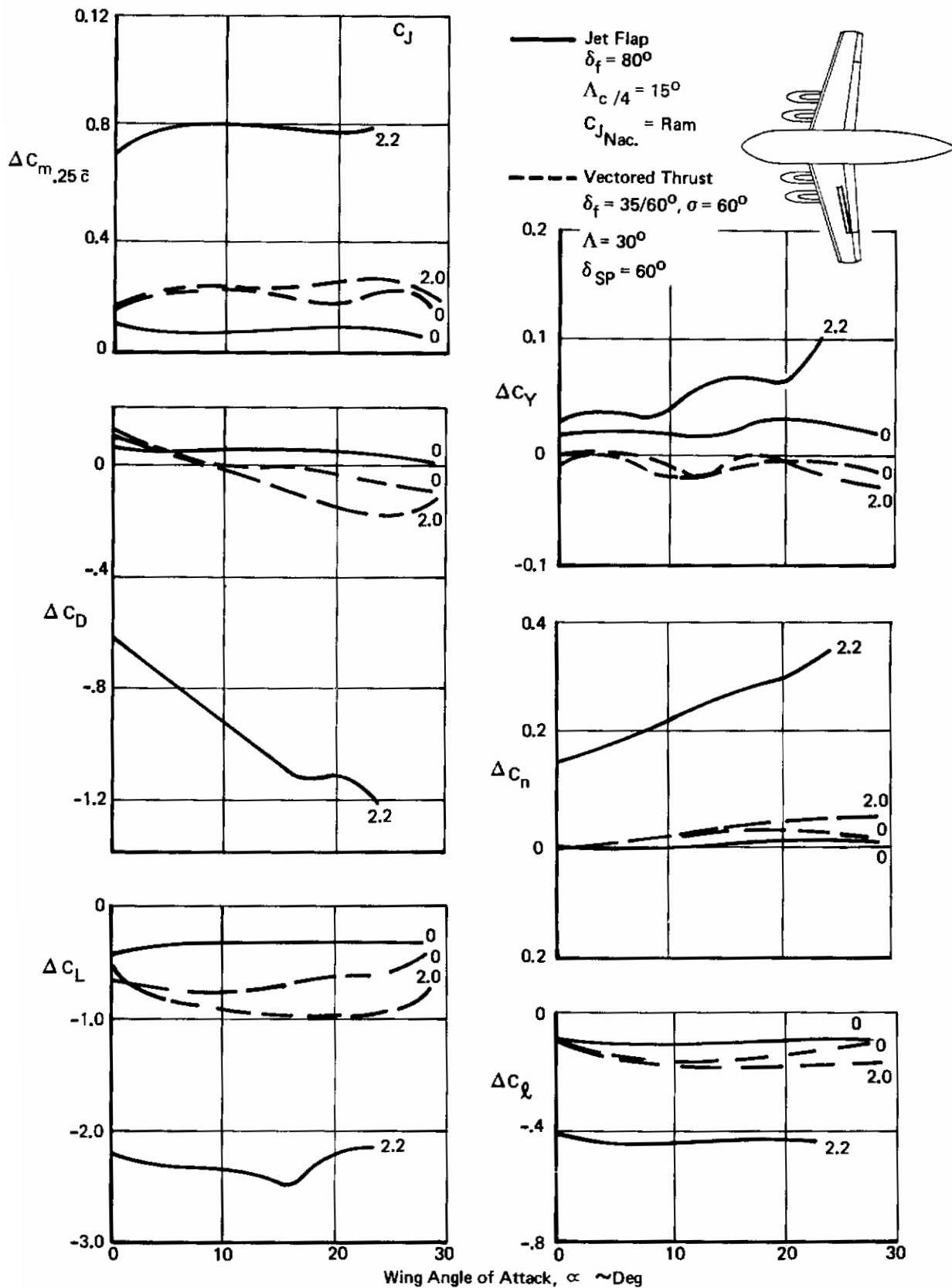


Figure 145: Spoiler Effects – Jet Flap and Vectors Thrust

Contrails

$\Lambda_{c/4} = 15^\circ$
 $AR = 8$
 Full Span Flaps, $\delta_f = 80^\circ$
 $\delta_f \text{ Ail} = 80/0^\circ$
 $C_{J \text{Nac.}} = \text{Ram}$

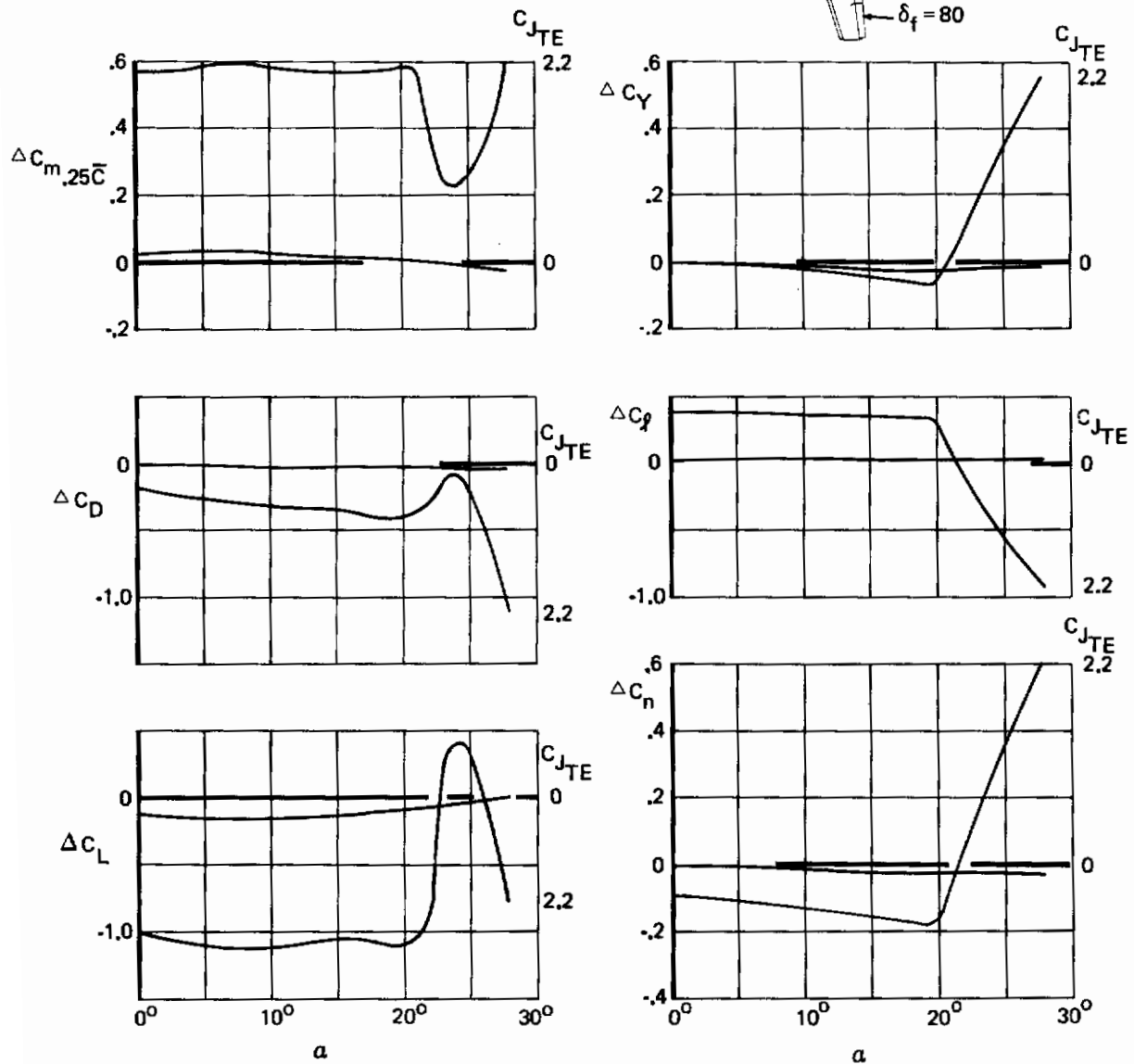
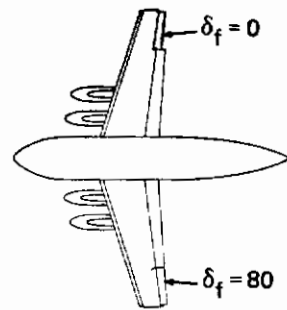


Figure 147: Jet Flap Aileron – No Blowing on Upgoing Aileron

aft from under-wing nacelles. These effects were determined to be very significant. Alternate configurations having the nacelles mounted above the wing have been suggested, and in fact, were proposed on the IBJF "baseline" a airplane designed early in the STAI.* Configurations representative of the IBJF baseline configuration were not tested since the interference effects should be minimal if the engine exhaust was not deflected downward. Significant additional lift augmentation could, in fact, be gained by using the flaps behind the nacelles as Coanda surfaces to turn the residual nacelle exhaust flow (Ref.7), thereby creating an Upper Surface Blown flap.

5.2.1 Effect of Dividing Total Thrust Between Nacelle and Jet Flap

The jet flap and powered nacelle have been run with several combination of thrust coefficient adding up to a total C_J of approximately 2.0. Lift and drag for these conditions are summarized in Figure 148. This shows the large variation in lift and flight path angle available from the same amount of total thrust. Further variation is, of course, possible by vectoring the residual thrust.

5.2.2 Residual Nacelle Thrust Interference Effects

Interference effects of the residual nacelle thrust on lift, drag, and pitching moment at an angle of attack of eight degrees and a jet flap deflection of 80° are shown as a function of both nacelle residual and jet flap thrust coefficient, Figure 149. Interference effects on lift and drag are nearly independent of residual nacelle C_J over the range tested but strongly dependent on trailing edge jet flap thrust coefficient. Unfortunately time and the difficulty of adequately visualizing the flow did not permit a flow visualization investigation of this phenomenon to determine how the jet sheet had been affected. The pitching moment interference is very small and trends with nacelle thrust could not be established.

Interference effects have been summarized as a function of wing angle of attack, jet flap angle, and jet flap thrust coefficient for $C_{J_{NAC}} = 2.0$, Figure 150. In general, interference effects increase with increasing flap angle as the flap jet sheet becomes steeper.

The data indicate that residual nacelle thrust has only a small effect on pitching moment below the stall angle of attack no matter what the jet flap thrust coefficient, Figure 151. Lift interference increases rapidly with jet flap thrust coefficient up to $C_{J_{TE}} = 0.5$ and then becomes nearly independent of $C_{J_{TE}}$.

5.2.3 Ground Effect

As an airplane operating at the very high lift levels required for STOL operation comes into ground effect, lift may be reduced by the effects of the image bound vortex reducing the velocity at

*For details, see Appendix B of Ref. 12

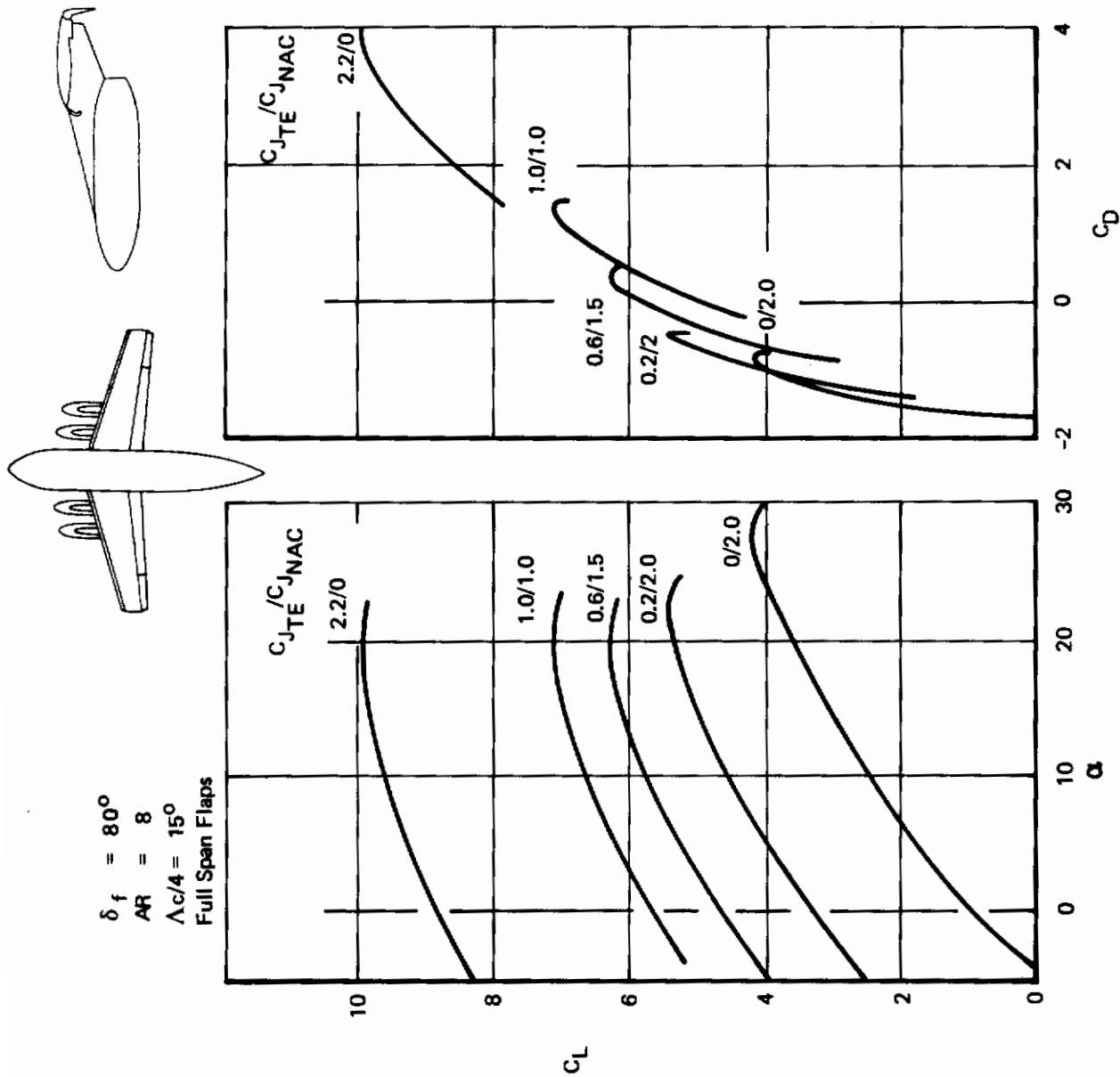
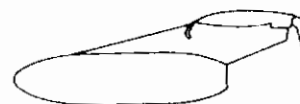
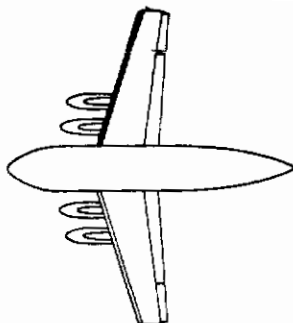


Figure 148: Effect of Thrust Division Between Nacelle and Jet Flap

Contrails

$\Lambda_{c/4} = 15^\circ$
 AR = 8
 Full Span Flaps, $\delta_f = 80^\circ$



Nac. Spanwise Location % $\eta = 27/43.5$
 Height Below WDP = $h/\bar{c} = 0.406$

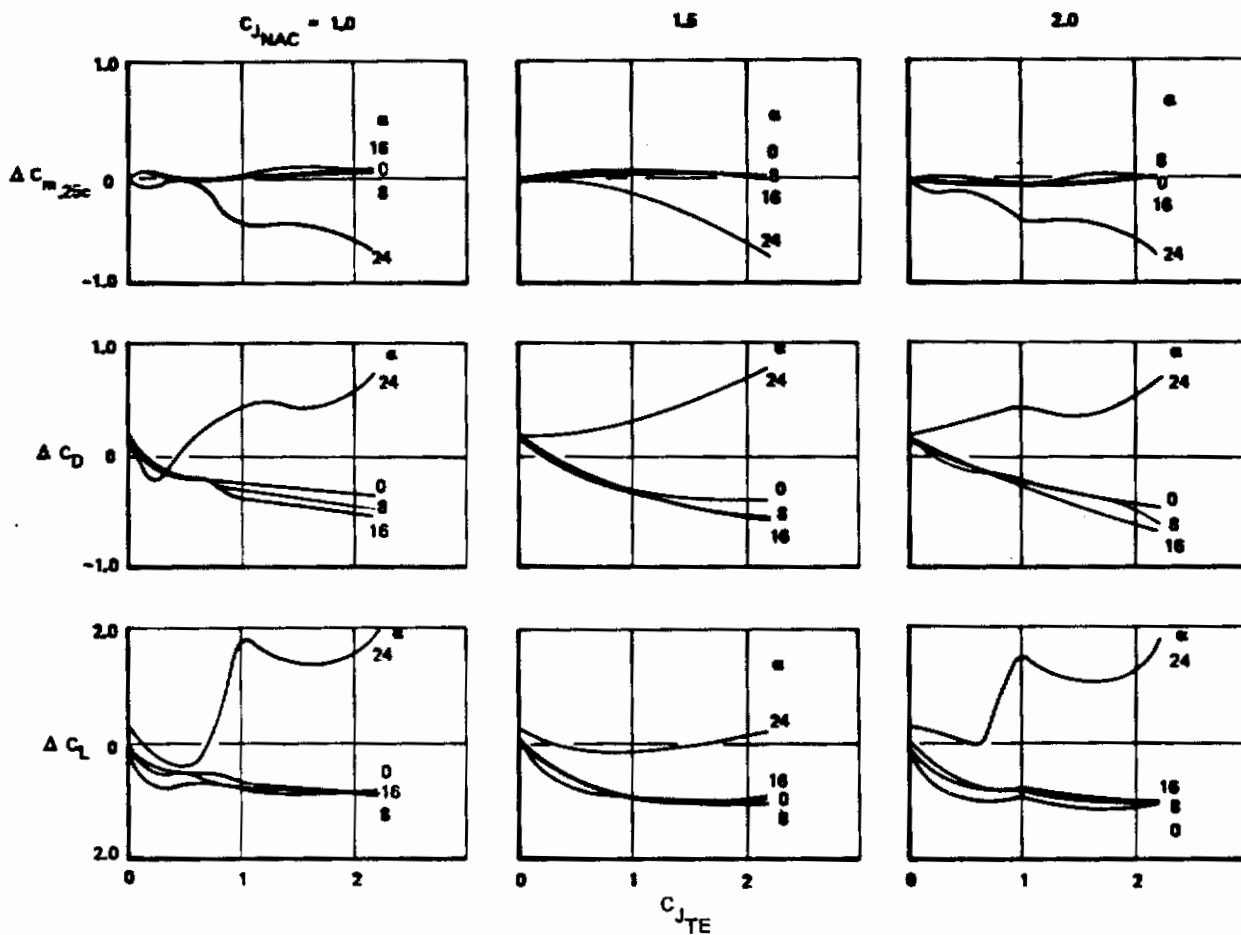


Figure 149: Effect of Jet Flap Thrust Coefficient on Residual Nacelle Thrust Interference — $\delta_f = 80^\circ$

Contrails

Sweep $\Lambda = 15^\circ$ AR = 8.0
 NAC Spanwise Location % $\eta = 27/43.5$
 Height Below WDP = $h/\bar{c} = 0.406$
 Full Span Flaps
 Free Air

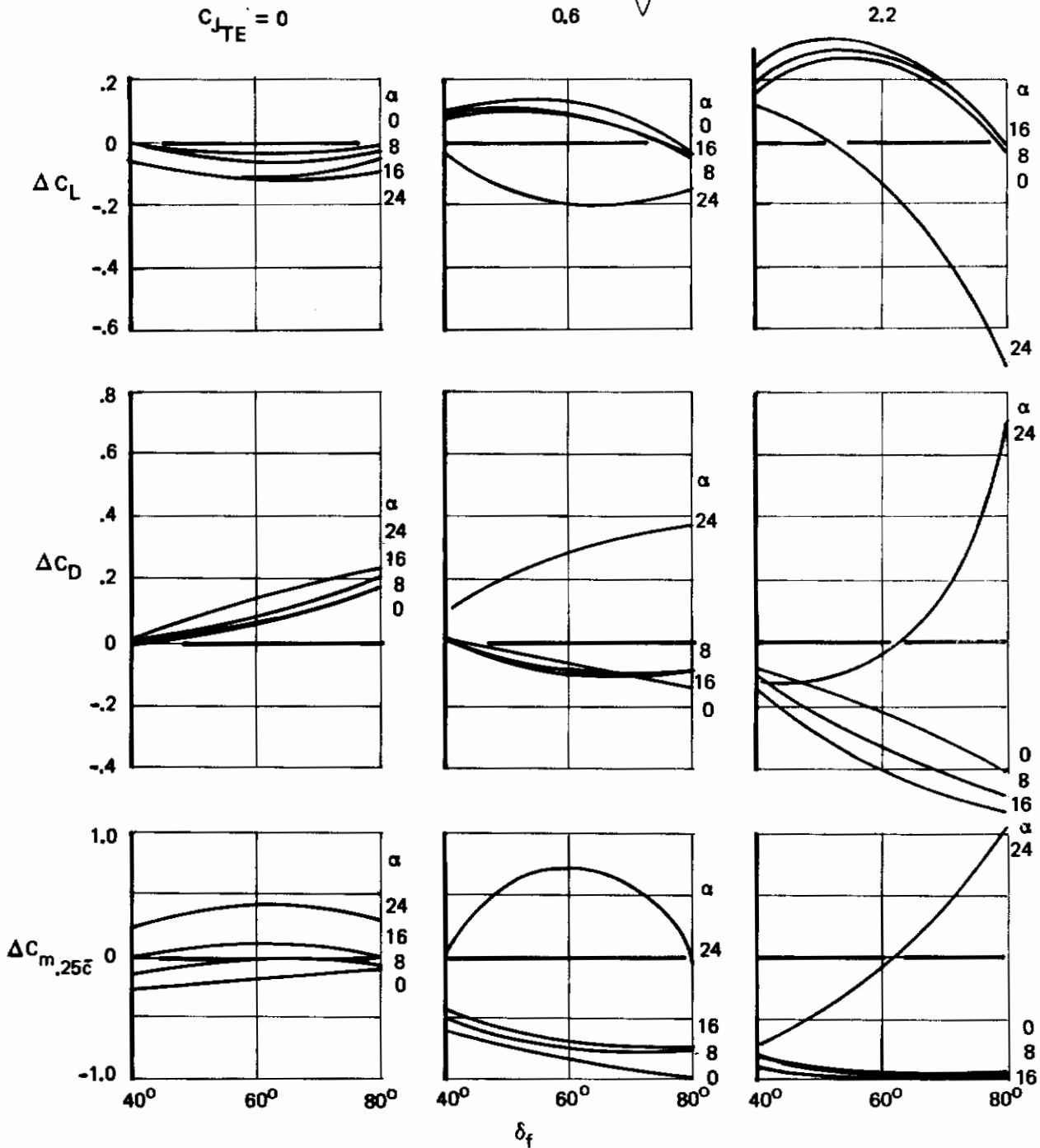
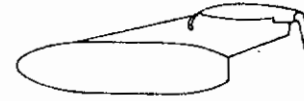
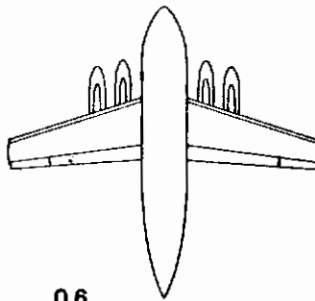
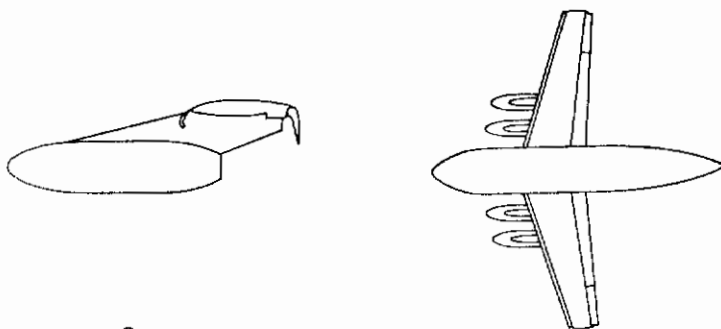


Figure 150: Effect of Jet Flap Angle and Thrust Coefficient on Residual Nacelle Thrust Coefficient ($C_{J_{Nac}} = 2.0$)

Contrails



Sweep $\Lambda = 15^\circ$ AR = 8
 NAC Spanwise Location % $\eta = 27/43.5$
 Height Below WDP = $h/\bar{c} = 0.406$
 Full Span Flaps
 Free Air

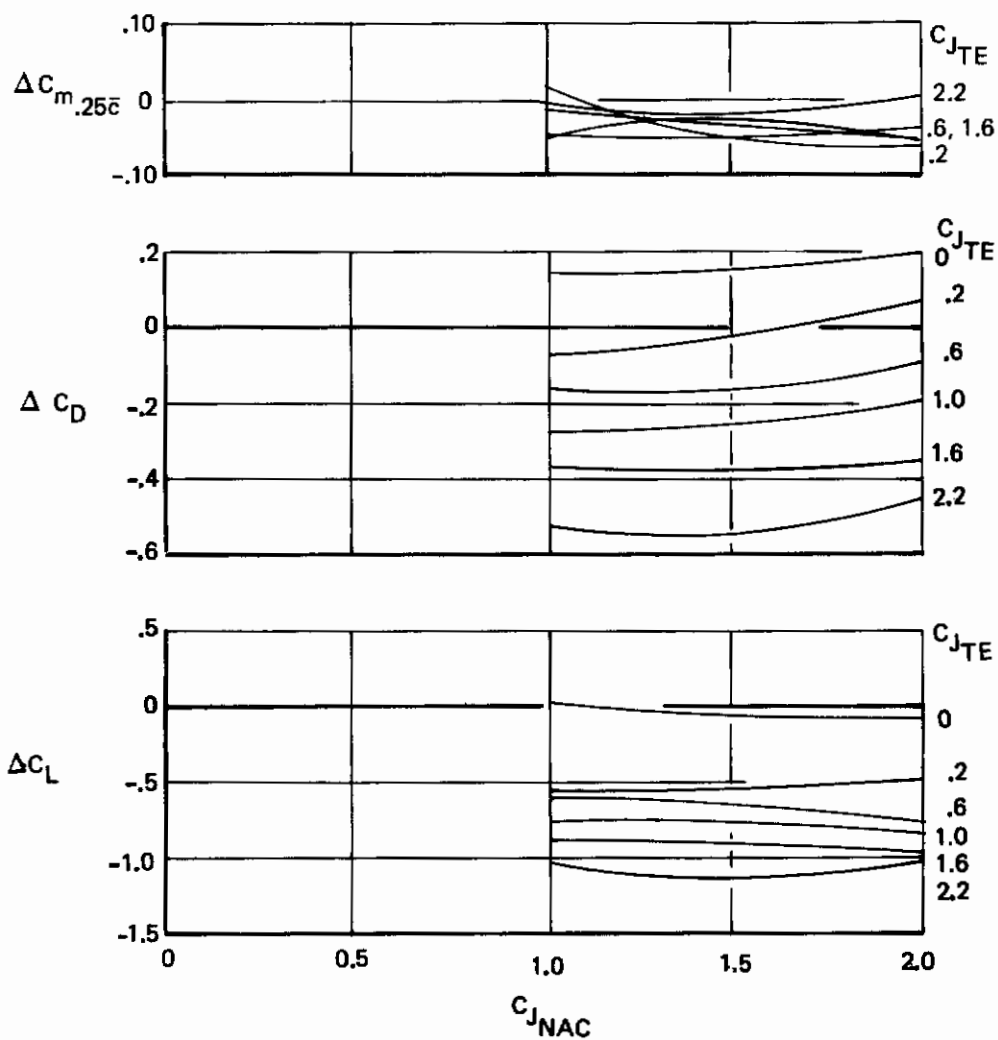


Figure 151: Effect of Residual Nacelle Thrust Level on Interference $\delta_f = 80^\circ$, $\alpha_w = 8^\circ$

the wing. This effect is shown in Figure 152 at zero angle of attack for the nacelle at ram pressure ratio and at $C_J = 1.6$. These data were determined using a moving belt ground plane. While the variation of aerodynamic coefficients with height follows the trend expected for ram pressure ratio, both lift and pitching moment are relatively unaffected by height above the ground plane for $C_{J_{NAC}} = 2.0$ and $\delta_f = 80^\circ$.

Residual nacelle thrust effects were also examined in ground proximity over an angle of attack range for jet flap deflection of 40° . Sting contact with the ground plane limited ground effect testing to a maximum angle of attack of 8° . A comparison of free air and ground effect interference for 40° flaps, Figure 153, shows that interference changes significantly between free air and ground effect. In fact, the drag interference changes sign.

5.3 Flow Survey

A limited amount of flow survey testing was done using a 17-tube rake. Figures 154 and 155 presented some downwash and sidewash data which represent effective angles that would be felt by the horizontal and vertical tails for typical tail location.

The downwash curves show that with no jet flap blowing the effect of nacelle thrust is to shift downwash by a small positive amount and to straighten the curve at higher angles of attack. With jet flap thrust coefficient of 2.2, the effect of residual nacelle thrust is to significantly reduce downwash angle. This is due to the large reduction in lift that results from the nacelle thrust interference.

Residual nacelle thrust has no effect on sidewash at the vertical tail. Jet flap blowing reduces the slope of σ versus β .

5.4 Augmentor Wing Jet Flap

The augmentor wing jet flap is a powered lift concept that was not included in the STAI wind tunnel studies. Boeing has been involved with this concept through its independent research, through a technical data interchange agreement with the deHavilland Company of Canada, and under NASA Contract NAS 2-6344 which included two-dimensional wind tunnel and static augmentor testing. In order to lend additional perspective to the jet flap as a candidate for STOL powered lift, a short summary of the augmentor wing is presented here.

A comparison between a pure jet flap and an augmentor wing jet flap on the same two-dimensional model is shown in Figure 156. The data indicate that the "pure" jet flap actually has a lower attachment C_J than the augmentor wing jet flap as indicated by the knee of the lift at $\alpha = -2^\circ$ versus C_J curve, but that the two are very similar at high C_J . The augmentor wing has higher $C_{l_{max}}$ above $C_J = 1.0$ and always has lower drag.

Contrails

$$\Lambda_{c/4} = 15^\circ$$

$$AR = 8$$

75% Span Flaps

$$C_{J_{TE}} = 1.6$$

— $C_{J_{NAC}} = \text{RAM}$

- - - $C_{J_{NAC}} = 2.0$

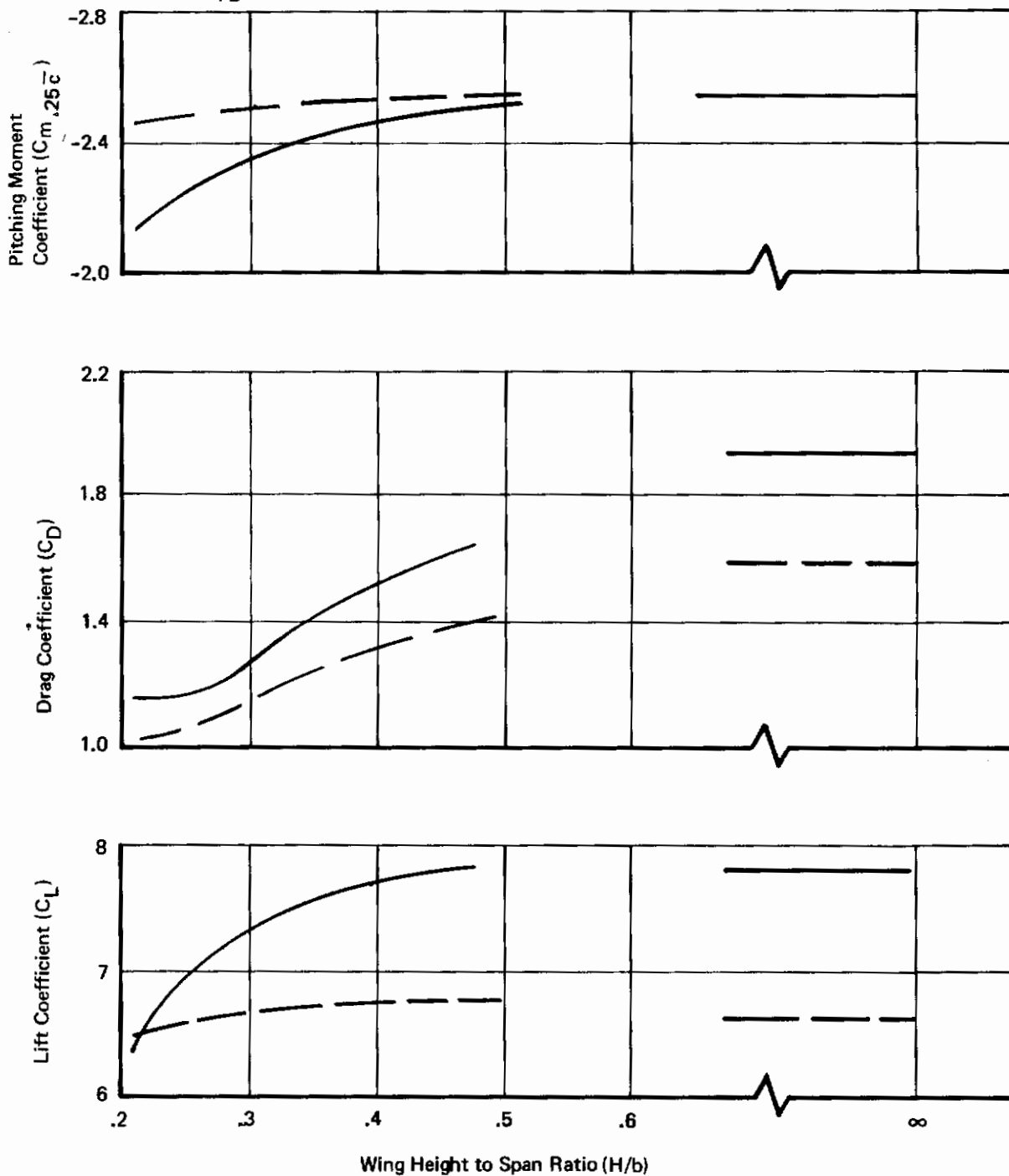
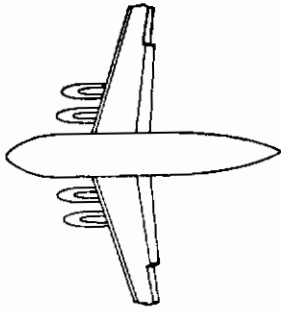


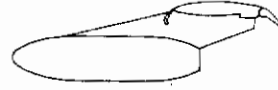
Figure 152: Ground Effect on Jet Flap Characteristics



$\Lambda_{c/4} = 15^\circ$

AR = 8

75% Span Flaps, $\delta_f = 40^\circ$



Nac Spanwise Location % $\eta = 27/43.5$

Height Below WDP (h/\bar{c}) = 0.406

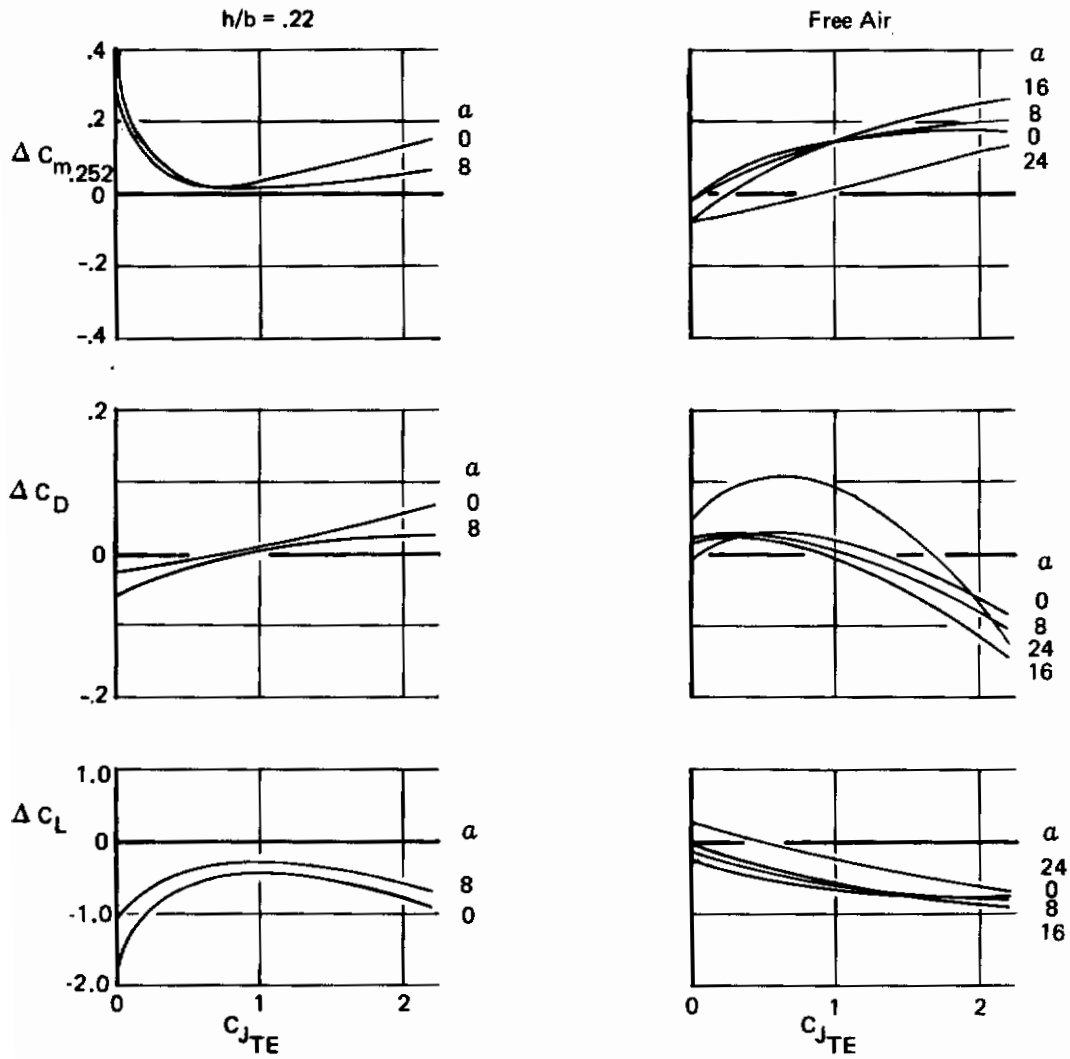


Figure 153: Effect of Ground Proximity on Residual Nacelle Thrust Interference Effects – $C_{J_{Nac.}} = 2.0$

Sweep $\Lambda c/4 = 15^\circ$ $AR = 8.0$
 NAC Spanwise Location $\% \eta = 27/43.5$
 Height Below WDP $= h/\bar{c} = 0.406$
 Full Span Flaps, $\delta_f = 80^\circ$
 $l_H/\bar{c} = 4.4$
 $Z_H/\bar{c} = 1.57$

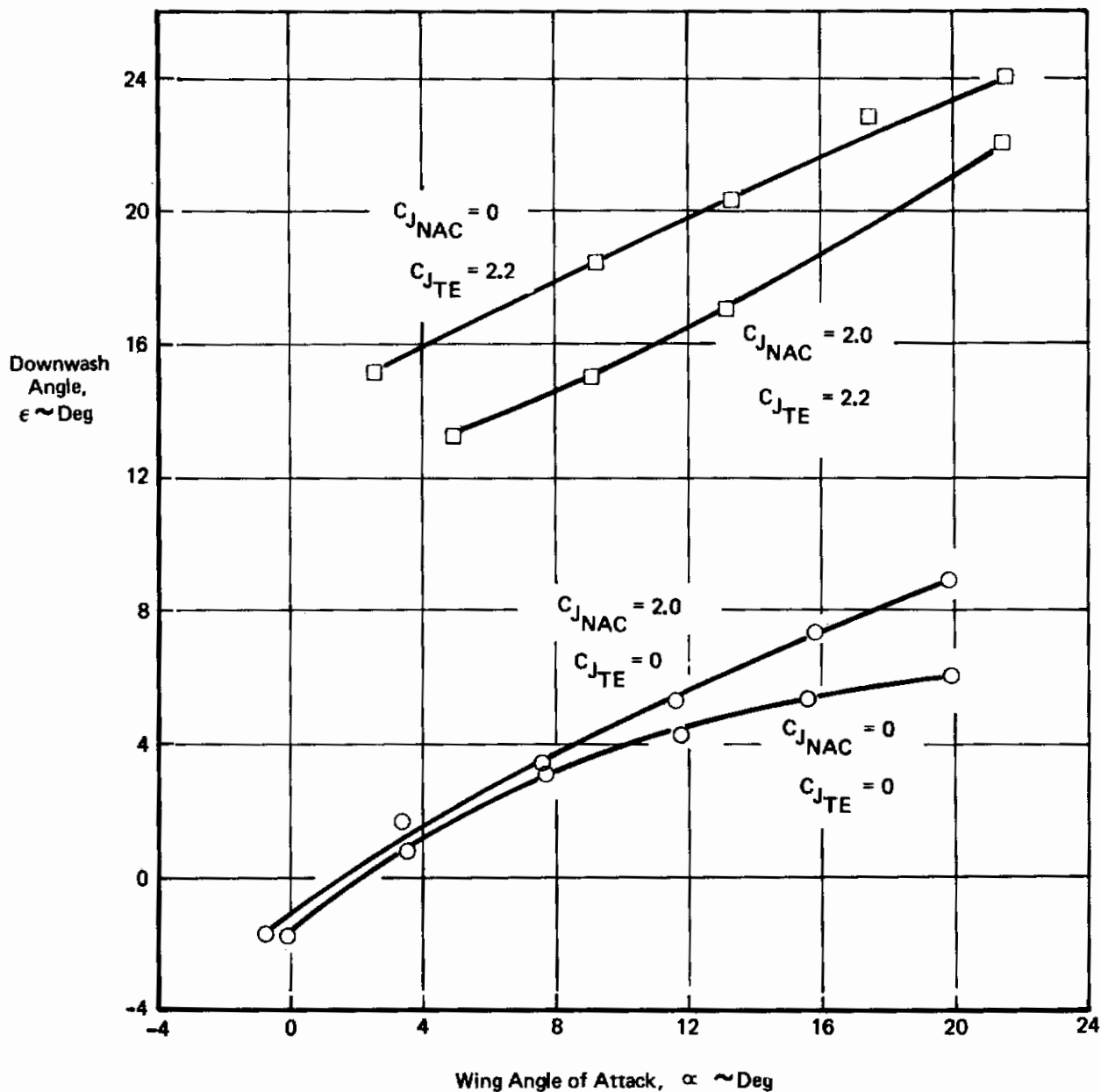


Figure 154: Effects of Power on Downwash – Free Air

Sweep 15° AR = 8.0
 NAC Spanwise Location % $\eta = 27/43.5$
 Height Below WDP = $h/\bar{c} = 0.406$
 Fullspan Flaps, $\delta_f = 80^\circ$
 Free Air
 $l_{V/\bar{c}} = 3.75$

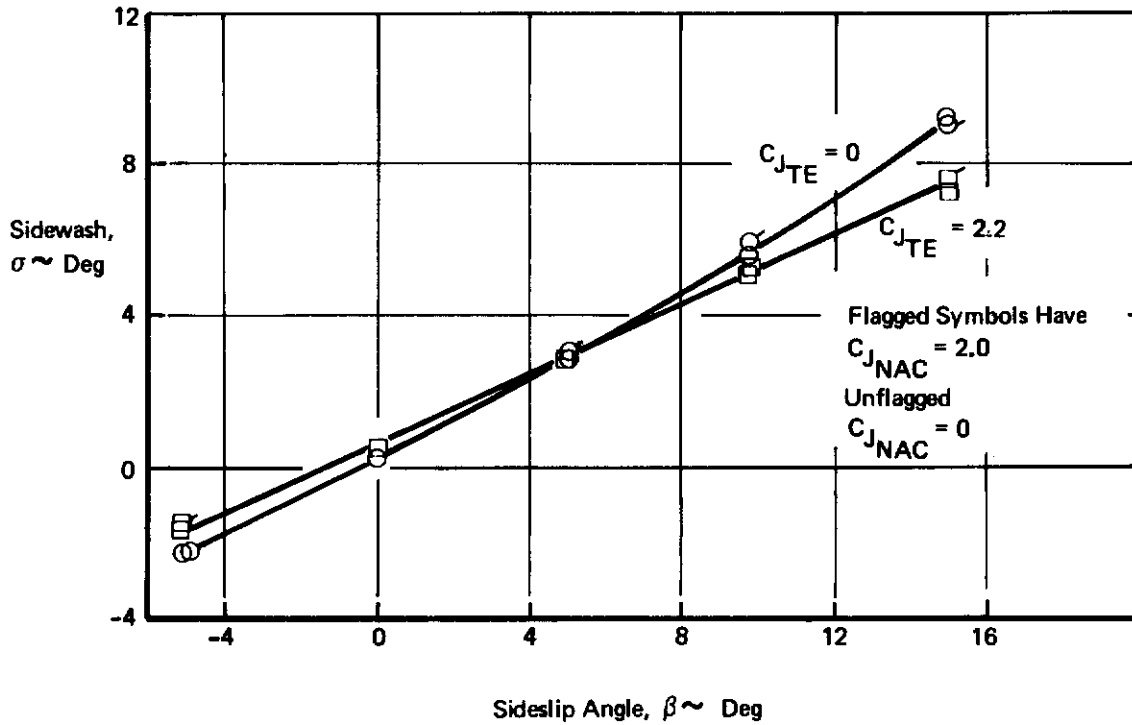


Figure 155: Effect of Sideslip Angle on Sidewash

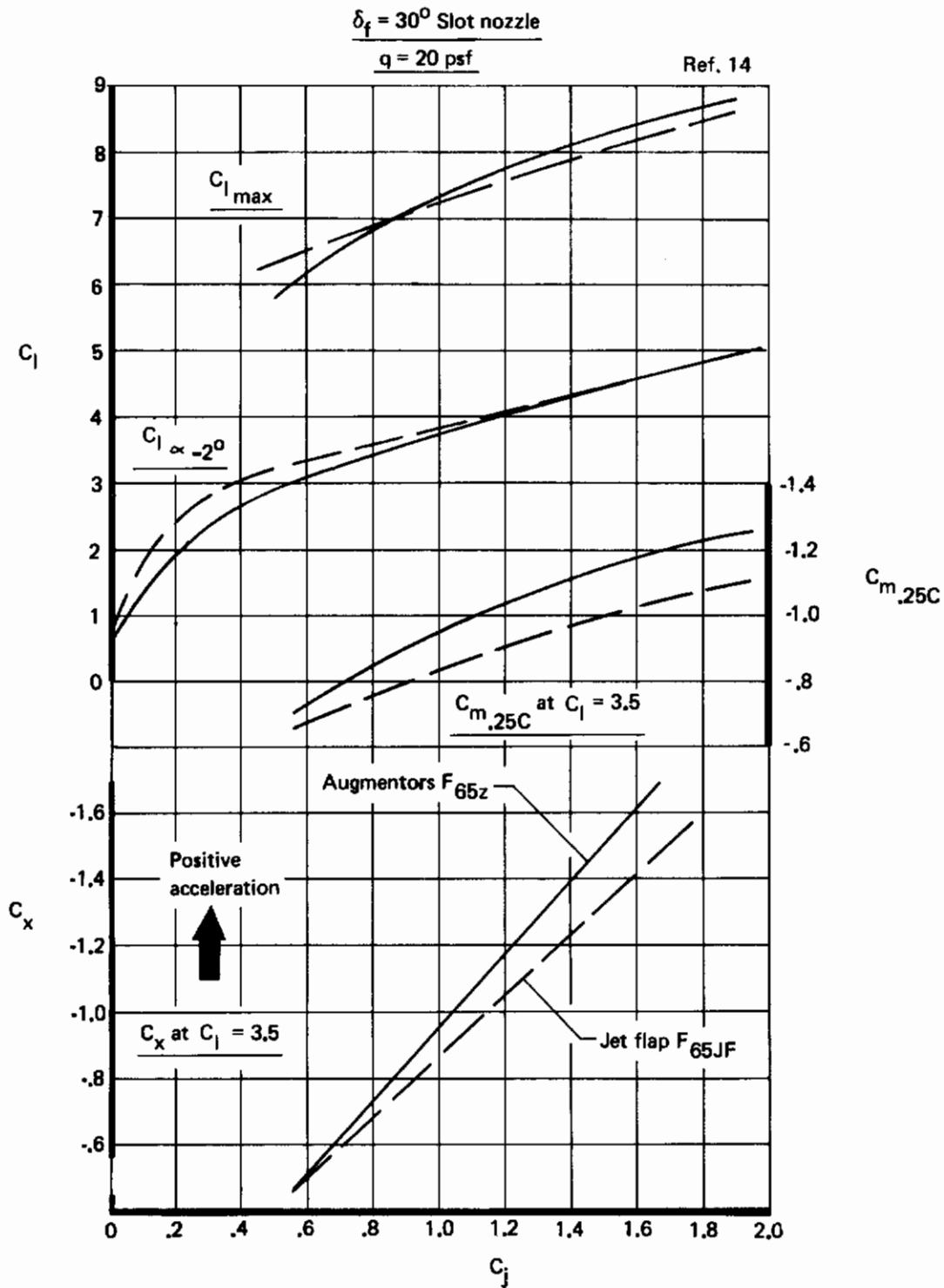


Figure 156: Comparison of Performance of Jet Flap and Augmentors at $q = 20$ psf

Contrails

A definition of geometry parameters for the augmentor wing is given in Figure 157. The aerodynamic performance of an augmentor flap is related to its static thrust augmentation characteristics. Statically the deflected augmentor flap is a curved ejector and the static thrust augmentation ratio is a function of the geometric parameters which govern the entrainment and mixing of the ejector flow. These include:

- o Throat area ratio (l_T/h_E)
- o Mixing length (C_f/h_E)
- o Diffuser angle
- o Inlet geometry
- o Location of primary nozzle exit
- o Primary nozzle geometry

Also, the aerodynamic performance of an augmentor wing at forward speed depends strongly upon avoiding flow separation from the shroud upper surface. Shroud flow separation tends to increase with flap deflection, angle of attack, and reduction of nozzle thrust coefficient. It also depends upon intake door angle and shroud and flap position.

The effects of some augmentor variables on static thrust augmentation is shown in Figure 159 .

Some typical two dimensional aerodynamic wind tunnel test data from NASA-sponsored Boeing tests are shown in Figures 160 and 161.

Boeing has also modified a deHavilland Buffalo into an augmentor wing configuration for the NASA. This airplane is now being flown for flight research purposes by the NASA Ames Research Center.

Enough flight testing has been done to get a preliminary indication if full scale performance can be predicted from wind tunnel data. The data obtained thus far, Figure 161, are very encouraging in that they lend confidence in the use of wind tunnel data and theoretical methods to predict full scale airplane characteristics.

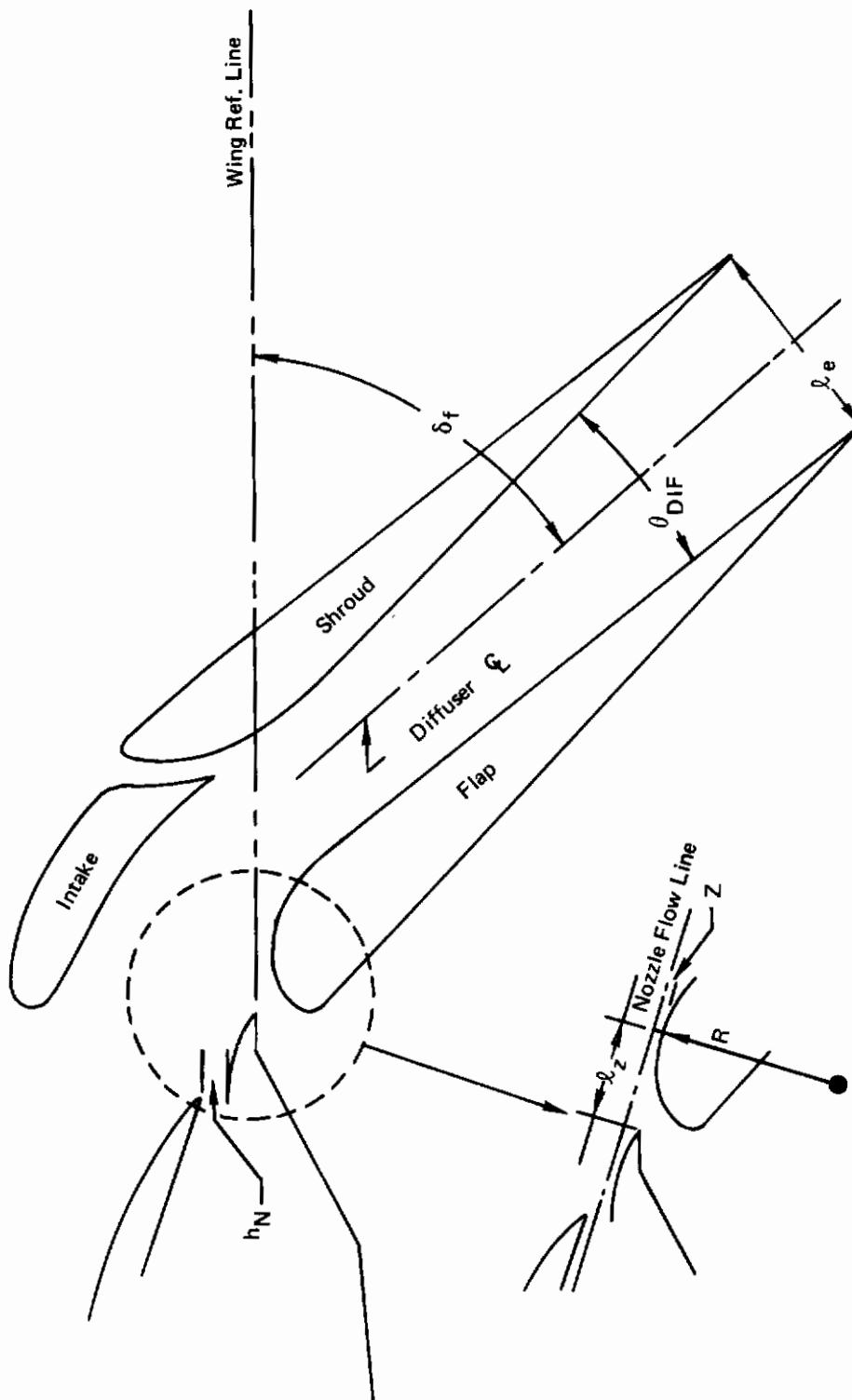


Figure 157 : Definition of Geometry Parameters

REF. 14

$C_f/C = .27$

$C_f/h_N = .50$

Slot nozzle

$\delta_f = 30^\circ$

NPR = 2.53

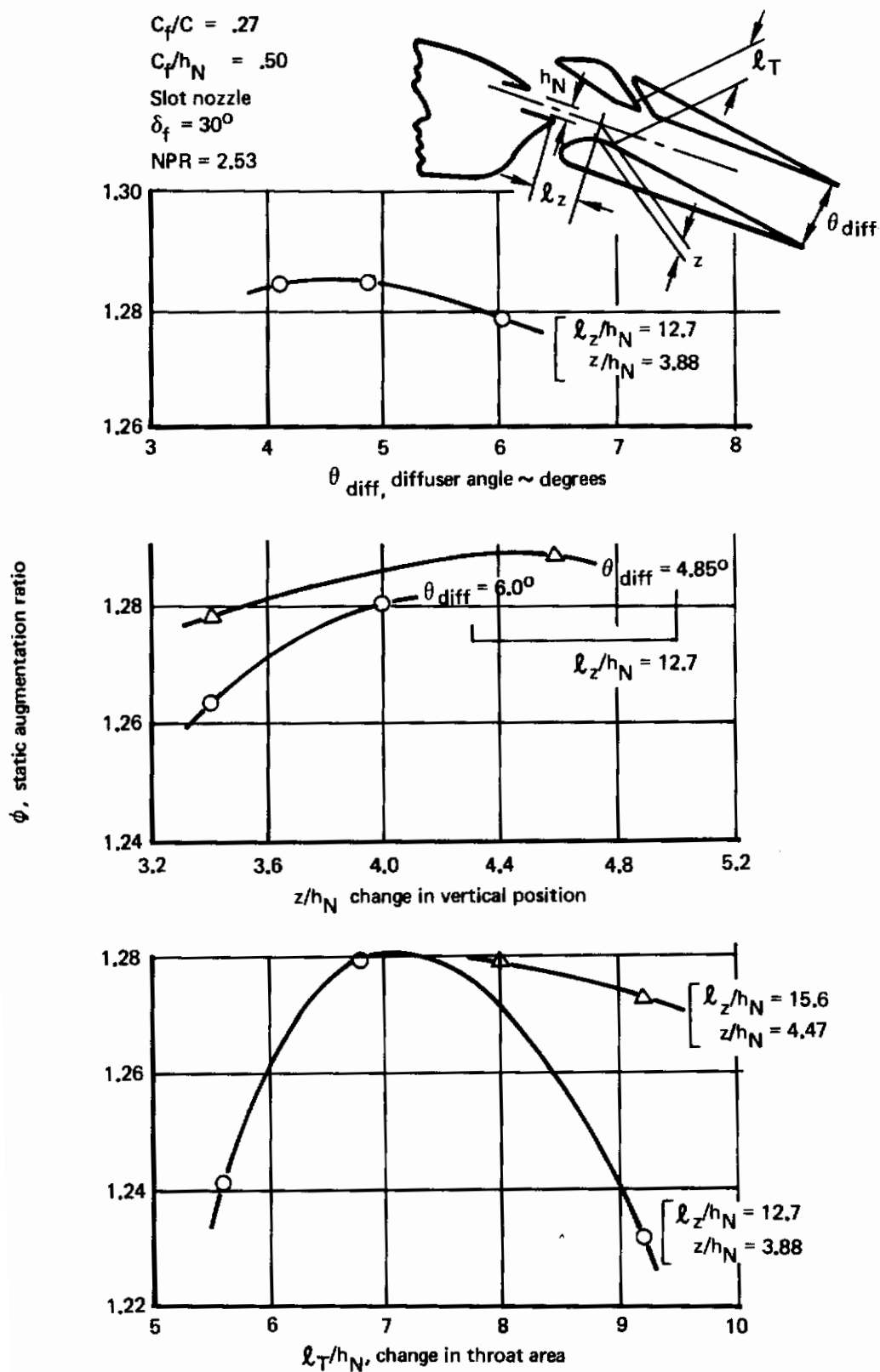


Figure 158: Effect of Augmentor flap Geometry on Static Thrust Augmentation Ratio

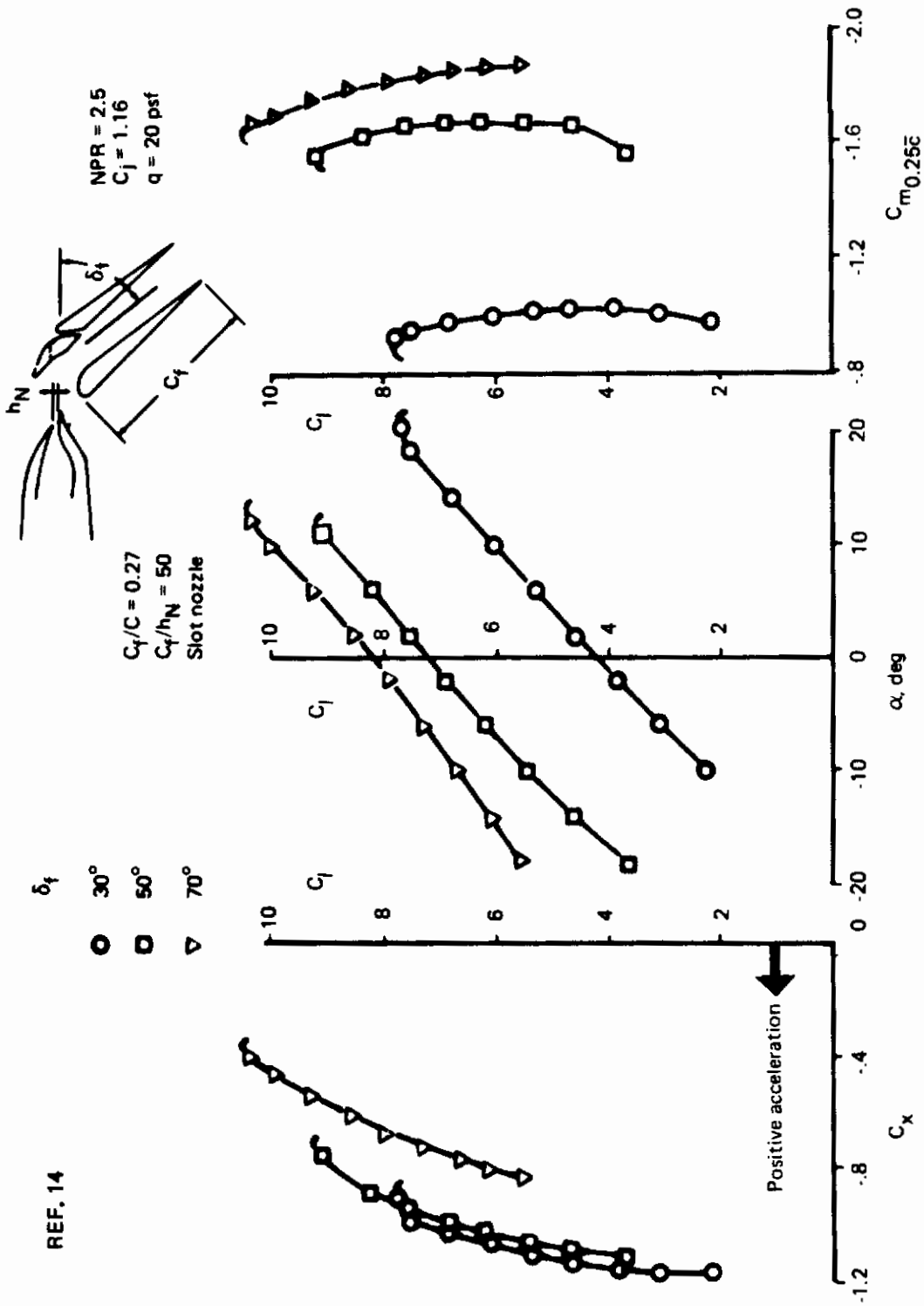


Figure 159: Representative 2-D Aerodynamic Data for the Augmentor Wing at $C_j = 1.16$

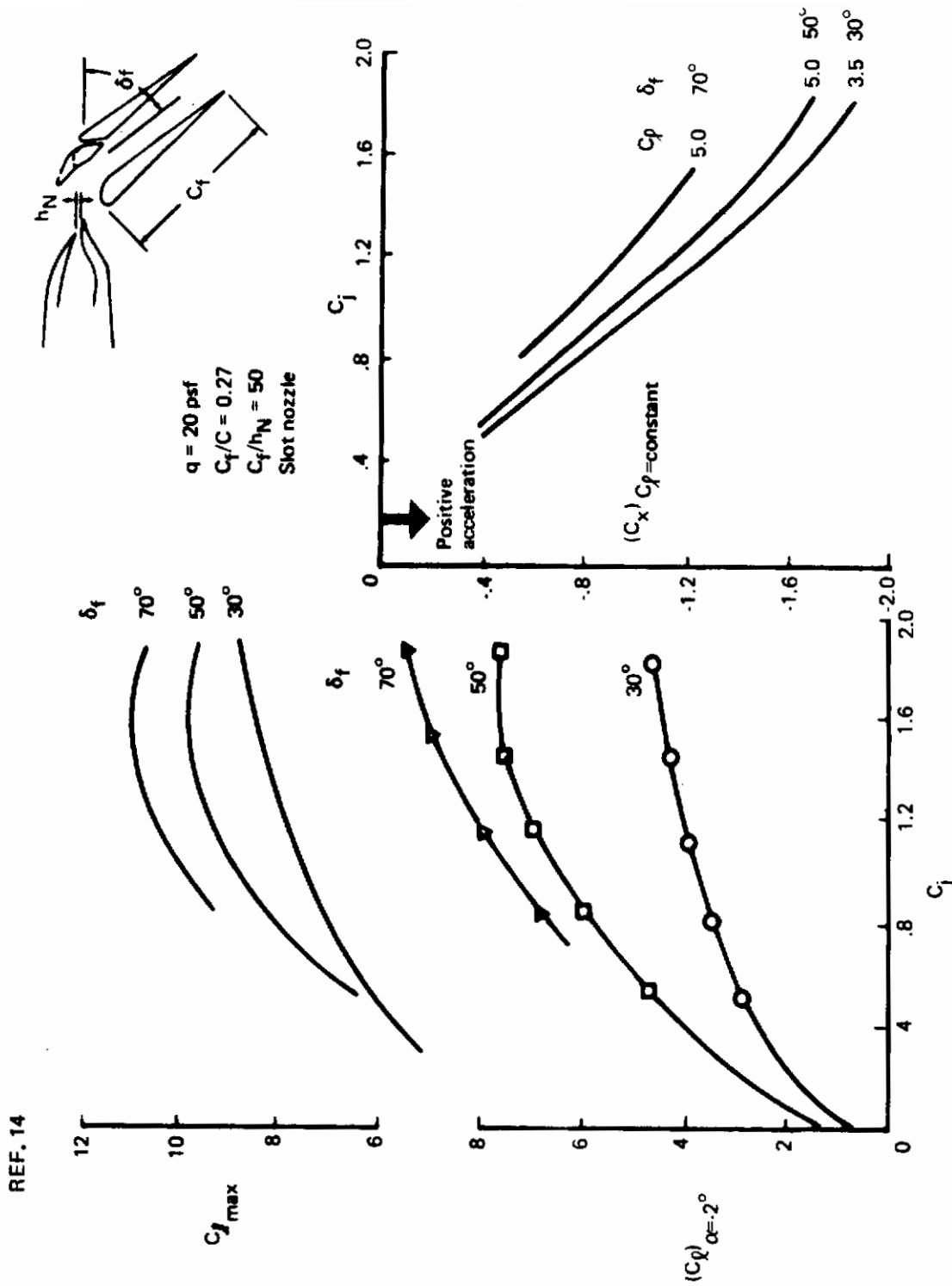


Figure 160: Variation of Lift and Streamwise Force with C_j for the Augmentor Wing

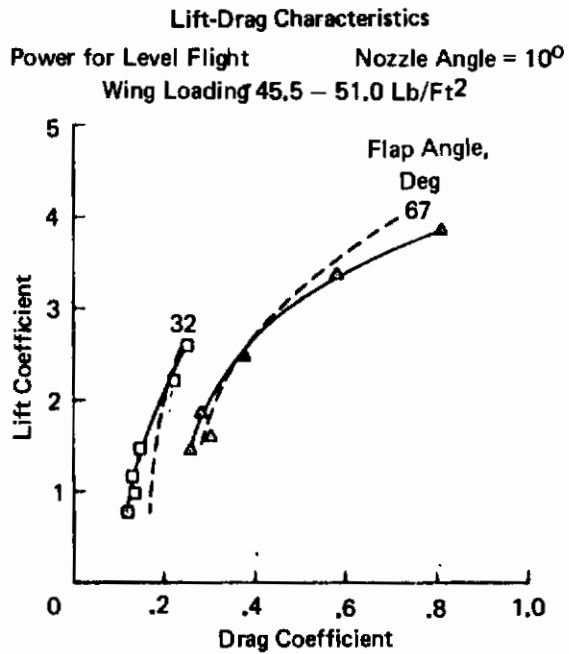
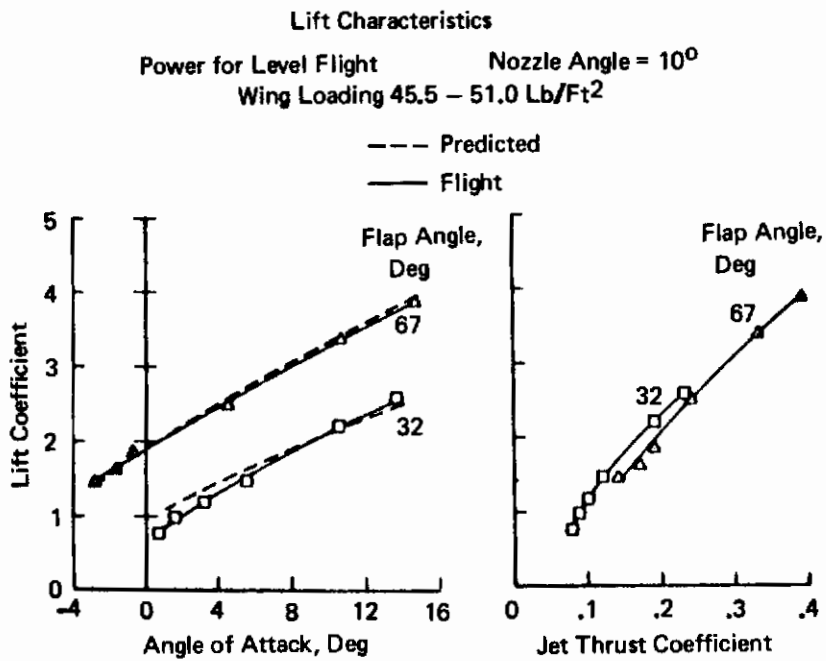


Figure 161: Predicted versus Flight Test Aerodynamic Characteristics for the NASA Program Augmentor Wing Buffalo

APPENDIX

DETAILED COMPONENT DESCRIPTIONS AND ORDINATES WING AND FLAP

<u>Description</u>	<u>Dwg. Ref. No.</u>
Wing Ordinates at WBL 8.427	1204-5
Wing Ordinates at WBL 23.175	1204-8
Wing Ordinates at WBL 48.998	1204-9
Wing Spanwise Thickness	1204 Model
Leading-Edge Krueger Flap Ordinates	1204-20
Aft Flap Ordinates at WBL 4.214	1204-34
Aft Flap Ordinates at WBL 8.427	1204-35
Aft Flap Ordinates at WBL 16.855	1204-36
Aft Flap Ordinates at WBL 23.175	1204-37
Aft Flap Ordinates at WBL 25.282	1204-38
Aft Flap Ordinates at WBL 48.998	1204-39
Main Flap Ordinates at WBL 4.214	1204-41
Main Flap Ordinates at WBL 8.427	1204-42
Main Flap Ordinates at WBL 16.855	1204-43
Main Flap Ordinates at WBL 23.175	1204-44
Main Flap Ordinates at WBL 25.282	1204-45
Main Flap Ordinates at WBL 48.998	1204-46
Fore Flap Ordinates at WBL 4.214	1204-47
Fore Flap Ordinates at WBL 8.427	1204-48
Fore Flap Ordinates at WBL 16.855	1204-49
Fore Flap Ordinates at WBL 23.175	1204-50
Fore Flap Ordinates at WBL 25.282	1204-51
Fore Flap Ordinates at WBL 48.998	1204-52
Flap Gap Settings Table ($\delta_f = 20, 30, 48, 55^\circ$)	1204-93
Flap Gap Settings Table ($\delta_f = 35^\circ$)	1204-236

Contrails

DWG. REF. NO. 1204-5

<u>% CHD .</u>	<u>STA. INS.</u>	<u>UPPER ORD.</u>	<u>LOWER ORD.</u>
0.00	0.000	0.000	0.000
.25	.033	.144	-.105
.50	.066	.209	-.141
.75	.099	.257	-.167
1.25	.166	.329	-.205
2.5	.331	.452	-.263
5.0	.662	.613	-.347
7.5	.993	.713	-.412
10.0	1.324	.788	-.470
12.5	1.655	.846	-.525
15.0	1.986	.895	-.574
20.0	2.649	.969	-.667
25.0	3.311	1.017	-.741
30.0	3.973	1.055	-.797
35.0	4.635	1.078	-.835
40.0	5.297	1.084	-.843
45.0	5.959	1.083	-.827
50.0	6.622	1.074	-.789
55.0	7.284	1.049	-.731
60.0	7.946	1.001	-.659
65.0	8.608	.924	-.579
70.0	9.270	.824	-.495
80.0	10.594	.572	-.315
90.0	11.919	.289	-.138
100.0	13.243	.005	-.005

WING ORDINATES AT WBL 8.427

Contours

DWG. REF. NO. 1204-8

<u>% CHD.</u>	<u>STA. INS.</u>	<u>UPPER ORD.</u>	<u>LOWER ORD.</u>
0.00	0.000	0.000	0.000
.25	.025	.101	-.071
.50	.050	.146	-.095
.75	.076	.180	-.113
1.25	.126	.231	-.137
2.5	.252	.319	-.175
5.0	.504	.433	-.230
7.5	.756	.503	-.274
10.0	1.008	.556	-.314
12.5	1.260	.596	-.351
15.0	1.512	.629	-.385
20.0	2.017	.680	-.450
25.0	2.521	.712	-.502
30.0	3.025	.738	-.542
35.0	3.529	.753	-.568
40.0	4.033	.758	-.573
45.0	4.537	.757	-.562
50.0	5.042	.752	-.535
55.0	5.546	.736	-.493
60.0	6.050	.704	-.443
65.0	6.554	.650	-.388
70.0	7.058	.581	-.330
80.0	8.066	.404	-.208
90.0	9.075	.205	-.089
100.0	10.083	.005	-.005

WING ORDINATES AT WBL 23.175

Contours

DWG. REF. NO. 1204-9

<u>% CHD.</u>	<u>STA. INS.</u>	<u>UPPER ORD.</u>	<u>LOWER ORD.</u>
0.00	0.000	0.000	0.000
0.25	.011	.045	-.032
0.50	.023	.066	-.043
0.75	.034	.081	-.051
1.25	.057	.104	-.062
2.5	.114	.144	-.079
5.0	.228	.195	-.104
7.5	.341	.227	-.124
10.0	.455	.251	-.141
12.5	.569	.269	-.159
15.0	.683	.284	-.174
20.0	.910	.307	-.203
25.0	1.138	.321	-.226
30.0	1.365	.333	-.244
35.0	1.593	.340	-.256
40.0	1.820	.342	-.259
45.0	2.048	.342	-.254
50.0	2.275	.339	-.241
55.0	2.503	.332	-.223
60.0	2.630	.318	-.200
65.0	2.958	.294	-.175
70.0	3.185	.262	-.149
80.0	3.640	.182	-.094
90.0	4.095	.092	-.040
100.0	4.550	.005	-.005

WING ORDINATES AT WBL 48.998

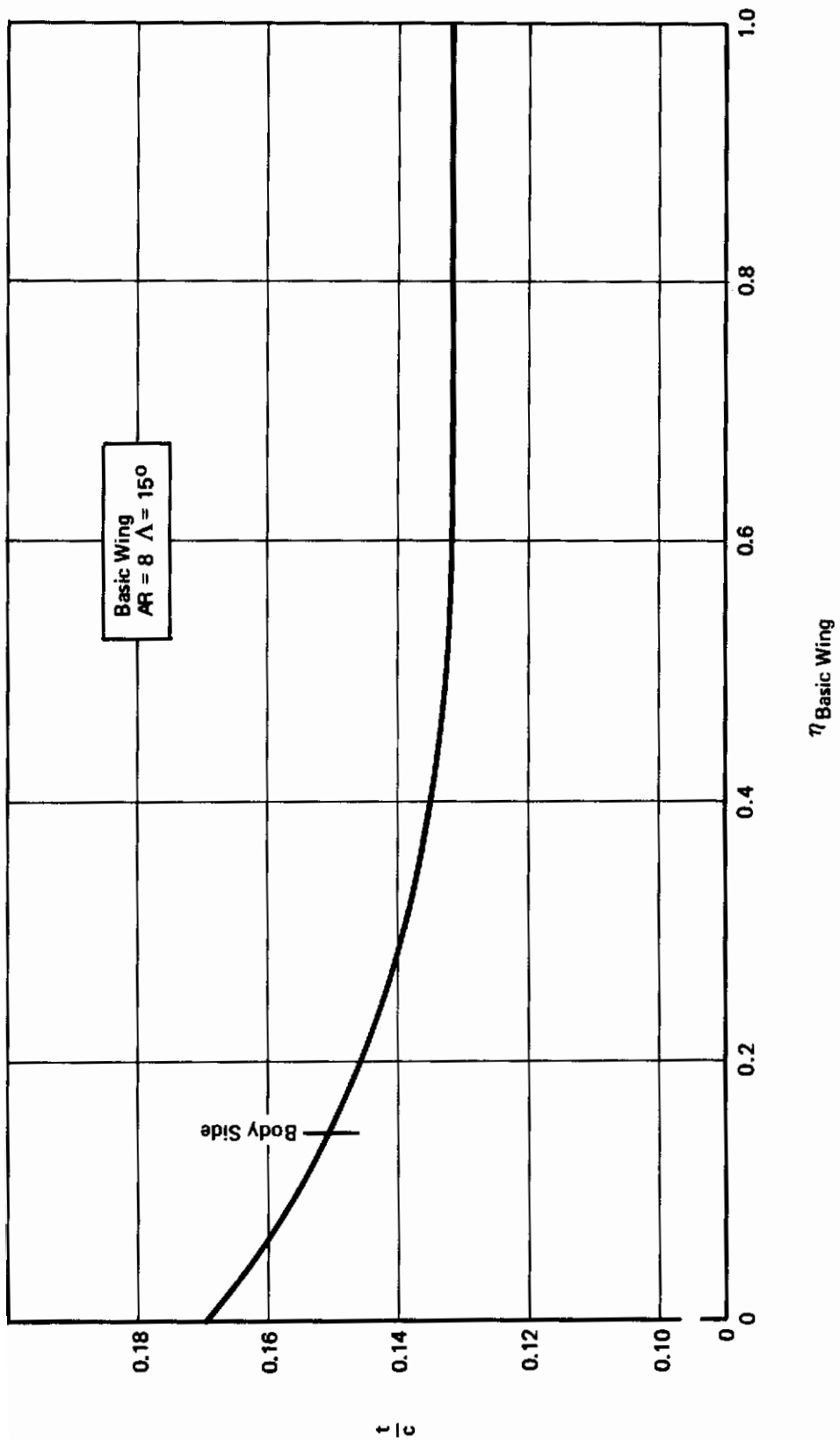


Figure 162: Wing Spanwise Thickness Distribution

Contours

DWG. REF. NO. 1204-20

<u>STA. INS.</u>	<u>UPPER ORD.</u>	<u>LOWER ORD.</u>
0.000	0.000	0.000
.007	.071	—
.011	—	-.068
.031	—	-.116
.042	.155	—
.067		-.159
.107	.235	—
.126	—	-.193
.184	—	-.193
.196	.298	—
.229	—	-.163
.290	.345	+.129
.390	.377	.189
.495	.396	.200
.605	.405	.200
.718	.403	.200
.866	.382	.200
1.024	.343	.200
1.179	.290	.194
1.314	.228	.168
1.436	.162	.124
1.547	.091	.071
1.600	.055	.040
1.677	0.0	-.010

LEADING-EDGE KRUEGER FLAP ORDINATES

Contours

DWG. REF. NO. 1204-34

<u>STA. INS.</u>	<u>UPPER ORD.</u>	<u>LOWER ORD.</u>
0.000	-.083	-.083
.014	-.033	-.128
.042	+.007	-.151
.071	+.033	-.159
.099	.056	-.163
.170	.103	-.159
.240	.134	-.159
.382	.179	-.159
.523	.196	-.159
.665	.196	-.159
.806	.186	-.159
.948	.166	-.159
1.089	.139	-.159
1.231	.108	-.159
1.372	.075	-.159
1.514	.041	-.159
1.655	.008	-.008

AFT FLAP ORDINATES AT WBL 4.214

Contrails

DWG. REF. NO. 1204-35 1204-35

<u>% CHD.</u>	<u>STA. INS.</u>	<u>UPPER ORD.</u>	<u>LOWER ORD.</u>
88.3	0.000	-.073	-.073
88.4	.013	-.029	-.112
88.6	.040	+.006	-.132
88.8	.066	.029	-.140
89.0	.093	.049	-.142
89.5	.159	.090	-.140
90.0	.225	.118	-.140
91.0	.358	.157	-.140
92.0	.490	.172	-.140
93.0	.622	.172	-.140
94.0	.755	.163	-.140
95.0	.887	.145	-.140
96.0	1.020	.122	-.140
97.0	1.152	.094	-.140
98.0	1.284	.065	-.140
99.0	1.417	.036	-.140
100.0	1.549	+.007	-.007

AFT FLAP ORDINATES AT WBL 8.427

Contrails

DWG. REF. NO. 1204-36

<u>% CHD.</u>	<u>STA. INS.</u>	<u>UPPER ORD.</u>	<u>LOWER ORD.</u>
88.3	0.000	-.058	-.058
88.4	.011	-.023	-.090
88.6	.034	+.005	-.106
88.8	.057	+.023	-.112
89.0	.080	.040	-.115
89.5	.137	.072	-.112
90.0	.194	.095	-.112
91.0	.309	.126	-.112
92.0	.423	.137	-.112
93.0	.538	.138	-.112
94.0	.652	.131	-.112
95.0	.766	.117	-.112
96.0	.881	.098	-.112
97.0	.995	.076	-.112
98.0	1.109	.053	-.112
99.0	1.224	.029	-.112
100.0	1.338	.006	-.006

AFT FLAP ORDINATES AT WBL 16.855

Contours

DWG. REF. NO. 1204-37

<u>% CHD.</u>	<u>STA. INS.</u>	<u>UPPER ORD.</u>	<u>LOWER ORD.</u>
88.3	0.000	-.050	-.050
88.4	.010	-.020	-.078
88.6	.030	+.004	-.092
88.8	.050	.020	-.097
89.0	.071	.034	-.099
89.5	.121	.062	-.097
90.0	.171	.082	-.097
91.0	.272	.109	-.097
92.0	.373	.119	-.097
93.0	.474	.119	-.097
94.0	.575	.113	-.097
95.0	.676	.101	-.097
96.0	.776	.085	-.097
97.0	.877	.066	-.097
98.0	.978	.045	-.097
99.0	1.079	.025	-.097
100.0	1.180	.005	-.005

AFT FLAP ORDINATES AT WBL 23.175

Contours

DWG. REF. NO. 1204-38

<u>% CHD</u>	<u>STA. INS.</u>	<u>UPPER ORD.</u>	<u>LOWER ORD.</u>
88.3	0.000	-.048	-.048
88.4	.010	-.019	-.074
88.6	.029	+.004	-.088
88.8	.048	.019	-.092
89.0	.067	.033	-.094
89.5	.116	.060	-.092
90.0	.164	.078	-.092
91.0	.260	.104	-.092
92.0	.356	.114	-.092
93.0	.453	.114	-.092
94.0	.549	.108	-.092
95.0	.645	.096	-.092
96.0	.742	.081	-.092
97.0	.838	.063	-.092
98.0	.934	.043	-.092
99.0	1.031	.024	-.092
100.0	1.127	.005	-.005

AFT FLAP ORDINATES AT WBL 25.282

Contrails

DWG. REF. NO. 1204-39

<u>% CHD.</u>	<u>STA. INS.</u>	<u>UPPER ORD.</u>	<u>LOWER ORD.</u>
88.3	0.000	-.023	-.023
88.4	.004	-.009	-.035
88.6	.014	+.002	-.041
88.8	.023	.009	-.044
89.0	.032	.015	-.045
89.5	.055	.028	-.044
90.0	.077	.037	-.044
91.0	.123	.049	-.044
92.0	.168	.054	-.044
93.0	.214	.054	-.044
94.0	.259	.051	-.044
95.0	.305	.046	-.044
96.0	.350	.038	-.044
97.0	.396	.030	-.044
98.0	.441	.020	-.044
99.0	.487	.011	-.044
100.0	.532	+.002	-.002

AFT FLAP ORDINATES AT WBL 48.998

Contrails

DWG. REF. NO. 1204-41

<u>% CHD.</u>	<u>STA. INS.</u>	<u>UPPER ORD.</u>	<u>LOWER ORD.</u>
70.88	-.003	-.365	-.365
71.0	0.000	-.325	-.398
71.1	.014	-.249	-.432
71.3	.042	-.166	-.467
71.5	.071	-.106	-.485
71.8	.113	-.033	-.498
72.0	.141	+.007	-.500
73.0	.283	.172	-.482
74.0	.424	.292	-.482
75.0	.566	.378	-.482
76.0	.707	.448	-.482
77.0	.849	.502	-.482
78.0	.990	.538	-.482
79.0	1.132	.551	-.482
80.0	1.273	.554	-.482
81.0	1.415	.551	-.482
83.0	1.698	.521	-.482
85.0	1.980	.481	-.241
86.0	2.122	.458	-.216
87.0	2.263	.432	-.173
88.0	2.405	.402	-.083
89.0	2.546	.370	+.056
90.0	2.688	.339	.136
91.0	2.829	.305	.179
92.0	2.971	.272	.199
93.0	3.112	.239	.196
94.4	3.310	+.194	+.179

MAIN FLAP ORDINATES AT WBL 4.214

Contrails

DWG REF NO 1204-42

<u>% CHD.</u>	<u>STA. INS.</u>	<u>UPPER ORD.</u>	<u>LOWER ORD.</u>
70.88	-.003	-.320	-.320
71.0	0.000	-.272	-.349
71.1	+.013	-.218	-.378
71.3	.040	-.145	-.407
71.5	.066	-.093	-.425
71.8	.106	-.029	-.436
72.0	.132	+.006	-.439
73.0	.265	.151	-.422
74.0	.397	.256	-.422
75.0	.530	.332	-.422
76.0	.662	.393	-.422
77.0	.794	.436	-.422
78.0	.927	.471	-.422
79.0	1.059	.483	-.422
80.0	1.192	.486	-.422
81.0	1.324	.483	-.422
84.0	1.589	.457	-.422
85.0	1.854	.422	-.211
86.0	1.986	.401	-.189
87.0	2.119	.378	-.151
88.0	2.251	.352	-.073
89.0	2.384	.324	+.049
90.0	2.516	.297	.119
91.0	2.649	.268	.157
92.0	2.781	.238	.174
93.0	2.913	.209	.171
94.4	3.099	.170	.157

MAIN FLAP ORDINATES AT WBL 8.427

Contrails

DWG REF NO 1204-43

<u>% CHD.</u>	<u>STA. INS.</u>	<u>UPPER ORD.</u>	<u>LOWER ORD.</u>
70.98	-.002	-.257	-.257
71.0	+0.000	-.235	-.275
71.1	.011	-.176	-.304
71.3	.034	-.117	-.328
71.5	.057	-.070	-.342
71.8	.091	-.020	-.351
72.0	.114	+.005	-.353
73.0	.229	.122	-.339
74.0	.343	.206	-.339
75.0	.457	.270	-.339
76.0	.572	.316	-.339
77.0	.686	.351	-.339
78.0	.800	.375	-.339
79.0	.915	.388	-.339
80.0	1.029	.391	-.339
81.0	1.144	.388	-.339
83.0	1.372	.367	-.339
85.0	1.601	.339	-.170
86.0	1.716	.323	-.152
87.0	1.830	.304	-.122
88.0	1.944	.283	-.058
89.0	2.059	.261	+.040
90.0	2.173	.239	.096
91.0	2.287	.215	.126
92.0	2.402	.192	.140
93.0	2.516	.168	.138
94.4	+2.676	+.137	+.126

MAIN FLAP ORDINATES AT WBL 16.855

Contrails

DWG REF NO 1204-44

<u>% CHD.</u>	<u>STA. INS.</u>	<u>UPPER ORD.</u>	<u>LOWER ORD.</u>
70.98	-.002	-.222	-.222
71.0	0.00	-.188	-.242
71.1	0.000	-.151	-.262
71.3	.030	-.101	-.282
71.5	.050	-.064	-.294
71.8	.081	-.020	-.302
72.0	.101	+.004	-.304
73.0	.202	.105	-.292
74.0	.302	.177	-.292
75.0	.403	.232	-.292
76.0	.504	.272	-.292
77.0	.605	.302	-.292
78.0	.706	.325	-.292
79.0	.807	.335	-.292
80.0	.907	.337	-.292
81.0	1.008	.335	-.292
83.0	1.210	.317	-.292
85.0	1.412	.292	-.146
86.0	1.512	.278	-.131
87.0	1.613	.262	-.105
88.0	1.714	.244	-.050
89.0	1.815	.225	+.034
90.0	1.916	.206	.083
91.0	2.017	.186	.109
92.0	2.117	.165	.121
93.0	2.218	.145	.119
94.4	2.359	+.119	.109

MAIN FLAP ORDINATES AT WBL 23.175

Contrails

DWG REF NO 1204-45

<u>% CHD.</u>	<u>STA. INS.</u>	<u>UPPER ORD.</u>	<u>LOWER ORD.</u>
70.98	-.002	-.212	-.212
71.0	0.000	-.180	-.231
71.1	.010	-.144	-.250
71.3	.029	-.096	-.270
71.5	.048	-.062	-.281
71.8	.077	-.019	-.289
72.0	.096	+.004	-.291
73.0	.193	.100	-.279
74.0	.289	.170	-.279
75.0	.385	.220	-.279
76.0	.482	.260	-.279
77.0	.578	.289	-.279
78.0	.674	.310	-.279
79.0	.770	.320	-.279
80.0	.867	.322	-.279
81.0	.963	.320	-.279
83.0	1.156	.302	-.279
85.0	1.348	.279	-.140
86.0	1.445	.266	-.125
87.0	1.541	.250	-.100
88.0	1.637	.233	-.048
89.0	1.734	.215	+.033
90.0	1.830	.196	+.079
91.0	1.926	.177	+.104
92.0	2.023	.158	+.116
93.0	2.119	.139	+.114
94.4	2.254	+.113	+.104

MAIN FLAP ORDINATES AT WBL 25.282

Contours

DWG REF NO 1204-46

<u>% CHD.</u>	<u>STA. INS.</u>	<u>UPPER ORD.</u>	<u>LOWER ORD.</u>
70.98	-.001	-.100	-.100
71.0	0.000	-.085	-.109
71.1	.005	-.068	-.118
71.3	.014	-.046	-.127
71.5	.023	-.029	-.133
71.8	.036	-.009	-.136
72.0	.046	+.002	-.137
73.0	.091	.047	-.132
74.0	.137	.080	-.132
75.0	.182	.104	-.132
76.0	.228	.123	-.132
77.0	.273	.136	-.132
78.0	.318	.147	-.132
79.0	.364	.151	-.132
80.0	.410	.152	-.132
81.0	.455	.151	-.132
83.0	.546	.143	-.132
85.0	.637	.132	-.066
86.0	.682	.126	-.059
87.0	.728	.118	-.047
88.0	.774	.118	-.023
89.0	.819	.118	+.015
90.0	.864	.118	+.037
91.0	.910	.118	+.049
92.0	.956	.118	+.055
93.0	1.001	.118	+.054
94.4	1.065	+.059	+.049

MAIN FLAP ORDINATES AT WBL 48.998

Contrails

DWG REF NO 1204-47

<u>% CHD.</u>	<u>STA. INS.</u>	<u>UPPER ORD.</u>	<u>LOWER ORD.</u>
68.4	0.000	-.365	-.365
68.6	.028	-.216	-.501
68.8	.057	-.149	-.536
69.0	.085	-.100	-.551
69.3	.127	-.042	-.558
69.6	.170	+.010	-.548
70.0	.226	.066	-.508
70.5	.297	.133	-.418
71.0	.368	.188	-.276
72.0	.509	.279	+.007
73.0	.651	.345	.174
74.0	.792	.398	.294
75.0	.934	.441	.380
76.0	1.075	.478	.450
76.7	1.174	+.501	+.485

(FLAP CHECK ORDINATES)

0.000	-.0825	-.0825
.130	+.130	-.196
.680	.292	+.059
1.520	.075	.062

FORE FLAP ORDINATES AT WBL 4.214

Contrails

DWG REF NO 1204-48

<u>% CHD.</u>	<u>STA. INS.</u>	<u>UPPER ORD.</u>	<u>LOWER ORD.</u>
68.4	0.000	-.320	-.320
68.6	.026	-.189	-.439
68.8	.053	-.131	-.470
69.0	.079	-.089	-.483
69.3	.119	-.036	-.487
69.6	.159	+.009	-.480
70.0	.212	.058	-.445
70.5	.278	.116	-.366
71.0	.344	.164	-.241
72.0	.477	.244	+.006
73.0	.609	.302	.153
74.0	.742	.349	.257
75.0	.874	.387	.333
76.0	1.006	.419	.394
76.7	1.099	.439	.425

(FLAP CHECK ORDINATES)

0.000	-.044	-.044
.125	+.154	-.146
.580	+.264	+.044
1.385	+.036	+.023

FORE FLAP ORDINATES AT WBL 8.427

Contrails

DWG REF NO 1204-49

<u>% CHD.</u>	<u>STA. INS.</u>	<u>UPPER ORD.</u>	<u>LOWER ORD.</u>
68.4	0.000	-.257	-.257
68.6	.023	-.152	-.353
68.8	.046	-.105	-.378
69.0	.069	-.070	-.388
69.3	.103	-.028	-.393
69.6	.137	+.007	-.386
70.0	.183	.048	-.358
70.5	.240	.094	-.295
71.0	.297	.132	-.194
72.0	.412	.196	+.008
73.0	.526	.243	.122
74.0	.640	.281	.207
75.0	.755	.311	.271
76.0	.869	.337	.317
76.7	.949	.353	.342

(FLAP CHECK ORDINATES)

0.000	-.013	-.013
.109	+.150	-.104
.260	.208	-.068
.423	.224	+.018
.760	.174	.079
1.161	.011	0.00

FORE FLAP ORDINATES AT WBL 16.855

Contrails

DWG REF NO 1204-50

<u>% CHD.</u>	<u>STA. INS.</u>	<u>UPPER ORD.</u>	<u>LOWER ORD.</u>
68.4	0.000	-.222	-.222
68.6	.020	-.131	-.304
68.8	.040	-.091	-.326
69.0	.060	-.060	-.335
69.3	.091	-.024	-.339
69.6	.121	+.006	-.333
70.0	.161	.041	-.308
70.5	.212	.081	-.254
71.0	.262	.114	-.167
72.0	.363	.169	+.007
73.0	.464	.210	.105
74.0	.565	.242	.178
75.0	.665	.268	.231
76.0	.766	.291	.273
76.7	.837	.306	.295

(FLAP CHECK ORDINATES)

0.000	0.000	0.000
.12	.148	-.087
.25	.188	-.047
.357	.195	+.011
.700	.137	+.066
1.170	+.006	-.005

FORE FLAP ORDINATES AT WBL 23.175

Contrails

DWG REF NO 1204-52

<u>% CHD.</u>	<u>STA. INS.</u>	<u>UPPER ORD.</u>	<u>LOWER ORD.</u>
68.4	0.000	-.100	-.100
68.6	.009	-.059	-.137
68.8	.018	-.041	-.147
69.0	.027	-.027	-.151
69.3	.041	-.011	-.153
69.6	.055	+.003	-.150
70.0	.073	.019	-.139
70.5	.096	.036	-.115
71.0	.118	.051	-.076
72.0	.164	.076	+.003
73.0	.209	.095	.047
74.0	.255	.113	.081
75.0	.300	.127	.105
76.0	.346	.138	.124
76.7	.378	.143	.133

(FLAP CHECK ORDINATES)

0.000	-.02	-.02
.078	+.077	-.035
.155	.090	+.002
.300	.069	+.030
.462	.009	-.003

FORE FLAP ORDINATES AT WBL 48.998

Contracts

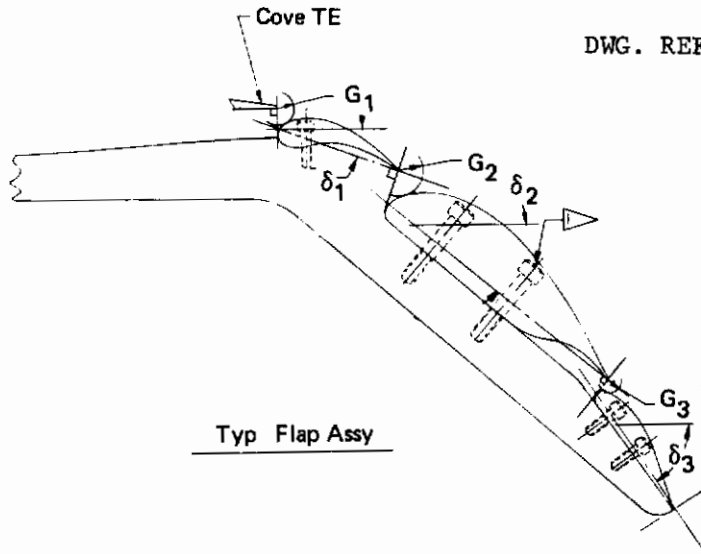
DWG REF NO 1204-51

<u>% CHD.</u>	<u>STA. INS.</u>	<u>UPPER ORD.</u>	<u>LOWER ORD.</u>
68.4	0.000	-.212	-.212
68.6	.019	-.125	-.291
68.8	.038	-.087	-.311
69.0	.058	-.058	-.320
69.3	.087	-.023	-.324
69.6	.116	+.006	-.318
70.0	.154	.039	-.295
70.5	.202	.077	-.243
71.0	.250	.109	-.160
72.0	.347	.162	+.007
73.0	.443	.200	.100
74.0	.539	.231	.171
75.0	.636	.256	.221
76.0	.732	.277	.261
76.7	.799	.291	.281

(FLAP CHECK ORDINATES)

0.000	-.009	-.009
.115	+.143	-.083
.340	+.187	+.011
.550	+.164	+.062
.760	+.098	+.052
.969	+.006	-.006

FORE FLAP ORDINATES AT WBL 25.282



<u>FORE FLAP</u>		<u>MAIN FLAP</u>		<u>AFT FLAP</u>		<u>LOCATION WBL *</u>
δ_1	G_1	δ_2	G_2	δ_3	G_3	
5°	.261	20°	.394	30°		9.000
10°	.219	30°	.328	40°	.132	
20°	.184	48°	.276	60°		
22°	.157	55°	.236	70°		
5°	.234	20°	.351	30°		15.700
10°	.195	30°	.292	40°	.117	
20°	.164	48°	.246	60°		
22°	.140	55°	.210	70°		
5°	.205	20°	.308	30°		22.300
10°	.172	30°	.257	40°	.103	
20°	.145	48°	.216	60°		
22°	.123	55°	.185	70°		
5°	.187	20°	.280	30°		26.700
10°	.156	30°	.233	40°	.093	
20°	.131	48°	.196	60°		
22°	.112	55°	.168	70°		
5°	.171	20°	.257	30°		30.300
10°	.143	30°	.214	40°	.086	
20°	.120	48°	.180	60°		
22°	.103	55°	.154	70°		

FLAP GAP SETTINGS

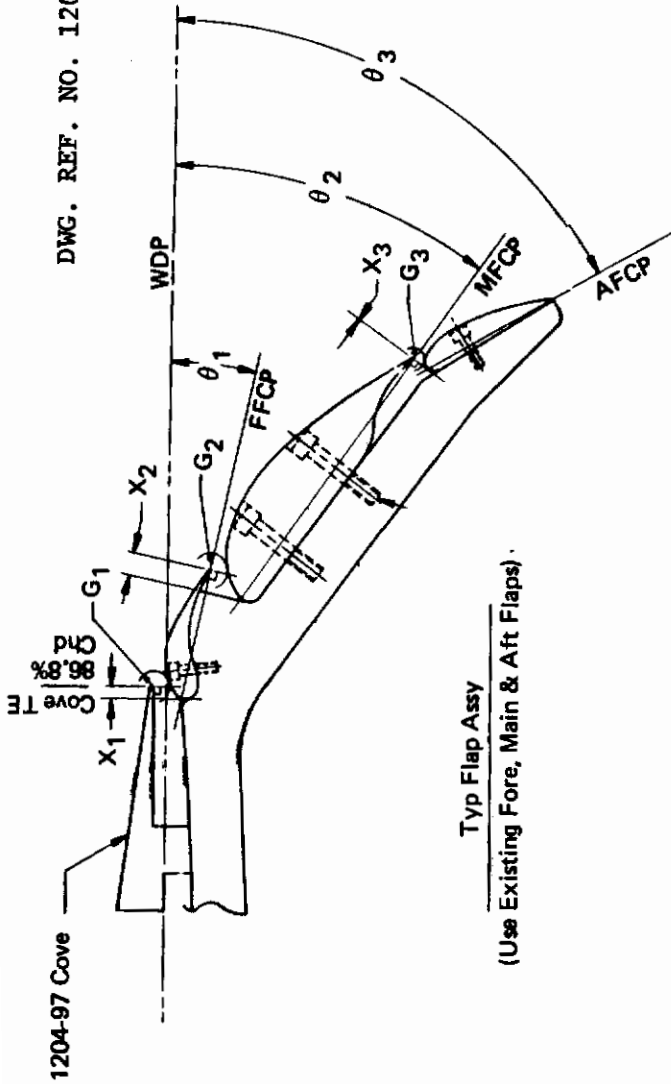
Contrails

FORE FLAP		MAIN FLAP		AFT FLAP		LOCATION
δ_1	G ₁	δ_2	G ₂	δ_3	G ₃	WBL
						*
5°	.162	20°	.243	30°		
10°	.135	30°	.203	40°	.081	32.400
20°	.113	48°	.170	60°		
22°	.097	55°	.146	70°		
5°	.150	20°	.225	30°		
10°	.125	30°	.188	40°	.075	35.200
20°	.105	48°	.158	60°		
22°	.090	55°	.135	70°		
5°	.141	20°	.212	30°		
10°	.117	30°	.176	40°	.071	37.300
20°	.099	48°	.148	60°		
22°	.085	55°	.127	70°		
5°	.126	20°	.189	30°		
10°	.105	30°	.157	40°	.063	40.900
20°	.088	48°	.132	60°		
22°	.075	55°	.113	70°		
5°	.115	20°	.173	30°		
10°	.096	30°	.144	40°	.058	43.400
20°	.081	48°	.121	60°		
22°	.069	55°	.104	70°		
5°	.097	20°	.146	30°		
10°	.081	30°	.122	40°	.049	47.500
20°	.068	48°	.102	60°		
22°	.058	55°	.088	70°		
20°	.113	48°	.170	40°	.081	32.400
20°	.113	48°	.170	80°	.081	
20°	.105	48°	.158	40°	.075	35.200
20°	.105	48°	.158	80°	.075	
20°	.099	48°	.148	40°	.071	37.300
20°	.099	48°	.148	80°	.071	
20°	.088	48°	.132	40°	.063	40.900
20°	.088	48°	.132	80°	.063	
20°	.113	48°	.170	0°	.045	32.400
20°	.105	48°	.158	0°	.041	35.200
20°	.099	48°	.148	0°	.039	37.300
20°	.088	48°	.132	0°	.035	40.900

*NOTE: This is inboard side of flap bracket.

FLAP GAP SETTINGS (Continued)

DWG. REF. NO. 1204-236



Typ Flap Assy

(Use Existing Fore, Main & Aft Flaps)

WBL LOCATION	FORE FLAP		θ_1	MAIN FLAP		θ_2	AFT FLAP		θ_3	BRACKET THICKNESS	
	X_1	G_1		X_2	G_2		X_3	G_3			
9.000	.092	.197	12°	.156	.249	35°	60°	0	.125	.50	.50
15.700	.082	.175		.140	.222			0	.111	.50	.50
22.300	.072	.154		.123	.195			0	.098	.50	.50
26.700	.065	.140		.112	.177			0	.089	.375	.375
30.300	.060	.128		.103	.163			0	.081	.375	.375
32.400	.057	.122		.097	.154			0	.077	.25	.25
35.200	.053	.113		.090	.143			0	.071	.25	.25
37.300	.049	.106		.085	.134			0	.067	.25	.25
40.900	.044	.094		.075	.119			0	.060	.25	.25
43.400	.040	.086		.069	.109			0	.055	.25	.25
47.500	.034	.073	12°	.058	.093	35°	60°	0	.046	.25	.25

FLAP BRACKETS AND GAP SETTING TRIPLE SLOT - 12°, 35° and 60°

Contrails

REFERENCES

1. Analysis of Wind Tunnel Data - Unpowered Characteristics, STOL Tactical Aircraft Investigation, D180-14411-2, The Boeing Company, Seattle, Wa., Dec. 1972.
2. Analysis of Wind Tunnel Data - Effect of Vectored Thrust on Lift, Drag and Pitching Moment, STOL Tactical Aircraft Investigation, D180-14411-3, The Boeing Company, Seattle, Wa., Dec. 1972.
3. Analysis of Wind Tunnel Data - Effect of Vectored Thrust on Longitudinal and Lateral Stability, STOL Tactical Aircraft Investigation, D180-14411-4, The Boeing Company, Seattle, Wa., Dec. 1972.
4. Analysis of Wind Tunnel Data - Control Power With Vectored Thrust, STOL Tactical Aircraft Investigation, D180-14411-5, The Boeing Company, Seattle, Wa., Dec. 1972.
5. Analysis of Jet Flap Wind Tunnel Data, STOL Tactical Aircraft Investigation, D180-14411-6, The Boeing Company, Seattle, Wa., Dec. 1972.
6. Aerodynamic Technology: Design Compendium, Vectored Thrust and Mechanical Flaps, STOL Tactical Aircraft Investigation, D180-14409-1, The Boeing Company, Seattle, Wa., Dec. 1972.
7. Effects of Jet-Exhaust Location on the Longitudinal Aerodynamic Characteristics of a Jet V/STOL Model, NASA TN D-5333, National Aeronautics and Space Administration, Langley Research Center, July 1969.
8. An 0.06 Scale, MST STOL Development Model, A Low Speed Wind Tunnel Test of MX 1204B-4, Data Report - BVWT 097, The Boeing Company, Philadelphia, Pa., Dec. 1972.
9. An 0.06 Scale, MST STOL Development Model, A Low Speed Wind Tunnel Test of MX 1204B-5, Data Report - BVWT 099, The Boeing Company, Philadelphia, Pa., Dec. 1972.
10. An 0.06 Scale MST STOL Development Model, A Low Speed Wind Tunnel Test of MX 1204B-6, Data Report - BVWT 101, The Boeing Company, Philadelphia, Pa., Dec. 1972.
11. An 0.06 Scale, MST STOL Development Model, A Low Speed Wind Tunnel Test of MX 1204B-6, Data Report - BVWT 103, The Boeing Company, Philadelphia, Pa., Dec. 1972.
12. Carroll, R.H. et. al., Configuration Definition Medium STOL Transport with Vectored Thrust/Mechanical Flaps, STOL Tactical Aircraft Investigation, D180-14409-1, The Boeing Company; Seattle, Wa., Dec. 1972.

Contrails

13. Phelps, A. E., et. al., Preliminary Low-Speed Wind Tunnel Investigation of a Semispan STOL Jet Transport With an Upper-Surface Blown Jet Flap, NASA LWP-1022, National Aeronautics and Space Administration, January 7, 1972.
14. Wang, T., et. al., Design Integration and Noise Studies for Jet STOL Aircraft, NASA CR-114286, National Aeronautics and Space Administration, May 1972.
15. Quigley, H. C., and Vomaske, R. F., Preliminary Results of Flight Tests of an Augmentor Wing Jet STOL Research Aircraft, STOL Technology Conference, NASA AMES Research Center, October 17-19, 1972.
16. Monk, J. R., STOL Wind Tunnel Test Program, Program Description, STOL Tactical Aircraft Investigation, D180-14279-1, The Boeing Company, Seattle, Wa., Dec. 1971.

UNCLASSIFIED

Security Classification

DOCUMENT CONTROL DATA - R&D		
<small>(Security classification of title, body of abstract and indexing annotation must be entered when the overall report is classified).</small>		
1. ORIGINATING ACTIVITY (Corporate author) Boeing Aerospace Company P. O. Box 3999 Seattle, Washington 98124		2a. REPORT SECURITY CLASSIFICATION UNCLASSIFIED
		2b. GROUP ---
3. REPORT TITLE STOL TACTICAL AIRCRAFT INVESTIGATION - Analysis of Wind Tunnel Data: Vectored Thrust/Mechanical Flaps and Internally Blown Jet Flaps		
4. DESCRIPTIVE NOTES (Types of report and inclusive dates) Final Technical Report, 8 June 1971 - 8 December 1972		
5. AUTHORS (First name, middle initial, last name) John R. Monk, Jerry L. Lee, J. Patrick Palmer		
6. REPORT DATE May 1973	7a. TOTAL NO. OF PAGES 286	7b. NO. OF REFS 16
8a. CONTRACT OR GRANT NO. F33615-71-C-1757	9a. ORIGINATOR'S REPORT NUMBERS AFFDL TR-73-19, Volume IV	
b. Project No. 643A		
c.	9b. OTHER REPORT NO(S) (Any other numbers that may be assigned this report)	
d.	D180-14411-1	
10. DISTRIBUTION STATEMENT Approved for public release; distribution unlimited		
11. SUPPLEMENTARY NOTES	12. SPONSORING MILITARY ACTIVITY Air Force Flight Dynamics Laboratory Wright-Patterson AFB, Ohio 45433	
13. ABSTRACT This document presents the analysis of 728 hours of testing, conducted in the Boeing V/STOL 20 x 20 ft. Wind Tunnel, on a model of a medium STOL transport with vectored thrust and jet flap powered-lift systems. The work is part of the STOL Tactical Aircraft Investigation, U. S. Air Force Flight Dynamics Laboratory Contract Number F33615-71-C-1757, (A Study of the Aerodynamic and Flight Controls Technology of Vectored Thrust for STOL Transport Aircraft). The interactions between the two powered lift systems and the basic airplane aerodynamics are presented for a systematic series of configuration changes which include sweep and nacelle location.		

DD FORM 1 NOV 65 1473
DI 4802 1030 ORIG. 3/71
PART 1 OF 3

UNCLASSIFIED
Security Classification

UNCLASSIFIED
Security Classification

14.	KEY WORDS	LINK A		LINK B		LINK C	
		ROLE	WT	ROLE	WT	ROLE	2T
	Wind Tunnel Test Vectored Thrust Jet Flaps						

FORM
DD 1 NOV 65 1473
D1 4802 1030 ORIG. 3/71
PART 2 OF 3

UNCLASSIFIED
Security Classification

*U.S. Government Printing Office: 1973 - 758-425/20